PB90-172230

Potential Effects of Global Climate Change on the United States. Appendix F. Air Quality

(U.S.) Environmental Protection Agency, Washington, DC

May 89

U.S. Department of Commerce
National Technical Information Service
NTIS

REPORT DOCUMENTATION PAGE

1. REPORT NO.
EPA-230-05-89-056

2.

3. Recipient's Accession No.
PB90 172230/AS

4. Title and Subtitle
The Potential Effects of Global Climate Change on the U.S.
Appendix F: Air Quality

5. Report Date
1989, December

6.

7. Author(s)
Joel Smith and Dennis Tirpak (eds)

8. Performing Organization Rept. No.

9. Performing Organization Name and Address
U.S. Environmental Protection Agency
Office of Policy, Planning and Analysis (PM220)
401 M Street, SW
Washington, DC 20460

10. Project/Task/Work Unit No.

11. Contract(C) or Grant(G) No.
(C)
(G)

12. Sponsoring Organization Name and Address
U.S. Environmental Protection Agency
Office of Policy, Planning, and Analysis (PM220)
401 M Street, SW
Washington, DC 20460

13. Type of Report & Period Covered
Final

14.

15. Supplementary Notes

16. Abstract (Limit: 200 words)

This appendix contains back-up research studies for The Potential Effects of Global Climate Change on the United States report for Congress (1989).

17. Document Analysis a. Descriptors
Climate Change Effects
Greenhouse Effect
Global Warming
Air Quality

b. Identifiers/Open-Ended Terms

c. COSATI Field/Group

18. Availability Statement
No restriction on distribution

19. Security Class (This Report)
Unclassified

20. Security Class (This Page)
Unclassified

21. No. of Pages

22. Price

(See ANSI–Z39.18) *See Instructions on Reverse* OPTIONAL FORM 272 (4–77)

United States
Environmental Protection
Agency

Policy, Planning,
And Evaluation
(PM-221)

EPA-230-05-89-056
June 1989

PB90-172230

EPA

The Potential Effects Of Global Climate Change On The United States

Appendix F
Air Quality

REPRODUCED BY
U.S. DEPARTMENT OF COMMERCE
NATIONAL TECHNICAL INFORMATION SERVICE
SPRINGFIELD, VA. 22161

Printed on Recycled Paper

THE POTENTIAL EFFECTS OF GLOBAL CLIMATE CHANGE ON THE UNITED STATES:

APPENDIX F - AIR QUALITY

Editors: Joel B. Smith and Dennis A. Tirpak

OFFICE OF POLICY, PLANNING AND EVALUATION
U.S. ENVIRONMENTAL PROTECTION AGENCY
WASHINGTON, DC 20460

MAY 1989

TABLE OF CONTENTS

Page

APPENDIX F: AIR QUALITY

PREFACE iii

CLIMATE CHANGE AND ITS INTERACTIONS WITH AIR CHEMISTRY: PERSPECTIVES AND RESEARCH NEEDS 1-1
J.E. Penner, P.S. Connell, D.J. Wuebbles, and C.C. Covey

SENSITIVITY OF A REGIONAL OXIDANT MODEL TO VARIATIONS IN CLIMATE PARAMETERS 2-1
Ralph E. Morris, Mike W. Gery, Mei-Kao Liu, Gary E. Moore, Christopher Daly, and Stanley M. Greenfield

PREFACE

The ecological and economic implications of the greenhouse effect have been the subject of discussion within the scientific community for the past three decades. In recent years, members of Congress have held hearings on the greenhouse effect and have begun to examine its implications for public policy. This interest was accentuated during a series of hearings held in June 1986 by the Subcommittee on Pollution of the Senate Environment and Public Works Committee. Following the hearings, committee members sent a formal request to the EPA Administrator, asking the Agency to undertake two studies on climate change due to the greenhouse effect.

> One of the studies we are requesting should examine the potential health and environmental effects of climate change. This study should include, but not be limited to, the potential impacts on agriculture, forests, wetlands, human health, rivers, lakes, and estuaries, as well as other ecosystems and societal impacts. This study should be designed to include original analyses, to identify and fill in where important research gaps exist, and to solicit the opinions of knowledgeable people throughout the country through a process of public hearings and meetings.

To meet this request, EPA produced the report entitled *The Potential Effects of Global Climate Change on the United States*. For that report, EPA commissioned fifty-five studies by academic and government scientists on the potential effects of global climate change. Each study was reviewed by at least two peer reviewers. The Effects Report summarizes the results of all of those studies. The complete results of each study are contained in Appendices A through J.

Appendix	**Subject**
A	Water Resources
B	Sea Level Rise
C	Agriculture
D	Forests
E	Aquatic Resources
F	Air Quality
G	Health
H	Infrastructure
I	Variability
J	Policy

GOAL

The goal of the Effects Report was to try to give a sense of the possible direction of changes from a global warming as well as a sense of the magnitude. Specifically, we examined the following issues:

- sensitivities of systems to changes in climate (since we cannot predict regional climate change, we can only identify sensitivities to changes in climate factors)
- the range of effects under different warming scenarios
- regional differences among effects
- interactions among effects on a regional level

- national effects
- uncertainties
- policy implications
- research needs

The four regions chosen for the studies were California, the Great Lakes, the Southeast, and the Great Plains. Many studies focused on impacts in a single region, while others examined potential impacts on a national scale.

SCENARIOS USED FOR THE EFFECTS REPORT STUDIES

The Effects Report studies used several scenarios to examine the sensitivities of various systems to changes in climate. The scenarios used are plausible sets of circumstances although none of them should be considered to be predictions of regional climate change. The most common scenario used was the doubled CO_2 scenario ($2XCO_2$), which examined the effects of climate under a doubling of atmospheric carbon dioxide concentrations. This doubling is estimated to raise average global temperatures by 1.5 to 4.5°C by the latter half of the 21st century. Transient scenarios, which estimate how climate may change over time in response to a steady increase in greenhouse gases, were also used. In addition, analog scenarios of past warm periods, such as the 1930s, were used.

The scenarios combined average monthly climate change estimates for regional grid boxes from General Circulation Models (GCMs) with 1951-80 climate observations from sites in the respective grid boxes. GCMs are dynamic models that simulate the physical processes of the atmosphere and oceans to estimate global climate under different conditions, such as increasing concentrations of greenhouse gases (e.g., $2XCO_2$).

The scenarios and GCMs used in the studies have certain limitations. The scenarios used for the studies assume that temporal and spatial variability do not change from current conditions. The first of two major limitations related to the GCMs is their low spatial resolution. GCMs use rather large grid boxes where climate is averaged for the whole grid box, while in fact climate may be quite variable within a grid box. The second limitation is the simplified way that GCMs treat physical factors such as clouds, oceans, albedo, and land surface hydrology. Because of these limitations, GCMs often disagree with each other on estimates of regional climate change (as well as the magnitude of global changes) and should not be considered to be predictions.

To obtain a range of scenarios, EPA asked the researchers to use output from the following GCMs:

- Goddard Institute for Space Studies (GISS)
- Geophysical Fluid Dynamics Laboratory (GFDL)
- Oregon State University (OSU)

Figure 1 shows the temperature change from current climate to a climate with a doubling of CO_2 levels, as modeled by the three GCMs. The figure includes the GCM estimates for the four regions. Precipitation changes are shown in Figure 2. Note the disagreement in the GCM estimates concerning the direction of change of regional and seasonal precipitation and the agreement concerning increasing temperatures.

Two transient scenarios from the GISS model were also used, and the average decadal temperature changes are shown in Figure 3.

FIGURE 1. TEMPERATURE SCENARIOS

GCM Estimated Change in Temperature from $1xCO_2$ to $2xCO_2$

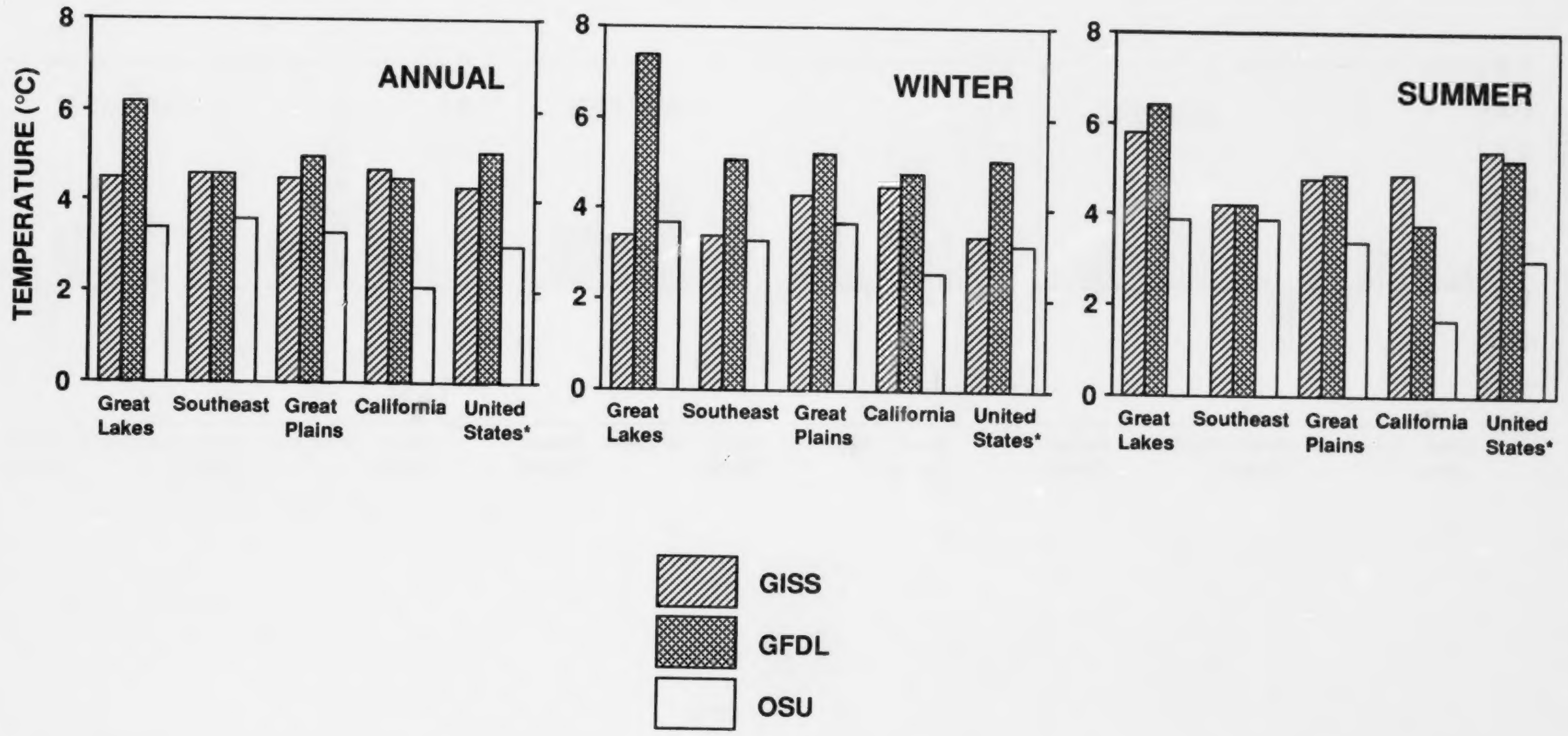

* Lower 48 States

FIGURE 2. PRECIPITATION SCENARIOS

GCM Estimated Change in Precipitation from $1xCO_2$ to $2xCO_2$

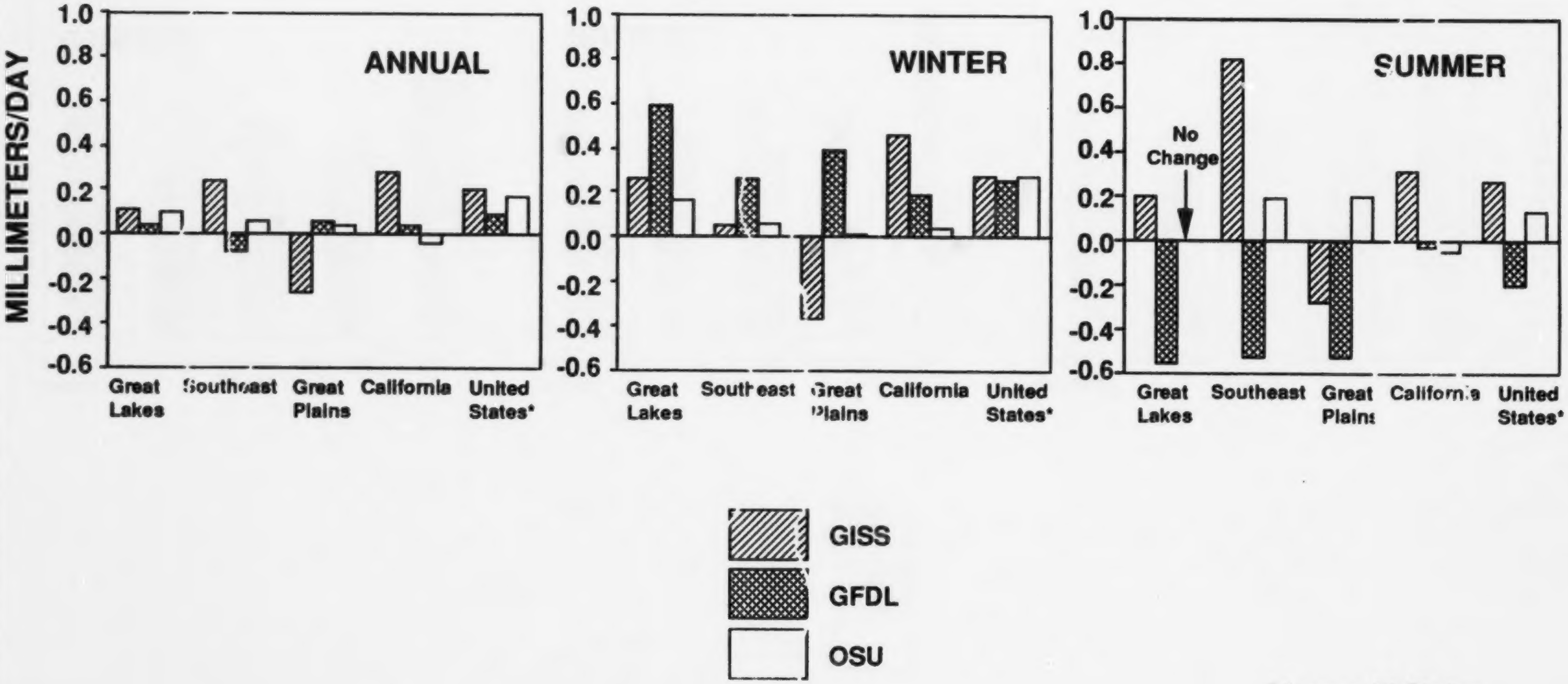

* Lower 48 States

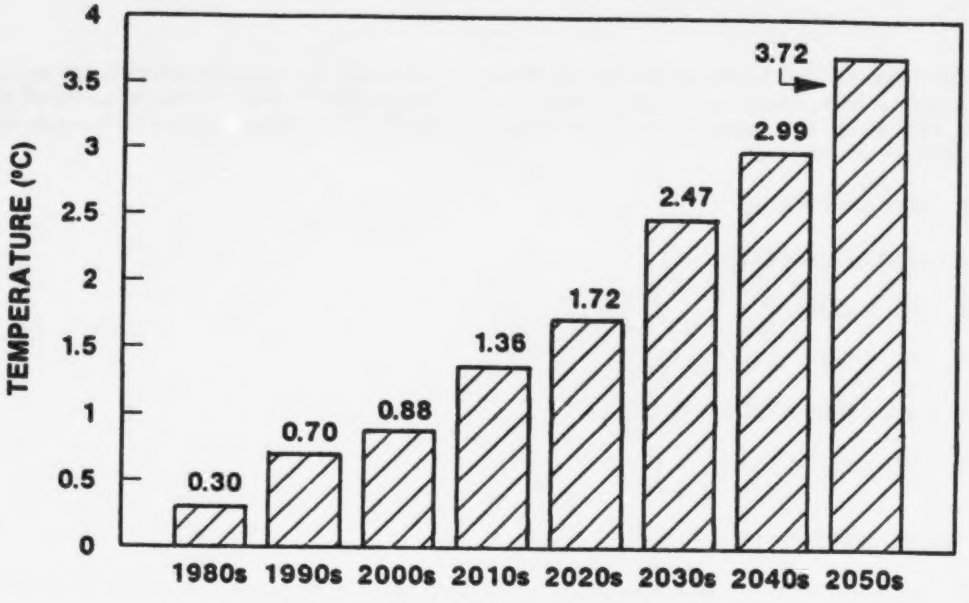

TRANSIENT SCENARIO A

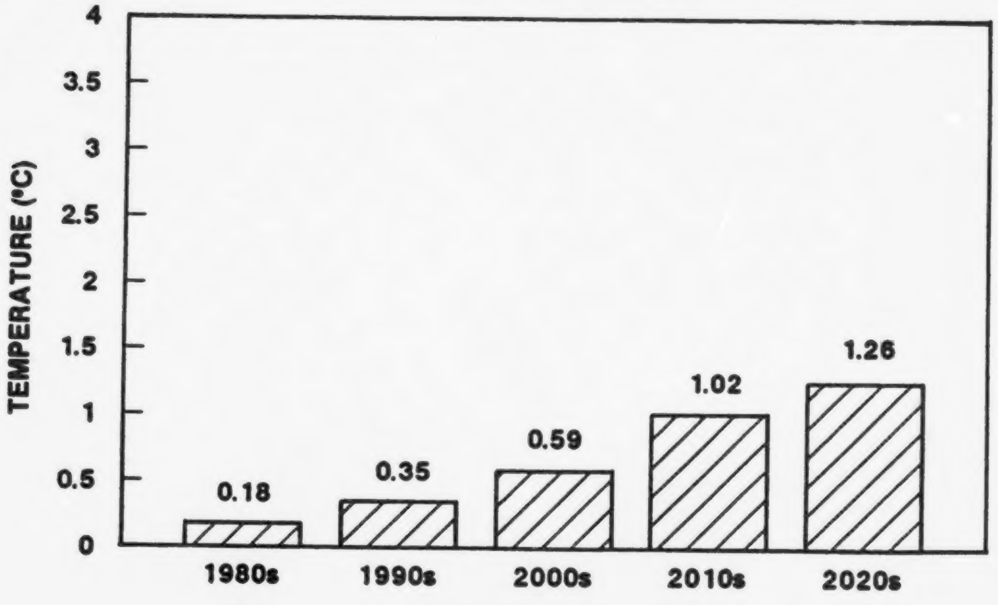

TRANSIENT SCENARIO B

FIGURE 3. GISS TRANSIENTS "A" AND "B" AVERAGE TEMPERATURE CHANGE FOR LOWER 48 STATES GRID POINTS.

EPA specified that researchers were to use three doubled CO_2 scenarios, two transient scenarios, and an analog scenario in their studies. Many researchers, however, did not have sufficient time or resources to use all of the scenarios. EPA asked the researchers to run the scenarios in the following order, going as far through the list as time and resources allowed:

1. GISS doubled CO_2
2. GFDL doubled CO_2
3. GISS transient A
4. OSU doubled CO_2
5. Analog (1930 to 1939)
6. GISS transient B

ABOUT THESE APPENDICES

The studies contained in these appendices appear in the form that the researchers submitted them to EPA. These reports do not necessarily reflect the official position of the U.S. Environmental Protection Agency. Mention of trade names does not constitute an endorsement.

CLIMATE CHANGE AND ITS INTERACTIONS WITH AIR CHEMISTRY: PERSPECTIVE AND RESEARCH NEEDS

by

J.E. Penner
P.S. Connell
D.J. Wuebbles
C.C. Covey
Lawrence Livermore National Laboratory
University of California
Livermore, CA 94550

Interagency Agreement No. DW89932676-01-1

NOTE[1]

The working title of this report and the title that appears in the LLNL Scope of Work is Estimates of the Interactions Between Urban/Regional Air Quality and Changes in Tropospheric Chemistry and Climate. The current report title was chosen to emphasize the importance of interactions at all spatial scales between local/urban and global in understanding the effects of climate change from the perspective of atmospheric photochemical processes.

---

[1] This work was performed under the auspices of the U.S. Department of Energy under Contract W-7405-Eng-48, with the partial support of the U.S. Environmental Protection Agency under Interagency Agreement DW89932676-01-0. However, it does not necessarily reflect the Agency's views and no official endorsement should be inferred from it. We thank Stan Grotch for useful discussions concerning his research on GCM intercomparison and allowing us to use some unpublished results. We would also like to thank John DiBari, Matthew Hopper, and Steven Giles, who participated in the ISME-sponsored LLNL summer study program, for their contributions. Thanks are also due to Peter Finkelstein, Joseph Bufalini, Anne Thompson, and Ralph Cicerone for their useful comments and careful reviews of the original manuscript.

CONTENTS

Page
CHAPTER 1: INTRODUCTION 1-1

CHAPTER 2: TRENDS IN GLOBAL ATMOSPHERIC COMPOSITION AND CLIMATE 1-4
GLOBAL DISTRIBUTIONS AND TRENDS OF ATMOSPHERIC SPECIES 1-4
CO_2 1-8
CH_4 1-9
N_2O 1-10
Cl- and Br-containing Industrial Compounds 1-10
Other Trace Constituents of Importance With Possible Trends 1-11
Nitrogen Oxides 1-12
Carbon Monoxide 1-12
Natural and Anthropogenic Higher Hydrocarbons 1-13
Global Background Stratospheric Aerosol 1-13
Global Background Tropospheric Aerosol 1-13
THE CLIMATE SYSTEM 1-14
Global Annual Average Radiative Forcing 1-14
Additional Climate Variables 1-16
ATMOSPHERIC COMPOSITION CHANGE AND GLOBAL CLIMATE 1-19
Direct Radiative Impacts 1-19
Climate Feedback Response to Direct Radiative Forcing Changes 1-20
Photochemical Forcings of Global Climate Change 1-20
Climate Responses to Composition Changes from the Historical Record 1-22
Global Climate Projections 1-23

CHAPTER 3: URBAN/REGIONAL CHEMISTRY AND CLIMATE CHANGE 1-24
URBAN AND REGIONAL OXIDANT FORMATION 1-24
Formation of Oxidant 1-24
Effect of Climate Change on Oxidant Formation 1-25
ACID RAIN AND ACID DEPOSITION 1-35
Formation of Acidic Species 1-35
Effect of Climate Change on Acid Rain and Acid Deposition 1-36

CHAPTER 4: GLOBAL CHEMISTRY AND CLIMATE INTERACTIONS 1-38
TROPOSPHERIC OH 1-38
Sources and Sinks of OH 1-38
Impact of Climate Change on Tropospheric OH 1-39
Climate Implications of OH Abundance Change 1-41
TROPOSPHERIC O_3 1-41
Sources and Sinks of O_3 1-43
Impacts of Climate Change on Tropospheric Ozone 1-44
OTHER CLIMATE CHANGE FEEDBACKS ON GLOBAL ATMOSPHERIC COMPOSITION 1-45

CHAPTER 5: MODELING CAPABILITIES AND LIMITATIONS 1-47
GENERAL CIRCULATION MODELS 1-48
GLOBAL CHEMISTRY MODELS 1-51
URBAN/REGIONAL MODELS 1-53
Bridging Across Spatial Scales 1-65

CHAPTER 6: CONCLUSIONS AND RESEARCH NEEDS 1-67

REFERENCES 1-70

CHAPTER 1

INTRODUCTION

Man's ability to impact the local environment has been evident for some time. Since the pioneering studies of Haagen-Smit in the 1950s to explain and understand the photochemical formation of smog, we have been aware that fossil fuel emissions can impact local air quality (see Leighton, 1961, and references therein). During the 1960s and 1970s, we became increasingly aware of the impacts of the long-range transport of fossil fuel emissions. These impacts manifest themselves on a more continental scale, the regional scale of acid rain and acid deposition, for example (Albritton et al., 1987).

During the last two decades as well, it has become increasingly clear that man's activities can also result in changes to much larger areas, areas which are global in scope (see NRC, 1983, and NRC, 1984). On these scales, not only may the chemistry of the atmosphere change, but the climate of our planet may change as well. The most obvious changes to climate are driven by increases in CO_2, a species whose lifetime is so long that other than its impact on temperatures and therefore reaction rate constants, it has no obvious interaction with chemistry. However, more recently, trends in more minor species, for example, CH_4, N_2O, and halocarbons, have been documented. These species interact radiatively in the atmosphere to alter temperatures. They also interact chemically in the atmosphere to impact other species whose lifetimes are much shorter (e.g., tropospheric OH and stratospheric O_3).

With the increasing awareness of climate change and the possibility of global chemical changes to the atmosphere, it becomes important to ask whether these global changes might impact regional chemistry in such a way as to obviate or otherwise hinder some of the programs already legislated or under contemplation and designed to help reduce local and regional air pollution. The issue is non-trivial because the effects of climate change are manifold and will be felt differently in different seasons and different areas around the world. Furthermore, the atmospheric chemical system as a whole will impact regional chemistry by impacting boundary and background concentrations leading to a need to understand not only regional chemical changes but global ones as well. Finally, global chemical changes have the potential to feed back and change climate so that the effects cannot be fully known until the entire) climate/chemistry system is understood.

This paper attempts to outline and estimate the interactions between climate change and atmospheric chemistry that need investigation on both local and/or regional and global scales. The problem is not simply one of estimating temperature change and running chemical models we already possess to get an answer. The ways that a changing climate influences atmospheric chemistry include not only temperature and precipitation changes, but changes to atmospheric transport processes, changes to the budgets of species with biological sources (which respond to temperature and moisture changes), changes to vegetative cover which would alter deposition rates, changes in the rate of export of pollutants from the urban/regional environment to the global one, etc. Furthermore, changes in atmospheric chemical composition will lead to climate change. Figure 1.1 gives an overview of the climate/chemistry system and the interactions that it will be necessary to understand in order to predict the future state of our planet. The responses of these various subsystems may be highly coupled to both each other and the climate change itself. For example, climate change has the potential to alter water vapor concentrations. Changes in the concentration of water vapor would profoundly alter many species concentrations by impacting atmospheric OH concentrations, because OH acts as a scavenger for many pollutants. Changes to H_2O will also impact tropospheric O_3 concentrations. Because O_3 absorbs infrared radiation, these changes will feed back to alter the climate. As another example, climate change also has the potential to alter the biological sources and sinks of certain gases. Because biological processes supply many of the species of radiative importance in the troposphere, changes in these sources will feed back to alter the climate response.

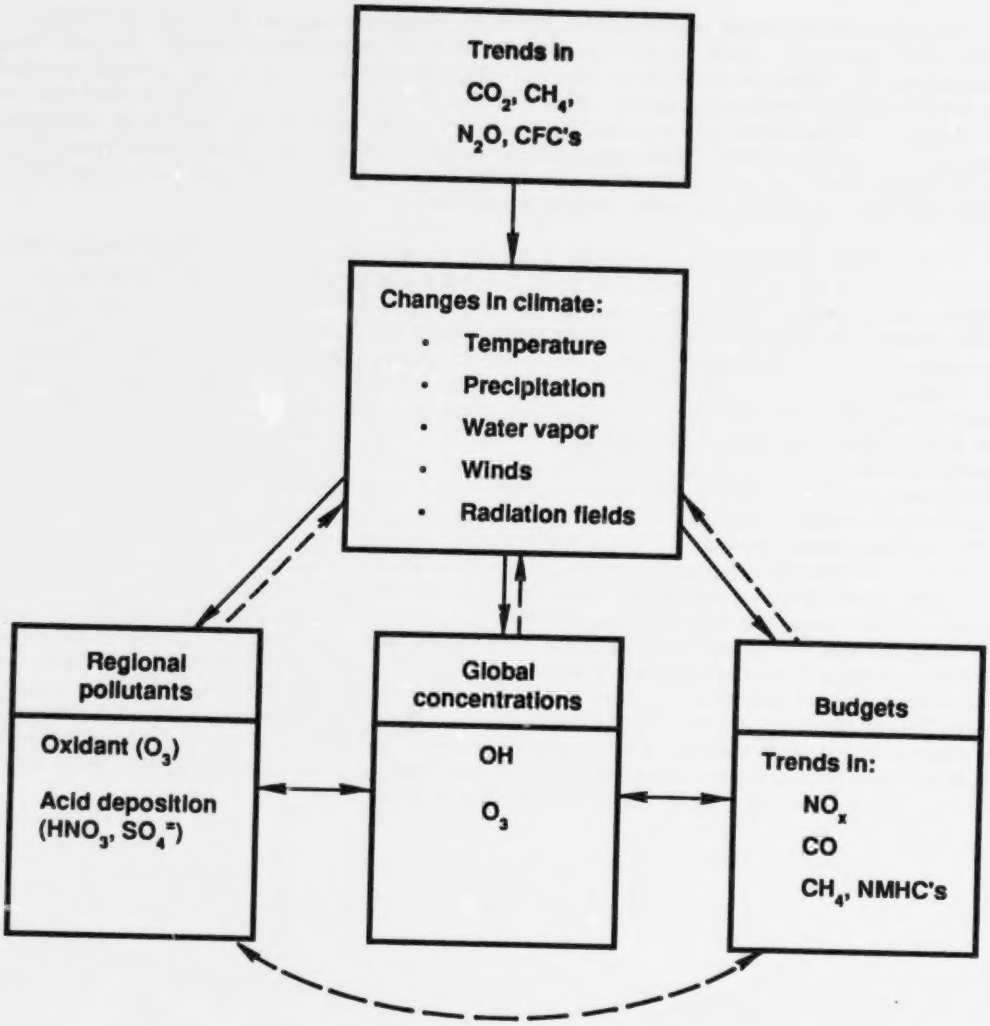
Trends in
CO_2, CH_4, N_2O, CFC's
Changes in climate:
• Temperature
• Precipitation
• Water vapor
• Winds
• Radiation fields
Regional pollutants
Oxidant (O_3)
Acid deposition (HNO_3, $SO_4^=$)
Global concentrations
OH
O_3
Budgets
Trends in:
NO_x
CO
CH_4, NMHC's

Figure 1.1. Processes interconnecting climate and global and regional chemistry.

Changes in global chemistry will be intimately tied to changes in regional chemistry and changes on one scale will affect changes on others. Just as the globally averaged temperature response to a given change in composition will be manifested by different changes in various different regions, the "average" composition change will be different in different regions. Determination of how this all ties together to feed back on the climate change is a formidable problem indeed. In this paper, we make a first attempt at examining this problem, by (1) a discussion of possible compositional changes on both regional and global scales from the variety of changes that may be introduced by climate change, and potential climate changes resulting from compositional change and (2) a discussion of needed research.

In the following, we begin with a review of climate change and a discussion of the evidence that leads us to believe that it is indeed an issue that will be facing man in the near future. Chapter 3 attempts to define the ways in which climate change might impact local and regional oxidant formation and regional acid rain formation. Chapter 4 outlines how climate change might impact global chemistry, in so far as tropospheric OH and tropospheric O_3 are concerned. Chapter 5 discusses the variety of models available today to address these issues. A short review of the capabilities of general circulation models to treat climate change is followed by a discussion of our ability to treat "global" chemistry (i.e., large-scale compositional changes generally treated by a great deal of spatial averaging) and regional chemistry (i.e., higher resolution treatments with predictions confined to specific locations). A central problem that we face is that the grid resolution of general circulation models is much larger than that typically needed in regional chemistry models. We have not yet developed the tools needed to translate the meteorological changes predicted by general circulation models to the changes that will drive regional chemistry changes. A related problem concerns the fact that no two general circulation models agree as to what the regional meteorological changes related to a change in climate might be. A similar problem plagues our ability to link global chemistry models to regional chemistry models. In this case the treatments available today not only differ in grid resolution but also in dimensionality--with "global" chemical models being at most two dimensional, while the most sophisticated and realistic regional models are three dimensional. Chapter 5 summarizes some of these issues and Chapter 6 gives a set of research areas that will need substantial support and effort in order to better define how climate change might impact atmospheric chemistry. These issues concern not only the issues of predicting changes across several spatial scales, but also issues concerning our understanding of atmospheric budgets. Because of the spatial heterogeneity in the troposphere, the budgets of many of the gases contributing to changes in the composition and climate are poorly understood. This is a second area where substantial effort is needed.

CHAPTER 2

TRENDS IN GLOBAL ATMOSPHERIC COMPOSITION AND CLIMATE

This report attempts, in part, to provide a synopsis of our ability to define how certain kinds of changes in the global climate may affect atmospheric chemistry in both a regional and global context. Thus, the global climate changes considered here include both secular trends in average climate statistics and changes in moments of the distribution of climate variables related to the controlling variables of regional air chemistry. While understanding the basis of possible future change in quantities such as annual average global surface temperature is a difficult problem receiving current attention, understanding the potential for changes in higher moments of the distributions of climate variables is even more complex and much less studied. But consideration of such changes remains important given the desire to characterize extreme events as well as average properties of regional air chemistry.

The external driver for the closely coupled terrestrial atmosphere/biosphere/ocean/land surface system is the solar energy input and the details of its spectral distribution. Intrinsic solar variability and the Earth's orbital elements produce weather and climate trends and variability on time scales ranging from seasonal to cosmic, some systematic and some apparently random. We are interested here in trends and variability in addition to the celestial component, which can be ascribed, in many cases, to human population and industrial and agricultural activities. The time scales of these changes are generational or political, ranging from decades to centuries. In this chapter, we will present an overview of relevant aspects of the climate system and the reasons for expecting significant trends on these time scales. An overview of the interactions of climate with atmospheric trace constituents and chemistry are shown in Figure 2.1.

GLOBAL DISTRIBUTIONS AND TRENDS OF ATMOSPHERIC SPECIES

From the standpoint of regional air chemistry, which involves questions of near surface abundances of oxidants like ozone, wet and dry deposition of acidic species and transport and lifetimes of trace atmospheric constituents, the climate variables of interest include moments of the distributions of temperature, precipitation, clouds, and boundary layer meteorology. In the basic global sense, these variables are controlled by surface and atmospheric temperature and water. The distributions of temperature and water are in turn controlled by solar and long-wave radiation transfer involving the surface and the atmosphere. The radiative properties of the atmosphere, that is absorption and emission of energy in the range from the infrared to the ultraviolet by atmospheric constituents, and the albedo of clouds and the Earth's surface are then the fundamental quantities and processes of interest in understanding the climate. It happens that both the radiative properties of the atmosphere, through the medium of the abundances of trace constituents, and the surface albedo are susceptible to modification by modern man (Wang et al., 1986; Dickerson and Cicerone, 1986; Ramanathan et al., 1987).

More or less well-mixed atmospheric constituents include those species listed in Table 2.1. Of these constituents, in order of relative importance according to current concentrations, H_2O, CO_2, O_3, CH_4, N_2O and potentially CFC-11 and CFC-12 are significant in atmospheric radiative transfer (Luther and Ellingson, 1985; Ramanathan et al., 1987). Of these all but H_2O and O_3 have established abundance trends thought to be directly traceable to emissions of human industrial and agricultural activity. (Note: there are indications that the distribution of O_3 is also changing.) H_2O and O_3, in addition to many other of the trace constituents listed above, may also be increasing, but trend detection is made difficult because of inadequate monitoring and/or spatial and temporal heterogeneity of distributions. Ozone and other photochemically produced species are subject to indirect modification of their abundances and distributions by trends in directly emitted source species.

We summarize below and in Table 2.2 current knowledge of global-scale observed abundance trends and budgets of many of these directly emitted atmospheric constituents. Atmospheric abundances of these trace constituents are controlled by the rates and spatial distributions of emissions (production) and losses.

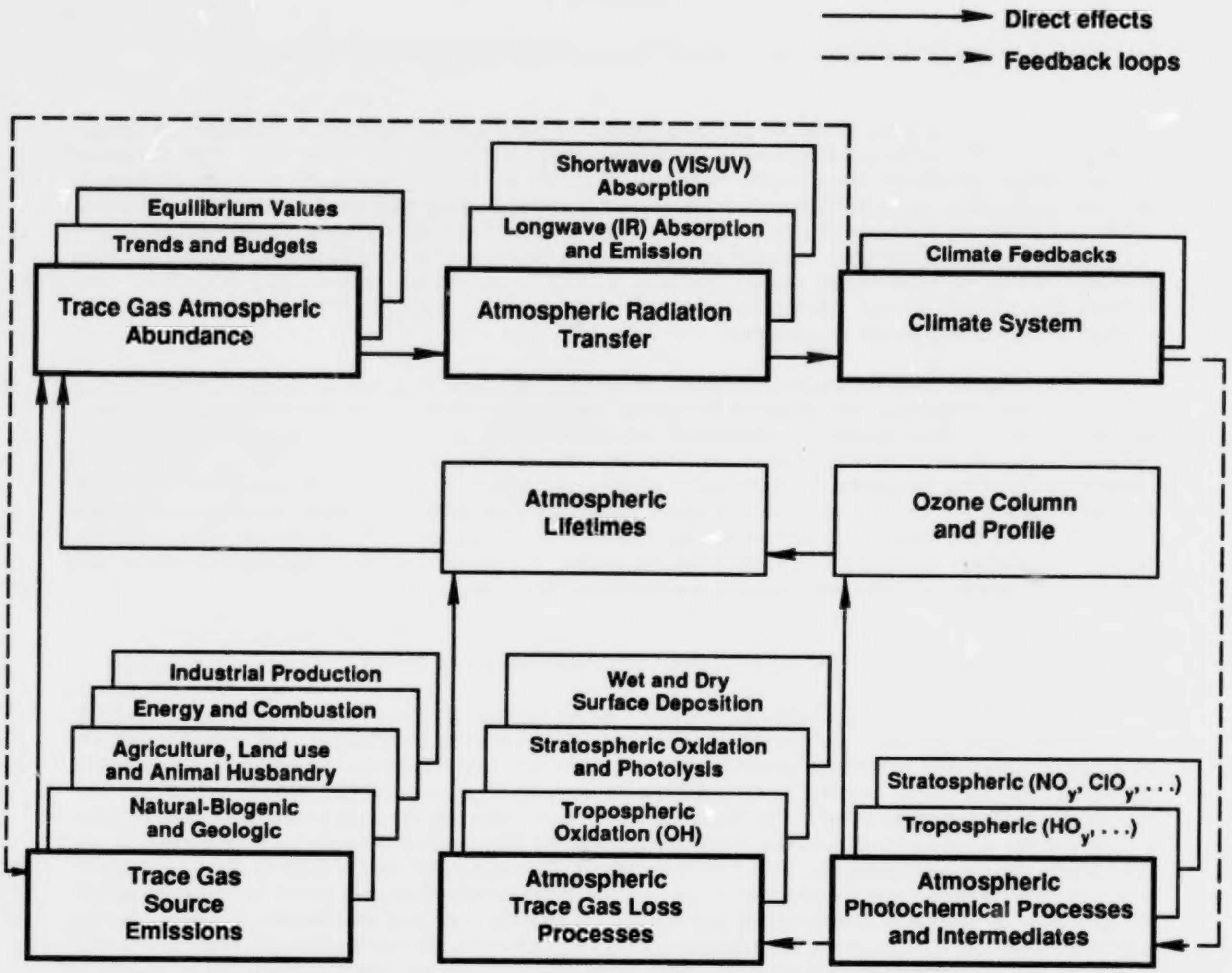
Direct effects
Feedback loops
Equilibrium Values
Trends and Budgets
Trace Gas Atmospheric Abundance
Shortwave (VIS/UV) Absorption
Longwave (IR) Absorption and Emission
Atmospheric Radiation Transfer
Climate Feedbacks
Climate System
Atmospheric Lifetimes
Ozone Column and Profile
Industrial Production
Energy and Combustion
Agriculture, Land use and Animal Husbandry
Natural-Biogenic and Geologic
Trace Gas Source Emissions
Wet and Dry Surface Deposition
Stratospheric Oxidation and Photolysis
Tropospheric Oxidation (OH)
Atmospheric Trace Gas Loss Processes
Stratospheric (NO_y, ClO_y, . . .)
Tropospheric (HO_y, . . .)
Atmospheric Photochemical Processes and Intermediates

Figure 2.1. Climate/chemistry system.

Table 2.1

Trace Constituent	Abundance		
	%	ppm	ppb
Nitrogen (N_2)	78		
Oxygen (O_2)	21		
Water (H_2O)	0-2		
Argon (Ar)	0.9		
Carbon dioxide (CO_2)	0.034		
Neon (Ne)		18.2	
Helium (He)		5.2	
Methane (CH_4)		1.7	
Krypton (Kr)		1.1	
Hydrogen (H_2)		0.56	
Nitrous oxide (N_2O)			300
Carbon monoxide (CO)			90
Xenon (Xe)			87
Ozone (O_3) troposphere			20-400*
Ammonia (NH_3)			<1
Ethane (C_2H_6)			0.8
Methyl chloride (CH_3Cl)			0.6
Carbonyl sulfide (OCS)			0.5
CFC-12 (CF_2Cl_2)			0.35
CFC-11 ($CFCl_3$)			0.2
Formaldehyde (CH_2O)			0.2
Sulfur dioxide (SO_2)			0.1
Nitrogen oxides (NO, NO_2)			0.05-100*
Other CFCs			<0.15
Many other species			<0.1

---

* Higher values representative of highly polluted conditions.

Table 2.2. Established and Suspected Trace Species Trends

Trace Constituent	Estimated Annual Increase	Importance for Climate	References
CO_2	0.4%	Absorbs infrared radiation; affects stratospheric O_3	d, l
CH_4	1.1%	Absorbs infrared radiation; affects tropospheric O_3 and OH; affects stratospheric H_2O and O_3	a, l
N_2O	0.2%	Absorbs infrared radiation; affects stratospheric O_3	k, l
$CFCl_3$	5.0%	Absorbs infrared radiation; affects stratospheric O_3	b, l
CF_2Cl_2	5.0%	Absorbs infrared radiation; affects stratospheric O_3	c, l
CH_3CCl_3	5.0%	Absorbs infrared radiation; affects stratospheric O_3	l
CHF_2Cl	12.0%	Absorbs infrared radiation; affects stratospheric O_3	e, l
$CFCl_2CF_2Cl$	10.0%	Absorbs infrared radiation; affects stratospheric O_3	f, l
Tropospheric O_3	0.8%*	Absorbs uv and infrared radiation	i
Stratospheric O_3	-0.3%**	Absorbs uv and infrared radiation	j
CO	≈1%	Involved in tropospheric O_3 and OH cycles	g, h
NO_x	?	Involved in O_3 and OH cycles and precursor of acidic nitrates	
NMHC	?	Involved in tropospheric O_3 and OH cycles	
$(CH_3)_2S$	?	Produces CCN which can alter cloud albedo; forms SO_2	
OCS	?	Forms aerosol in stratosphere which alters albedo	
CS_2	?	May be major source of OCS in the troposphere	
SO_x	?	Major precursor of acid rain	
H_2S	?	Major natural source for SO_2	
Tropospheric OH	-?	Scavenger for many atmospheric pollutants, including CH_4, CH_3CCl_3, CH_3F_2Cl	

* In lower troposphere.
** In upper stratosphere.

References:
a. Blake and Rowland (1988)
b. Cunnold et al. (1983a)
c. Cunnold et al. (1983b)
d. Keeling (1983)
e. Khalil and Rasmussen (1981)
f. Khalil and Rasmussen (1985a)
g. Khalil and Rasmussen (1988)
h. Risland and Levine (1985)
i. Tiao et al. (1986)
j. Watson (1988)
k. Weiss (1981)
l. WMO (1985)

Observed non-zero trends indicate an imbalance of production and losses related to changes in either or both processes. Changes in production or loss rates can be currently continuing or, particularly for long-lived species, the result of past events. Uncertainties in the understanding of the budgets of most of the important source species makes the prediction of future abundance trends difficult, even for species with well-defined current abundance trends. Although trends are listed for tropospheric and stratospheric ozone based on recent evaluations of available data from ozonesondes, ground-based measurements, and satellite measurements, there are many uncertainties associated with the data that determine these trends, and therefore the trends for ozone should be regarded cautiously.

CO_2

Carbon dioxide is the single most important trace constituent from the standpoint of global climate change, as its radiative impact is second only to H_2O and its emission source has a significant direct anthropogenic fraction (Wang et al., 1986; Ramanathan et al., 1987). It does not participate directly in photochemistry and is well-mixed in the troposphere and stratosphere. Many recent primary sources and reviews are available discussing the many complex elements of the global biogeochemical carbon cycle (DOE, 1985b; NRC, 1983). We touch here only on the most salient features.

Millenial scale long-term natural variability of the CO_2 atmospheric abundance is closely related to climate variability. Records generated both by proxy techniques and recovery of ancient air trapped in glacial ice show the CO_2 abundance cycling between 200 and 300 ppm as the climate cycled from glacial to interglacial conditions (Barnola et al., 1987; Genthon et al., 1987). Inferred rates of change at the end of the last glacial period are similar in magnitude to that currently observed. However variability during the millenium prior to 1800 (and the start of growth in large scale land use changes and industrial activity) appears smaller, in the range of 260 to 285 ppm. In the period since 1800, both direct and proxy methods, including archived spectroscopic plates, tree rings, bubbles in ice and wet chemical measurements, show a secular trend of increase to the current level of 345 ppm (Gammon et al. in DOE, 1985b).

A continuous record of CO_2 abundance at Mauna Loa, Hawaii, using a precise technique, is available starting in 1958 (Keeling, 1983). More recently, continuous surface abundance records from additional sites at a variety of latitudes in both hemispheres provide sufficient information to portray seasonal and latitudinal variations superimposed on the secular global abundance trend (WMO, 1985). Currently, the secular trend in global surface abundance averages about 1.4 ppm/year (3×10^{15} gC/year), or about 0.4%/year. At Mauna Loa, the trend of increase has been monotonic since the beginning of the record in 1958, with some indication that the rate of increase has slowed over the last decade (Keeling, 1983; WMO, 1985). A seasonal cycle in CO_2 abundance is observed at northern middle and high latitudes peaking in the winter with a maximum amplitude of about 15 ppm (3×10^{16} gC). Interannual variability in the secular trend appears to be on the order of 1 ppm, about the, same magnitude as the current annual trend.

Biogeochemical cycling of carbon among the atmosphere, biosphere, surface, oceans and sediments covers time scales from geologic to seasonal. The largest reservoir of carbon (>99.999%) and the largest loop in the cycle is the formation and weathering of carbonate rocks, involving tectonic processes and taking place on a geologic time scale. Total burdens in the atmosphere, oceans, biosphere and soils (exclusive of subfossil and fossil deposits) are all of the order 1×10^{18} gC, with perhaps a 500-year characteristic time constant for CO_2 loss from this system. Annual respiration of the oceans and biosphere is of the order 1×10^{17} gC. Annual variability in the processes controlling biological productivity and near surface ocean uptake, driven for example by El Niño/Southern Oscillation (ENSO) events, can be of the order of 1×10^{15} gC. The current anthropogenic exogenous CO_2 production from land use changes and fossil fuel burning is about 6×10^{15} gC/year (WMO, 1985).

It appears that the CO_2 atmospheric abundance increase between 1800 and the early 20th century was driven by changes in land use affecting the partitioning of carbon between biosphere and atmosphere. Direct emission by fossil fuel combustion became the dominant term in CO_2 increase early in this century and continuing to the present. A significant fraction, perhaps 40%, of the anthropogenic release of CO_2 is partitioned into the oceans by a net annual ocean uptake (WMO, 1985).

Much effort has gone into a quantitative understanding of the historical CO_2 record and associated human activities as a basis for prediction of future trends. Quantitative models describing uptake and chemical and biological processes in the ocean, the sensitivity to vegetation changes of carbon fluxes from terrestrial ecosystems, the role of subfossil (e.g., peat) deposits, and fossil fuel consumption are required to derive the small net terms as differences of source and sink fluxes in the carbon budget. Significant uncertainties remain in all of these areas.

Predicting the future atmospheric abundance of CO_2, and thus its radiative impact and contribution to climate change, requires knowledge of the carbon cycle and how it partitions non-equilibrium CO_2 emission inputs. The ability to predict future emissions is based on the ability to predict future trends in global population and economic growth and energy consumption patterns as well as any possible effects of future responses to observed climate change and alternative energy-producing technologies. Clearly uncertainties will remain large. A possible view of the future is an average annual increase in atmospheric abundance over the next century of about 0.5%/year (NRC, 1983; Edmonds et al., 1984; Bolin et al., 1986; Mintzer, 1987). The CO_2 abundance at the end of the next century would, in this case, be about twice the average abundance over the last several thousand years.

CH_4

The modern abundance record for CH_4 (Rinsland et al., 1985b) starts in 1951 with information from spectroscopic plates which can be precisely analyzed to give an abundance of 1.14 ppm in Europe at that time. Sporadic measurements between 1965 and 1977 during the development of the high-precision gas chromatography/flame ionization detection method for CH_4 show a clearly increasing abundance over this period (Ehhalt, 1985). Finally, continuous records with high precision are available since 1979, with globally distributed sampling yielding information on the latitudinal dependence of seasonal variability (Blake and Rowland, 1986, 1988; Khalil and Rasmussen, 1983a). The record has also been extended back over thousands of years by analysis of air encapsulated in glacial bubbles.

The glacial air bubble record shows a constant CH_4 abundance of about 0.7 ppm until several centuries before present, followed by an observed increasing abundance (Craig and Chou, 1982; Khalil and Rasmussen, 1982; Rasmussen and Khalil, 1984; Stauffer et al., 1985, 1988). Connecting the 1.14 ppm abundance in 1951 with a similarly derived spectroscopic value of 1.58 ppm in 1981 implies an average annual increase over 30 years of 1.1% (Rinsland et al., 1988). The continuous record between 1979 and present shows an average annual increase around 1% with significant interannual variability. A seasonal cycle is observed at most latitudes, generally with a minimum in the summer and with a poleward increase in amplitude. The present average abundance is about 1.7 ppm in the northern hemisphere and 1.6 ppm in the southern hemisphere.

The atmospheric abundance of CH_4 represents a balance primarily between biogenic sources and photochemical sinks in the troposphere and stratosphere. The solubility of CH_4 is sufficiently low that the ocean is not an important reservoir. The current atmospheric burden is about 3.5×10^{15} gC (Wuebbles and Edmonds, 1988). The atmospheric lifetime resulting from reaction with OH can be estimated by comparison to another species, CH_3CCl_3, also predominantly destroyed by OH and with a similar lifetime. From knowledge of the kinetic rate constants for reaction of OH with CH_4 and CH_3CCl_3 and the ALE observational data on the lifetime of CH_3CCl_3 (Prinn et al., 1983), the CH_4 lifetime must be about 11 years and the calculated annual CH_4 loss by reaction with OH is around 3.2×10^{14} gC. Uptake by biological processes in dry soils contributes perhaps $7\text{-}8 \times 10^{12}$ gC/year to the sink. Accumulation in the atmosphere is observed to be about 1% or 0.017 ppm/year, corresponding to 3.5×10^{13} gC. The global source term is thus constrained to be roughly 3.6×10^{14} gC/year (WMO, 1985; Wuebbles and Edmonds, 1988). The equilibrium atmospheric abundance for this emission term and lifetime is around 2.0 ppm, so that the methane abundance should be expected to increase, exclusive of compensating atmospheric changes or source reductions.

Apportioning the total source term among the many known CH_4 sources is a difficult problem (WMO, 1985; Wuebbles and Edmonds, 1988). Three major sources, enteric fermentation in ruminant animals, rice paddies and natural wetland emissions, are thought to be of roughly equivalent magnitude (7-10 x 10^{13} gC/year). Abiogenic emissions related to fossil fuels and biomass burning may be important (3-4 x 10^{13} gC/year). The sensitivity of emission to many variables in an ecosystem and to such things as specific strains of rice restricts the potential to generalize individual field studies to the globe. It appears that perhaps 60% of the total source term can be directly ascribed to human activities. Investigation of the $^{13}C/^{12}C$ ratio of atmospheric CH_4 and its trend, in comparison to the isotopic composition of known source emissions, may result in better definition of relative source magnitudes in the future.

The currently observed imbalance of the source and sink strengths in the atmospheric CH_4 budget can arise from either an increasing source strength or an increasing atmospheric lifetime (decreasing sink) or both. Documentation of increases in the global cattle population and rice paddy cultivation area exist over the last several decades. The area of natural wetlands may be decreasing with land use development. Several recent studies (Khalil and Rasmussen, 1985b; Levine et al., 1985; Thompson and Kavanaugh, 1986) ascribe a fraction (0.2-0.8%) of the CH_4 increase to a decrease in global OH abundance. Because of the many uncertainties in source characterization, little confidence should be placed at present in predictions of future CH_4 abundance, although it appears likely that levels above 2.0 ppm will be reached sometime in the next century.

N_2O

Nitrous oxide is a long-lived (lifetime approximately 150 years), well-mixed trace constituent with a current global average abundance of about 310 ppb (WMO, 1985). Continuous records at several sites since 1978 show a 1 ppb deficit in the southern hemisphere relative to the northern and a global trend of increase of about 0.2%/year (Weiss, 1981; Khalil and Rasmussen, 1983b). Trends measured at northern hemisphere stations are larger than for the southern stations, suggesting an increasing interhemispheric disparity. Measurements extending back to 1961 are consistent with the 0.2%/year trend (WMO, 1981). Preliminary results on bubbles of glacial air suggest an N_2O abundance of 270-280 ppb in 1600 (Pearman et al., 1985).

The sink for atmospheric N_2O appears to be limited to photolysis in the stratosphere and reaction with electronically excited atomic oxygen. From the observed distribution and models of stratospheric photochemical processes (WMO, 1985), the magnitude of the sink can be calculated to be 1 x 10^{13} gN/year. The global atmospheric burden is 1.5 x 10^{15} gN, implying a lifetime of 150 years. The observed global trend in abundance corresponds to an annual increase of 2-3 x 10^{12} gN, or as much as 25% of the implied source strength of about 1.4 x 10^{13} gN/year. Probably about half of this source is contributed by natural emissions from tropical and subtropical forests, attributed to microbial nitrification processes in the soil. Perhaps a third of the source can be assigned to conversion of fuel nitrogen in combustion processes, dominated by coal combustion but with a contribution from biomass burning. The remaining sources are spread among ocean emissions, indicated by observed N_2O supersaturation of surface waters, and soil emissions from temperate and boreal forests, cultivated soils and fertilized soils. The magnitude of the combustion source is similar to the magnitude of the implied source imbalance, leading several authors to suggest that the current increase can be attributed essentially entirely to the anthropogenic combustion source (e.g., Weiss, 1981).

The sink term is essentially fixed in the absence of large changes in stratospheric ozone abundance, so that a continued positive trend is likely. An equilibrium abundance around 400 ppb is implied by the current source strength. However, continued increase in the fossil fuel combustion source term is also likely as use of coal increases. Changes in tropical land uses may also have short- and long-term effects that may contribute to or mitigate source strength increases. These considerations support projecting the observed trend of 0.2%/year into the future.

Cl- and Br-Containing Industrial Compounds

Sporadic surface and balloon measurements of the atmospheric abundance of CFC-11 and CFC-12 showed, starting in the late 1960s, that these industrially produced compounds were accumulating in the atmosphere and were essentially well-mixed in the troposphere. A program of precise, continuous, absolute measurements at five sites sampling marine air at mid and low latitudes in both hemispheres commenced in 1978 (Cunnold et al., 1983a,b; WMO, 1985). The average annual growth rates observed are around 5% for both CFC-11 and CFC-12, with current levels of about 220 ppt for CFC-11 and 350 ppt for CFC-12. Most emission sources are in the northern hemisphere, producing an interhemispheric gradient of about 10%, with higher abundances in the northern hemisphere. The current southern hemispheric trend is larger than that in the northern hemisphere, however, tending to reduce the gradient.

From the observed increase in atmospheric burden and the history of emissions, atmospheric lifetimes of around 75 years for CFC-11 and 111 years for CFC-12 can be derived (WMO, 1985). These are consistent within error limits of model-derived values, considering loss only by stratospheric photolysis. There is no evidence that processes other than stratospheric photolysis are significant atmospheric sinks for CFC-11 and CFC-12.

Although lifetimes for CFCs with respect to stratospheric photolysis will be somewhat sensitive to perturbations of the stratospheric ozone column, future CFC atmospheric abundances can be calculated with some confidence assuming knowledge of future global emission rates. The current burden of CFC-11 is about 5.5×10^{12} g, with current annual emissions of about 2.6×10^{11} g. For CFC-12, the current burden is about 7.7×10^{12} g, global annual emissions about 4.1×10^{11} g. If the current levels of emission were to continue indefinitely, CFC-11 and CFC-12 would eventually reach abundances of around 800 ppt and 2.6 ppb, respectively, assuming no change in lifetimes.

Future emission rate projections for these compounds are, however, highly uncertain. Even neglecting the possibility of future global emissions regulations connected to the interaction of CFCs with stratospheric ozone, economic projections of future production and emission depend on estimates of uncertain growth in quantities including population, gross national product per capita, and development of new technology, among others (Hammitt et al., 1987). Especially uncertain are projections in new markets and developing (Third World) economies. With the announcement of the 1987 Montreal Protocol designed to limit future emissions of CFC-11 and CFC-12 in particular, continuing compounded growth of emissions seems unlikely. But achieving emission rates in equilibrium with current abundances would require substantial emission reductions, to 25% of the current emission rate for CFC-11 and only about 1/8th of the current rate for CFC-12. Consequently, without substantial cuts in emissions, some continued increase in atmospheric abundance is inevitable. The atmospheric concentrations of several brominated halocarbons, namely CF_2ClBr and CF_3Br, which are used in fire extinguishing, are increasing rapidly (10-30%/year). Although their concentrations are small (~1 pptv), they could have potentially significant effects on atmospheric chemistry and climate in the next century (WMO, 1985; Wuebbles and Edmonds, 1988).

Other Trace Constituents of Importance With Possible Trends

There are many other surface-emitted trace atmospheric constituents with direct or indirect potential climatic impacts for which good global records and firm trend indications are lacking at present. For many of these constituents, the difficulties in determining global average abundances and secular trends are related to short atmospheric lifetimes and the implied spatial and temporal heterogeneity of their distributions. We will briefly discuss nitrogen oxides ($NO_x = NO + NO_2$), carbon monoxide (CO), higher hydrocarbons and global background tropospheric aerosol. NO_x, CO, and NMHC (non-methane hydrocarbons) affect climate processes indirectly through their participation in tropospheric photochemistry affecting both OH and O_3 (see Chapter 4). Tropospheric O_3 has important direct effects on radiation, and OH is predominantly responsible for controlling the lifetimes of oxidizable species, including CH_4 and hydrogen-containing halocarbons (e.g., CH_3CCl_3). Tropospheric aerosol can scatter solar radiation and absorb both solar and longwave energy. The net surface-troposphere effect of increased aerosol can be either warming or cooling, depending on the albedo of the underlying surface and other factors.

Nitrogen Oxides

The nitrogen oxides, NO and NO_2 as natural constituents play several roles in tropospheric and stratospheric chemistry. They are involved in tropospheric photochemistry producing both ozone and hydroxyl radicals, which in turn act as major atmospheric oxidants. NO and NO_2 are observed to be globally distributed trace tropospheric constituents, with abundances ranging from 10 ppt in remote clean marine air to the ppb level at clean continental sites. There is no direct observational evidence for a secular trend in the global average tropospheric abundance, but there are many reasons to infer an increased level relative to levels earlier in this century.

The tropospheric odd-nitrogen sources total perhaps 5×10^{13} gN/year with a large uncertainty (Logan, 1983). Fossil fuel combustion accounts for about 40% or 2×10^{13} gN/year, and biomass burning, lightning, and soil emissions for perhaps 20% each. There is a small contribution from the stratosphere, where odd-nitrogen is produced in the oxidation of N_2O. The loss processes include dry deposition and photochemical oxidation to HNO_3 followed by rainout. Both are highly variable in time and space. The extent of correlation of the source emission with the tropospheric sink is important in determining the $NO+NO_2$ lifetime, which can vary from a day to a week. Specifying a global average lifetime and thus a global burden or average abundance is therefore difficult.

The inference of a positive global abundance trend follows from the importance of fossil fuel combustion as a source of nitrogen oxides and the evidence that the increase in fuel nitrogen emissions is responsible for the observed N_2O increase. Further, there is evidence for nitric acid increases in precipitation from ice cores from 1895 to 1978 (Neftel et al., 1985). Likewise, estimates of global NO_x emissions from fossil fuel usage indicate growth from 1966 to 1980 (Hameed and Dignon, 1988). However, even a rough estimate of the future trend cannot be made based on current knowledge. There is accumulating evidence, which will be discussed below, for the importance of PAN and other organic nitrates as longer-lived reservoirs for the nitrogen oxides with the ability to transport odd nitrogen on global scales in the mid-troposphere.

Carbon Monoxide

The reaction of carbon monoxide (CO) with the hydroxyl radical (OH) serves as the dominant sink process for CO as well as a major conversion pathway of OH to other forms of HO_x. Abundance records for CO are currently being generated at several points around the globe (WMO, 1985). The current northern hemispheric average surface abundance is around 150 ppb, about twice the average southern hemispheric abundance. A seasonal cycle with a winter maximum is evident at or below the 25% level, with higher amplitude at higher latitudes. Substantial variability, related to the spatial inhomogeneity of sources and the 1- to 4-month atmospheric lifetime, is also observed. This variability and the generally short duration of continuous records makes the detection of a secular trend difficult. Early reported results range from no trend different from zero, discernible at high southern latitudes, to 5% per year observed at Cape Meares, Oregon, between 1979 and 1982 (WMO, 1985). Analysis of spectroscopic plates from 1951 and 1981 shows an average annual increase of about 2% over Europe between these times (Rinsland and Levine, 1985). Recent measurements at six sites indicate a global trend of about 1%/year (Khalil and Rasmussen, 1988).

The global atmospheric burden of CO is about 2×10^{14} gC. The global sink can be estimated at about 1×10^{15} gC/year, fixing the global source at about the same value. About 85% of the sink term is the reaction of CO with OH forming CO_2 and HO_2, with the remainder attributable to soil uptake. From studies of combustion processes and analysis of the global extent of fossil fuel combustion and biomass burning, direct anthropogenic emissions of CO comprise about half of the total source term (Logan et al., 1981; Kavanaugh, 1987; WMO, 1985). The remaining sources are natural burning and the atmospheric oxidation of CH_4, natural tropical and temperate higher hydrocarbons, and anthropogenic hydrocarbons.

The importance of anthropogenic combustion as a source of CO and the larger abundance observed in the northern hemisphere, where the sources are concentrated, suggest strongly that CO levels are higher now than earlier in this century and before. The trends derived from the recent data records indicate that the

CO abundance is continuing to increase. Predicting the future behavior of both the source and sink terms is, however, difficult at present. In considering the sink term, the tropospheric OH abundance is affected by many other species, including H_2O, CO, O_3, NO_x, and CH_4, in a complicated photochemical interdependence. The prediction of a future OH trend is problematical. Because the short lifetime of CO keeps sources and sinks in approximate balance, a continued increase in CO abundance will depend not just on continued emission by combustion but on a continuing increase in the rate of combustion emissions of the sort that produce CO.

Natural and Anthropogenic Higher Hydrocarbons

A very large number of Cn (n=2-8+) hydrocarbons can be found throughout the global troposphere in abundances ranging from 10's of ppt to the ppb level and higher (NRC, 1984). Values near source regions, such as forests and urban areas, are at the high end of this range and can be significantly higher locally. Lifetimes range from hours to several days with respect to oxidation by OH. The paucity of observations and the large variability in abundances do not support global average characterizations at present. The importance of the anthropogenic component of the source term varies with individual hydrocarbons but can be significant for the lighter species. Because they are sources of CO and are consumed reactants in the $NO_x/HO_x/O_3$ photochemical system, future changes in higher hydrocarbon abundances must be considered in predicting the climate interaction with atmospheric composition and chemistry.

Global Background Stratospheric Aerosol

The chief aerosol found in the stratosphere is composed of condensed sulfuric acid vapor (H_2SO_4) and water vapor. The globally distributed unperturbed background aerosol found in the lower stratosphere, termed the Junge layer, has a visible optical depth less than 0.01 (WMO, 1985). Its source is thought to be oxidation of surface-emitted carbonyl sulfide, OCS (NRC, 1984; WMO, 1985). OCS is present at about 500 ppt in the troposphere, has a long tropospheric lifetime, and is mixed efficiently into the stratosphere. OCS oxidation can be initiated by photolysis and by OH, producing SO_x species and eventually sulfuric acid. The extremely low vapor pressure of sulfuric acid, about 60 ppt at 215 K, allows condensation into aerosol at very low abundance levels. Other surface-emitted sulfur-containing species, for example SO_2, DMS, and CS_2, do not persist long enough in the troposphere to be transported to the stratosphere.

A state of unperturbed background stratospheric aerosol may be relatively rare, however, as frequent volcanic eruptions inject significant quantities of SO_2 directly into the lower and mid stratosphere. Recent major eruptions include Agung in 1963 and El Chichon in 1982. The subsequent sulfuric acid aerosol clouds can over a period of months be distributed globally at optical densities that overwhelm the natural background aerosol. The stratosphere's relaxation to background optical density has a characteristic time on the order of years, so that the average state of stratospheric aerosol could be considered as partially perturbed by volcanic emissions.

The Antarctic stratospheric aerosol implicated in the spring ozone hole phenomenon is probably different in composition from the global sulfuric acid aerosol. In addition to water, it probably contains a significant proportion of nitric acid (HNO_3) and may incorporate hydrochloric acid (HCl) as well. The chief Antarctic aerosol precursors are stratospheric water vapor and gas phase NO_x and Cl-containing species. Its formation is related to the very low stratospheric temperatures reached in the Antarctic winter.

Given the importance of episodic volcanic injections to the global stratospheric aerosol burden, it is unlikely that human activities could introduce an observable trend into the stratospheric aerosol abundance. In the case of Antarctic aerosol, Blake and Rowland (1988) have made the suggestion that the secular trend in methane may have increased formation through the increase in stratospheric water vapor formed by methane oxidation in the stratosphere.

Global Background Tropospheric Aerosol

Background tropospheric aerosol is variable in its composition as well as its spatial and temporal distribution (Wang et al., 1986). The major types of aerosol composition are soot, sulfate, maritime, crustal, and

While quantitative predictions of trends are not currently available, development of techniques for such prediction is being pursued. Aerosol physicochemical processes, important at the regional level, include coagulation, growth/shrinkage by condensation/evaporation, nucleation of fresh aerosol at some threshold size, thermodynamic equilibrium between aerosol and the gas phase, cloud processing of aerosol, and wet and dry removal processes. Model representations of the microphysics of aerosol formation and growth and the aerosol size distribution have been discussed by Suck and Brock (1979) and Seigneur et al. (1986).

THE CLIMATE SYSTEM

Global Annual Average Radiative Forcing

The most fundamental planetary climate variable could be considered to be the planetary annual average surface temperature. Considering an atmosphere transparent to radiation and in the absence of a significant internal planetary heat source, this temperature is controlled by the solar energy input and the surface albedo of the planet. The surface temperature adjusts so that the planetary emission of heat to space balances the solar energy input. Annually and globally averaged, about 340 W m^{-2} of solar energy strikes the earth and 30% is reflected back to space, leaving about 240 W m^{-2} to be absorbed. Of the 100 W m^{-2} reflected back to space, clouds account for about two-thirds of the loss and the surface for about an eighth, with atmospheric Rayleigh scattering reflecting the rest. Were the atmosphere transparent to infrared radiation, the surface temperature would simply adjust to balance the absorbed insolation and would be about 255°K.

Although the total absorbed and emitted energy of the surface-atmosphere system balance at 240 W m^{-2}, the fluxes of processes transferring energy within the system, between the surface and atmosphere and within the atmosphere itself, can exceed the net 240 W m^{-2} net solar input. Actually, about 70 of the 240 W m^{-2} in absorbed insolation are absorbed by trace constituents, aerosol, and clouds in the atmosphere (Ramanathan et al., 1987). In addition, since the earth's observed average surface temperature is 288°K, about 390 W m^{-2} is radiated upward from the surface, so that trace atmospheric constituents must be responsible for trapping the excess surface-emitted infrared radiation. The earth-atmosphere system must be in balance with the solar energy input, so that the effective radiating temperature of the earth and its atmosphere must be lower than the surface temperature. This is accomplished by the climate system in two steps; first, the atmosphere is not transparent to outgoing infrared radiation by virtue of H_2O, CO_2, clouds, and other trace constituents and second, the temperature of the atmosphere decreases with altitude in the troposphere.

The surface, then, absorbs about 170 W m^{-2} of solar insolation and about 320 W m^{-2} of infrared energy emitted by the atmosphere. To balance the 490 W m^{-2} total input, the earth's surface releases about 100 W m^{-2} in the form of sensible and latent heat in addition to the 390 W m^{-2} emission of infrared radiation. About 20 W m^{-2} of the surface radiation is emitted directly to space, primarily in the 7-13 μ wavelength "window" between the H_2O vapor and CO_2 absorption bands. The atmosphere's energy input totals 540 W m^{-2}, 70 in direct solar, 370 in surface infrared emissions, and 100 in sensible and latent heat. Of the 540 W m^{-2} in atmospheric infrared emission, 320 is emitted downward to the earth's surface and 220 is emitted to space, with about 90 emitted by clouds and the remaining 130 W m^{-2} by trace constituents. Water vapor, clouds, and CO_2 are responsible for about 90% of the atmospheric radiation trapping. Methane, N_2O, and O_3 contribute the remaining 10%. A schematic diagram of the global average components of the earth's energy balance is shown is Figure 2.2.

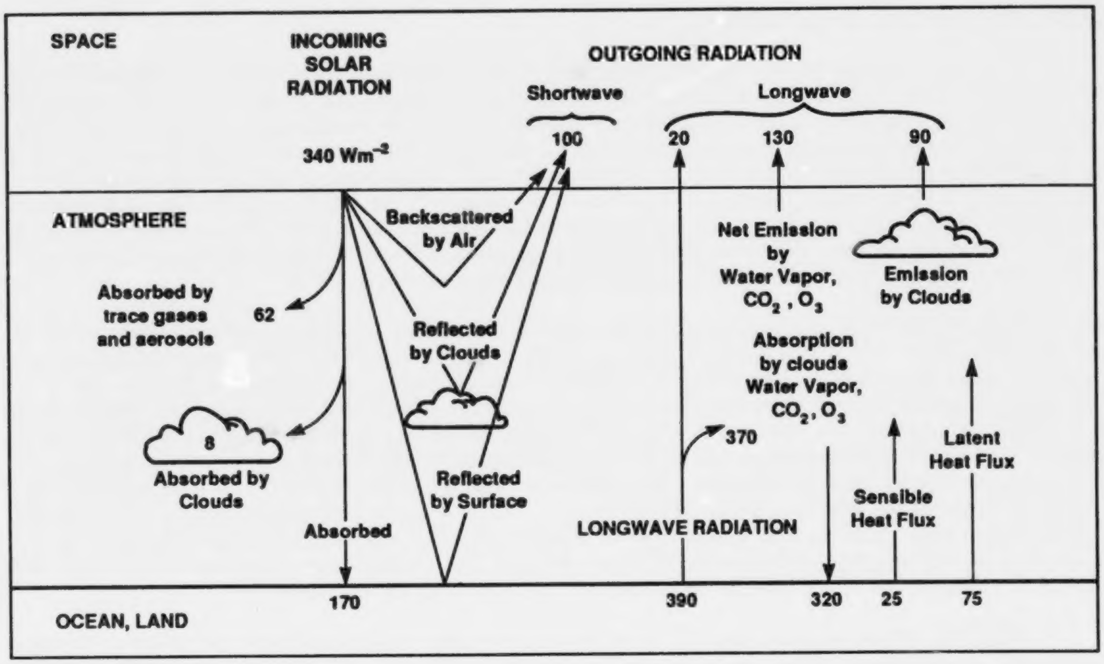
SPACE
INCOMING SOLAR RADIATION
340 Wm^{-2}
OUTGOING RADIATION
Shortwave
100
Longwave
20
130
90
ATMOSPHERE
Backscattered by Air
Absorbed by trace gases and aerosols
62
Reflected by Clouds
8
Absorbed by Clouds
Absorbed
Reflected by Surface
Net Emission by Water Vapor, CO$_2$, O$_3$
Emission by Clouds
Absorption by clouds Water Vapor, CO$_2$, O$_3$
370
Latent Heat Flux
Sensible Heat Flux
LONGWAVE RADIATION
OCEAN, LAND
170
390
320
25
75

Figure 2.2. Schematic diagram of the global average components of the earth's energy balance.

In the troposphere, dynamics driven by the direct solar surface warming and the hydrologic cycle actively mix the air on time scales shorter than the time scales of energy transport by radiative processes. Consequently, the surface and the troposphere can be considered as a tightly coupled system from the radiative standpoint. In the consideration of climate change, the details of the vertical profiles of absorption and emission of energy within the troposphere are much less important than the net radiative flux changes measured at the tropopause (Ramanathan et al., 1987; Potter and Cess, 1984). Because the stratosphere is, on the other hand, stable with respect to vertical mixing and can be considered to be in radiative equilibrium, the nature of the vertical profiles of absorbing and emitting species like O_3 are of greater importance to the stratospheric climate.

Additional Climate Variables

The actual response of the climate system to the observed trends in atmospheric constituents discussed above involves more than the direct changes in radiative forcing, with respect to predicting both annual average temperature changes and the specific climate variables that most directly affect regional air quality and chemistry. Strong feedbacks within the surface/atmosphere/ocean/cryosphere system modify the net global radiative response to changes in atmospheric constituent abundances. Couplings also exist between atmospheric dynamics and hydrology and the budgets and photochemistry of the trace constituents, so that potential changes in dynamics and clouds and precipitation will produce another level of feedback to the climate.

Many potentially important climate feedback processes have been identified. Figures 2.3 and 2.4 give a schematic portrayal of important feedback processes. Because water vapor and clouds are the principal constituents responsible for reflecting, absorbing and emitting radiation in the atmosphere, while snow and ice cover on the surface contribute significantly to surface albedo at higher latitudes, most feedbacks involve processes affecting the hydrologic cycle. These include the dependence of absolute humidity on temperature, the extent of cloud cover and cloud properties (optical depth and radiating temperature), the dependence of the tropospheric temperature profile on humidity, and the temperature dependence of the extent of surface coverage by snow and ice. The abundance of water vapor in the stratosphere appears to be controlled by the temperature of the tropical tropopause, through which air entering the stratosphere passes, and the photochemical oxidation of CH_4. Increases in the temperature of the low-latitude tropopause may result from an altered surface-atmosphere radiative balance and may increase stratospheric water vapor, with subsequent feedback on surface temperatures and stratospheric photochemistry. Some of these feedback processes remain poorly quantified. In the case of the various cloud feedbacks, even some of the signs are in doubt.

The close coupling of the surface and the troposphere, however, appears to enforce at least a degree of simplification on the consideration of climate change impacts on tropospheric regions. In a global sense, the climate change remains a result of the change in net fluxes at the tropopause. The exact nature of the original source of radiative perturbation (for example, the particular trace gas emission scenario) and the combination of resulting climate feedbacks are of lesser importance in determining climate change than the global net radiative result. The extent to which regional climate change is independent of the original forcing is unclear. This general conclusion probably fails, for example, at high latitudes where the importance of snow and ice albedo impacts may be much greater with respect to other types of forcing than they are globally.

Refined understanding of potential changes in the climate variables that directly affect local and regional air quality and chemistry, that is regional temperature extremes and distributions, precipitation patterns and distributions, wind patterns and near surface temperature profiles, requires an understanding of how net tropopause radiative forcing changes affect the details of the surface-troposphere system. Two lines of investigation are being followed in the climate research community. First, three-dimensional general circulation model depictions of the physics of the atmosphere, land surface, and upper oceans, including more or less detailed treatment of atmospheric radiative transport, can produce climate variable statistics on the spatial scale of a hundred kilometers. The capabilities and limitations of such models will be discussed below. Second, the record of CO_2 abundance over geologic history shows a variation that correlates with the temperature record.

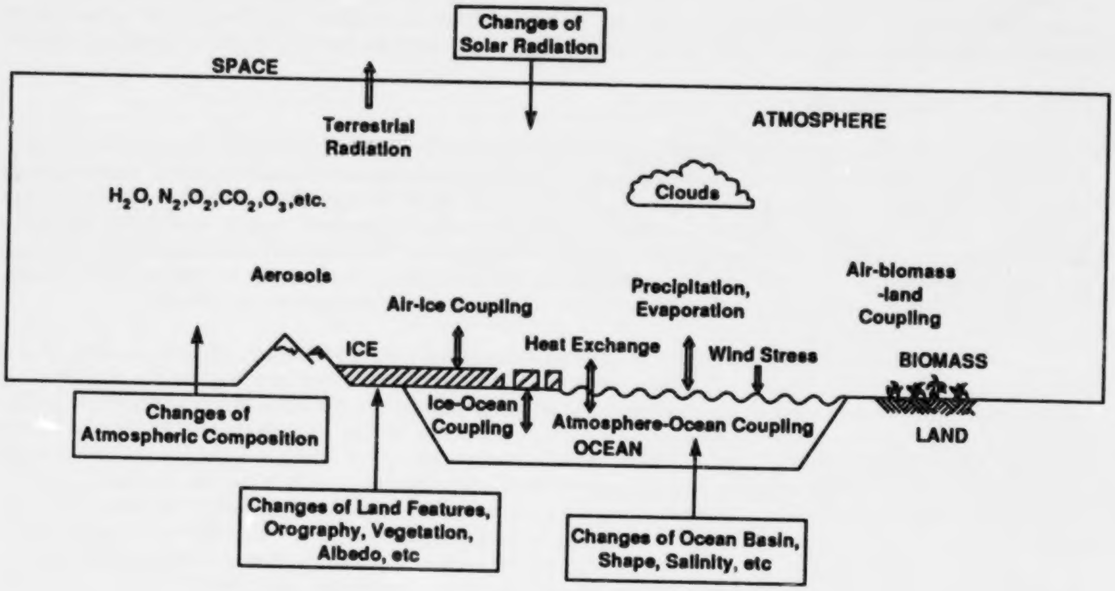
Changes of Solar Radiation
SPACE
Terrestrial Radiation
ATMOSPHERE
$H_2O, N_2, O_2, CO_2, O_3$, etc.
Clouds
Aerosols
Air-ice Coupling
Precipitation, Evaporation
Air-biomass -land Coupling
ICE
Heat Exchange
Wind Stress
BIOMASS
Ice-Ocean Coupling
Atmosphere-Ocean Coupling
OCEAN
LAND
Changes of Atmospheric Composition
Changes of Land Features, Orography, Vegetation, Albedo, etc
Changes of Ocean Basin, Shape, Salinity, etc

Figure 2.3. The prinicipal interactions among the components of the atmosphere-ocean-ice-land surface climate system and some examples of external changes that may cause climatic variations. Source: Gates (1979).

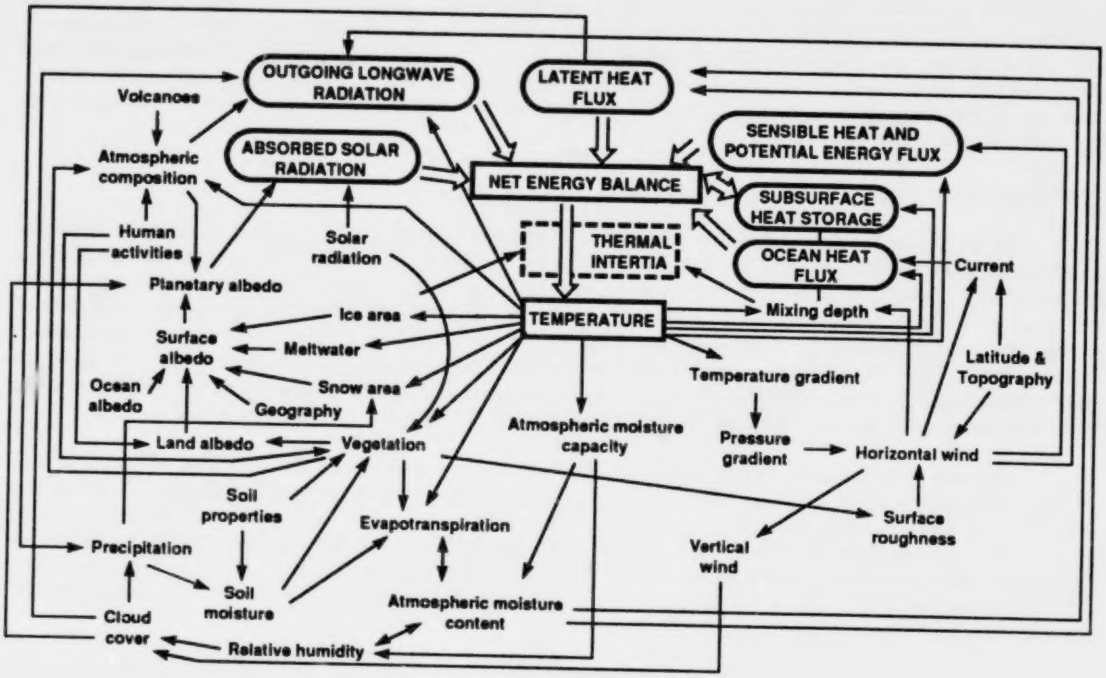
OUTGOING LONGWAVE RADIATION
LATENT HEAT FLUX
Volcanoes
Atmospheric composition
ABSORBED SOLAR RADIATION
SENSIBLE HEAT AND POTENTIAL ENERGY FLUX
NET ENERGY BALANCE
SUBSURFACE HEAT STORAGE
Human activities
Solar radiation
THERMAL INTERTIA
OCEAN HEAT FLUX
Current
Planetary albedo
Ice area
TEMPERATURE
Mixing depth
Surface albedo
Meltwater
Latitude & Topography
Ocean albedo
Snow area
Temperature gradient
Geography
Atmospheric moisture capacity
Pressure gradient
Land albedo
Vegetation
Horizontal wind
Soil properties
Evapotranspiration
Surface roughness
Precipitation
Vertical wind
Soil moisture
Atmospheric moisture content
Cloud cover
Relative humidity

Figure 2.4. Schematic illustration of climatic cause and effect (feedback) linkages and variables that are often included in numerical models of the climate system. Source: Robock (1985).

From the relative timing of fluctuations in the CO_2 and temperature records, there is some indication that the CO_2 changes may be causal, in addition to orbital variability and other factors. If other climate variables can be deduced from proxy records with precision, the past climate information may be useful for predicting future response to trace constituent trends.

ATMOSPHERIC COMPOSITION CHANGE AND GLOBAL CLIMATE

The evidence for observed nonzero trends in many trace atmospheric constituents and the prospects for continued changes have been briefly summarized above. The direct global annual average radiative effects of constituent abundance changes can be calculated and compared in the absence of climate, biological, and photochemical feedback processes. The climate feedback terms, chiefly involving water vapor and clouds, are determined by the total radiative forcing change and do not depend on the nature of the assumed trace constituent change scenario. This is not true, however, of the photochemistry and source and sink feedbacks, which are unique to each constituent. Quantitative estimates in the following section were taken largely from Ramanathan et al. (1987) and Wang et al. (1986).

Direct Radiative Impacts

The direct, feedback-free radiative effect of an abundance change in a trace atmospheric constituent can be estimated using radiative-convective models in which humidity and cloudiness, for example, are fixed while the constituent abundance is altered. For the prototypical case of the doubling of CO_2, the change in net radiative flux at the tropopause is about 4 W m^{-2}. About two-thirds of the effect is tropospheric reduction of outgoing infrared radiation, the remaining third an increase in downward emission from the stratosphere. Because the atmosphere is already optically thick in the wavelength regions of CO_2 absorption, the radiative effect of changing CO_2 is a logarithmic function of the abundance. The extensive overlap of the CO_2 absorption bands with those of H_2O must be carefully considered in radiative transfer calculations for CO_2.

The current abundances of CH_4 and N_2O together contribute a total radiative forcing of around 3.5 W m^{-2}, but as absorbers at wavelengths with larger atmospheric transmittance, forcing changes per molecule are around 30 and 130 times that for CO_2, respectively. Because they are present at much lower abundances than CO_2, the absolute impact of their increase is reduced with respect to CO_2. However, assuming the continuation of current growth rates, the radiative impact of doubled CH_4 (after 70 years) would be about 25% of the impact of the 50% increase in CO_2 that would be expected in 70 years. N_2O and CH_4 are considerably less important than CO_2 in affecting stratospheric temperatures.

Many of the industrially emitted CFC compounds have their principal infrared absorption bands around 10 μ. These compounds are generally much more efficient infrared absorbers than CO_2 on a per molecule basis because of larger band strengths, high atmospheric optical transmittance at their absorption wavelengths, and the peaking of the surface emission in the 10-μ wavelength region. Much smaller abundance increases, of the order of 1 ppb, can produce a radiative forcing change as large as 20% of the forcing change of a CO_2 doubling.

Ozone absorbs both incoming solar radiation in the ultraviolet and visible regions and terrestrially emitted infrared radiation in a band centered at 9.6 μ. Acting as a net source of heat in the stratosphere, ozone absorbs about 12 W m^{-2} of solar radiation and 8 W m^{-2} of terrestrial infrared radiation. Stratospheric ozone reradiates about 4 W m^{-2}, 60% of that to space. Because the direct absorption of incoming solar radiation in the stratosphere by ozone is the major stratospheric heating term, stratospheric ozone has both heating and cooling influences on the surface-troposphere system. The net direct radiative effect of stratospheric ozone change depends on the balance of increased (decreased) tropospheric solar flux with decreased (increased) downward infrared emission from the cooler (warmer) stratosphere. For ozone in the troposphere, however, both direct solar absorption and infrared trapping warm the surface-troposphere system. Although the current tropospheric ozone column is only about 10% of the stratospheric column, representative computations show that a 25% decrease in tropospheric ozone results in a net flux change of -0.5 W m^{-2} at the tropopause, while a 25% decrease in stratospheric ozone (a larger decrease than is currently projected) produces a net flux change tropopause, coincidentally a region where a complex combination of photochemical and transport phenomena control the ozone abundance.

The net effects of aerosols on radiative fluxes are very sensitive to aerosol optical properties so that, in many instances, conclusions about the sign of the effect are difficult. In the case of Arctic aerosol, which appears to be related to long-range transport of continental pollution and conceivably could have a secular trend, the effect is likely to be tropospheric warming.

Climate Feedback Response to Direct Radiative Forcing Changes

On the principle that the surface-troposphere system responds to the total net radiative forcing of the several trace constituents that contribute, the climate feedback response should be relatively independent of the particular emission scenario assumed. The flux changes resulting from individual constituent changes also appear to be approximately additive. This results from the high optical transmissivity of the atmosphere near 10 μ where most important trace constituent absorption features occur and from the lack of significant overlap of the various absorption features.

The radiative forcing for a doubling of CO_2 is around 4 W m^{-2}, and the estimated surface temperature increase in the absence of any climate feedback processes is calculated to be in the range 1.2 to 1.3°K at equilibrium. From the results of radiative-convective and general circulation models that incorporate climate feedback responses, the surface temperature change associated with doubled CO_2 is in the range 1.5 to 4.5°K, with most GCM results falling in the upper end of this range. The climate feedback factor then, defined as the ratio of the computed surface temperature change to the zero feedback change, falls in the range 1.2 to 3.75. The expected range of the global surface temperature change from the direct radiative effects of any combination of trace constituent abundance changes can then be scaled, given the results above, by comparison of the radiative model results for the net flux change for the doubled CO_2 scenario with a trace gas scenario.

Photochemical Forcings of Global Climate Change

In addition to changes in direct radiative forcing by trends in trace species, changes in the atmospheric radiation balance can be forced through photochemical modification of atmospheric composition. Many of the radiatively important atmospheric trace constituents are also photochemically important participants in processes that control ozone abundances and the lifetimes and budgets of trace species. We noted above that small changes in net radiative forcings are additive with respect to their impact on the surface-troposphere system. On the other hand, photochemical processes affecting atmospheric composition are in general coupled and nonlinear, and their effects on atmospheric composition are not additive. The estimation of the net radiative impact of changes mediated by photochemistry is usually specific to the details of a scenario of coupled trace gas abundance and emission trends.

We will discuss the climate-photochemistry process interactions in two identified significant cases, tropospheric OH and tropospheric and stratospheric ozone, in some detail in Chapter 4. Here, we briefly present a summary of results from several recent studies estimating the indirect climate impacts of radiative-photochemical interactions using various types of radiative models. Although the effects of the photochemical feedback processes can be described in isolation, the various feedbacks are, in general, also closely coupled with each other, so that the net effect depends on the simultaneous operation of all the processes. The abundances and distributions of three families of photochemically active species, O_x, HO_x, and NO_x, are prominent in many of the chemical feedbacks on climate.

The global average tropospheric abundance of the short-lived, photochemically generated hydroxyl radical, OH, is the crucial quantity in determining the lifetimes of many reduced atmospheric trace constituents and the oxidizing or scavenging ability of the atmosphere. The tropospheric OH abundance can be affected through perturbing HO_x production processes,

$$O_3 + h\nu\ (< 310\ \text{nm}) = O(^1D) + O_2$$

$$O_3 + h\nu\ (< 310\ \text{nm}) = O(^1D) + O_2$$

$$O(^1D) + H_2O = 2\ OH$$

$$OH + HC = \ldots = nHO_x + \text{other products} \qquad (2.1)$$

perturbing loss processes,

$$OH + NO_2 + M = HNO_3 + M$$

$$HO_2 + HO_2 = H_2O_2 + O_2$$

$$OH + HO_2 = H_2O + O_2$$

$$OH + CH_4 = H_2O + CH_3 \qquad (2.2)$$

and perturbing the OH/HO_2 ratio,

$$OH + CO\ (+O_2) = HO_2 + CO_2$$

$$HO_2 + NO = OH + NO_2 \qquad (2.3)$$

The tropospheric relative humidity in climate models is relatively insensitive to surface/troposphere temperature change, so that surface/tropospheric warming produces an increase in absolute water vapor abundance. All else being equal, an increase in tropospheric OH follows. Depending on assumptions concerning the distribution of NO_x, reductions in CH_4 and O_3 (through HO_x catalyzed loss) can result (Thompson and Cicerone, 1986a,b). In one study (Hameed and Cess, 1983) this negative feedback on radiative warming of the troposphere resulted in a 10% reduction on the surface temperature increase.

On the other hand, positive trends in the CH_4 and CO abundances can bring about reduction in OH, with a subsequent positive feedback on the lifetime and abundance of CH_4 (and other hydrocarbons, including partially halogenated species). In the presence of a sufficient NO_x concentration, tropospheric ozone can also be increased by the mechanism

$$OH + CH_4\ (+O_2) = H_2O + CH_3O_2$$

$$CH_3O_2 + NO = CH_3O + NO_2$$

$$NO_2 + h\nu = NO + O$$

$$O + O_2 + M = O_3 + M \qquad (2.4)$$

Model studies indicate that the radiative impacts of increased ozone produced by this mechanism can be of similar magnitude to the direct CH_4 radiative forcing change (Wang et al., 1986).

The importance of the distribution and abundance of global tropospheric NO_x is highlighted in the two preceding paragraphs. As discussed above, there is no concrete evidence for a secular trend, but a strong inference can be made that increasing anthropogenic combustion (including aircraft operating in the upper troposphere) results in increasing abundances. As NO_x is the catalyst for tropospheric ozone production, increased tropospheric ozone can also be inferred. Ramanathan et al. (1987) estimate that the resulting surface-troposphere radiative heating by this process during the 70s could be a third of the CO_2-induced warming over the same period.

A second category of climate-chemistry interactions involves stratospheric ozone and stratospheric climate. Stratospheric ozone is the primary absorber of solar radiation between 200 and 350 nm and the primary determinant of the surface flux of UVB radiation. Current indications are that positive trends in N_2O or CFCs, separately, will reduce stratospheric ozone, with the Cl-containing compounds of greater concern at present. Together, the effect of increased N_2O is to mitigate the CFC-related ozone decrease. Positive trends in CO_2, CH_4, and stratospheric water vapor act to increase stratospheric O_3 by reducing the efficiency of the NO_x and ClO_x catalyzed odd oxygen loss processes. The greatest radiative impact on the surface-troposphere system arises from changes in lower stratospheric ozone. Predicting the sign of these changes requires a full treatment of the complex ozone-controlling stratospheric photochemistry, including seasonal and latitudinal dependence. Ramanathan et al. (1987) suggest that the importance of these considerations for surface warming can be on the order of 25% of the direct CFC radiative effect, for constant current CFC emissions at steady state.

Climate Responses to Composition Changes from the Historical Record

Assembling an estimate of the direct and indirect radiative effects of trends in atmospheric composition as discussed above depends on the completeness and veracity of a variety of radiative and radiative-photochemical models. However, evidence from the climate record of responses to compositional change would directly incorporate the effects of feedback processes, and there exists the possibility that conclusions on climate change could be made independent of models. Indeed, there is strong evidence that significant compositional variability with respect to CO_2 extends into the past, prior to any anthropogenic perturbation of the atmosphere (Genthon et al., 1987). The CO_2 variability also seems to be tied intimately to climate variability on at least two widely separated time scales and by two independent processes.

On time scales exceeding 500,000 years, the abundance of atmospheric carbon dioxide is maintained by the balance of losses through weathering of calcium-silicate rocks by rain containing dissolved CO_2 and emission as a byproduct of tectonic processes (Kasting et al., 1988). This system provides a negative feedback between temperature and CO_2 that is proposed to maintain habitable conditions on Earth over a range of solar energy input.

On the shorter time scale of the glacial-interglacial cycle (160,000 years), recently reported results of records with a sampling resolution of 2,000-4,000 years of the climate-related ^{18}O and D isotopic abundances (Jouzel et al., 1987) and occluded CO_2 from the Vostok Antarctic ice core (Barnola et al., 1987) show a strong correlation of the profiles extending back to the last interglacial (warm) period. There are many subtleties and complexities in interpreting the ice core records, but in a simple linear multivariate analysis Genthon et al. (1987) concluded that more than half of the 11°C glacial-interglacial Antarctic surface temperature variability could be assigned to the CO_2 abundance variations. The effect on surface temperature of the direct global radiative forcing of the 200 to 300-ppm CO_2 change was calculated to be 0.6°C, compared to a direct orbital forcing effect of 0.2°C. It appears, subject to the difficulties mentioned below, that the long term or glacial condition climate feedback factor (5 to 14) may be larger than the climate feedbacks included in GCM models of the present atmosphere (1.2 to 3.75). Difficulties in interpretation include the uncertain global significance of the Antarctic surface temperature record and the extent to which the effects of the 200- to 300-ppm CO_2 glacial-interglacial variability can be related to the current situation with CO_2 at 345 ppm (and increasing) and with contributing increases in other constituents. It is clear from the ice core record that the global climate and atmospheric infrared radiative transfer are intimately connected.

On the still shorter time scale of decades to centuries before present, construction of the global temperature record and attribution of any trends to the effects of changes in trace constituent radiative forcing have received much attention (DOE, 1985a). Difficulties arise in evaluating the accuracy and representativeness of the temperature record and in accounting for the time lag in climate response to radiative forcing changes that results from the time constant of the atmosphere-ocean interaction. Accounting for the observed NH temperature increase of about 0.6°C since 1850 with current GCM models requires that about half of the calculated equilibrium climate response to the CO_2 increase has not yet been realized because of slow transport of heat in the ocean. The observed warming is thus not inconsistent with the observed CO_2 increase (Ramanathan et al., 1987), but firm conclusions are hampered by natural climate variability.

Global Climate Projections

There have been a number of recent studies of the future climate impacts of trends in atmospheric composition, including trends in CO_2 and other trace constituents discussed above. The climate impact can be quantified in terms of global equilibrium surface temperature change, with consideration of the time response of the climate system (particularly the ocean response) necessary to predicting the actual time evolution of the global temperature change over the next century. The general conclusion from the body of recent studies is that the trends in trace constituents other than CO_2 can be expected to approximately double the surface warming that is expected to occur as a result of the CO_2 increase in isolation (see, for example, Ramanathan et al., 1987).

Predicting the future climate response with the use of models of various sorts requires decisions in five broad areas. First, the basic scenario of future trace constituent source emissions must be developed. As discussed above, emission scenarios can involve questions in demographics, energy use and policy, economics, technology, agriculture and land use, atmospheric, photochemistry, bioscience on a range of scales, marine and geosciences, and many interdisciplinary areas. Scenarios have often been based on extension of currently observed atmospheric abundance trends, but it can be important to account for economic or physical couplings of emissions strengths that make particular combinations of source emissions or abundance trends more or less likely.

The second and third steps are the calculation of the direct and indirect radiative effects of abundance changes. These require the capability to treat radiative transfer in the atmosphere in both solar and longwave regions, as well as photochemical processes in both the troposphere and stratosphere. These two steps are coupled, especially in the stratosphere where radiatively driven temperature change can have profound impact on the photochemistry, so that these areas are best treated together.

The fourth problem is the magnitude of the climate sensitivity or response to radiative forcing. Under consideration here are the climate feedback processes that amplify the response of the surface-troposphere system to the net radiative forcing change imposed by the trace constituent changes in the assumed scenario. With the effects of these processes established, global equilibrium surface temperature perturbations can be quantified. Fifth and last, the time response of the surface-atmosphere-ocean system must be taken into account so that time-dependent surface temperature change can be predicted.

As a consequence of the many large uncertainties in at least the scenario and climate response aspects, climate change predictions are more appropriately made in terms of (broad) likely ranges rather than specific values. (Similarly, the impacts on the regional topics discussed in this report can be construed as sensitivities over a range of possible input and boundary condition values.) As an example of studies of climate-chemical interactions projecting climate change into the next century, Ramanathan et al. (1987) consider three scenarios generally characterized by liberal, conservative, and intermediate views of the extension of currently observed abundance trends. The range of global equilibrium temperature change for the 50-year period ending in 2030 is 0.8 to 4.1°K, incorporating uncertainties in both scenario and climate sensitivity. The range of realized temperature change over this period is about 0.5 to 1.2°K, including uncertainty in the rate of ocean thermal diffusivity. These area substantial fractions of the 11°K glacial-interglacial temperature contrast deduced from the Vostok Antarctic ice core.

CHAPTER 3

URBAN/REGIONAL CHEMISTRY AND CLIMATE CHANGE

The above discussion shows that a significant climate change can be expected to occur during the next century. The effect of CO_2 doubling alone can be expected to lead to global average temperature increases of between 1.5 and 4.5°C. Additional temperature increases are expected from the increased concentrations of CFCs, CH_4, and N_2O. Furthermore, more subtle changes that have not yet been fully established may also be occurring, such as an increase in tropospheric O_3. These changes would also add to the predicted temperature rise.

The temperature increases associated with the trends in trace species discussed above are globally averaged temperature changes. Not all regions, however, will experience the same temperature increase; furthermore, changes other than just a temperature increase can be expected. These changes could include, for example, changes in cloud types and amounts, changes in meteorological conditions in a given region, and changes in background free tropospheric concentrations of a variety of species. This variety of changes will affect the chemical processes that take place on urban and regional scales and lead to oxidant formation and acid deposition. It is important to try to understand the effects of these changes on regional chemistry, because we have already implemented emissions control policies that may not be appropriate for a climatically different future. New policies that are implemented should account for the possibility that climate change will alter the formation of oxidant and acid deposition. Below we discuss some of the possible changes that need better understanding.

URBAN AND REGIONAL OXIDANT FORMATION

Elevated urban and regional oxidant concentrations result from the interaction of sunlight, NO_x, and NMHCs. The tendency to form oxidant (primarily ozone) depends, therefore, on the concentrations of hydrocarbons and nitrogen oxides, on the availability of sunlight, and on the rate coefficients of certain key photochemical reactions (which depend on temperature). As will be shown, climate change can alter this tendency dramatically, although few quantitative estimates are available. Below, we first discuss the mechanisms of oxidant formation, and then describe the ways in which climate change might impact urban and regional oxidant formation.

Formation of Oxidant

In very clean areas, where NO_x concentrations are about 20-50 ppt, O_3 is generally destroyed by photochemical reaction sequences initiated by the reaction of CO with OH:

$$CO + OH = CO_2 + H$$

$$H + O_2 + M = HO_2 + M$$

$$HO_2 + O_3 = OH + 2\,O_2$$

$$\text{Net: } CO + O_3 = CO_2 + O_2 \qquad (3.1)$$

As NO_x is added to this system, the reaction of HO_2 with O_3 in (3.1) becomes slower than the corresponding reaction of HO_2 with NO, creating a reaction sequence which produces O_3:

$$CO + OH = CO_2 + H$$

$$H + O_2 + M = HO_2 + M$$

$$HO_2 + NO = OH + NO_2$$

$$NO_2 + h\nu = NO + O$$

$$O + O_2 + M = O_3 + M$$

$$\text{Net: } CO + 2\,O_2 = CO_2 + O_3 \qquad (3.2)$$

If NMHCs are then added to the system, the reaction sequence leading to O_3 production can be even faster. This is because as NMHCs react, they tend to increase the pool of hydroxyl radical species (OH, HO_2, as well as higher organic forms of peroxy and peroxyl radicals), leading to more conversions of NO to NO_2 in reaction sequences similar to (3.2). The sequence of reactions leading to O_3 production can be initiated by the reaction of OH with NMHCs as well as by reaction of OH with CO. Thus the sequence becomes:

$$NMHC + OH + O_2 = RO_2$$

$$RO_2 + NO + O_2 = HO_2 + NO_2 + RCHO$$

$$HO_2 + NO = OH + NO_2$$

$$2(NO_2 + h\nu = NO + O)$$

$$2(O + O_2 + M = O_3 + M)$$

$$\text{Net: } NMHC + 4\,O_2 = 2\,O_3 + RCHO \qquad (3.3)$$

where RCHO is a carbonyl compound and R- is a hydrocarbon radical. These processes can be moderated locally. In areas with high NO_x and lower NMHC/NO ratios, the reaction $NO_2 + OH + M \rightarrow HNO_3 + M$ can serve to decrease hydroxyl, which is necessary to initiate the O_3-producing sequence. Also, nitrogen oxides which are primarily emitted as NO remove O_3 directly via: $NO + O3 \rightarrow NO_2 + O_2$. This second reaction leads to a net reduction in O_3 until a steady-state ratio for NO/NO_2 is established. After this, the reaction of NO with O_3 is balanced by photolysis of NO_2 followed by O atom attachment to O_2 to reform O_3. However, the potential for higher oxidant concentrations where emissions of NMHC and NO_x are high is clearly possible and experienced in many urban areas. A greater degree of complexity in the photochemical mechanism also follows with the production from radical precursors of peroxyacetyl nitrates (PAN compounds) and other organic nitrates. Therefore, any climate change that substantially alters these concentrations can alter O_3 formation. Such possibilities are discussed below.

Effect of Climate Change on Oxidant Formation

Several scenarios of climate or global chemical change have the potential for altering oxidant levels. Table 3.1 summarizes the types of climate change parameters that are important for regional chemistry. Below, the specific effects of these changes on oxidant formation are discussed.

A change in temperature will alter oxidant formation rates directly by influencing the rates of chemical reaction. Figure 3.1 shows the peak ozone concentration reached in a box model calculation of ozone formation as a function of the assumed atmospheric temperature and of the initial HC to NO_x ratio (see Atherton and Penner, 1988, for a description of the box model and initial conditions). For urban conditions, with a HC/NO_x ratios near 7, a 5 degree temperature increase (from 298 to 303°K) might be expected to raise O_3 levels by 0.05 ppm or 20%. Most of the O_3 response to temperature is due to the strong temperature dependence of the

Table 3.1. Climate Change Parameters Important for Regional Chemistry

1. A change in the average maximum or minimum temperature and/or changes in their spatial distribution and duration leading to a change in reaction rate coefficients and the solubility of gases in cloud water solution.

2. A change in stratospheric O_3 leading to a change in photolysis rate coefficients.

3. A change in the frequency and daily pattern of cloud cover and types of cloud formed leading to a change in photolysis rate coefficients and heterogeneous rates of conversion of SO_2.

4. A change in the frequency and intensity of stagnation episodes or a change in the depth of the planetary boundary layer and its diurnal cycle leading to more or less mixing of polluted air with background air.

5. A change in background boundary layer and/or free tropospheric concentrations of water vapor, hydrocarbons, NO_x,and O_3 (due to changes in mixing processes or sources such as lightning for NO_x) leading to more or less dilution of polluted air in the boundary layer with background air and layering the chemical transformation rates in both the boundary layer and the free troposphere.

6. A change in the vegetative and/or soil emissions of hydrocarbons and NO_x which are sensitive to temperature and/or light levels leading to changes in their concentrations.

7. A change in deposition rates to vegetative surfaces whose stomatal resistance is a function of temperature, light intensity and other factors leading to changes in concentrations.

8. A change in energy usage or technology leading to a change in energy-related emissions and their concentrations.

9. A change in secondary aerosol formation leading to changes in photolysis rates, the planetary albedo, and heterogeneous reaction rates.

10. A change in circulation and/or precipitation patterns leading to a change in the abundance of pollutants deposited locally versus exported off the continent.

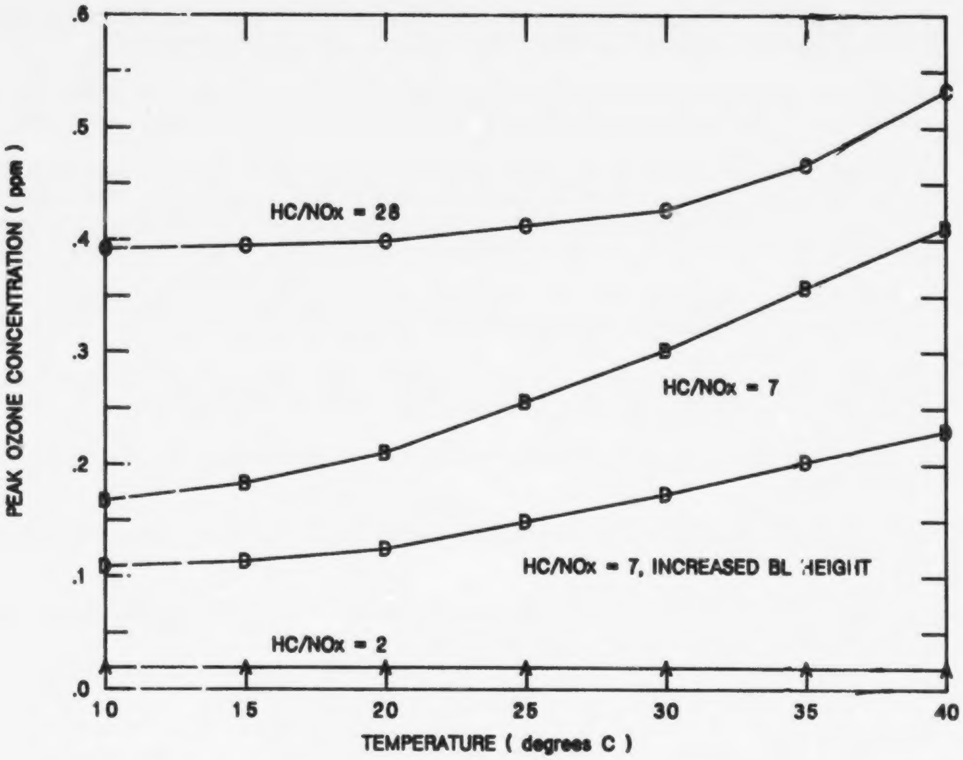

Figure 3.1. The effect of temperature on the peak O_3 concentrations predicted in a box model calculation of urban O_3 formation. Calculations are shown for three hydrocarbon to NO_x ratios. The effect of increasing the boundary layer depth for the case with a hydrocarbon to NO_x ratio of 7 is also shown.

thermal decomposition of PAN:

$$PAN = RCO_3 + NO_2$$

$$k = 2 \times 10^{16}\, e^{12542/T}\, s^{-1} \qquad (3.4)$$

When PAN forms by combination of peroxy acetyl radicals (RCO_3) with NO_2, it sequesters the NO_x and peroxy radicals that contribute to ozone formation in a non-reactive form (although PAN itself is a harmful irritant). When temperatures are raised, more NO_x and RCO_3 radicals are available for O_3 production, and, as shown in Figure 3.1, over an 8-hour period, the effect on O_3 production can be pronounced, especially at intermediate HC/NO_x ratios. At very high or very low HC/NO_x ratios, the effect is not as pronounced. At high HC/NO_x ratios, the reaction sequence which produces O_3 is very fast so that the peak O_3 concentration is not greatly changed by the sequestering of NO_x by PAN. At low HC/NO_x ratios, the mixture of hydrocarbons and NO_x are not reactive enough to significantly affect O_3 buildup in an 8-hour period, but one might expect a larger change at later times or over a several day period. Apparently, an increase of temperatures can significantly exacerbate oxidant problems.

A change in stratospheric O_3 concentrations would alter oxidant formation by altering the surface UV flux, thereby changing photolysis rates. O_3, and in particular, stratospheric O_3, is responsible for absorbing much of the UV radiation below 300 nm. Changes to the column abundance of O_3 would thus change the amount of shortwave radiation available in the troposphere. In the reaction sequence outlined above, only the photolysis of NO_2 is shown. The photolysis of NO_2 is not expected to be significantly altered by a change in the column concentration of O_3, because most of its photolysis occurs by absorption of longer wavelength photons (between 350 and 400 nm). However, several species that are intimately involved in the production of O_3 have significant absorption cross-sections at shorter wavelengths. These include H_2CO, CH_3CHO, H_2O_2, O_3, etc. Table 3.2 gives an estimate of the photolysis cross-sections for these species calculated at ground level for zenith angle of 45 degrees for three levels of column O_3 abundance calculated using the LLNL one-dimensional model of the stratosphere and troposphere (Wuebbles, 1981). The maximum to minimum change in O_3 represents a 25% decrease in column O_3.

Table 3.2. Photolysis Rate Constants at the Surface as a Function of Overhead O_3 Column

REACTANT:	CH_3CHO	CH_2O	CH_2O	NO_2	H_2O_2	O_3	O_3
PRODUCTS:	CH_3+CHO	H_2+CO	$H+HCO$			$O(^3P)$	$O(^1D)$
O_3 Column*	Photodissociation rate constants (s^{-1})						
8.0E18	4.4E-6	2.50E-5	2.09E-5	7.90E-3	7.10E-6	4.80E-4	2.18E-5
7.2E18	4.9E-6	2.55E-5	2.20E-5	7.92E-3	7.30E-6	4.84E-4	2.60E-5
6.0E18	5.7E-6	2.63E-5	2.40E-5	7.95E-3	7.80E-6	4.91E-4	3.47E-5

* Note: Units are molecules cm^{-2}.

Figure 3.2 gives the ozone production during an 8-hour simulation using these three sets of photolysis rate constants for a simulation in the box model with a HC/NO_x ratio of 7. Similar runs at HC/NO_x ratios of 2 and 28 showed a much smaller O_3 response. According to these calculations, if stratospheric O_3 decreases by 25%, urban oxidant formation could increase by about 10% or by 0.03 ppm.

These results may be contrasted with those reported by Gery et al. (1987) and Liu and Trainer (1987). Gery et al. report peak O_3 changes ranging from -7% to +47% for an O_3 column decrease of 33%. Their study only considered conditions in which an urban area had already attained the 0.12 ppm standard for O_3. The range of results they report is apparently a function of the specific HC/NO_x ratio used in each model run and also of the latitude, base temperature, and meteorology used. Liu and Trainer (1987) also calculated the response of tropospheric ozone to a column ozone change. They considered a range of NO_x conditions and scaled the NMHC concentrations with NO_x for NO_x concentrations above 1 ppb. For areas impacted by urban emissions NO_x ranging from 1 to 10 ppb), they calculated a 10-15% increase in surface ozone resulting from a 20% decrease in column ozone. In very clean areas, photochemistry acts to destroy ozone, and they calculated a decrease of up to 35% for surface ozone resulting from a 20% decrease in column ozone.

Cloud cover changes can directly alter O_3 production by changing photolysis rates. For example, on very cloudy days, no significant photochemical production occurs, because too little sunlight reaches the surface. Urban and regional oxidant models have varying sophistication in their ability to account for cloud cover. One simple technique is to decrease all photolysis rates in proportion to the amount of partial cover. Using this technique, one can estimate the impact on O_3 production using the box model. The impacts are illustrated in Figure 3.3 for a HC/NO_x ratio of 7. Clearly, as illustrated there, the amount of cloud cover is a significant climate element for oxidant formation. Furthermore, cloud amounts reflect the degree of convective intensity. Such activity acts to redistribute pollutants vertically with potentially important consequences for global as well as regional chemistry.

The highest oxidant concentrations are developed during stagnation episodes. These episodes are characterized by surface winds that are generally small (0-3 m/s) leading to little mixing of pollutants in the horizontal, high-pressure systems with higher than normal temperatures, and decreased ventilation associated with decreased vertical mixing and boundary layer depth. If the frequency of these episodes were to change, this would clearly impact the number of days in which high oxidant concentrations were experienced. In addition, of course, as discussed above, any change in the intensity of any one of these characteristics would alter the intensity of the oxidant episode.

The depth of the boundary layer influences the level of oxidant formation by restricting or enhancing mixing of pollutants into tropospheric background air. Over continental areas, the boundary layer is generally low at night, grows to heights as high as 1,000-2,000 m, during daylight hours as the ground temperature heats, and then reforms near the surface again at night. If the maximum height of the boundary layer were to increase as a result of a higher surface heat flux, concentrations would decrease within the boundary layer, allowing for decreased oxidant formation. This is illustrated using the box model in Figure 3.1. Doubling the ventilation rate decreases the amount of ozone formed during an 8-hour period by about 40% for a HC/NO_x ratio of 7. The results obtained here with the simple box model are in qualitative agreement with the results of sensitivity studies from trajectory models (e.g., Derwent and Hov, 1988) and from more complete grid-based photochemical models (see, for example, the studies quoted in the review by Seinfeld, 1988; as well as Penner et al., 1983; and Seigneur et al., 1981). The above studies also explore the effects of altered meteorological conditions. Of course, specific areas will have different sensitivities.

Pollutants which have mixed throughout the boundary layer the previous day, will become part of the "free" troposphere during this process. If the winds above the boundary layer are strong, these pollutants will be advected and diffused away from the region of concern, but with light winds they may be incorporated into the boundary layer during its growth on the following day. Pollutants which are part of the "free" troposphere are generally represented in a photochemical model through boundary conditions. Thus, to the extent that boundary layer injection processes are altered by climate change, we can also expect changes to the free tropospheric concentrations of NO_x and hydrocarbons. Other climate-induced changes will, of course, add to

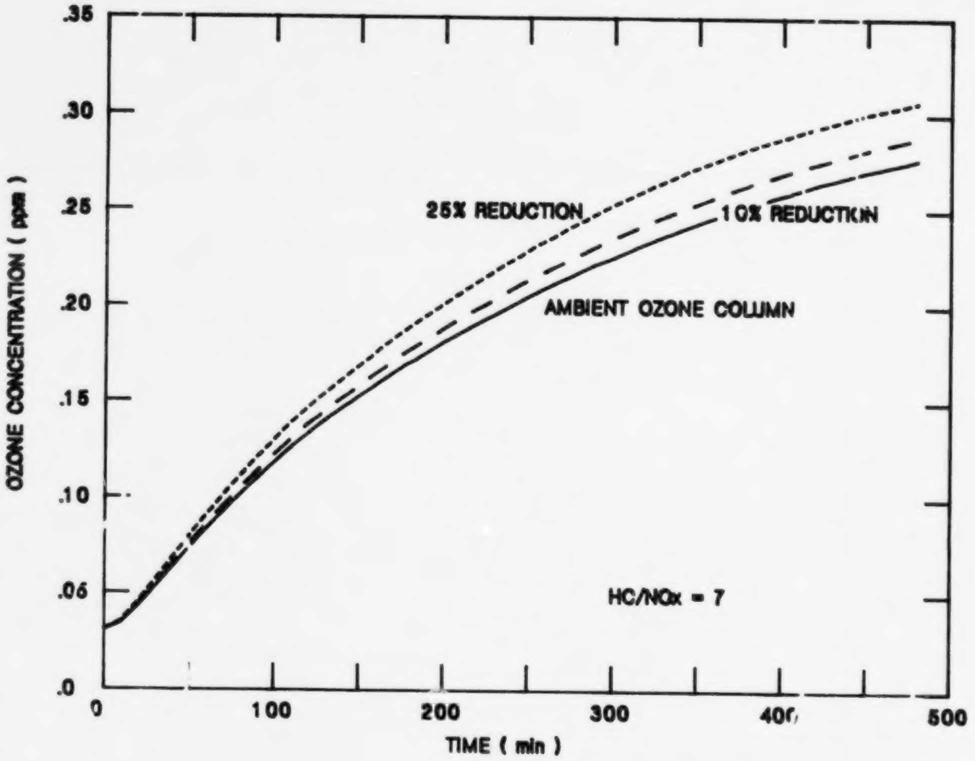

Figure 3.2. The effect of changes in the column O_3 abundance on urban O_3 formation. The ambient O_3 column was assumed to be 8.0 x 10^{18} molecules cm^{-2}. The other two cases represent column O_3 decreases of 10 and 25%.

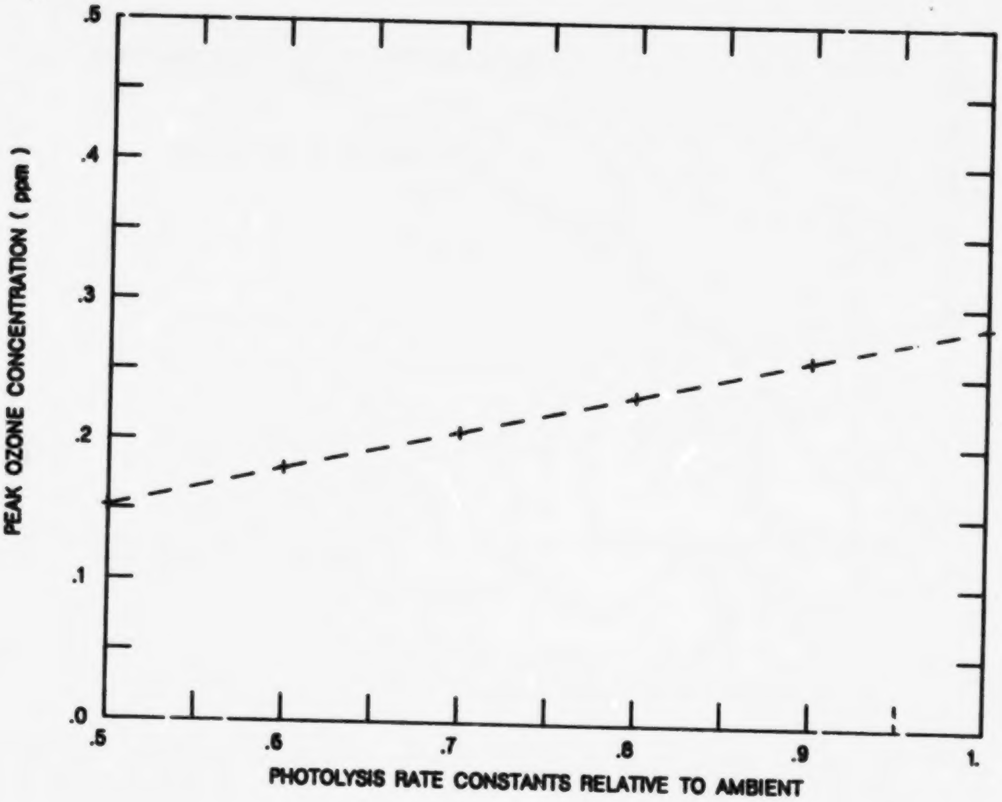

Figure 3.3. The effect of cloud cover changes on the peak O_3 concentrations predicted in a box model calculation of urban O_3 formation. The presence of clouds was assumed to decrease all photolysis rates by the same ratio.

this dynamically caused alteration of free tropospheric concentrations. These changes include changes in the water vapor concentration as well as changes in the anthropogenic emission of NO_x and NMHCs due to a change in energy usage. Also, a change in the natural fluxes of hydrocarbons and nitrogen oxides due to the climate change would lead to changes in free tropospheric concentrations. Also, because lightning is a significant source of free tropospheric NO_x, a change in the frequency of lightning could alter background NO_x concentrations. Finally, changes to background free tropospheric HC and NO_x concentrations will likely cause changes to the free tropospheric ozone concentration. These background concentrations, as well, impact urban and regional oxidant concentrations. Sensitivity studies of the response of grid-based models to changes in boundary conditions give some indication of the importance of this source of change (Seinfeld, 1988; Penner et al., 1983; Seigneur et al., 1981).

As stated above, changes to the natural emissions of hydrocarbons and NO_x can alter background tropospheric concentrations. Both soil NO_x emissions and vegetative hydrocarbon emissions appear to increase exponentially with temperature (Williams et al., 1987; Lamb et al., 1985). Vegetative hydrocarbon emissions are also dependent on light intensity. Changes in emissions will also contribute directly to changes in urban and regional concentrations of HC and NO_x that contribute to O_3 formation. In the urban atmosphere, the sensitivity may not be large because the proportion of ozone formation that can be attributed to vegetative hydrocarbon emissions and soil NO_x emissions are generally small (see Penner, 1984; Lurmann et al., 1983). Figure 3.4 demonstrates the changes in peak O_3 concentration over an 8-hour simulation for a simulation in which vegetative HC fluxes were increased exponentially in response to a temperature increase following the relationship determined by Lamb et al. (1985). (See Penner, 1984, for a description of the treatment of natural hydrocarbon emissions in the box model). The curve is quite similar to that obtained by a straightforward change in the temperature. Of course, the response of regional ozone may be more dramatic. In addition to changes in natural hydrocarbons and NO_x emission rates, deposition may change. Deposition of many pollutants takes place on vegetative surfaces. The stomatal resistance of leaves is a function of temperature as well as light intensity and other parameters (Baldocchi et al., 1987). Deposition rates might therefore be expected to change as a result of climate change, possibly affecting air chemistry.

A change in energy usage and the emissions from energy usage as a result of climate change will obviously lead to HC and NO_x emission changes as well. If temperatures increase, we can expect summertime usage of air conditioners to increase, perhaps with a proportional increase in emissions from power plants. Evaporative emissions from vehicles and refueling would also increase. A simple estimate of the episodic impact of these emission increases on urban ozone can be obtained from studies of the effect of emissions reductions. Increases in NO_x will, in many urban areas, lead to local decreases in O_3 (although downwind concentrations could increase). Increases in hydrocarbon emissions would increase local and downwind O_3 concentrations. The study of Penner and Connell (1987), for example, showed that a 30% increase of NO_x emissions led to an O_3 decrease of 25 to 35% at a location near the urban center where the largest ozone concentrations were experienced, but an expanded area of O_3 increase above the federal standard downwind of the central urban region. A 30% increase in hydrocarbon emissions increased peak O_3 at all locations, with an increase of 25 to 35% at the location where the highest ozone concentration was recorded. These changes were calculated for changes in areawide emissions from all sources. The quantitative model results will be different, of course, for different urban areas or if only increases in power usage were considered (see also Seigneur et al., 1981; Penner et al., 1983; Derwent and Hov, 1988, as well as studies quoted in Seinfeld, 1988).

Finally, changes in the amount of secondary aerosol can affect oxidant formation through effects on photodissociation processes. The amount of secondary aerosol would likely change as a result of both temperature and water vapor changes (Schere, 1988). The estimates of potential urban and regional O_3 change from various climate-related perturbations are summarized in Table 3.3. Because some climate perturbations lead to increases in O_3 and some lead to decreases, further work is needed to fully assess the expected change. However, as shown in Table 3.3, the response of urban and regional ozone to climate change is potentially significant.

Table 3.3 Estimated Change in Urban Ozone

Climate-driven Perturbation	Estimated O_3 Change*	Notes
T increase from 25° to 30°C	+20%	
Increase biogenic emissions of NMHC consistent with a a 5°C temperature increase	3-10%	Could be larger in regions where biogenic emissions are more important
25% decrease in column O_3 abundance	+10%	This work and Liu and Trainer (1987)
	-7% to +47%	Gery et al. (1987)
Increase cloudiness leading to a 10% decrease in photolysis rates	-10%	
Increase boundary layer depth by 2	-50%	

---

[*] Estimated using a simple box model of urban photochemistry with initial $HC/NO_x = 7$. See Atherton and Penner (1988) for details.

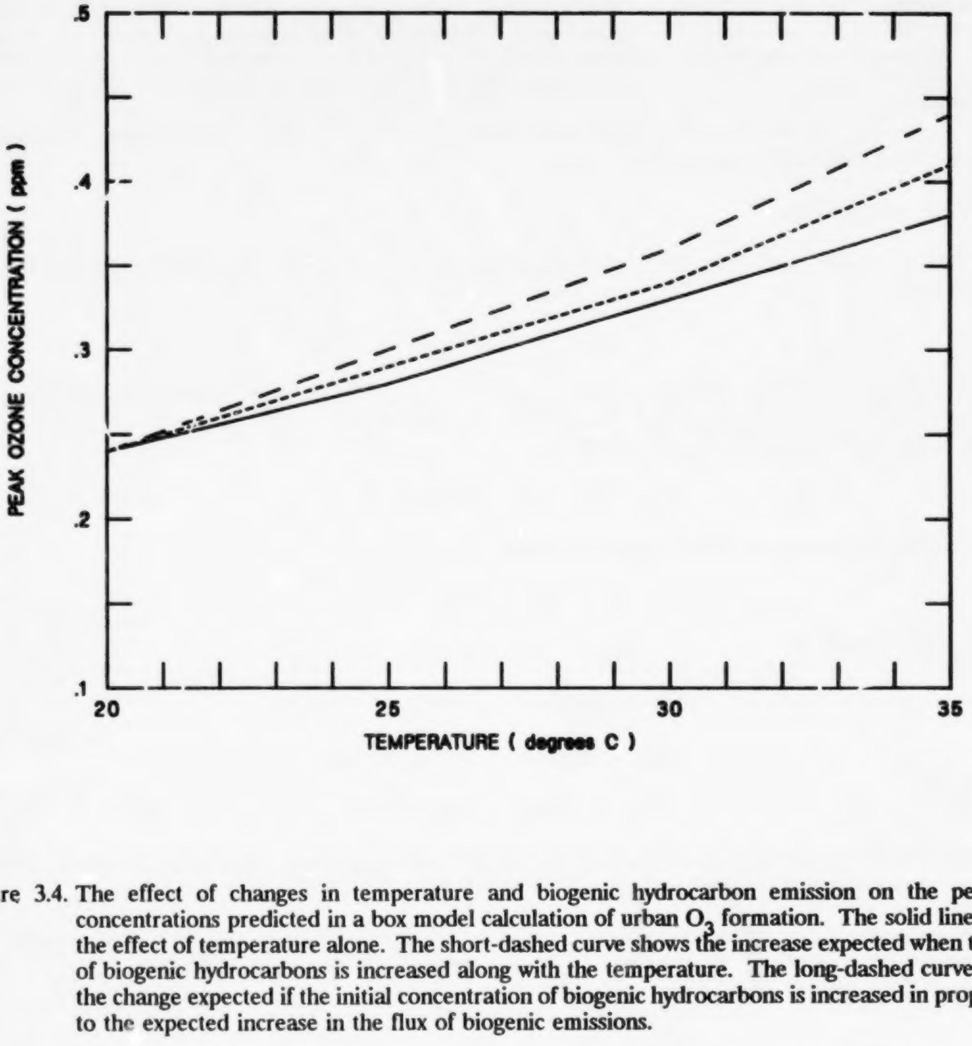

Figure 3.4. The effect of changes in temperature and biogenic hydrocarbon emission on the peak O_3 concentrations predicted in a box model calculation of urban O_3 formation. The solid line shows the effect of temperature alone. The short-dashed curve shows the increase expected when the flux of biogenic hydrocarbons is increased along with the temperature. The long-dashed curve shows the change expected if the initial concentration of biogenic hydrocarbons is increased in proportion to the expected increase in the flux of biogenic emissions.

ACID RAIN AND ACID DEPOSITION

Emissions of NO_x and SO_2 into the atmosphere lead to the formation of nitric and sulfuric acid via a number of complex heterogeneous and homogeneous chemical pathways. In addition, organic acids may form from non-methane hydrocarbons (NMHC), which add to the abundance of acidic species. Once conversion to acid species has occurred, surface deposition may take place via either dry or wet processes. The effect of a particular change in climate on the rates of transformation of NO_x, SO_2, and NMHC to their acidic forms and on their method of delivery to the Earth's surface will depend on which pathway is dominant in any given situation. Here we review the chemical pathways thought to be primarily responsible for the conversion of NO_x, SO_2, and NMHC to NO_3^-, SO_4^{-2}, and organic acids. We speculate about the impacts that any given climate change might have on these conversion rates. No comprehensive statement about sensitivity is possible, because no comprehensive model results that integrate over a number of specific situations are available. However, we indicate situations wherein a change might occur.

Formation of Acidic Species

Nitrogen oxides (NO and NO_2) are emitted primarily as NO. NO is rapidly converted to NO_2 via reaction with O_3:

$$NO + O_3 = NO_2 + O_2 \qquad (3.5)$$

with smaller contributions from reactions with HO_2 and RO_2 (see reactions 3.3). NO and NO_2 are converted to a variety of other species by a number of different gas phase reactions. Conversion to HNO_3 takes place primarily in the gas phase during daylight hours via:

$$NO_2 + OH + M = HNO_3 + M \qquad (3.6)$$

At night and in clouds, other reaction sequences, such as:

$$NO_2 + O_3 = NO_3 + O_2$$

$$NO_3 + NO_2 = N_2O_5$$

$$N_2O_5 + H_2O(aq) = 2\ HNO_3 \text{ or } 2\ NO_3^-$$

$$NO_3 + H_2O(aq) = HNO_3 \text{ or } NO_3^-$$

$$NO_3 + RCHO = NO_3 + RCO \qquad (3.7)$$

may also be important. In reaction (3.7) above, RCHO indicates an aldehyde, but similar gas phase reactions of NO_3 with aromatics and terpenes also occur (Morris and Niki, 1974; Atkinson et al., 1984).

Conversion of SO_2 to SO_4^{-2} occurs via a number of pathways that involve both homogeneous and heterogeneous (aqueous phase) mechanisms. Gas phase conversion is thought to occur via:

$$SO_2 + OH = HSO_3$$

$$HSO_3 + O_2 = HO_2 + SO_3$$

$$SO_3 + H_2O = H_2SO_4 \qquad (3.8)$$

while the aqueous phase conversion occurs primarily via:

$$SO_2 + H_2O_2 = H_2SO_4$$

$$SO_2 + O_3 + H_2O = H_2SO_4 + O_2$$

At high concentrations, metal ions in solution can also catalyze the conversion of SO_2 to SO_4^{-2} by O_2. Sulfate particles may be formed by attachment of the gas phase H_2SO_4 formed in reaction (3.8) to pre-existing particles or by the evaporation of cloud drops whose residue consists of H_2SO_4 formed in the aqueous phase. Which process is most important has not been determined. Further, the relative importance of the subsequent incorporation of sulfate particles into precipitation versus the aqueous conversion of SO_2 to SO_4^{-2} during precipitation events remains uncertain.

Formic and acetic acid can account for a significant fraction of the acidity in precipitation (Galloway et al., 1982; Keene et al., 1983; Keene and Galloway, 1984; Norton, 1985), although their relative importance globally to that of the acidity from nitric and sulfuric acid is currently unknown. Their formation mechanism involves both gas-phase and aqueous phase processes, but the relative importance of these processes is also unknown (see discussion in Albritton et al. (1987) and also Atkinson and Lloyd (1984), Calvert and Stockwell (1984), Chapman and Sklarew (1986), Graedel and Goldberg (1983), and Chameides (1984)). Because so little is known, the effect of climate change on the conversion of NMHC to organic acids is not considered below.

Effect of Climate Change on Acid Rain and Acid Deposition

Given the mechanisms of acid formation discussed above, it is immediately clear that changes to climate could impact the rates and mechanisms leading to acid deposition. For example, cloud cover may change, leading to a change in the rates of heterogeneous conversion of SO_2 to SO_4^{-2}. Alternatively, precipitation patterns may change, leading to a change in the spatial areas affected by acid precipitation. Prediction of these changes is currently beyond the capability of GCMs (see Chapter 5). Furthermore, except for models of episodic events, we still cannot properly delineate the relative role of conversion rates in clouds versus conversion rates in dry air so that estimating the global and seasonal effects of cloud cover changes is not possible. However, we can illustrate the climate and chemistry changes that are expected to impact the rates of SO_2 conversion to sulfate. These types of climate change include the following:

1) A change in average tropospheric temperatures and/or their regional distribution.

2) A change in stratospheric O_3 concentrations.

3) A change in the background concentrations of O_3, H_2O, NO_x, and NMHCs

4) A change in circulation patterns.

5) A change in the frequency and type of clouds formed.

6) A change in precipitation patterns.

An increase in temperature can impact conversion of SO_2 to SO_4^{-2} in several ways. Walcek and Chang (1988) used results from the RADM model (Chang et al., 1987) to estimate that gas phase conversion rates of SO_2 to SO_4^{-2} would be increased as a result of temperature increase in both the boundary layer and free troposphere. However, in their model aqueous phase conversion rates were a factor of 3 larger than the gas phase conversion rates. Increases in temperature caused a decrease of the H_2O_2 production rate, which may be associated with decreases in aqueous conversion rates of SO_2. The solubility of SO_2 also decreases at higher temperature, although the aqueous oxidation rate constants increase.

A decrease in stratospheric O_3 concentrations can alter the conversion rate of SO_2 to SO_4^{-2} by increasing the UV flux in the troposphere, thereby increasing photolysis rates. The most important species impacted will be H_2O_2. Since H_2O_2 acts to efficiently convert SO_2 to SO_4^{-2} in cloud water and because its concentration can be limiting in this process, an increase in H_2O_2 concentrations will quantitatively increase the conversion of SO_2 to SO_4^{-2}.

A change in the background concentrations of the species involved in the conversion of SO_2 to SO_4^{-2} or of NO_x to HNO_3 will alter acid formation rates. These species include O_3, H_2O (which determines the concentrations of H_2O_2 and OH), NO_x, and NMHCs. The background concentrations of these species can be altered by climate change through a number of different mechanisms, none of which is easily quantified given the state of today's knowledge. For example, a general warming of the climate is expected to lead to increases in the concentration of water vapor, if it is assumed that the relative humidity remains constant. Also, as discussed above, both NO_x and NMHCs have natural sources that are sensitive to temperature and precipitation. Thus, a change in climate that affects temperature and precipitation patterns will lead to a change in the natural fluxes of NO_x and NMHCs. Further, both these species have large fluxes associated with energy usage. If this is altered as a result of climate change, the flux of NO_x and NMHCs from energy usage will change. It is not possible, at this time, to estimate how background concentrations might respond to these flux changes; three-dimensional models are needed that account for all the sources of these species in a realistic manner. However, it can be stated that changes are expected and that these changes will alter the rates of acid formation. Sensitivity tests with the RADM model confirm this observation (Brost, 1988), but it is not clear, at the present time, how to relate these tests to climate change. Given that H_2O, NO_x, and NMHC concentrations will change, it can also be stated that the background concentration of O_3 will change, since its chemistry depends intimately on the levels of these species. Walcek and Chang (1988), for example, estimated that a 10% increase in ozone concentrations would increase the gas phase oxidation of SO_2 in the boundary layer, while decreasing SO_4^{-2} production in the free troposphere. A 10% increase in background water vapor was estimated to increase gas phase production rates of SO_4^{-2} and H_2O_2 in both the boundary layer and free troposphere. However, these estimates were not based on fully coupled model calculations.

Potentially the most significant climate-change effect could be a change in average cloud liquid water content. Hales (1988) used a cloud/chemistry model of a cyclonic storm to estimate that changes in temperature would lead to substantial changes in precipitation amount at constant relative humidity. The deposition rate of SO_4^{-2} is thereby strongly affected. By changing the pH of cloud water, these effects could also alter the roles of H_2O_2 and O_3 in the conversion of SO_2 to SO_4^{-2}.

Finally, if circulation and precipitation patterns change, the amount of acid deposited locally can change. Galloway et al. (1984) have estimated that the amount of sulfur exported off the east coast of North America is 30 to 35% of that emitted over land areas. A slowing of winds or a change of circulation patterns, possibly as an increased seasonal duration of summer-like conditions, for example, could change the ratio of deposition to export in a manner that significantly alters regional deposition. Sensitivity studies reported by Brost (1988) confirm that changes in meteorology can be quite important. Further, precipitation can occur in a variety of storm types which have different impacts on the redistribution of pollutants and on their mixing. Therefore, the venting of acid precursors to the upper atmosphere and/or the reaction times available for formation of sulfate could change if the types of clouds and storm systems change.

CHAPTER 4

GLOBAL CHEMISTRY AND CLIMATE INTERACTIONS

It has been established through long-term measurement records that global changes in radiatively important species (e.g., CO_2, CH_4, N_2O, CFCs) are occurring at significant rates, and models have been used to demonstrate that these will drive development of a significant change to climate. As the above discussion shows, changes in climate and global chemistry have the capacity to influence both acid deposition and urban and regional oxidant formation. Other climate-related changes in global atmospheric composition that have significant implications may also be inferred. These include perturbation of tropospheric and stratospheric ozone driven by emissions of hydrocarbons and NO_x (in the troposphere) and emissions of CFCs and other halocarbons (in the stratosphere). In addition, composition changes induced by climate change can feed back through various processes to produce further climate change. One example of a feedback loop involves change in tropospheric OH concentration, which then alters the lifetimes and transport of radiatively active species. Another involves climate-driven change in tropospheric O_3, which in turn directly impacts climate in its role as an absorber and emitter of solar and infrared radiation. Furthermore, O_3 is intimately involved in production of hydroxyl. Below, we outline some of the feedback loops and estimate, where possible, the sensitivities and consequences.

TROPOSPHERIC OH

The hydroxyl radical, OH, is the primary tropospheric chemical scavenger of CH_3CCl_3, CH_3Cl, CH_3Br, and other hydrogen-containing halocarbons, as well as of CH_4, NMHCs, CO, DMS, H_2S, NO_2, and SO_2. Some of these species (several halocarbons and CH_4) are directly responsible through their radiative properties for part of the expected climate change. A change in global OH concentration will alter the lifetimes of some of the species driving the climate change, and thereby modify their abundances and radiative effects. Further, OH and other closely related species in the HO_x family play a central role in the conversion of SO_2 to SO_4^{-2} and NO_2 to HNO_3 in the homogeneous phase, by direct reaction of SO_2 and NO_2 with OH. In solution, H_2O_2, formed homogeneously by HO_2 disproportionation, acts to convert SO_2 to SO_4^{-2} in clouds. Likewise, the HO_x family plays a central role in $O_3$3 production by oxidizing NO to NO_2, by removing active forms of NO_x, and by initiating the oxidation of hydrocarbons in the atmosphere. Below we describe first the sources and sinks of OH, then we consider how climate change could influence its concentration, and finally we speculate on related climate-chemistry feedback processes.

Sources and Sinks of OH

The major source for OH and for HO_x (HO, HO_2, H_2O_2, HNO_3, etc.) in the background global troposphere is the reaction of an excited state of atomic oxygen, $O(^1D)$, with H_2O:

$$H_2O + O(^1D) = 2\,OH \qquad (4.2)$$

The $O(^1D)$ in reaction (4.1) is generated by photolysis of O_3 near 300 nm:

$$O_3 + \nu h\nu\ (\lambda < 310\ \text{nm}) = O_2 + O(^1D) \qquad (4.2)$$

In regions of high NMHC concentration, the oxidation of these species can also add to the HO_x family by radical chain-branching reactions:

$$\text{NMHC} + OH = ...HO_2 + RO_2 \qquad (4.3)$$

which lead to OH production after reactions with NO or O_3 that convert HO_2 and RO_2 to OH.

In addition to these direct sources of OH (and HO_x), the abundance of the hydroxyl radical is controlled by fast reactions interconverting OH with other members of the HO_x and RO_x families (HO_2, H_2O_2, HNO_3, RO, RO_2, RCO_3, etc.). The rates of these radical chain-propagating reactions depend on the local concentrations of NO, CO, O_3, CH_4, NMHCs, and on local photolysis rate constants, particularly that for H_2O_2.

A variety of radical chain-terminating reactions remove OH and HO_x from the troposphere including:

$$OH + H_2O_2 = H_2O + HO_2$$

$$OH + HO_2 = H_2O + O_2$$

$$OH + NO_2 + M = HNO_3 + M \qquad (4.4)$$

and

$$HO_2 + HO_2 = H_2O_2 + O_2 \qquad (4.5)$$

followed by the heterogeneous removal of H_2O_2 and HNO_3 by precipitation. A suite of other reactions also remove HO_x but are currently thought to be less important than those listed here.

Impact of Climate Change on Tropospheric OH

Given the importance of H_2O, CH_4, CO, NO, O_3, and tropospheric solar fluxes to tropospheric OH abundance, it is clear that, to the extent that climate would impact the concentrations of these species and photolysis rate constants, a change in climate would alter OH. As noted above, reaction with OH provides the major chemical scavenging mechanism for a variety of species in the troposphere. In particular, the primary removal mechanisms for CO and CH_4 are by reaction with OH. These reactions are also the most important direct conversion reactions for OH on a global basis. They cycle OH to other forms in the HO_x family, modifying the ratio of OH to HO_x. The importance of these interactions in HO_x chemistry implies that increases in CO and CH_4 abundances can lead to decreases in OH. Similarly, increases in tropospheric NO and O_3 can lead to increases in OH by enhancing cycling reactions that convert HO_2 to OH. Whether these effects on OH will be offsetting is a problem requiring higher-dimensional tropospheric chemical models to understand and integrate in detail.

Because water vapor is a parent compound for OH and other HO_x species, changes to its concentration would alter the concentration of tropospheric OH. Tropospheric water vapor is in balance with an evaporation and transpiration source from the oceans, soils, and plants and the precipitation sink. Global increases in temperature, driven by a climate change, are expected to lead to changes in the tropospheric water concentration. If the sources of water vapor are not perturbed by changes in vegetative cover and if circulation patterns do not lead to more frequent precipitation events, then the concentration of H_2O might be expected to increase. We note that global average relative humidity tends to remain almost constant with warming in climate model experiments (Ramanathan et al., 1987). Of course, changes in precipitation patterns and/or frequency and changes in vegetation patterns would make this simple picture more complex. As a simple estimate, a 2 degree increase in temperature could be associated with a 10-30% increase in tropospheric H_2O levels, implying a few percent increase in OH and other HO_x family members (Thompson et al., 1988), all else being equal.

Reaction of O_3 with HO_2 cycles HO_x back to OH. Therefore, increases in the tropospheric concentration of O_3 would lead to increases in OH. As discussed below, tropospheric O_3 concentrations may be increasing as a result of direct emissions of NO_x, NMHCs, and CH_4 as well as through indirect changes in the emissions of these species (and others) which are driven by a climate change. Because of the role of NO in partitioning HO_x and because of the large variation in the concentration of NO between remote oceanic areas and continental areas, an increase in O_3 by a factor of 2 could increase OH by perhaps 10% over ocean areas and by probably greater than 10% over the continents (Thompson et al., 1988). These changes might, of course, feed back on the concentration perturbation of O_3 and would be better estimated using a fully coupled global model.

Also, increases in the concentrations of halocarbons and N_2O are driving changes that are calculated to lead to a net decrease in stratospheric O_3. Stratospheric cooling, as driven by increases in CO_2 and other infrared emitters, acts to increase stratospheric O_3 (Penner, 1980). These direct effects of emissions and indirect effects of climate change are calculated to have caused only small changes in stratospheric O_3 at present. However, larger changes could occur in the future if the existing balance of processes is perturbed. Because most of the ozone column resides in the stratosphere and because ozone is responsible for much of the atmospheric opacity below 300 nm, these changes would alter tropospheric OH by changing photolysis rate constants for any species with significant absorption in this range (see Table 3.1). In particular, absorption by ozone leading to the formation of $O(^1D)$ would change, creating a change in the direct source of HO_x and OH. Further, an increase in the photolysis rate for H_2O_2 could affect HO_x loss rates. A decrease in column O_3 of 20% would lead to an OH increase of roughly 15% over continental areas (Thompson et al., 1988; Liu and Trainer, 1987).

Another mechanism for climate impact on OH concerns the magnitude of the source of OH created by the oxidation of NMHC. Trainer et al. (1987) have estimated that in areas of low NO_x concentrations, the concentration of OH might be decreased by as much as a factor of 2 in the first 100 m above ground level as a result of biogenic emission of isoprene and terpenes. The emission of biogenic hydrocarbons is exponentially dependent on temperature (Lamb et al., 1985). An increase of 5°K could lead to an increase in the biogenic emission of hydrocarbons by more than a factor of 3. An estimate of the impact on global OH concentrations is difficult because the importance of the role of NMHC in the global budget for OH is not well defined. However, it is clear that locally, at least, these changes would lead to decreases in OH, although the global consequence (for removal of CFCs, CH_4, etc.) cannot be estimated at this time.

Likewise, temperature increases can impact the bacterial source of CH_4. Reaction of CH_4 with OH is a net sink for OH in a low NO_x environment, although the net effect of CH_4 oxidation on HO_x depends on the oxidation pathway (Logan et al., 1981). Because the bacterial source of CH_4 is about 50% of the total source (Khalil and Rasmussen, 1983a) and because CH_4 emissions are exponentially dependent on temperature, an increase of 5°K could lead to almost a 50% increase in the total (bacterial plus anthropogenic) source strength of CH_4 (Hameed and Cess, 1983). The estimated increase in atmospheric abundance of CH_4 would be larger than the increase in its source strength because the concentration of OH would decrease as CH_4 is increased.

As discussed above, reaction of NO with HO_2 is important in partitioning H_x between HO_2 and OH, particularly over continental areas where the concentration of NO is elevated. Bacterial sources of NO_x could also be increased by an increase in temperature. Using the relationship of Williams et al. (1987), a 5 degree increase in temperature, for example, could lead to an increased bacterial emission of about a factor of 3. Because the sources of NO_x are so poorly defined (Logan, 1983), the effect of this change in emissions on continental NO_x concentrations is uncertain. However, rough estimates suggest a local increase in OH over continental areas of approximately 5% for a 10% increase in NO_x (Thompson et al., 1988).

Bacterial processes in soils act as a small sink for atmospheric CO, and emission of CO by plants acts as a source. Temperature changes could also impact these sources and produce a small change on tropospheric OH.

Finally, changes in tropospheric temperatures themselves create important changes in reaction rates that are strongly temperature dependent. In particular, the reaction of CH_4 with OH has an activation energy of 1710°K. An increase of 5°K would increase this reaction rate by 10%. The reaction of OH with NO_2 is sensitive to temperature, as are the reactions of OH and HO_2 with O_3. Model estimates using the LLNL 1-D troposphere/stratosphere model (Wuebbles, 1981) imply that an increase in temperature by 5°K could decrease OH by a few percent, if all other concentrations are held constant.

Any prediction of future changes in global-average tropospheric OH abundances depends on accounting for the simultaneous action of the many coupled HO_x-controlling processes outlined above. Significant uncertainties area encountered even in investigation of implied trends of OH abundance in the recent past. In studies of the CH_4 trend, it is considered plausible that a decline in OH abundance (and associated increase in CH_4 lifetime) accounts for 20-80% of the observed increase in atmospheric CH_4 abundance over the previous few centuries (Khalil and Rasmussen, 1985b; Thompson and Cicerone, 1986a,b; Thompson and Kavanaugh, 1986; Levine et al., 1985). But unresolved uncertainties in CO, NO_x, and NMHC trends, as well as global distribution of NO_x sources, lifetimes, and abundances contribute to the wide range of possible recent change. Considering the troposphere as a whole, it is thought that the current situation is NO_x-poor with respect to net HO_x production by CH_4 and NMHC oxidation (Logan, 1987). Projected increases in these compounds are thus likely to lead to continued decrease in total tropospheric OH abundance, as is shown by Isaksen and Hov (1987) in a 2-D model study of coupled perturbations to the troposphere. This average conclusion includes, however, significant regional diversity, in which some areas of the troposphere may be characterized by OH increase. Isaksen and Hov (1987) also find that OH is increased slightly in their model when NO_x, CO, CH_4, and NMHC are assumed to increase concurrently. The changes in OH from the various climate-related perturbations discussed are summarized in Table 4.1. Clearly, the changes are subtle and will require fully coupled models that can address local as well as global changes.

Climate Implications of OH Abundance Change

The connection between average tropospheric OH abundance, CO and CH_4 lifetimes, and climate has been mentioned above. If, as seems likely, CO and CH_4 continue to increase, the average OH abundance should decrease, subsequently enhancing the tropospheric concentration of CH_4 above the value resulting from the direct effect of increases in the emissions of these species (Penner et al., 1977) and leading to a larger climate impact. Other species of radiative or stratospheric photochemical importance (e.g., hydrogen-containing halocarbons) that are primarily destroyed by reaction with OH will be similarly affected in what appears to be a positive feedback mechanism. This direct effect of a decrease in OH, however, is moderated by the increases in O_3 that also occur as a result of CH_4 and CO increases (in regions of sufficient NO_x) (see, for example, Isaksen and Hov, 1987, and Thompson and Cicerone, 1986a,b). As discussed above, increases lead to OH increases. Thus, to evaluate the effect of these changes it is important to account for all these species in a coupled system that also accounts for the long-range transport of the longer-lived species from source to remote regions.

TROPOSPHERIC O_3

In Chapter 3, we discussed how changes in climate could alter O_3 production on urban and regional scales. One factor discussed there, which could contribute to these changes, was a change in the background tropospheric ozone concentration. A change in background O_3 (see also Chapter 2) is also important for a change in climate itself. O_3 absorbs infrared radiation near 9.6 μ. At current concentrations it absorbs roughly 4% of the longwave energy emitted at the surface of the earth. An increase in tropospheric O_3 of 15% could lead to a temperature increase of about 0.1 degrees (Ramanathan et al., 1987). Tropospheric ozone concentrations are the result of a balance between transport of roughly 5×10^{10} molecules cm^{-2} s^{-1} from the stratosphere (Levy et al., 1985), surface deposition to land and vegetation estimated to be of similar magnitude, and photochemical sources and sinks whose magnitudes are estimated to be comparable to or larger than the stratospheric source (NRC, 1984). Because tropospheric ozone abundances can be controlled variously by global scale transport, regional scale transport, and photochemistry, the distribution and lifetime of tropospheric ozone are significantly heterogeneous in time and space. Perturbations to the photochemical source and sink for tropospheric O_3 could come about directly via modulation of the emissions of anthropogenic hydrocarbons and NO_x, and/or indirectly via changes to the natural sources of these species. Below we discuss first the sources, sinks, and chemistry of global tropospheric ozone and then a set of mechanisms that could connect changes in climate to changes in tropospheric ozone.

Table 4.1. Estimated Change in Global OH

Climate-driven Perturbation	Change in OH	Reference
+5°C	few percent	LLNL 1-D model
10-30% increase in H_2O	few percent	Thompson et al. (1988)
2 x O_3 in troposphere	~10% over ocean	Thompson et al. (1988)
Increase biogenic NMHC emissions	Current emissions decrease OH by a factor of 2 near surface; no estimate for effect of increased emissions	Trainer et al. (1987)
10% increase in NO_x	+5%	Thompson et al. (1988)
Simultaneous increase in CO, CH_4, NMHC	Decrease in OH	Isaksen and Hov (1987)
Simultaneous increase in CO, CH_4, NO_x, NMHC	Increase in OH	Isaksen and Hov (1987)

Sources and Sinks of O_3

The production and accumulation of ozone in the stratosphere produces a mole fraction gradient in the region of the tropopause down which ozone is transported by eddy motions, mainly at midlatitudes. This source of tropospheric ozone is observed directly and can be inferred from observations of radioactive tracers of stratospheric origin. Agreement among observations and models of various dimension sets the global average magnitude of this source in the range of 3 to 12 x 10^{10} molecules cm^{-2} s^{-1} (4-15 x 10^{14} g/year) (see Levy et al., 1985 and papers quoted therein). This ozone is introduced into a region in which ozone photochemical lifetimes are long (order of months), so that further mixing by transport within the troposphere occurs over global scales.

Ozone is known to be taken up on contact with leaf surfaces, soils, and to a lesser extent water and snow surfaces. Global average estimates of the total surface deposition of ozone lie in the range 5-15 x 10^{14} g/year (NRC, 1984), essentially the range of the estimated stratospheric source. General circulation model simulations including the stratospheric source and surface loss, but no tropospheric photochemistry, successfully emulate in remote regions the large-scale observed features of the free tropospheric ozone distribution and its seasonal dependence (Levy et al., 1985).

However, estimates of tropospheric photochemical production and loss magnitudes are, in most cases, larger than the stratospheric source and surface loss terms (see, for example, Logan et al., 1981). It is clear that in some regions of the troposphere, with urban smog being the extreme example, photochemical processes dominate the ozone budget. In regions with little NO_x, however, net O_3 loss can occur. The ozone produced near urban areas can be transported to remote areas, as well, contributing to global O_3 production (Vukovich et al., 1985). Thus, the sign and magnitude of the net tropospheric photochemical term for O_3 remains uncertain.

Tropospheric photochemical ozone loss can occur through the reactions:

$$O_3 + h\nu\ (\lambda < 310\ \text{nm}) = O(^1D) + O_2$$

$$O(^1D) + H_2O = 2\ OH \qquad (4.6)$$

and

$$OH + O_3 = HO_2 + O_2$$

$$HO_2 + O_3 = OH + 2\ O_2 \qquad (4.7)$$

The importance of the second loss mechanism depends on both the HO_x and NO_x abundance. The primary source for tropospheric HO_x is reaction (4.6) above. In the presence of sufficient NO, HO_2 reacts to form NO_2:

$$HO_2 + NO = OH + NO_2 \qquad (4.8)$$

The ozone lost by reaction with OH in (4.7) can be regenerated, through reaction (4.8), after photolysis of NO_2:

$$NO_2 + h\nu\ (\lambda < 410\ \text{nm}) = NO + O$$

$$O + O_2 + M = O_3 + M \qquad (4.9)$$

Measurements of ozone in the remote marine troposphere, where NO was observed at levels of only 10 ppt (Davis et al., 1987; Ridley et al., 1987), imply the importance of local photochemical ozone loss.

If peroxy radicals are produced by reactions other than the reaction of OH and O_3, then reactions (4.8) and (4.9) provide a photochemical source of ozone. Tropospheric photochemical ozone production is qualitatively similar to production in photochemical urban smog. In general, peroxy radicals are generated in the OH-initiated oxidation of CO, CH_4, and higher hydrocarbons (NMHC) which are capable of oxidizing NO to NO_2, leading to ozone formation after NO_2 photolysis. For CO, one ozone molecule can be produced for each CO oxidized. In the complete oxidation of CH_4 to CO_2 and H_2O where sufficient NO is present, between 3 and 4 ozone molecules can be produced for each CH_4 reactant molecule, with H_2CO as an important intermediate (Logan et al., 1981). Generally, higher hydrocarbon complexity is associated with higher ozone-forming potential.

Observations at Niwot Ridge, Colorado, show the importance of photochemical formation of ozone in clean continental air (Fehsenfeld et al., 1983). A clear diurnal variation in the measured ozone abundance is seen in the summer, which is related to oxidation of anthropogenic and natural hydrocarbons. Based on a theoretical interpretation of their observations, Liu et al. (1987) propose that summertime photochemical production of ozone over the United States as a region may reach 1×10^{12} molecules cm^{-2} s^{-1}, an order of magnitude larger than the global average stratospheric source. They suggest also that the accumulation of anthropogenic NO_x in the winter may contribute to observed seasonal enhancement of springtime ozone at Mauna Loa.

Given the wide range of NO_x and O_3 photochemical lifetimes encountered in the troposphere and the complexity of NO_x-related photochemistry, understanding the current global tropospheric ozone budget will depend on the availability of diagnostic models. These models of photochemistry and transport must include the complexity of anthropogenic and natural source distributions and strengths for NO_x and a variety of hydrocarbons as well as boundary layer and free tropospheric transport at a spatial resolution better than existing global circulation models.

Impacts of Climate Change on Tropospheric Ozone

In Chapter 3 above, we discussed the potential impact of climate change on ozone and oxidant formation in urban and regional settings that are often already strongly perturbed by anthropogenic emissions. In individual urban cases, the effects of climate change are commingled with the dominant effects of local trends in emission characteristics and fluxes. The global sum of all local anthropogenic emissions may also be affecting ozone in the previously unperturbed background troposphere (see, for example, Vukovich et al., 1985). There is evidence of an increase in tropospheric ozone over the last 10-20 years from several Northern Hemisphere observing stations with consistent long-term records, including some remote sites (Oltmans and Komhyr, 1986; Logan, 1985). Liu et al. (1987) propose that the statistically significant winter and spring increasing trends at Mauna Loa and Hohenpeissenberg are the result of increasing anthropogenic emission fluxes of NO_x and NMHC directly affecting atmospheric trace constituent composition.

But as large uncertainties remain in the understanding of the current tropospheric ozone budget and controlling processes, predictions of the effects of climate change on tropospheric ozone must be considered speculative. A number of processes related to climate and composition change, including stratospheric ozone perturbation and trends in NO_x, CH_4, CO, and NMHC emissions and budgets, are potentially capable of affecting tropospheric ozone. These processes are important, as with tropospheric ozone itself, over a range of spatial and temporal scales. A comprehensive coupled analysis over all scales is a problem for the future, but speculations can be made about various aspects.

Two possible areas in which stratospheric properties can affect tropospheric chemistry are the downward flux of ozone from the stratosphere and the downward flux of solar UV radiation impinging on the troposphere. The magnitude of the source of ozone mixed downward across the tropopause depends on the lower stratospheric ozone abundance and the dynamics of the stratosphere-troposphere exchange process. Some current photochemical model calculations show that for some stratospheric perturbations of the sort that might be expected to occur over the next several decades, upper stratospheric ozone depletion is associated with lower stratospheric ozone increase, often termed "self-healing" (WMO, 1985). Upper tropospheric ozone might then be expected to increase, in the absence of dynamical changes reducing the stratosphere-troposphere exchange rate.

Decreases in the overhead burden of ozone result in increases in the photochemically active solar flux that drives ozone photochemical production. Model results simulating clean continental or urban air (Liu and Trainer, 1987; Whitten and Gery, 1986) show that the increase in actinic flux produces an increase in ozone. In the remote troposphere with very low NO_x, this relationship does not hold, however (Liu and Trainer, 1987).

The direct impact of composition trends on global tropospheric ozone operates through ozone forming photochemical precursors. In photochemical model calculations of clean continental or urban air, increases in NO_x, CH_4, CO, and NMHC are all related to increased tropospheric ozone, via the reaction mechanisms discussed above. There are many subtleties, however, which complicate quantitative predictions. Liu et al. (1987) infer from data obtained at Niwot Ridge, a clean continental site, that ozone production is a nonlinear function of NO_x and NMHC emission strength. The impact on predictive modeling is that calculations of tropospheric ozone distributions will be sensitive to details of the dispersion of NO_x and related reservoir species such as PAN. Models of lower dimension, in which NO_x emissions are effectively rapidly dispersed zonally or over large regions, can overpredict photochemical ozone formation rates. Isaksen and Hov (1987) have applied a 2-D tropospheric model to the question of the interaction of trends in CO, CH_4, and NO_x and their effects on ozone and OH over a period representing 1965 to 1995. Using simple assumptions of combined annual rates of growth or decline, they find that, in general, the sense and magnitude of ozone change is tied to the assumed NO_x trend. When NO_x is held fixed or increases, increases in CO or CH_4 result in increasing O_3 (and decreasing OH). When NO_x is assumed to decline, O_3 decreases also, even though CO, CH_4, and NMHC are concurrently increasing.

These results and those for tropospheric OH clearly demonstrate the importance of understanding the global distribution of NO_x in three dimensions over the range of scales from urban to global. Of particular pertinence is the significance of long-range transport of NO_x in the form of organic nitrates and peroxynitrates. The summer lifetime for NO_x is on the order of a day or less in the planetary boundary layer. The lifetime of PAN with respect to thermal decomposition is highly dependent on temperature and can be on the order of weeks or months in the middle troposphere. Singh et al. (1985) have speculated that PAN could serve to convey NO_x released in the boundary layer to the remote troposphere, where it plays an important role in affecting the background global abundances of OH and ozone.

OTHER CLIMATE CHANGE FEEDBACKS ON GLOBAL ATMOSPHERIC COMPOSITION

We summarized in Chapter 2 the trends in atmospheric composition that are the drivers for perturbation of atmospheric radiative transfer and climate change. Chapter 3 and Chapter 4 above discuss the effects that the expected climate change may have on regional and global tropospheric photochemistry. The temperature dependence of CH_4 and NMHC emissions by plants and soils mentioned above demonstrates another level of interaction. The changing emissions of trace species that are expected to drive climate change are also functions of climate change variables, through both natural and anthropogenic (economic) mechanisms.

A distinction can be made, in considering the interaction of climate change and anthropogenic source gas emissions, between the effects of actual climate change and those of anticipated climate change. Anticipated climate change can bring about reductions, which may or may not be mandated, in production and emissions related to efficiency improvements in equipment and processes, exploitation of alternatives and straightforward regulation of emissions. A current example is the Montreal Protocol on the production of several halocarbon compounds thought to act to deplete stratospheric ozone abundance. The decreases (or slowing of the rates of increase) in atmospheric abundances of several CFCs and the related stabilization of stratospheric ozone, which are expected to result from application of this agreement, will affect the future global atmosphere in the areas of surface and tropospheric ultraviolet fluxes, stratospheric climate, and surface-tropospheric climate. It is possible that means may be found to reduce combustion-related emissions in anticipation of global warming.

Decreases in the overhead burden of ozone result in increases in the photochemically active solar flux that drives ozone photochemical production. Model results simulating clean continental or urban air (Liu and Trainer, 1987; Whitten and Gery, 1986) show that the increase in actinic flux produces an increase in ozone. In the remote troposphere with very low NO_x, this relationship does not hold, however (Liu and Trainer, 1987).

The direct impact of composition trends on global tropospheric ozone operates through ozone forming photochemical precursors. In photochemical model calculations of clean continental or urban air, increases in NO_x, CH_4, CO, and NMHC are all related to increased tropospheric ozone, via the reaction mechanisms discussed above. There are many subtleties, however, which complicate quantitative predictions. Liu et al. (1987) infer from data obtained at Niwot Ridge, a clean continental site, that ozone production is a nonlinear function of NO_x and NMHC emission strength. The impact on predictive modeling is that calculations of tropospheric ozone distributions will be sensitive to details of the dispersion of NO_x and related reservoir species such as PAN. Models of lower dimension, in which NO_x emissions are effectively rapidly dispersed zonally or over large regions, can overpredict photochemical ozone formation rates. Isaksen and Hov (1987) have applied a 2-D tropospheric model to the question of the interaction of trends in CO, CH_4, and NO_x and their effects on ozone and OH over a period representing 1965 to 1995. Using simple assumptions of combined annual rates of growth or decline, they find that, in general, the sense and magnitude of ozone change is tied to the assumed NO_x trend. When NO_x is held fixed or increases, increases in CO or CH_4 result in increasing O_3 (and decreasing OH). When NO_x is assumed to decline, O_3 decreases also, even though CO, CH_4, and NMHC are concurrently increasing.

These results and those for tropospheric OH clearly demonstrate the importance of understanding the global distribution of NO_x in three dimensions over the range of scales from urban to global. Of particular pertinence is the significance of long-range transport of NO_x in the form of organic nitrates and peroxynitrates. The summer lifetime for NO_x is on the order of a day or less in the planetary boundary layer. The lifetime of PAN with respect to thermal decomposition is highly dependent on temperature and can be on the order of weeks or months in the middle troposphere. Singh et al. (1985) have speculated that PAN could serve to convey NO_x released in the boundary layer to the remote troposphere, where it plays an important role in affecting the background global abundances of OH and ozone.

OTHER CLIMATE CHANGE FEEDBACKS ON GLOBAL ATMOSPHERIC COMPOSITION

We summarized in Chapter 2 the trends in atmospheric composition that are the drivers for perturbation of atmospheric radiative transfer and climate change. Chapter 3 and Chapter 4 above discuss the effects that the expected climate change may have on regional and global tropospheric photochemistry. The temperature dependence of CH_4 and NMHC emissions by plants and soils mentioned above demonstrates another level of interaction. The changing emissions of trace species that are expected to drive climate change are also functions of climate change variables, through both natural and anthropogenic (economic) mechanisms.

A distinction can be made, in considering the interaction of climate change and anthropogenic source gas emissions, between the effects of actual climate change and those of anticipated climate change. Anticipated climate change can bring about reductions, which may or may not be mandated, in production and emissions related to efficiency improvements in equipment and processes, exploitation of alternatives and straightforward regulation of emissions. A current example is the Montreal Protocol on the production of several halocarbon compounds thought to act to deplete stratospheric ozone abundance. The decreases (or slowing of the rates of increase) in atmospheric abundances of several CFCs and the related stabilization of stratospheric ozone, which are expected to result from application of this agreement, will affect the future global atmosphere in the areas of surface and tropospheric ultraviolet fluxes, stratospheric climate, and surface-tropospheric climate. It is possible that means may be found to reduce combustion-related emissions in anticipation of global warming.

Analysis of the actual effects of climate change on anthropogenic emissions is far beyond the scope of this report, but we offer a few general speculations. Domestic energy consumption is a function of ambient temperature and should respond to changes in the temperature frequency distribution. Changes in temperature, frost dates, precipitation patterns, and water availability can certainly affect the choice of crops and could, for example, affect methane emissions.

Natural biospheric sources of CO_2, CH_4, CO, NMHC, and NO_x will also be affected by climate change. The CO_2 atmospheric abundance record shows both the seasonal variability of photosynthesis and respiration patterns of plants and variability related to ENSO climate perturbation events (WMO, 1985). It is not clear whether long-term temperature and precipitation changes can produce a secular trend in the distribution of carbon between the atmosphere, the biosphere, and the oceans, which would affect the CO_2 atmospheric abundance trend. For CH_4, wetland emissions are thought to be the major natural source. Clearly changes in the areal extent of wetlands resulting from climatological changes in the hydrologic cycle, as well as the temperature dependence of biologic activity, will affect the CH_4 source flux. This effect could be exacerbated by the enhanced warming in tundra and permafrost regions that is predicted by some general circulation models.

Finally, other interdependences of photochemistry and the climate system can be envisioned which cannot be quantified at present. For example, cloud cover plays a major role in atmospheric radiative transfer in both the visible and infrared wavelength regions. Biological activity in the oceans produces the short-lived sulfur species H_2S and dimethyl sulfide. They are oxidized in part to produce sulfate aerosol particles, which act as cloud condensation nuclei. If the fluxes of these species are affected by warming of the ocean surface water, changes in CCN concentration and cloud cover or properties could result. The DMS/cloud/albedo interconnection has been invoked recently to explain the Cretaceous-Tertiary extinction event in the following manner (Rampino and Volk, 1988). If a large proportion of ocean plankton were suddenly killed by darkness (following comet impact), the DMS emissions, CCN, and global cloud cover and albedo would all decrease. The Earth would then warm substantially, disrupting the saurian ecosystem. This is, of course, conjecture, but it illustrates the complexity of the climate system.

CHAPTER 5

MODELING CAPABILITIES AND LIMITATIONS

So far we have discussed a number of interactions between climate change and air chemistry that may affect the future state of the atmosphere. In this section we focus our attention on the availability of models to treat these scientific issues. Our purpose here is twofold. We want to assess the capabilities of present day models, and also to advocate construction of new models that are needed to improve the assessments of effects discussed above. To obtain better predictions of the effect of climatic changes upon global, regional, and local air chemistry, we must combine a number of different models that simulate different physical processes and operate on varying scales--for example, global-scale climate models, regional-scale weather models, and chemistry models. The question of how to couple models in a workable fashion is dealt with in the final part of this section.

Why use models? Put bluntly, the answer is that we have no choice if we wish to predict the future, or even to predict a range of possibilities for the future (the typical situation in environmental forecasting). Measurements of relevant quantities in the laboratory and in the field are indispensable for understanding the atmosphere. Such measurements, of course, cannot by themselves tell us what to expect as Earth's climate changes; to answer that question we must use some sort of theory or model to extrapolate from the present to the future.

Models in science can be extremely simple, but in atmospheric science they are often complex enough to require substantial use of supercomputers. Such is often the case with the models discussed below. These models are physically based; that is, they solve mathematical equations that express the laws of physics and the experimentally determined behavior of atmospheric constituents (e.g., chemical reaction rates). Accordingly, one might hope for the construction of one "perfect" model encompassing all relevant atmospheric processes, which would yield detailed and reliable forecasts of atmospheric conditions at all points on the globe. In practice, however, such a goal is not feasible. A model that kept track of all chemical and atmospheric properties of interest on local scales, and that extended over the entire globe, would overwhelm the capacity of even the best present day or foreseeable supercomputer. And even if a "super-supercomputer" were to arise, uncertainties in the input to such a machine--such as chemical reaction rates--would probably render the "perfect" model's output questionable.

Fortunately, there is a realistic alternative. A hierarchy of models have already been developed and applied to the various atmospheric processes (Schneider and Dickinson, 1974). For processes of interest in this report, the models have served to conceptualize theoretical understanding and thereby provide a foundation for the construction of coupled models. As we shall see, joining different models must be approached with caution, but could result in a useful degree of predictive power for effects connecting urban, regional, and global scale air chemistry and global scale climate.

Prediction of air quality on regional and local scales from the global climate obviously requires models which resolve the variability of wind, temperature, and other parameters of interest over the three dimensions of latitude, longitude, and altitude. A detailed discussion of these three-dimensional models will be found below. First, however, it is appropriate to mention models with more limited resolution; these have been and will continue to be useful in identifying key factors affecting global climate and its simulation by three-dimensional models. Table 5.1 depicts the hierarchy of one-, two-, and three-dimensional models. Most climate models fall into one of three categories: energy balance models (EBMs), radiative-convective models (RCMs), and general circulation models (GCMs). EBMs, as their name suggests, compute the average surface temperature by assuming a balance between solar energy absorbed by the Earth-atmosphere system and infrared radiation (IR) radiated by Earth to space (North et al., 1981); typically this calculation is performed for a number of latitude bands from the Equator to the Poles, but the variation of temperature with altitude is not explicitly considered. Thus, EBMs generally cannot handle the vertical exchanges of IR and solar radiation, or the vertical transport of heat by means of turbulent convection, by any means other than crude empirical parameterizations. RCMs,

Table 5.1

MODEL TYPE	TYPICAL RESOLUTION			LIMITATIONS
	Altitude	Latitude	Longitude	
EBM	none	5°-10°	none	overly empirical
RCM	0.1 km	none	none	no horizontal variations
2D GCM	1-5 km	2°-10°	none	no longitudinal variations
3D GCM	1-5 km	2°-10°	5°-10°	sub-gridscale processes

in contrast, are specialized to calculate just such radiative and convective transfers of energy (Ramanathan and Coakley, 1978)--but at the price of averaging over all horizontal variations, i.e., lumping land and ocean areas into one "average" surface type and ignoring the significant variations in solar energy amounts that are received at different latitudes, seasons, and times of day.

GCMs simulate not only radiative and convective energy transports, but also atmospheric circulation (winds), together with temperature, cloudiness, and precipitation over the globe; these are the most detailed models available to simulate climatic change (Saltzman, 1983). Some GCMs are two-dimensional, resolving their parameters in latitude and altitude, but not longitude. These models can either compute atmospheric circulation from the input of solar energy, with assumed constraints on atmospheric temperature (Wuebbles et al., 1987) or compute both atmospheric temperature and circulation self-consistently (Saltzman, 1978); in both cases, however, longitude-varying features ("eddies") cannot be explicitly calculated and must, therefore, either be parameterized using approximate empirical relationships or ignored altogether. Two-dimensional circulation models have been particularly useful in investigating connections among solar and infrared energy transfer, atmospheric circulation, and chemistry (Wuebbles et al., 1987). It has been difficult to address such problems with three-dimensional GCMs without consuming prohibitive amounts of computer time. However, many important atmospheric phenomena--for example, the development and movement of the "fronts" that characterize midlatitude weather systems--cannot be represented in a model that ignores or parameterizes eddies. This limitation may apply to important physical processes that transport chemical species. Thus it is likely that in the future, efforts to understand the interconnection between climate and air chemistry will increasingly make use of three-dimensional general circulation models.

GENERAL CIRCULATION MODELS

Three-dimensional GCMs are essentially the same as the computer models used for modern weather forecasting (Haltiner and Williams, 1980). The output of GCMs, however, is used not to forecast the occurrence of specific weather events, such as a storm occurring at a particular time and place, but rather to study longer-term changes in climate that occur over broader scales, such as changes in globally averaged temperature, or regional drought. A key assumption in GCM studies is the notion that while the forecast of specific weather events beyond a few weeks into the future is impossible, the prediction of more general climatic trends is possible.

GCMs calculate in straightforward fashion the time evolution of atmospheric structure and circulation, using well-known laws of classical physics such as conservation of mass, energy, and momentum. To solve the equations on a computer, however, it is necessary to divide the atmosphere into a large number of boxes and to solve for only the average temperature, wind, etc., within each box. With today's computers each box can be made no smaller than roughly a kilometer in height and a few degrees of latitude and longitude in its horizontal dimension; otherwise there would be too many boxes for the computer to handle in a reasonable amount of time. Therefore, present day GCMs must either ignore the "sub-gridscale" phenomena that take place on horizontal scales smaller than roughly a hundred kilometers, or parameterize these phenomena in terms of empirical relationships and grossly simplified physics, rather than explicitly simulate them from well-understood physical laws. Such phenomena include many of concern to this report, including the formation of clouds and the turbulent mixing of atmospheric pollutants near the planetary surface (Figure 5.1).

What justification, then, do we have for believing the results of GCMs? As we shall see, there are many details of GCM simulations of climate that are flawed, but there are good reasons for optimism about the ability to predict climatic change with GCMs. The fact that GCMs correctly simulate the cycle of the seasons, which is in effect a climatic change driven by known forcing (the variations in the amount of sunlight received at different latitudes over the year), is one confidence-builder (Schneider and Londer, 1984). Another is the recent series of successes in GCM simulations of past climates that are known through the geologic record (COHMAP, 1988) and even, to a limited extent, of the atmospheric states of other planets (Leovy, 1985).

It is therefore not unrealistic to hope that GCMs can provide analysis of global and regional climatic change of relevance to local, regional, and global air chemistry. GCMs are the most "complete" models available for studying the atmosphere and climate in all its aspects--the transmission of solar and infrared radiation, the generation of winds ("dynamics"), the hydrological cycle, and the interaction of the atmosphere with the oceans. GCM simulations of some of these processes are available only in crude form and require further development, but even in their present state GCMs are useful for studying interactions among the various components of the climate system. The following discussion of GCM flaws and limitations should be taken in a spirit of cautious optimism.

The main impediment to using GCM simulations of climatic change on a regional scale is that present day models give inconsistent results on this scale. As an example, we consider the increase in surface air temperature (ΔT) caused by the greenhouse effect of doubling the atmospheric concentration of carbon dioxide. The globally averaged temperature increase obtained by different GCMs spans the range from roughly 2°C to 5°C (NRC, 1982) with more recent models converging toward the higher end of this range (Schlesinger and Mitchell, 1985; Manabe, 1986; Wilson and Mitchell, 1987). As we consider increasingly detailed aspects of climate prediction, however, the agreement among the models diminishes and finally disappears. Grotch (1988) has compared ΔT among the more recent models, using as a quantitative measure of consistency the statistical correlations between results for different model pairs; 100% correlation would indicate perfect agreement, while scores much less than 50% indicate essentially no agreement. Grotch finds that for the Northern Hemisphere winter season, correlation scores for broad latitude bands are in the range of 80-95%, but when more limited areas, 12° latitude by 15° longitude, are considered, the correlations drop to 50-80%; these fall further to 40-70% when 40° by 5° areas are used for comparison between the models. In other words, although the models display considerable agreement on global and broad continental scales, they show virtually no agreement when their results are compared over smaller areas--for example, individual states in the U.S.--which are precisely the scales we are interested in for predictions of local and regional air quality.

Of course, consistency among models is not by itself a sufficient condition for accuracy of simulation (consistent models could all be equally wrong) but it is surely necessary to first understand why the models give different results. This problem is being directly addressed in a major initiative, sponsored by the U.S. Department of Energy, to intercompare the GCM-simulated climatic changes (Grotch, 1988). Since the models all solve the same equations for large-scale atmospheric circulation and temperature structure, the fault presumably lies in the parameterization of small-scale processes discussed above. Sub-gridscale parameterization has been identified as responsible for one inconsistency among GCMs, the presence or absence of summertime drought in the American Midwest as a consequence of CO_2 doubling (Manabe and Wetherald, 1986; MacCracken et al., 1986). Mitchell and Warrilow (1987) and Meehl and Washington (1988) conclude that the appearance of this drought in GCMs depends critically upon the assumptions made about the ability of the soil to hold moisture. In the words of Mitchell and Warrilow (1987), "the magnitude of them simulated summer drying is dependent on the [assumed] physical attributes of the soil, and in certain regions can be reduced or

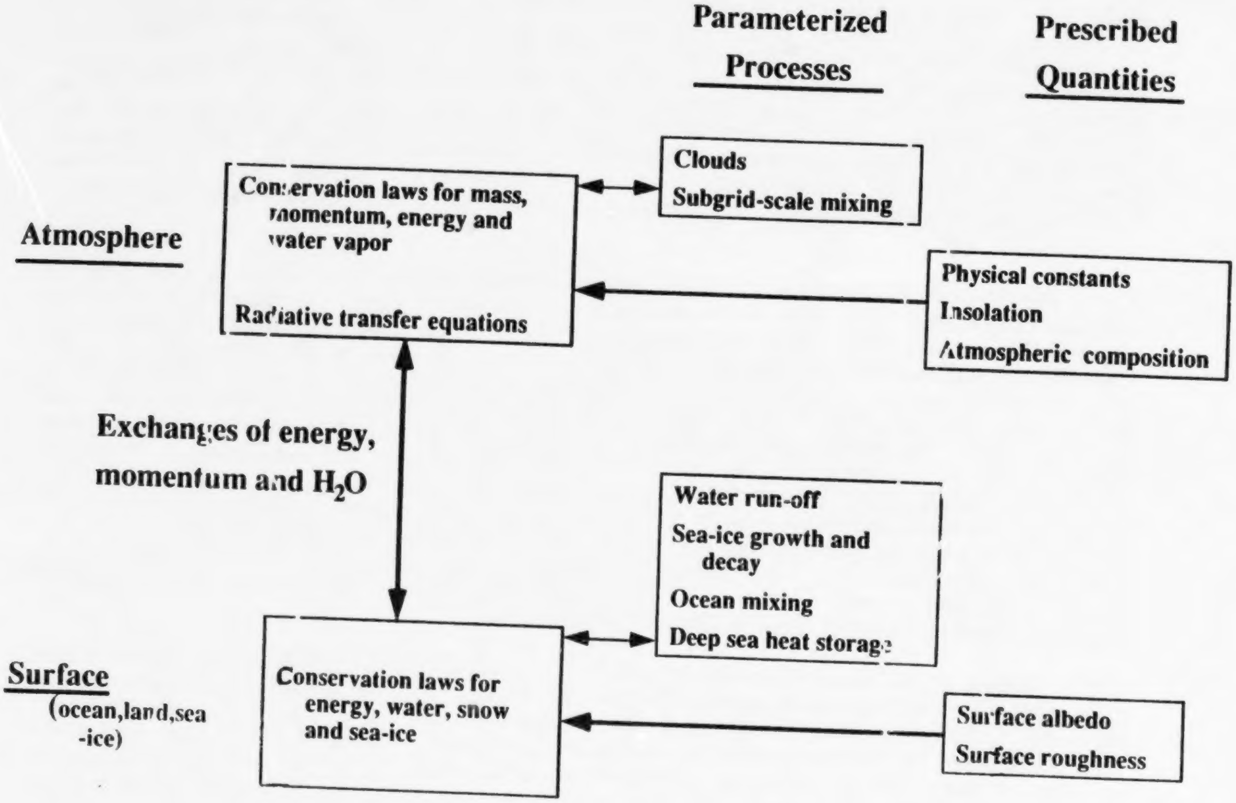
Parameterized Processes
Prescribed Quantities
Atmosphere
Conservation laws for mass, momentum, energy and water vapor
Radiative transfer equations
Clouds
Subgrid-scale mixing
Physical constants
Insolation
Atmospheric composition
Exchanges of energy, momentum and H2O
Water run-off
Sea-ice growth and decay
Ocean mixing
Deep sea heat storage
Surface
(ocean,land,sea-ice)
Conservation laws for energy, water, snow and sea-ice
Surface albedo
Surface roughness

Figure 5.1. Processes and interactions represented in a typical climate model (from Taylor and Grotch, 1987).

even reversed by an alternative, but equally plausible, treatment of run-off [of water into streams and rivers]..." The lesson is that seemingly minor differences in a model's parameterization of small-scale processes can lead to major errors in he model's simulation of regional and local details of climate.

A number of processes come to mind as candidates for improved parameterization. Some are of direct import to the transport and dispersal of atmospheric pollutants, such as turbulence in the boundary layer near the planetary surface (Deardorff, 1972; Mellor and Yamada, 1974) and convection and cloud formation (Arakawa and Schubert, 1974; Kuo, 1974). Others do not directly influence local and regional air quality but are significant factors in the determination of climate, for example, in addition to the question of soil moisture discussed above, the behavior of sea ice (Semtner, 1984) and the upper mixed layer of the ocean (Niiler and Kraus, 1977). A variety of workable parameterizations for GCMs are given in the references cited above; what is needed now is a systematic intercomparison of how the parameterizations affect GCM simulations in detail. Of course, the GCM results must be compared not only with each other but also with the real world's climate. Toward this end an enhanced global observing system, probably emphasizing remote sensing from space, is needed (NASA, 1986).

Finally, we must emphasize that realistic time-dependent analysis of climatic change is not generally available from GCMs. For example, the simulations of CO_2 greenhouse warming discussed above all refer to an equilibrium response; in the simulations, atmospheric CO_2 concentration is abruptly doubled and maintained thereafter at a constant level until the model achieves a steady-state climate, which is then analyzed as the "response to CO_2 doubling." The actual climatic change the world undergoes in response to steadily increasing carbon dioxide is a complicated affair, with different components of the climate system--air, land, and ocean--approaching equilibrium at different rates; the resulting climate patterns do not necessarily resemble the equilibrium response (Schneider and Thompson, 1981). Simulations of this time-dependent process are difficult to perform because it is necessary to consider not only the circulation of the atmosphere but also the circulation of the ocean as it slowly responds to the new climate; what is required is an ocean GCM coupled to an atmospheric GCM, an unwieldy combination that consumes great amounts of supercomputer time. The small number of coupled time-dependent ocean/atmosphere simulations performed to date (e.g., Spelman and Manabe, 1984; Nihoul, 1985; Sperber et al., 1987) involve unsatisfactory simplifications such as idealized geography (Thompson and Schneider, 1982) and limited run times.

In summary, GCMs are essentially the same weather prediction models that have been extensively used for decades--with steadily increasing accuracy (Haltiner and Williams, 1980)--by national weather services around the world. GCMs are used to forecast not specific weather events but rather more general climatic trends. Their ability to do so is difficult to determine since the opportunities for comparison with the real world are far more limited than is the case with numerical weather prediction, but indications are that current GCMs give generally reliable climate simulations for the largest spatial scales, that is, the scales of large continents or of the entire globe. On the smaller scales of interest in this report, simulations are not yet reliable, but correction of the problem may be found by a thorough testing of sub-gridscale parameterizations, a straightforward task given commitment of sufficient resources.

GLOBAL CHEMISTRY MODELS

Development of computational models over the last two decades to study atmospheric chemical processes has revolutionized our understanding of global atmospheric chemistry. These models have allowed us to analyze, as well as appreciate, the nonlinear interactions between atmospheric chemical processes. They give us insight into the complexities of the interactions of these processes with radiative and dynamical processes in determining the distributions of atmospheric trace constituents. Global atmospheric models have also been extensively used in attempts to understand the impact that human activities are having on atmospheric chemistry, in particular on ozone concentrations in the troposphere and stratosphere.

Until the last few years, the one-dimensional (1-D) horizontally averaged model has been the mainstay for theoretical chemistry studies of the troposphere and stratosphere. Because of their computational efficiency, such models can treat the full complexity of the chemistry schemes needed to simulate these regions. Typical calculations can involve the simultaneous, coupled interactions of more than 30 species and over a hundred chemical and photochemical reactions, with detailed calculations of the diurnal variations in the solar flux as a function of altitude. Radiative processes can also be accounted for in these models, and it is now standard for temperature feedbacks on atmospheric chemistry to be included.

A severe limitation of the 1-D model lies in its crude representation of atmospheric transport processes. These models parameterize all transport effects in terms of vertical diffusion. This diffusive treatment is purely empirical, with a vertical diffusion coefficient based on observations of the temporal and spatial distributions of selected tracers. The derived diffusion coefficient is then applied equally to all atmospheric constituents in current models, although methods have recently been proposed (Holton, 1986) for species-dependent dynamically based transport parameterizations.

A further limitation of 1-D models is the obviously implied use of average global rates for photochemical reaction rates. Spatial correlations of short lifetime species cannot be directly simulated and this complicates interpretation of 1-D results, leading to controversy over the meaning of calculated distributions of various species. Nonetheless, the 1-D model remains a useful theoretical tool because it works--simulating well many of the important features in the vertical distributions of atmospheric constituents and comparing well with the globally averaged results of two-dimensional models for perturbed atmospheres.

Zonally averaged two-dimensional (2-D) models are now becoming the workhorse for studies of the global atmosphere. While the 1-D model can only provide information on the horizontally and annually averaged vertical profile, the 2-D model includes the important latitudinal and seasonal dependences in atmospheric processes. Two-dimensional models can, in principle, simulate the effects of zonally averaged meridional and vertical mean and eddy transports, while also accurately accounting for the meridional variations in photochemistry.

Recent 2-D models can include essentially the same chemistry and radiative transfer treatments as have been traditionally associated with 1-D models. As an example, the LLNL two-dimensional chemical-radiative-transport model calculates the concentrations of 30 atmospheric trace constituents at about 300 grid zones extending from pole to pole and from the ground to the stratopause. A complete radiative transfer submodel is used to determine solar heating and infrared cooling rates that then drive the diabatic circulation in the model and allow for trace species feedback effects on stratospheric temperatures. This and other 2-D models are being applied to extended time-dependent studies of anthropogenic effects on global ozone in research sponsored by NASA.

The ultimate fidelity of the two-dimensional model depends primarily on the accuracy with which the zonally averaged transport of trace constituents can be represented, and is limited by spatial and temporal heterogeneity of short-lived species. Theoretical advances have produced major improvements in the understanding and formulation of 2-D models in recent years. The theoretical basis for 2-D models, along with their associated limitations, is reasonably well understood. Significant uncertainties remain, especially regarding the treatment of eddy transport processes in these models, including the treatment of interactions between eddy and mean transport processes. Existing two-dimensional models do, however, provide a generally good description of the spatial and temporal variations of trace constituents, within the limitations of current observational data bases.

While the two-dimensional model has been brought to the level of being a sophisticated tool for diagnostic and assessment studies, its fundamental limitations suggest that we should ultimately turn to three-dimensional (3-D) models. Besides the difficulty in treating three-dimensional atmospheric dynamics in 1-D and 2-D models, these models are especially inadequate in the study of photochemical processes in the lower troposphere. The short chemical lifetimes of many lower atmospheric constituents when combined with the significant variations in land-based versus ocean-based source strengths require the development of 3-D chemistry models. The development of these models has been slow, however, because of the computational expense in treating realistic global atmospheric chemistry with a three-dimensional model. As a result, while there have been many studies of stratospheric chemical processes, theoretical modeling studies of chemistry processes in the troposphere have been limited in scope. While many studies with 1-D models exist and a few with 2-D models (e.g., Isaksen and Hov, 1987; Thompson and Cicerone, 1986; Thompson et al., 1988; Liu et al., 1987), global tropospheric chemistry studies are necessarily limited by the unavailability of 3-D models.

Although 3-D models with complete chemistry will not have meaningful results for several years, such models are being developed and already are being applied, in a limited manner and with limited chemistry, to scientific problems. Walton et al. (1987), using the LLNL 3-D model GRANTOUR, have investigated the effects of anthropogenic NO_x emissions on nitrate deposition on a global scale. Prather et al. (1987) have used the 3-D tropospheric chemistry model being developed at NASA GISS to study the relationship between emissions of chlorocarbons and observations expected at various sites. Each of these models uses winds, temperatures, and other input parameters based on calculations from GCMs.

In the future, it will be possible to fully couple 2-D and 3-D models with GCMs and other climate models. This coupling will be important to determining the role of chemistry-climatic feedbacks on the atmosphere, and to determining the effects that future climate change may have in modifying global chemistry, particularly to ozone and OH concentrations in the troposphere and stratosphere.

The above discussion has highlighted many of the current capabilities and limitations in modeling of global atmospheric chemistry. In addition, there are many remaining uncertainties that also affect our ability to model global chemistry. Uncertainties remain in the reaction rates and chemical schemes used in these models. Feedbacks between chemical processes and other atmospheric processes represented in the models are still poorly understood. For meaningful evaluations of future climate and chemical interactions in the atmosphere, further research and model development are required to overcome current limitations and to reduce remaining uncertainties.

URBAN/REGIONAL MODELS

Many different types of models have been developed to study atmospheric chemistry problems on urban to regional scales. These range from simple box models, with no consideration of meteorology effects, to complex three-dimensional models with internally derived mesoscale meteorology. In general, the complexity of actual meteorological structure, the effects of topography, the variability in emission sources, and the nonlinearity of relevant chemical mechanisms have indicated that, for many problems, simple box and trajectory (or Lagrangian puff) models are insufficient tools and that higher dimensional models are required. For this reason, our discussion of urban and regional models will be confined to describing the capabilities and limitations of existing multidimensional Eulerian models that include detailed treatments of emissions, atmospheric chemistry, transport, and other relevant processes.

Figures 5.2 and 5.3 give an indication of the complex interactions of atmospheric processes that are treated in urban/regional models. Current models have achieved a high degree of sophistication in their treatments of these processes. Some of the more important examples of urban and regional models are the Regional Acid Deposition Model (RADM) developed for the U.S. Environmental Protection Agency at the National Center for Atmospheric Research and at SUNY Albany (Chang et al., 1987), the Regional Oxidant Model (ROM) developed by the Environmental Protection Agency (Lamb, 1982, 1983, 1985, 1987), the Regional Transport Model developed by Systems Applications Inc. (Liu et al., 1984; Morris et al., 1987), and the Livermore Regional Air Quality model (LIRAQ) developed at Lawrence Livermore National Laboratory (MacCracken et al., 1978; Penner and Connell, 1987). Tables 5.2 through 5.5 give a short description of each of these models. These tables provide a guide to comparing the different approaches used by each group in modeling of urban and regional air quality.

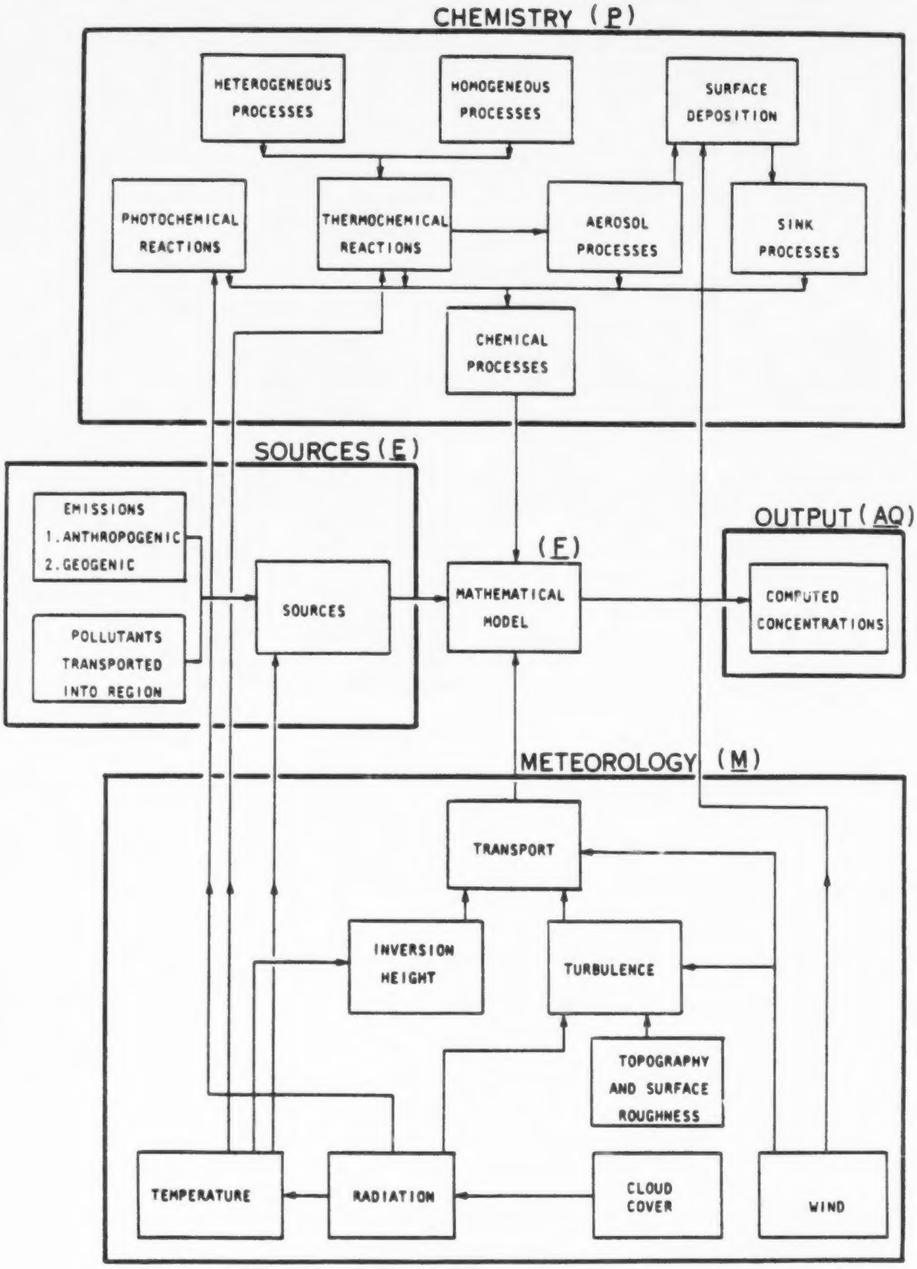
CHEMISTRY (P)
HETEROGENEOUS PROCESSES
HOMOGENEOUS PROCESSES
SURFACE DEPOSITION
PHOTOCHEMICAL REACTIONS
THERMOCHEMICAL REACTIONS
AEROSOL PROCESSES
SINK PROCESSES
CHEMICAL PROCESSES
SOURCES (E)
EMISSIONS
1. ANTHROPOGENIC
2. GEOGENIC
POLLUTANTS TRANSPORTED INTO REGION
SOURCES
(F)
MATHEMATICAL MODEL
OUTPUT (AQ)
COMPUTED CONCENTRATIONS
METEOROLOGY (M)
TRANSPORT
INVERSION HEIGHT
TURBULENCE
TOPOGRAPHY AND SURFACE ROUGHNESS
TEMPERATURE
RADIATION
CLOUD COVER
WIND

Figure 5.2. Elements of a mathematical model for relating pollutant emissions to ambient air quality (from McRae et al., 1982).

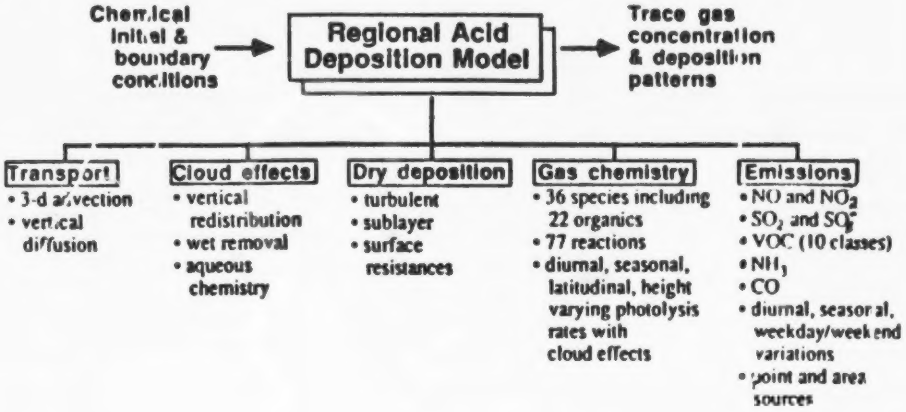
Chemical initial & boundary conditions
Regional Acid Deposition Model
Trace gas concentration & deposition patterns
Transport
• 3-d advection
• vertical diffusion
Cloud effects
• vertical redistribution
• wet removal
• aqueous chemistry
Dry deposition
• turbulent
• sublayer
• surface resistances
Gas chemistry
• 36 species including 22 organics
• 77 reactions
• diurnal, seasonal, latitudinal, height varying photolysis rates with cloud effects
Emissions
• NO and NO2
• SO2 and SO4=
• VOC (10 classes)
• NH3
• CO
• diurnal, seasonal, weekday/weekend variations
• point and area sources

Figure 5.3. Overview of a regional acid deposition model - RADM (from Chang et al., 1987).

The primary difference between urban models and regional models is the physical domain they attempt to simulate. An urban model, such as the one at LLNL mentioned above or the model at the California Institute of Technology (McRae et al., 1982), considers an area about 200 km by 200 km or smaller, a size appropriate to analyzing the production and transport of photochemical oxidant and other trace constituents important to air quality in an urban area on a single or several-day basis. Regional models, such as RADM or RTM, simulate atmospheric chemical and physical processes on much larger domains, on the order of 2,000 km by 2,000 km, about the size of the eastern third of the United States. These models are also used to study oxidant formation, with coarser resolution than urban models over these larger domains, and can, when appropriately designed, be used to study regional acid deposition ("acid rain"). Each of the models described here is spatially three-dimensional, containing multiple vertical layers to account for the effects of variations in transport and mixing with altitude, and to include interactions with the free troposphere.

Each of these models is designed to consider the effects of area and point source emissions of pertinent pollutants and pollutant precursors, chemical transformation processes, meteorological conditions influencing horizontal and vertical transport and dispersal, natural background trace gas concentrations, and dry deposition. In addition, models designed to study regional acid deposition, such as RADM, also include detailed representations of effects associated with clouds such as aqueous chemistry, scavenging, and sub-gridscale vertical transport of trace species. In general, the models designed primarily to study oxidant formation are not designed to study the formation and deposition of acidity; however, simulating either oxidant formation or acid deposition necessitates that similar treatments of many of the chemical and physical processes be included in both types of models.

The primary drivers in the simulation of air quality in these models are the inventories of emitted species and of meteorological conditions used as input parameters to the model derivations. Uncertainties in either the emissions or in the wind speed and direction can have a significant influence on the derived trace constituent concentrations. For example, Morris et al. (1987) suggest that their model's tendency in some calculations to underpredict ozone peak levels is likely related to deficiencies in the complex-terrain wind fields and in the inability of the model to resolve local NO emissions. Many of the models have based their representations of meteorology on interpolations and analyses from available observations. However, because spatial and temporal resolution of these measurements is often not sufficient, newer models such as RADM are using primitive equation meteorological models to generate the required input information. These mesoscale models allow for better internal consistency of dynamical, thermodynamic, and hydrologic processes. However, uncertainties still exist with this approach, as predicted meteorological fields tend to diverge from observed values after a few days unless observed data assimilation approaches are used (NAPAP, 1987).

A major problem with urban/regional models, particular in the assessment of impacts from climatic change, is their limitation to simulating episodes of only a few days. Computational expense and the lack of sufficient high-quality input data tend to limit the model calculations to being run episodically. The difficulty of representing seasonal to annual changes in climatology with such episodic-based models has not yet been resolved. Likewise, aggregating a subset of events to determine longer-term effects has not yet been shown to be a viable approach.

Overall, the current urban/regional models have demonstrated the capability to simulate many chemical and physical processes important to the transport and transformation of trace constituents determining air quality. However, many uncertainties still exist. The detailed chemical mechanisms used in these models have uncertainties associated with the kinetics of NMHC species, particularly aromatics, and with heterogeneous chemical processes. Parameterizations of gas and aqueous phase chemical interactions, the effects of clouds, and dry deposition need to be verified by observations. As discussed earlier, uncertainties in externally based input parameters, such as emission rates, initial and boundary conditions, temperature, winds, and other meteorological conditions, can produce errors in the model-derived species distributions.

Table 5.2. The Regional Oxidant Model - ROM (Shere, 1988)

Physical Domain

60 grid cells E-W
42 grid cells N-S
3 prognostic, 1 diagnostic vertical layers of spatially and temporally variable depth (<3000 m agl)
Typical domain size 1100 x 800 km.

Spatial Variables

λ,ϕ: horizontal curvilinear coordinates from grid origin in degrees.
z : distance above ground level in meters.

Grid Resolution

Horizontal: 1/6 degree latitude by 1/4 degree longitude

Vertical: Generally layers 1 and 2 represent the mixed layer during the day. Layer 1 is also used to represent any internal boundary layers present. Layer 3 is the cloud layer, extending from the cloud base to the tops of any convective-type clouds present. The depth of the diagnostic layer 0 is typically on the order of 30-50 m.

Chemical Scheme

Carbon bond 4 (CB-4.0 with 28 chemical species.

Hydrocarbon classes: ETH (ethylene), OLE (olefins), PAR (paraffins), FORM (formaldehyde), ALD2 (higher aldehydes, TOL (toluene), XYL (xylene and other aromatics), ISOP (isoprene), and NONR (non-reactive hydrocarbons except methane).

Homogeneous Chemistry

70 reactions.

Heterogeneous Chemistry

Sulfur compounds and primary and secondary aerosols not currently included.

Atmospheric Structure

Determined from observed data. Twice daily radiosonde reports and hourly surface meteorological data determine the basic meteorological variables. Temporal and spatial interpolation of observed variables: temperature, dew point, pressure, horizontal winds, and cloud cover and types.

Photolysis Treatment

Photolysis rate constant for NO_2, O_3 ($O(^1D)$path), FORM (radical products), FORM (stable products), and ALD2 (radical products) are determined individually during execution as functions of solar zenith angle and grid cell elevation. Table lookup of clear sky values (91 zenith angles and 10 elevations). Solar flux values from Dave radiative transfer model. The final values are scaled by a cloud transmissivity factor. Other values are linearly related to NO_2 photolysis constant.

Wind Field Generation

Hourly gridded horizontal wind fields are determined from interpolations of observed winds, based on mass conservation and minimum kinetic energy constraints. The only exception is for layer 1 during nighttime conditions when a prognostic shallow-water fluid model is used to determine the wind flows in the stable inversion layer closest to the ground.

Table 5.2. The Regional Oxidant Model - ROM (Schere, 1988) (continued)

Transport Treatment

Horizontal transport and diffusion are solved numerically in ROM with a biquintic polynomial technique that is independent of the Courant condition. Vertical exchange between layers is accomplished by mass conservation and the specification of turbulent vertical velocities at the layer interfaces. A unique convective cloud flux is also able to transport material from near the ground directly into the base of growing cumulus clouds in the third model layer, with little entrainment into intervening layers.

Chemistry Solution

Predictor-corrector version of the QSSA (quasi-steady state algorithm) that also computes a variable time step based on the photochemical lifetimes of key species. No explicit steady states are used and all species are transported.

Time-dependent Integration

The modeled concentrations are given by:

$c(t) = \Gamma(t)\, \gamma(t)\, \Upsilon(t)$

where Γ is the advective transport solution, γ is the normalized chemistry solution, and Υ is the normalized vertical flux solution. Each component is solved by forward time differencing with algorithms and time steps unique to each. Integration of the vertical flux and chemistry solutions is performed at 5-minute intervals, and integration of all three components is performed at 30-minute intervals.

Boundary Conditions

Lateral boundary concentrations for ozone are determined from selected monitoring stations located near the upwind edges of the domain and are updated every 12 hours. Values for other species are assumed to be near tropospheric background values, subject to the constraint that they be brought into chemical equilibrium with each other and with the specified ozone value. Boundary conditions at the top of the domain are assumed to be spatially and temporally invariant, and are the chemically equilibrated tropospheric background values.

Heterogeneous Deposition

No heterogeneous deposition.

Surface Deposition

Resistance theory model with deposition velocities taken from the literature.

Diurnal Effects

Incorporated in vertical layer structure. Layer 1, during the day, models approximately the lower 100 m of the well-mixed layer; at night, the layer expands to represent the radiative inversion layer, capped by a nocturnal jet. Layer 2, during the day, represents the bulk of the mixed layer; at night, it is a transport layer for the photochemical products. Layer 3, during the day, is the cloud layer, including direct vertical entrainment of near-surface air; at night, the layer is a transport layer for this material as well as photochemical products.

Table 5.2. The Regional Oxidant Model - ROM (Schere, 1988) (continued)

Sub-gridscale Processes

Layer 0 attempts to model the expected sub-gridscale variations of modeled concentrations based on the non-homogeneity of emissions sources within a grid cell. No transport is considered in this layer and NO_x scavenging of ozone within source plumes is considered to be instantaneous. Concentrations and concentration variances are estimated in this diagnostic approach.

Table 5.3. The RTM-III Model (Gery and Morris, 1988)

Physical Domain

User specified. Examples include:
Eastern U.S. (2080 x 1840 km)
Western Europe 34° x 12.5° (2232 x 1388 km)
Midwest/Southeast U.S. 42° x 35° (3820 x 3885 km)
Central California Phase I (210 x 340 km)
Central California Phase II (520 x 320 km).

Spatial Variables

3-D fields of constituents, T, H_2O (g), layer depths, u, v, w
2-D fields of surface wind speed, precipitation, cloud cover, emissions, surface characteristics.

Grid Resolution

User specified, to date 10-55 km.

Chemical Scheme

Carbon Bond 4 (CB-4.0) with 28 chemical species
Hydrocarbon classes: ETH (ethylene), OLE (olefins), PAR (paraffins), FORM (formaldehyde), ALD2 (higher aldehydes), TOL (toluene), XYL (xylene and other aromatics), ISOP (isoprene), and NONR (non-reactive hydrocarbons except methane).
Expansion to 33 species underway.

Homogeneous Chemistry

64 reactions, expansion to 81 reactions underway.

Heterogeneous Chemistry

Not treated.

Atmospheric Structure

Homogeneous tropospheric model.

Photolysis Treatment

Light and spectral distribution vary diurnally (zenith angle). Aerosol loading, molecular scattering, ozone column density and albedo also considered. Photolysis varies with light intensity and the spectral distribution for each species.

Wind Field Generation

Application dependent
Objective analysis (Eastern U.S.)
Dynamic meteorology models (Western Europe, Midwest/Southeast U.S.)
Hybrid diagnostic/dynamic models (Central California).

Transport Treatment

Sharp and Smooth Transport Algorithm (SHASTA).

Chemistry Solution

Quasi-Steady-State relationship with Crank-Nicholson integration scheme.

Table 5.3. The RTM-III Model (Gery and Morris, 1988) (continued)

Time-dependent Integration	Time steps range from 3 to 30 minutes depending on stability and convergence criteria.
Boundary Conditions	User specified, may be spatially and temporally varying.
Heterogeneous Deposition	Gaseous wet deposition uses solubility approach Particle wet deposition uses algorithms of Scott (1978).
Surface Deposition	Resistance theory model, diagnostic surface layer.
Diurnal Effects	Implemented for photolysis of individual species, emissions, and deposition.

Table 5.4. The Regional Acid Deposition Model - RADM (Chang et al., 1987)

Physical Domain
Horizontal 2000 x 2000 km
Troposphere depth.

Spatial Variables
3-D fields of constituents, T, u, v, q_v
2-D fields of precipitation, deposition, P_{surf}.

Grid Resolution
80 km horizontal, 80-8000 m vertical.

Chemical Scheme
36 species, 22 organics, 11 radicals.

Homogeneous Chemistry
77 reactions.

Heterogeneous Chemistry
8 reactions including aqueous SO_2 oxidation, nitric acid formation from aerosol/NO_3.

Atmospheric Structure
Predicted from meteorology model.

Photolysis Treatment
Full δ-Eddington radiative transfer model of troposphere with cloud effects.

Wind Field Generation
Meteorology model with hourly resolution.

Transport Treatment
Smolarkiewicz (corrected upstream).

Chemistry Solution
Exponential-assisted predictor-corrector.

Time-dependent Integration
Time steps range from <10 to 150 seconds.

Boundary Conditions
User specified, varying.

Heterogeneous Deposition
1-D cloud chemistry/scavenging model.

Surface Deposition
Resistance theory model.

Diurnal Effects
Fully implemented.

Table 5.5. The LLNL Regional Air Quality Model (Penner and Connell, 1987)

Physical Domain
Flexible, 100-200 km in horizontal
Currently 2 layers in vertical to approximately 2000 m.

Spatial Variables
Fixed horizontal spatial grid, time varying vertical grid
3-D fields of trace constituents, u, v, w
2-D fields of deposition.

Grid Resolution
1-5 km horizontal, 50-2000 m vertical.

Chemical Scheme
22 species, 5 lumped hydrocarbon classes, 3 organic radicals.

Homogeneous Chemistry
60 reactions.

Heterogeneous Chemistry
Not treated.

Atmospheric Structure
Daily sounding and surface measurements of wind speed, cloud cover. Model is currently isothermal.

Photolysis Treatment
Table lookup based on zenith angle from values generated by LLNL 1-D troposphere/stratosphere model, including effects of multiple-scattering and cloud coverage.

Wind Field Generation
From analysis of data with mass-consistent interpolation model, hourly resolution.

Transport Treatment
Smolarkiewicz (corrected upstream).

Chemistry Solution
Predictor-corrector with steady-state assumptions for some species.

Time-dependent Integration
Operator-splitting with base 10-minute advection time step. Variable time step chemistry solution.

Boundary Conditions
User specified constituent fields typically representing rural or ocean abundance levels, varying.

Heterogeneous Deposition
Not treated.

Table 5.5. The LLNL Regional Air Quality Model (Penner and Connell, 1987) (continued)

Surface Deposition
Resistance theory model.

Diurnal Effects
Zenith angle dependence of photolysis constants
Diurnal variation of mixed layer depth.

Bridging Across Spatial Scales

This chapter has discussed the tools available for evaluation of the interactions between climate change and atmospheric chemistry. Climate change is essentially the product of general circulation models. These predict precipitation patterns, wind patterns, global cloudiness, and temperature change with a resolution no better than several hundred kilometers. Because many important processes take place on smaller scales, these must be parameterized in the models, leading to inconsistent results on the scales important to regional chemistry. Figure 5.4 shows characteristics of typical current regional, global chemistry, and global climate models. Note that there are no arrows showing connections between existing models.

Regional and urban chemistry and deposition models need meteorological and climate change information on much smaller scales. Typically, an urban oxidant model would occupy much less than one grid square of a general circulation model. Regional models require a detailed description of the meteorology appropriate to, at most, several GCM grid points. A challenge for the future is to design a means for bridging across these spatial scales (assuming the GCM predictions for climate change on a regional basis become more robust). Some initial work in this direction has begun, but these initial efforts will require significant ongoing support to understand the level of confidence that might be placed in their predictions. A further challenge is to try to bridge the evident differences in time scales. GCM calculations attempt to predict statistics of the predicted climate averaged over a reasonably long period--i.e., one week or more. Regional and urban models have only been applied to particular episodes--with at most a several-day time period. A method for interpreting the results of the episodic predictions, within the context of the climate change statistics, must be devised.

The connections between global chemistry models and regional and urban models are even more tenuous. Three-dimensional chemistry models capable of treating the horizontally inhomogeneous gas concentrations evident in the global troposphere are only now beginning to be developed. Sub-grid-scale parameterizations that currently plague the GCM simulations will likely have impacts for the chemistry models as well. Further, sub-grid-scale parameterizations of chemistry are likely to be important in these models as well, because chemical processes that alter concentration distributions on urban and regional scales would need to be treated in some realistic fashion. It will likely be important to develop schemes to make the chemistry on these larger scales consistent with the chemical transformations that we know take place on smaller scales.

Unfortunately, little is known about the effect of chemical transformations across such spatial scales. Much research needs to be done, and, as appropriate, new modeling tools need to be developed to account for the necessary bridging across spatial scales. Modeling capabilities are needed not only to provide more accurate representation of urban processes in regional models or regional processes in global models, but also to provide meaningful input data from global models to regional to urban models.

Finally, regardless of our ability (or lack thereof) to physically link these modeling systems, our basic knowledge of the global tropospheric chemical system needs refinement and tuning. Our knowledge of biogeochemical cycles is crude at best. Therefore, our ability to confidently predict trace gas trends is crude, and certainly our ability to predict the impact of climate change on biologically emitted source gases is nearly nonexistent. Hence substantial effort is called for to truly understand the interactions of our planet's chemistry and climate systems.

Global chemistry models

- Explicit chemistry
- 1-D or 2-Dimensional
- Resolution: Entire hemisphere or 100's of kilometers of latitude
- Seasonal statistics

Climate models

- No chemistry
- 3-Dimensional
- Resolution ~ 100's kilometers
- Seasonal statistics

Regional chemistry models

- Parameterized HC chemistry
- 3-Dimensional
- Resolution ~ 5 - 10 kilometers
- Episodic event simulations

Figure 5.4. Characteristics of current models.

CHAPTER 6

CONCLUSIONS AND RESEARCH NEEDS

The primary purpose of this report has been to examine the possible interactions that may occur between a changing climate and atmospheric chemical processes. In particular, the focus has been on tropospheric chemistry and the interactions with climate change that could occur on spatial scales extending from the urban to regional to global. A number of conclusions can be drawn from the analyses presented, and many of these will be described below. While the potential for climate change in coming decades is also discussed in this report, it is not the major emphasis, and the discussion below will only attempt to cover a few highlights.

The single most significant finding in this study is that very little is known about the effects of such interactions, either on climate or on air quality. Few modeling studies or pertinent observational data exist that allow quantification of the effects that climate change could have on urban or regional or global chemistry, or vice versa. Likewise, little is known about the importance of chemical transformations that may occur in transition from the modeling of one spatial scale to another.

Some of the major findings of the analyses reviewed or developed in this report are:

1. There is sufficient evidence to indicate that atmospheric emissions and concentrations of radiatively and chemically important trace gases, such as CO_2, CH_4, N_2O, CF_2Cl_2, $CFCl_3$, and CO, are increasing, and have been increasing for a long time. These increases derive largely from human-related activities. Current analyses suggest that it is improbable that present trends toward increasing concentrations will be arrested or reversed in the near future. Predictions of future scenarios for their growth are limited by uncertainties in trace gas budgets and in forecasting economic growth, energy use, and other factors.

2. The direct effects from the radiative forcing from these gases on climate are not in question. However, there are many uncertainties associated with the climate feedback processes that will determine the eventual change in temperature and other climatic variables. Climate models indicate that global surface temperatures for a doubling of CO_2, the radiative equivalence of which could occur by mid-21st century, is in the range of 1.5 to 4.5°K, with general circulation models giving results in the upper end of this range.

3. General circulation models are in general agreement regarding the effects of climate change on a global basis, but are in substantial disagreement on the effects over specific regions. Representations of clouds, the planetary boundary layer, and surface processes all contribute to the uncertainties in determining the derived climate change. Currently, the results from GCMs should not be regarded as reliable indicators of regional effects from climate change.

4. The effects of climate change on urban and regional scale chemistry could be quite significant, but very little information currently exists on the sensitivity of air quality models to climatic parameters. The few studies available suggest that oxidant formation may be sensitive to changes in temperature, in stratospheric ozone, in cloud cover, in boundary layer depth, in background concentrations, and in induced emissions responses. No information exists on whether the frequency of stagnation episodes would be affected by climate change.

5. Likewise, little is known about how acid deposition would be affected by climate change. Types of climate change that could affect the conversion rate of SO_2 to sulfate and the acid deposition include changes in temperature, stratospheric ozone, background concentrations, circulation patterns, frequency and types of clouds formed, and precipitation patterns.

6. Interactions between climate change and global tropospheric chemistry primarily center around perturbations to the distributions of ozone and the hydroxyl radical. Changes in ozone, driven by increasing

concentrations of CO and NO_x for example, can have a direct impact on climate. At the same time, climate change can influence ozone concentrations. Hydroxyl radical is the primary chemical scavenger of such radiatively and chemically important gases as CH_4, NMHC, and CO; therefore, changes in OH concentrations, whether due to direct emissions of CH_4 or CO, or due to climate-induced changes in temperature or H_2O, can have a significant impact on the lifetimes and transport of radiatively active gases.

7. Studies of global tropospheric chemistry are currently limited due to unavailability of three-dimensional global scale models that can adequately account for the spatial variations in trace gas emissions and photochemistry.

8. Urban and regional emissions, particularly of NO_x and NMHC, may affect global scale tropospheric chemistry and thus affect climate. However, the chemical forms of these species by the time they reach the global scale are not well known nor represented adequately in current global models. Likewise, the extent to which O_3 formed from these precursors within the urban environment is exported to affect hemispheric backgrounds is unknown.

9. In general, the current modeling tools available, both in terms of climate models and air quality models, are insufficient to delineate meaningful diagnostic or prognostic analyses of all of the changes in climate parameters of interest.

The findings from this study lead naturally to the development of a list of important research needs. Research needed to provide a useful evaluation of the interactions between climate change and atmospheric chemistry, and to determine the effects of climate change on air quality, includes the following:

1. Biogeochemical cycles and the role of human-related emissions and removal processes need to be better understood through monitoring, specific process-oriented measurements, and theoretical model-based budget analyses. Global scale emissions inventories are needed to understand the causes of the increasing concentrations of important greenhouse and chemically active trace gases, and to make defensible projections of future emissions. The proper coupling of the effects of atmospheric chemistry and climate on trace gas concentrations with the dependence of future emissions on natural and human-related factors, including economic, energy use, agricultural and technological developments, needs to be considered in developing such scenarios.

2. Climate models, in particular general circulation models, require continued efforts to improve their simulation of climatic behavior, from global down to regional variations of climatic parameters. Better validation against observations is needed, again down to the regional scale. More accurate and physically complete treatments of important climatic feedback processes need to be investigated, including the representations of clouds, oceans, sea ice, and snow cover.

3. Global atmospheric models capable of treating the chemical, radiative, dynamical, and climatic interactions of the many important trace gases must be developed and tested. This is an active research area, but one still in its infancy, and efforts should be expanded. Two- and three-dimensional chemistry-transport models coupled to climate models are being developed.

4. Analogue techniques based on historical records need to be investigated and, perhaps through accounting for statistical and atmospheric chemical/physical theory, developed to provide an alternative means to understanding potential climate change effects down to regional scales. A necessary aspect of such analyses will be the determination of past causes of climate change.

5. The global distributions of essentially all relevant tropospheric trace gases and aerosols need to be determined. Laboratory and field measurements also need to assess the relevant physical properties of gas-phase and aerosol constituents. Of highest priority are measurements of O_3, OH, NO_x, CO, NMHCs, and aerosols. The processes involved in the production and removal of tropospheric ozone need to be determined.

6. Theories and specialized models will need to be developed to aid in the interpretation of experimental data, particularly for the synthesis and interpretation of global distributions and trend data, and for understanding of various processes, including biological and surface exchange, formation and growth of aerosols, and cloud and precipitation chemistry. Likewise, chemical theory should be tested through appropriate field and laboratory studies.

7. A high priority is the development of appropriate techniques to bridge spatial scales to provide meaningful input data for air quality models, and to provide more accurate representation of local processes in the regional models and regional processes in the global models. Realistic treatments of sub-grid-scale processes, such as chemical transformations or chemical-transport interactions, are needed to improve modeling capabilities. Analyses of the effects of climate change require higher resolution data than that directly available from climate models (even if their results were reliable). Localized mesoscale climate models, using input data from GCMs, may be necessary for determining regional effects of global climate change.

8. Methods need to be developed for determining the effects on air quality from climatic change. Sensitivity and uncertainty studies are needed to determine the key climatic variables requiring further analysis, but care must be taken that model parameterizations and simplifications of atmospheric processes do not unduly influence any sensitivity studies of urban and regional effects. These studies also need to determine the spatial and time scales for which climatic variables should be provided.

9. Schemes need to be developed to use urban and regional models beyond their normal episodic time range. Longer term analyses are necessary for determining the overall effects of climate change.

10. Development of existing air quality models should continue, particularly in terms of improving model representations of cloud processes (e.g., vertical mixing, aqueous chemistry), photolysis, and boundary layer/canopy interactions. The potential importance of secondary aerosol formation needs to be evaluated.

11. Additional atmospheric data bases are needed for assessing, evaluating, and validating urban/regional models. Critical treatments of average conditions in addition to pollution episodes are of particular importance from the standpoint of climate change and its effects on regional air quality.

12. Chemical kinetics data bases need further improvements for air quality studies, particularly for the rates of oxidation of aromatics and biogenic hydrocarbons.

13. The response of biogenic and anthropogenic emissions to climate change needs to be examined. Also, the latitudinal and seasonal dependence of the tropospheric water vapor/temperature feedback relationship needs to be studied.

REFERENCES

Albritton, D., F. Fehsenfeld, D., B. Hicks, J. Miller, S. Liu, J. Hales, J. Shannon, J. Durham, and A. Patrinos, NAPAP, Interim Assessment/The Causes and Effects of Acidic Deposition, Vol. III, 1987.

Arakawa, A., and W.H. Schubert, Interaction of Cumulus Cloud Ensembles with the Large-scale Environment, I, J. Atmos. Sci., 31, 674-701, 1974.

Atherton, C.S., and J.E. Penner, The Transformation of Nitrogen Oxides in the Polluted Troposphere, to be published, Tellus, 1988; also Lawrence Livermore National Laboratory UCRL-96343, Rev. 1, 1988.

Atkinson, R., and A.C. Lloyd, Evaluation of Kinetic and Mechanistic Data for Modeling of Photochemical Smog, J. Phys. Chem. Ref. Data, 13, 315-444, 1984.

Atkinson, R., C.N. Plum, W.P.L. Carter, A.M. Winer, and J.N. Pitts, Jr., Rate Constants for the Gas-phase Reactions of Nitrate Radicals with a Series of Organics in Air at 298 K, J. Phys. Chem., 88, 1210-1215, 1984.

Baldocchi, D.D., B.B. Hicks, and P. Camara, A Canopy Stomatal Resistance Model for Gaseous Deposition to Vegetated Surfaces, Atm. Env., 21, 91-101, 1987.

Barnola, J.M., D. Raynaud, Y.S. Korotkevich, and C. Lorius, Vostok Ice Core Provides 160,000-year Record of Atmospheric CO_2, Nature, 329, 408-414, 1987.

Blake, D.R. and F.S. Rowland, World-Wide Increases in Tropospheric Methane, 1978--1983, J. Atmos. Chem., 4, 43-62, 1986.

Blake, D.R. and F.S. Rowland, Continuing Worldwide Increases in Tropospheric Methane, 1978-1983, Science, 239 1123-1131, 1988.

Bolin, B., B.R. Doos, J. Jager, and R.A. Worrick, editors, The Greenhouse Effect, Climatic Change, and Ecosystems, J. Wiley and Sons, New York, 1986.

Brost, R.A., The Sensitivity to Input Parameters of Atmospheric Concentrations Simulated by a Regional Chemical Model, J. Geophs. Res., 93, 2371-2387, 1988.

Calvert, J.G., and W.R. Stockwell, The Mechanisms and Rates of the Gas Phase Oxidations of Sulfur Dioxide and the Nitrogen Oxides in the Atmosphere, in SO_2, NO, and NO_2 Oxidation Mechanism: Atmospheric Considerations, edited by J.G. Calvert, pp. 1-62, Butterworth, Boston, MA, 1984.

Chameides, W.L., The Photochemistry of a Remote Marine Stratiform Cloud, J. Geophys. Res., 89, 4739-4755, 1984.

Chang, J.S., R.A. Brost, I.S.A. Isaksen, S. Madronich, P. Middleton, W.R. Stockwell, and C.J. Walcek, A Three-Dimensional Eulerian Acid Deposition Model: Physical Concepts and Formulation, J. Geophys. Res., 92, 14681-14700, 1987.

Chapman, E.G., and D.S. Sklarew, Organic-inorganic Ion Relationships in North American Precipitation, Paper presented at the 191st American Chemical Society Meeting, New York, April, 1986.

COHMAP, Major Climatic Changes of the last 18,000 Years: Observations and Model Simulations, Cooperative Holocene Mapping Project, 1988.

Craig, H. and C.C. Chou, Methane: The Record in Polar Ice Cores, Geophys. Res. Lett., 9, 1221-1224, 1982.

Cunnold, D.M., R.G. Prinn, R.A. Rasmussen, P.G. Simmonds, F.N. Alyea, C.A. Cardelino, A.J. Crawford, P.J. Fraser, and R.D. Rosen, The Atmospheric Lifetime Experiment, 3, Lifetime Methodology and Application to 3 Years of $CFCl_3$ Data, J. Geophys. Res., 88, 8379-8400, 1983a.

Cunnold, D.M., R.G. Prinn, R.A. Rasmussen, P.G. Simmonds, F.N. Alyea, C.A. Cardelino, and A.J. Crawford, The Atmospheric Lifetime Experiment, 4, Results for CF_2Cl_2 Based on 3 Years of Data, J. Geophys. Res., 88, 8401-8414, 1983b.

Davis, D.D., J.D. Bradshaw, M.O. Rodgers, S.T. Sandholm, and S. KeSheng, Free Tropospheric and Boundary Layer Measurements of NO Over the Central and Eastern North Pacific Ocean, J. Geophs. Res., 92, 2049-2070, 1987.

Deardorff, J.W., Parameterization of the Planetary Boundary Layer for Use in General Circulation Models, Mon. Weather Rev., 100, 93-106, 1972.

Derwent, R. and O. Hov, Application of Sensitivity and Uncertainty Analysis Techniques to a Photochemical Ozone Model, J. Geophys. Res., 93, 5185-5199, 1988.

Dickinson, R.E. and R.J. Cicerone, Future Global Warming from Atmospheric Trace Gases, Nature, 319, 109-115, 1986.;

DOE, Detecting the Climatic Effects of Increasing Carbon Dioxide, edited by M.C. MacCracken and F.M. Luther, U.S. Department of Energy Report ER-0235, 1985a.

DOE, Atmospheric Carbon Dioxide and the Global Carbon Cycle, edited by J.R. Trabalka, U.S. Department of Energy Report ER-0239, 1985b.

Edmonds, J.A., J. Reilly, J.R. Trabalka, and D.E. Reichle, An Analysis of Possible Future Atmospheric Retention of Fossil Fuel CO_2, U.S. Department of Energy, report DOE/OR/21400-1, 1984.

Ehhalt, D.H., Methane in the Global Atmosphere, Environment, 27, (10): 6-12, 30-33, 1985.

Fehsenfeld, F.C., M.J. Bollinger, S.C. Liu, D.D. Parrish, M. McFarland, M. Trainer, D. Kley, P.C. Murphy, D.L. Albritton, A Study of Ozone in the Colorado Mountains, J. Atmos. Chem., 1 87-105, 1983.

Galloway, J.N., G.E. Likens, W.C. Keene, and M.M. Miller, The Composition of Precipitation in Remote Areas of the World, J. Geophys. Res., 87, 8771-8786, 1982.

Galloway, J.N., D.M. Whelpdale, and G.T. Wolff, The Flux of S and N Eastward from North America, Atmos. Environ., 18, 2595-2607, 1984.

Gates, W.L., The Physical Basis of Climate, in Proceedings of the World Climate Conference (WMO No. 537), World Meteorological Organization, Geneva, Switzerland, 112-131, 1979.

Genthon, C., J.M. Barnola, D. Raynaud, C. Lorius, J. Jouzel, N.I. Barkov, Y.S. Korotkevich, and V.M. Kotlyakov, Vostok Ice Core: Climatic Response to CO_2 and Orbital Forcing Changes Over the Last Climatic Cycle, Nature, 329, 414-418, 1987.

Gery, M.W., R.D. Edmond, and G.Z. Whitten, Tropospheric Ultraviolet Radiation Assessment of Existing Data and Effect on Ozone Formation, SYSAPP-87/191, 1987.

Graedel, T.E., and K.I. Goldberg, Kinetic Studies of Raindrop Chemistry, 1. Inorganic and Organic Processes, J. Geophys. Res., 88, 10865-10882, 1983.

Grotch, S., Regionally Intercomparing GCM Predictions with Historical Climate Data, in preparation, 1988.

Hales, J., paper presented at LLNL-EPA Workshop on Impacts of Climate Change, Chapel Hill, North Carolina, February, 1988 and Lawrence Livermore National Laboratory UCRL-99436, 1988.

Haltiner, G.J., and R.T. Williams, Numerical Prediction and Dynamic Meteorology, 2nd ed., John Wiley and Sons, New York, 1980.

Hameed, S., and R.D. Cess, Impact of a Global Warming on Biospheric Sources of Methane and its Climatic Consequences, Tellus, 35B, 1-7, 1983.

Hameed, S., and J. Dignon, Changes in the Geographical Distributions of Global Emissions of NO_x and SO_x from Fossil-fuel Combustion Between 1966 and 1980, Atmos. Env., 22, 441-449, 1988.

Hammitt, J.K., F. Camm, P.S. Connell, W.E. Mooz, K.A. Wolf, D.J. Wuebbles, and A. Bamezai, Future Emission Scenarios for Chemicals That May Deplete Stratospheric Ozone, Nature, 330, 711-716, 1987.

Holton, J.R., A dynamically Based Transport Parameterization for One Dimensional Photochemical Models of the Stratosphere, J. Geophys. Res., 91, 2681-2686, 1986.

Hov, O., Application of Sensitivity and Uncertainty Analysis Techniques to a Photochemical Ozone Model, J. Geophys. Res., 93, 5185-5199, 1988.

Isaksen, I.S.A., and O. Hov, Calculation of Trends in the Tropospheric Concentration of O_3, OH, CO, CH_4 and NO_x, Tellus, 39B, 271-285, 1987.

Jouzel, J., C. Lorius, J.R. Petit, C. Genthon, N.I. Barkov, V.M. Kotlyakov, and V.M. Petrov, Vostok Ice Core: A Continuous Isotope Temperature Record Over the Last Climatic Cycle (160,000 years), Nature, 329, 403-408, 1987.

Kasting, J.F., O.B. Toon, and J.B. Pollack, How Climate Evolved on the Terrestrial Planets, Scientific Am., 258, February 90-97, 1988.

Kavanaugh, M., Estimates of Future CO, N_2O, and NO_x Emissions from Energy Combustion, Atmos. Env., 21, 463-468, 1987.

Keene, W.C., J.N. Galloway, and J.D. Holden, Jr., Measurements of Weak Organic Acidity in Precipitation From Remote Areas of the World, J. Geophys. Res., 88, 5122-5130, 1983.

Keene, W.C., J.N. Galloway, Organic Acidity in Precipitation of North America, Atmos. Environ., 18, 2491-2497, 1984.

Keeling, C.D., The Global Carbon Cycle: What we know and could know from atmospheric, biospheric, and oceanic observations, in Proceedings of the CO_2 Research Conference: Carbon Dioxide, Science and Consensus, DOE CONF-820970, pp. II.3-II.62, U.S. Dept. of Energy, Washington, DC, 1983.

Khalil, M.A.K., and R.A. Rasmussen, Increase of $CHClF_2$ in the Earth's Atmosphere, Nature, 292, 823-824, 1981.

Khalil, M.A.K., and R.A. Rasmussen, Secular Trends of Atmospheric Methane (CH_4), Chemosphere, 11, 877-883, 1982.

Khalil, M.A.K., and R.A. Rasmussen, Sources, Sinks, and Seasonal Cycles of Atmospheric Methane, J. Geophys. Res., 88, 5131-5144, 1983a.

Khalil, M.A.K., and R.A. Rasmussen, Increase and Seasonal Cycles of Nitrous Oxide in the Earth's Atmosphere, Tellus, 35B, 161-169, 1983b.

Khalil, M.A.K., and R.A. Rasmussen, Tricholorotrifluoroethane (F-113) Trends at Pt. Barrow, Alaska, in Geophysical Monitoring for Climate Change, No. 13, Summary Report 1984, U.S. Department of Commerce, ERL/NOAA, Boulder, CO, 1985a.

Khalil, M.A.K., and R.A. Rasmussen, Causes of Increasing Atmospheric Methane: Depletion of Hydroxyl Radicals and the Rise of Emissions, Atmos. Environ., 19, 397-407, 1985b.

Khalil, M.A.K., and R.A. Rasmussen, Carbon Monoxide in the Earth's Atmosphere: Indications of a Global Increase, Nature, 332, 242-245, 1988.

Kuo, H.-L., Further Studies on the Influence of Cumulus Convection on Large-scale Flow, J. Atmos. Sci., 31, 1232-1240, 1974.

Lamb, B., H. Westbert, G. Allwine, and T. Quarles, Biogenic Hydrocarbon Emissions from Deciduous and Coniferous Trees in the United States, J. Geophys. Res., 90, 2380-2390, 1985.

Lamb, R.G., A Regional Scale (1000 km) Model of Photochemical Air Pollution, 1, Theoretical Formulation, Office of Research and Development Report, Environmental Science Research Laboratory, U.S. Environmental Protection Agency, 1982.

Lamb, R.G., A Regional Scale (1000 km) Model of Photochemical Air Pollution, 2, Input Processor Network Design, Office of Research and Development Report, Environmental Science Research Laboratory, U.S. Environmental Protection Agency, 1983.

Lamb, R.G., A Regional Scale (1000 km) Model of Photochemical Air Pollution, 3, Tests of Numerical Algorithms, Office of Research and Development Report, Environmental Science Research Laboratory, U.S. Environmental Protection Agency, 1985.

Lamb, R.G., Diagnostic Studies of Ozone in the Northeastern United States Based on Applications of the Regional Oxidant Model (ROM), APCA Conference on the Scientific and Technical Issues Facing Post-1987 Ozone Control Strategies, Hartford, Connecticut, November 16-19, 1987.

Leighton, P.A., Photochemistry of Air Pollution, Academic Press, New York, v, 300 pp., 1961.

Leovy, C.B., The General Circulation of Mars: Models and Observations, Adv. Geophys., 28, 327-346, 1985.

Levine, J.S., C.P. Rinsland, and G.M. Tennille, The Photochemistry of Methane and Carbon Monoxide in the Troposphere in 1950 and 1985, Nature, 318, 254-257, 1985.

Levy, H., II, J.D. Mahlman, W.J. Moxim, and S.C. Liu, Tropospheric Ozone: The Role of Transport, J. Geophys. Res., 90, 3753-3772, 1985.

Liu, M.K., R.E. Morris, and J.P. Killus, Development of a Regional Oxidant Model and Application to the Northeastern United States, Atmos. Environ., 18, 1145-1161, 1984.

Liu, S.C., M. Trainer, F.C. Fehsenfeld, D.D. Parrish, E.J. Williams, D.W. Fahey, G. Hubler, and P.C. Murphy, Ozone Production in the Rural Troposphere and the Implications for Regional and Global Ozone Distributions, J. Geophys. Res., 92, 4191-4207, 1987.

Liu, S.C., and M.Trainer, Response of the Tropospheric Ozone and Odd Hydrogen Radicals to Column Ozone Change, J. Atmos. Chem. 6, 221-233, 1988.

Logan, J.A., M.J. Prather, S.C. Wofsy, and M.B. McElroy, Tropospheric Chemistry: A Global Perspective, J. Geophys. Res., 86, 7210-7254, 1981.

Logan, J.A., Nitrogen Oxides in the Troposphere: Global and Regional Budgets, J. Geophys. Res., 88, 10,785-10,807, 1983.

Logan, J.A., Tropospheric Ozone: Seasonal Behavior, Trends, and Anthropogenic Influence, J. Geophys. Res., 90, 10,463-10,482, 1985.

Logan, J.A., private communication, 1987.

Lurmann, F.W., A.C. Lloyd and B. Nitta, Modeling Potential Ozone Impacts from Natural Hydrocarbons--II. Hypothetical Biogenic HC Emission Scenario Modeling, Atmos. Environ., 17, 1951-1963, 1983.

Luther, F.M. and R.G. Ellingson, Carbon Dioxide and the Radiation Budget, in Projecting the Climate Effects of Increasing Carbon Dioxide, M.C. MacCracken and F.M. Luther, editors, U.S. Department of Energy, report DOE/ER-0237, 1985.

MacCracken, M.C., D.J. Wuebbles, J.J. Walton, W.H. Duewer, and F.E. Grant, The Livermore Regional Air Quality Model: I. Concept and Development, J. Applied Met., 17, 254-272, 1978.

MacCracken, M.C., M.E. Schlesinger, and M.R. Riches, Atmospheric Carbon Dioxide and Summer Soil Wetness, Science, 234, 659-660, 1986.

Manabe, S., and R.T. Wetherald, Reduction in Summer Soil Wetness Induced by an Increase in Atmospheric Carbon Dioxide, Science, 232, 626-628, 1986.

Manabe, S. and R.T. Wetherald, Large-scale Changes in Soil Wetness Induced by an Increase in Atmospheric Carbon Dioxide, J. Atmos. Sci., 44, 1211-1235, 1987.

McRae, G.J., W.R. Goodin, and J.H. Seinfeld, Mathematical Modeling of Photochemical Air Pollution, California Institute of Technology, Environmental Quality Laboratory Report No. 18, 1982.

Meehl, G.A., and W.M. Washington, A Comparison of Soil Moisture Sensitivity in Two Global Climate Models, J. Atmos. Sci., (in press), 1988.

Mellor, G.L., and T. Yamada, A Hierarchy of Turbulence Closure Models for Planetary Boundary Layers, J. Atmos. Sci., 31, 1791-1806, 1974.

Mintzer, I.M., A Matter of Degrees: The Potential for Controlling the Greenhouse Effect, World Resources Institute Research Report #5, 1987.

Mitchell, J.F.B., and D.A. Warrilow, Summer Dryness in Northern Midlatitudes Due to Increased CO_2, Nature, 330, 238-240, 1987.

Morris, E.D., Jr., and H. Niki, Reaction of the Nitrate Radical with Acetaldehyde and Propylene, J. Phys. Chem., 78, 1337-1338, 1974.

Morris, R.E., S.D. Reynolds, and M.K. Liu, The Systems Applications, Inc. Regional Transport Model - Current status and future needs, APCA Conference on the Scientific and Technical Issues Facing Post-1987 Ozone Control Strategies, Hartford, Connecticut, November 16-19, 1987.

NASA, Earth System Science: Overview, National Aeronautics and Space Administration, Washington, DC, 1986.

National Acid Precipitation Assessment Program (NAPAP), Report on the peer review of the Regional Acid Deposition Model (RADM), Washington, DC, 1987.

Neftel, A., J. Beer, H. Oeschger, F. Zurcher and R.C. Finkel, Sulfate and Nitrate Concentrations in Snow from South Greenland 1895-1978, Nature, 314, 611-613, 1985.

Nihoul, J. (ed.), Coupled Ocean-Atmosphere Models, Elsevier Oceanography Series, Vol. 4, 767 pp., Elsevier, Amsterdam, 1985.

Niiler, P.P., and E.B. Kraus, One Dimensional Models of the Upper Ocean, in Modeling and Prediction of the Upper Layers of the Ocean, edited by E.B. Kraus, pp. 143-172, Pergamon Press, 1977.

North, G.R., R.F. Cahalan, and J.A. Coakley, Jr., Energy Balance Climate Models, Rev. Geophys. Space Phys., 19, 91-122, 1981.

Norton, R.B., Measurements of Formate and Acetate in Precipitation at Niwot Ridge and Boulder, Colorado, Geophys. Res. Lett., 12, 769-772, 1985.

NRC, Carbon Dioxide and Climate: A Second Assessment, U.S. National Research Council, National Academy Press, Washington, DC, 1982.

NRC, Changing Climate: Report of the Carbon Dioxide Assessment Committee, U.S. National Research Council, National Academy Press, Washington, DC, 1983.

NRC, Global Tropospheric Chemistry: A Plan for Action, U.S. National Research Council, National Academy Press, Washington, DC, 1984.

Oltmans, S.J., and W.D. Kohmyr, Surface Ozone Distributions and Variations From 1973-1984, Measurements at the NOAA Geophysical Monitoring for Climatic Change baseline observatories, J. Geophys. Res., 91, 5229-5236, 1986.

Pearman, G.I.P., D. Etheridge, F. deSilva, and P.J. Fraser, Evidence of Changing Concentrations of Atmospheric CO_2, N_2O and CH_4 from Air Bubbles in Antarctica, Nature, 320, 248-250, 1985.

Penner, J.E., M.B. McElroy, and S.C. Wofsy, Sources and Sinks for Atmospheric H_2: A Current Analysis with Projections for the Influence of Anthropogenic Activity, Planet. Space Sci., 25, 521-540, 1977.

Penner, J.E., Increases in CO_2 and Chlorofluoromethanes: Coupled Effects on Stratospheric Ozone, Proceedings of the Quadrennial International: Ozone Symposium, Aug. 4-9, 1980, Boulder, CO, 1980.

Penner, J.E., Modeling the Effect of Biogenic Hydrocarbon Emissions in the San Francisco Bay Area, APCA Specialty Meeting Proceedings on the Environmental Impact of Natural Emissions, Research Triangle Park, North Carolina, March, 1984; also Lawrence Livermore National Laboratory UCRL-89170, 1984.

Penner, J.E., and P.S. Connell, Pollutant Transport Study: Bay Area to North Central Coast Air Basin, Lawrence Livermore National Laboratory UCID-21287, 1987.

Penner, J.E., J.J. Walton, and T. Umeda, Air Quality Model Validation: Application to the San Francisco Bay Area and St. Louis, published in the proceedings of the 76th Annual Meeting of the Air Pollution Control Association, Atlanta Georgia, June 19-24, 1983.

Potter, G.L., and R.D. Cess, Background Tropospheric Aerosols: Incorporation Within a Statistical-Dynamical Climate Model, J. Geophys. Res., 89, 9521-9526, 1984.

Prather, M., M. McElroy, S. Wofsy, G. Russell, and D. Rind, Chemistry of the Global Troposphere: Fluorocarbons as Tracers of Air Motion, J. Geophys. Res., 92, 6579-6613, 1987.

Prinn, R.G., R.A. Rasmussen, P.G. Simmonds, F.N. Alyea, D.M. Cunnold, B.C. Lane, C.A. Cardelino, and A.J. Crawford, The Atmospheric Lifetime Experiments, 5, Results for CH_3CCl_3 based on three years of data, J. Geophys. Res., 88, 8415-8426, 1983.

Ramanathan, V., and J.A. Coakley, Jr., Climate Modeling Through Radiative-Convective Models, Rev. Geophys. Space Phys., 16, 465-489, 1978.

Ramanathan, V., L. Callis, R. Cess, J. Hansen, I. Isaksen, W. Kuhn, A. Lacis, F. Luther, J. Mahlman, R. Reck, and M. Schlesinger, Climate-Chemical Interactions and Effects of Changing Atmospheric Trace Gases, Rev. Geophys., 25, 1441-1482, 1987.

Rampino, M.R., and T. Volk, Mass Extinctions, Atmospheric Sulfur and Climatic Warming at the K/T Boundary, Nature, 332, 63-65, 1988.

Rasmussen, R.A. and M.A.K. Khalil, Atmospheric Methane in the Recent and Ancient Atmospheres: Concentrations, Trends, and Interhemispheric Gradient, J. Geophys. Res., 89, 11599-11605, 1984.

Ridley, B.A., M.A. Carroll, G.L. Gregory, Measurements of Nitric Oxide in the Boundary Layer and Free Troposphere Over the Pacific Ocean, J. Geophys. Res., 92, 2025-2047, 1987.

Rinsland, C.P. and J.S. Levine, Free Tropospheric Carbon Monoxide Concentrations in 1950 and 1951 Deduced from Infrared Total Column Amount Measurements, Nature, 318, 250-254, 1985a.

Rinsland, C.P., J.S. Levine, and T. Miles, Concentration of Methane in the Troposphere Deduced from 1951 Infrared Solar Spectra, Nature, 318, 245-249, 1985b.

Robock, A., An Updated Climate Feedback Diagram, Bul. Amer. Meteor. Soc., 66 786-787, 1985.

Saltzman, B., A Survey of Statistical-Dynamical Models of the Terrestrial Climate, Adv. Geophys., 20, 183-304, 1978.

Saltzman, B., (ed.), Theory of Climate, Part I: History and Application of General Circulation Models, Adv. Geophys., 25, 1983.

Schere, K., paper presented at LLNL-EPA Workshop on Impacts of Climate Change, Chapel Hill, North Carolina, February, 1988 and Lawrence Livermore National Laboratory UCRL-99436, 1988.

Schlesinger, M.E., and J.F.B. Mitchell, Model Projections of the Equilibrium Climatic Response to Increased Carbon Dioxide, in The Potential Climatic Effects of Increasing Carbon Dioxide, edited by M.C. MacCracken and F.M. Luther, U.S. Department of Energy, 1985.

Schneider, S.H., and R.E. Dickinson, Climate Modeling, Rev. Geophys. Space Phys., 12, 447-493, 1974.

Schneider, S.H., and S.L. Thompson, Atmospheric CO_2 and Climate: Importance of the Transient Response, J. Geophys. Res., 86, 3135-3147, 1981.

Schneider, S.H., and R. Londer, The Coevolution of Climate and Life, Sierra Club Books, San Francisco, 1984.

Seinfeld, J.H., Ozone Air Quality Models, A Critical Review, JAPCA, 38, 616-645, 1988.

Seigneur, C., T.W. Tesche, P.M. Roth, and L.E. Reid, Sensitivity of a Complex Urban Air Quality Model to Input Data, J. Appl. Meteoro., 20, 1020-1040, 1981.

Seigneur, C., A.B. Hudischewskyj, J.H. Seinfeld, K.T. Whitby, E.R. Whitby, J.R. Brock, and H.M. Barnes, Simulation of Aerosol Dynamics: A Comparative Review of Mathematical Models, Aerosol Sci. and Tech., 5, 205-222, 1986.

Semtner, A.J., Jr., On Modeling the Seasonal Thermodynamic Cycle of Sea Ice in Studies of Climatic Change, Climatic Change, 6, 27-37, 1984.

Singh, H.B., L.J. Salas, B.A. Ridley, J.D. Shetter, N.M. Donahue, F.C. Fehsenfeld, D.W. Fahey, D.D. Parrish, E.J. Williams, S.C. Liu, G. Hubler, and P.C. Murphy, Relationship Between Peroxyacetyl Nitrate and Nitrogen Oxides in the Clean Troposphere, Nature, 318, 347-349, 1985.

Spelman, M.J., and S. Manabe, Influence of Oceanic Heat Transport Upon the Sensitivity of a Model Climate, J. Geophys. Res., 89, 571-586, 1984.

Sperber, K.R., S. Hameed, W.L. Gates, and G.L. Potter, Southern Oscillation Simulated in a Global Climate Model, Nature, 329, 140-142, 1987.

Stauffer, B., G. Fisher, A. Neftel, and H. Oeschger, Increase of Atmospheric Methane Recorded in Antarctic Ice Core, Science, 229, 1386-1388, 1985.

Stauffer, B., E. Lochbronner, H. Oeschger, and J. Schwander, Methane Concentration in the Glacial Atmosphere Was Only Half that of the Preindustrial Holocene, Nature, 332, 812-814, 1988.

Suck, S.H. and J.R. Brock, Evaluation of Atmospheric Aerosol Particle Size Distribution Via Brownian Coagulation: Numerical Simulations, J. Aerosol Sci., 10, 581-590, 1979.

Taylor, K.E., and S.L. Grotch, Observational and Theoretical Studies of Greenhouse Climatic Effects, Lawrence Livermore National Laboratory UCRL-98087, 1987.

Thompson, A.M., and R.J. Cicerone, Possible Perturbations to Atmospheric CO, CH_4, and OH, J. Geophys. Res., 89, 10,853-10,864, 1986a.

Thompson, A.M., and R.J. Cicerone, Atmospheric CH_4, CO and OH from 1860 to 1985, Nature, 321, 148-150, 1986b.

Thompson, A.M., and M. Kavanaugh, Tropospheric CH_4/CO/NO_x: The Next Fifty Years, in Effects of Changes in Stratospheric Ozone and Global Climate, Vol. 2, United Nations Environmental Program Report, 1986.

Thompson, A.M., R.W. Stewart, M.A. Owens, and J.A. Herwehe, Sensitivity of Tropospheric Oxidants to Global Chemical and Climate Change, submitted to Atmos. Env., 1988.

Thompson, S.L., and S.H. Schneider, Carbon Dioxide and Climate: The Importance of Realistic Geography in Estimating the Transient Temperature Response, Science, 217, 1031-1033, 1982.

Tiao, G.C., G.C. Reinsel, J.H. Pedrick, G.M. Allenby, C.L. Mateer, A.J. Miller, and J.J. DeLuisi, A Statistical Trend Analysis of Ozonesonde Data, J. Geophys. Res., 91, 13121-13136, 1986.

Trainer, M., E.Y. Hsie, S.A. McKeen, R. Tallamraju, D.D. Parrish, F.C. Fehsenfeld, and S.C. Liu, Impact of Natural Hydrocarbons on Hydroxyl and Peroxy Radicals at a Remote Site, J. Geophys. Res., 92, 11879-11894, 1987.

Vukovich, F.M., J. Fishman and E.V. Browell, The Reservior of Ozone in the Boundary Layer of the Eastern United States and Its Potential Impact on the Global Tropospheric Ozone Budget, J. Geophs. Res., 90, 5687-5689, 1985.

Walcek, C., and J. Chang, paper presented at LLNL-EPA Workshop on Impacts of Climate Change, Chapel Hill, North Carolina, February, 1988 and Lawrence Livermore National Laboratory UCRL-99436, 1988.

Walton, J.J., D.J. Wuebbles, and S. Hameed, Simulation of Global Wet and Dry Deposition of Nitric Acid in a Three-Dimensional Chemistry-Transport Model, published in Acid Rain: Scientific and Technical Advances, R. Perry, R.M. Harrison, J.N.B. Bell, and J.N. Leater, editors, Selper Ltd., London, 1987.

Wang, W.-C., D.J. Wuebbles, W.M. Washington, R.G. Isaacs, and G. Molnar, Trace gases and Other Potential Perturbations to Global Climate, Rev. Geophys., 24, 110-140, 1986.

Watson, R., Executive Summary of the Ozone Trends Panel, NASA, 1988.

Weiss, R.W., The Temporal and Spatial Distribution of Tropospheric Nitrous Oxide, J. Geophys. Res., 86, 7185-7195, 1981.

Whitten, G.Z., and M.W. Gery, The Interaction of Photochemical Processes in the Stratosphere and Troposphere, in Effects of Changes in Stratospheric Ozone and Global Climate, Vol. 2, United Nations Environmental Program Report, 1986.

Williams, E.J., D.D. Parrish, and F.C. Fehsenfeld, Determination of Nitrogen Oxide Emissions from Soils: Results from a Grassland site in Colorado, United States, J. Geophys. Res., 92, 2173-2179, 1987.

Wilson, C.A., J.F.B. Mitchell, A Doubled CO_2 Climate Sensitivity Experiment with A Global Climate Model Including a Simple Ocean, J. Geophys. Res., 92, 13315-13344, 1987.

WMO, The Stratosphere 1981: Theory and Measurements, World Meteorological Organization, Global Ozone Research and Monitoring Project Report No. 11, 1981.

WMO, Atmospheric Ozone: 1985, Vols. 1 and 3, World Meteorological Organization, Global Ozone Research and Monitoring Project Report No. 16, 1985.

Wuebbles, D.J., A Summary of the LLNL One-Dimensional Model of the Troposphere and Stratosphere: 1981, Lawrence Livermore National Laboratory UCID-19185, 1981.

Wuebbles, D., P. Connell, K. Grant, R. Tarp, and K. Taylor, Initial Results of the LLNL 2D Chemical-radiative-transport Model, Lawrence Livermore National Laboratory UCID-21178, 1987.

Wuebbles, D.J., and J. Edmonds, A Primer on Greenhouse Gases, DOE/NBB0083 Report TR040, 1988.

SENSITIVITY OF A REGIONAL OXIDANT MODEL TO VARIATIONS IN CLIMATE PARAMETERS

by

Ralph E. Morris
Mike W. Gery
Mei-Kao Liu
Gary E. Moore
Christopher Daly
Stanley M. Greenfield
Systems Applications, Inc.
101 Lucas Valley Road
San Rafael, CA 94903

Contract Nos. CX-0001-4-0055 and PX-001-8-0436

CONTENTS

Page

CHAPTER 1: INTRODUCTION 2-1
- BACKGROUND 2-1
- METHODOLOGY 2-2
- UNCERTAINTIES 2-2

CHAPTER 2: REGIONAL MODELING OF OZONE FORMATION UNDER FUTURE CHANGES IN CLIMATE 2-3
- DEFINITION OF TEMPERATURE INCREASE 2-4
- EFFECTS OF TEMPERATURE CHANGE ON OTHER METEOROLOGICAL VARIABLES 2-5
  - Boundary Layer Heights 2-6
  - Cloudiness 2-6
  - Water Vapor Concentrations 2-6
  - Wind Fields 2-7
  - Stability 2-8
  - Emissions 2-8
- DEFINITION OF STRATOSPHERIC OZONE REDUCTION 2-9
- DEFINITION OF MODELING SCENARIOS 2-9
- UNCERTAINTIES 2-9
  - Definitions of the Climate Change Scenarios 2-9
  - Model Inputs 2-10
  - Model Limitations 2-10
- RESULTS OF THE SIMULATIONS -- CLIMATE CHANGE SCENARIO #1 2-10
  - Central California 2-11
  - Midwestern/Southeastern Region 2-13
- RESULTS OF THE SIMULATIONS -- CLIMATE CHANGE SCENARIO #2 2-15
- IMPLICATIONS OF THE ANALYSIS FOR AIR QUALITY CONTROLS 2-16

CHAPTER 3: THE SENSITIVITY OF OZONE CONCENTRATIONS TO CLIMATE VARIABILITY 2-85
- METHODOLOGY 2-85
  - Selection of Meteorological Variables 2-86
  - Classification of Meteorological Variables 2-87
- THE DATA BASE 2-87
  - RTM-III Simulations 2-87
  - RTM-III Input Variables 2-87
- SELECTION OF VARIABLES FOR THE ANALYSIS 2-92
  - Spatial Grouping of Variables 2-92
  - Temporal Grouping of Variables 2-93
  - Ranges of the Meteorological Variables within Episodes 2-95
- THE SENSITIVITY OF MAXIMUM DAILY OZONE CONCENTRATION TO THE METEOROLOGICAL VARIABLES 2-101
  - A General Conceptual Model 2-101
  - Correlational Analysis 2-101
  - Cluster Analysis 2-108
- THE FEASIBILITY OF USING METEOROLOGICAL CLASSIFICATION SCHEMES FOR PREDICTING OZONE CONCENTRATIONS 2-111

CHAPTER 4: RECOMMENDATIONS 2-112

REFERENCES 2-114

CHAPTER 1

INTRODUCTION[1]

BACKGROUND

Global atmospheric changes are expected to occur within the next several decades because of increases in levels of pollutants in the atmosphere. These changes are associated with (1) warming of the atmosphere due to the greenhouse effect of trace gases, (2) depletion of the stratospheric ozone layer, and (3) modification of tropospheric chemistry. The emitted materials responsible for those changes are carbon dioxide, carbon monoxide, methane, chlorofluoro-hydrocarbons, nitrous oxide, and other trace gases.

As atmospheric concentrations of the so-called greenhouse gases continue to increase, the potential climate change and consequent environmental impacts have become issues of great concern worldwide. Such climate changes could significantly affect the chemistry and dynamics of the troposphere and ultimately endanger human health and sensitive ecological systems. Of particular concern to many parties, including the Environmental Protection Agency (EPA) and National Park service (NPS), is the possibility that increased temperature and depletion of stratospheric ozone may result in increases in tropospheric concentrations of ozone. The resulting increased reactivity of the troposphere would also result in increased concentrations of other photochemically active species, such as hydrogen peroxide and peroxyacetyl nitrate. Hydrogen peroxide is believed to be one of the principal chemicals in the formation of sulfate and consequently acid deposition, by acting as an oxidizer of sulfur dioxide, while increased concentrations of ozone and peroxyacetyl nitrate may result in significant damage to forest ecosystems.

To provide an initial estimate of the possible effects of future climate changes on tropospheric oxidant concentrations, the EPA, through an interagency agreement with the NPS, funded a preliminary study that examined the effects of future climate changes on urban air quality at several U.S. cities (Gery et al., 1987). Specifically, this study used a computer simulation model, OZIPM3, a simple photochemical trajectory box model, to study the effects of increased temperature and decreased stratospheric ozone on ozone formation. The results indicated that, if anticipated climate changes do occur, most of the cities studied will not be able to meet the current National Ambient Air Quality Standard (NAAQS) for ozone (0.12 ppm) without more emission controls than are currently envisioned.

This preliminary study, however, did not estimate the effects of future climate changes on ozone concentrations in the rural atmosphere. The simulation model used in the study, OZIPM3, does not completely simulate the complex interaction between the processes of transport, diffusion, chemistry, and deposition nor does it include any feedback mechanisms between these processes. In addition, because the model does not divide the atmosphere into more than one vertical layer, it does not properly account for emission, meteorological, and chemistry variations with height, which may be important in both urban and rural environments. Therefore, the purpose of the study reported here was to examine the ability of another model to assess the effects of future climate change on tropospheric air quality. This model, the RTM-III, is an Eulerian three-dimensional regional oxidant model that has been developed over several years (Liu et al., 1984; Morris et al., 1987).

---

[1] Although the information in this report has been funded wholly or partly by the U.S. Environmental Protection Agency under Contract Nos. CX-0001-4-0055 and PX-0001-8-0436, it does not necessarily reflect the Agency's views, and no official endorsement should be inferred from it.

METHODOLOGY

This study involved two tasks. The first task was to examine past RTM-III calculations of regional ozone concentrations in order to estimate the sensitivity of the model to changes in climate. Ozone concentrations predicted by the model were related to meteorological input parameters in order to gain insight into how potential future perturbations of these meteorological parameters will affect ozone concentrations. The second task was to determine the sensitivity of the RTM-III to changes in climate by simulating a base case of current climate conditions and potential future climate sensitivity scenarios. (The results of the second task are reported in Chapter 2, and those of the first task in Chapter 3.)

To estimate the sensitivity of RTM-III calculations of ozone to climatic change, past model simulations were re-analyzed and the meteorological conditions used as input were classified into sets of variables. The predicted ozone concentrations associated with these sets of meteorological conditions were then examined to determine their sensitivity to variations in climatic conditions.

We then applied an updated version of the RTM-III to two modeling domains: one covering central California and the other covering the midwestern and southeastern United States. For each modeling domain the model was exercised for a base case of current temperature and ultraviolet light conditions, and for a future climate scenario reflecting the effects of global warming. The model's ozone concentration predictions were then analyzed to determine the sensitivity of the model's predictions of tropospheric air quality to climate changes.

This study provides a preliminary estimate of the sensitivity of calculations of air quality to climate changes, and should help identify those climate parameters to which the calculations are most sensitive. These results will help focus future research on the effects of possible changes in climate on air quality.

UNCERTAINTIES

The use of air quality simulation models (AQSM) to estimate changes in air quality due to changes in climate conditions is beset with limitations because of the quantitative uncertainty associated with assumptions about global climate change. Current climate models can only provide general indications of the direction of future climate changes; AQSMs, however, require specific meteorological inputs. Thus, for this preliminary estimate of the sensitivity of AQSM calculations of ozone concentrations to potential climate modifications, we used an AQSM (the RTM-III) to simulate current climate meteorological conditions and a simple modification of these conditions that reflects the general direction of potential climate changes. In no way do we claim that the future climate scenarios described here represent actual future climate conditions, only that they include some of the basic features predicted by climate models, namely, increased temperature and UV radiation.

CHAPTER 2

REGIONAL MODELING OF OZONE FORMATION UNDER FUTURE CHANGES IN CLIMATE

The continued release of emissions of carbon dioxide (CO_2) and other trace gases has in recent years led to the concern that these trace gases will result in a global warming of the atmosphere by blocking the escape of thermal infrared radiation. This phenomenon is commonly referred to as the greenhouse effect (Dickinson and Cicerone, 1986; Ramanathan et al., 1985; Wang et al., 1986). To quantify the amount of global warming expected in the future, general circulation models (GCMs) and other climate models have been exercised with various estimates of future loadings of trace gases in the upper atmosphere. We analyzed the predictions of climate change from four GCMs to obtain two representative future climate scenarios: a 4°C temperature increase and a combination of a 4°C temperature increase with a 10% reduction in stratospheric ozone.

In this section we report the results of simulations of current climate conditions and two future climate scenarios using a regional air quality model, the RTM-III. The maximum daily ozone concentrations calculated by the model are presented along with an interpretation of the impact of possible climate changes on air quality management.

Our future climate scenarios were based on results from the following four GCMs:

National Center for Atmospheric Research (NCAR) Community Climate Model (CCM) model

National Aeronautics and Space Administration (NASA) Goddard Institute of Space Studies (GISS) model

National Oceanic and Atmospheric Administration (NOAA) General Fluid Dynamics Laboratory (GFDL) model

Oregon State University (OSU) model

Current estimates of the emission and retention of manmade CO_2 in the atmosphere indicate a distinct possibility that atmospheric concentrations of CO_2 will double within the next century. Under these conditions, several GCMs predict an increase in the global average surface temperature at sea level of from 1 to 5°C. The above four GCMs models predict that the doubling of CO_2 concentrations would increase the global average temperature in the range of 2 to 5°C (Wuebbles and Penner, 1988). The presence of other trace gases, in addition to CO_2, would increase the global warming further. Although the four GCMs generally agree on the level of increase of global average temperature, they do not agree in their predictions of temperature increases in specific regions, such as California. Studies conducted by Lawrence Livermore National Laboratory (LLNL) and others indicate that current GCMs cannot, as yet, provide meaningful results for specific regions of interest.

Because of these limitations, translating the output of GCMs to hourly average temperature increases for a specific region of interest, as required by a regional air quality model such as the RTM-III, is problematic. The temporal and spatial scales of a GCM (decades and thousands of kilometers) are not compatible with those of a model like RTM-III (hours and 10 to 50 km). Because of difficulties in adapting the GCM output to a regional model and the discrepancies in the predictions of the GCMs for many climate variables, we have assumed simply that the temperature increases by 4°C throughout the modeling region. A temperature increase of 4°C is in the higher range of increases in global average temperature predicted by the four GCMs (2°C to 5°C) yet is well within the range of those predictions. In fact, temperature increases in central California and the midwestern/southeastern U.S. could be substantially larger than 4°C since the GCM simulations we analyzed considered the effects of doubling CO_2 concentrations on temperature increases. The effects of increases of other trace gases, or a more than doubling of the CO_2 concentrations, would result in a higher temperature increase. Of course it is also possible that the GCMs may be overpredicting increases in temperature due to uncertainties in the GCM calculations. Nevertheless, the fact remains that atmospheric concentrations of CO_2 are rising and all of the results of climate models we studied agree that this will result in an increase in global average temperature.

DEFINITION OF TEMPERATURE INCREASE

The 4°C temperature increase predicted by the climate models is a global, sea-level, annual average value. In general, the increases predicted by the GCMs are relatively higher in polar regions and lower at the equator. The modeling regions in the study reported here lie in the mid latitudes, thus the temperature increases should be between those at the equator and at the polar regions. Although the four GCMs are in general agreement when predicting the global average temperature effects of a doubling of CO_2 concentrations, they are less in agreement when examining changes in temperature for specific regions. For example, the four models predict that, under a doubling of the CO_2 concentrations, the summer average temperature for the eight westernmost states would increase in the range of 2.5 to 5°C, while in the eastern United States the temperature increase would range from 2.5 to 5.5°C. These results support the assumption of a 4°C temperature increase for the central California and midwestern/southeastern regions.

A consideration in defining this increased temperature scenario is how to relate this 4°C average increase to the temperature fields used as input to the RTM-III, which vary diurnally and by vertical layer. For the present study it was decided to add 4°C to each grid cell in each layer for each hour of the episode. While this approach may be viewed as an oversimplification of the actual phenomena, it is not unrealistic, as is discussed below.

None of the output from the GCMs is reported to have sufficient temporal and spatial resolution to resolve the temperature increases as hourly variations for a specific region. There is some speculation that the increase in global average temperature would have a greater impact on the nightime low temperature than on the daytime maximum. However, in the absence of better information, it will be assumed that the 4°C increase in surface temperature occurs uniformly throughout the diurnal cycle.

The next consideration in the definition of the increased temperature climate scenario is how to relate the temperature increase to the vertical layers of the RTM-III. The RTM-III contains three vertical layers. The first layer corresponds to the mixed layer. For daytime hours the top of this first layer is defined by an inversion below which rapid convective mixing occurs. It would appear that, because of rapid vertical mixing within this layer, an increase in surface temperature would result in a uniform temperature increase throughout the layer. For nighttime hours this first layer in RTM-III is defined as a shallow layer, usually approximately 50 to 150 meters thick. Since the top of this layer is usually defined by the magnitude of the wind speed and represents a mechanically well-mixed layer from the friction velocity and Coriolis parameter (Yu, 1978), any increase in the surface temperature would occur throughout the mixed-layer of the RTM-III.

The second layer in the RTM-III is a very thin layer (200 to 650 meters thick) that represents a transition between the mixed layer and an inversion layer (the third layer aloft). This transition layer has a special function in the application of the RTM-III to central California. During the day the wind fields in the San Joaquin Valley are dominated by upslope flows near the surface, which are compensated by return flows aloft. Between the upslope winds at the surface and downslope return flow aloft is a shallow transition layer in which the slope flows counteract each other, resulting in a dead air space. Because of such convergence zones, there is significant transport between this transition layer and the mixed layer. At night a similiar situation exists, except that the direction of the flow regimes is reversed, with the mixed layer containing the downslope (drainage) flows. Again there is some interaction between the mixed layer and the transition layer in the convergence zones, especially in the valley, where the pooling of the drainage flows causes an uplifting of the air. It appears that the second layer is tied to the mixed layer quite strongly; this is borne out by the RTM-III simulations, in which the ozone predictions in the second layer are closer to those in the mixed layer than the third layer (Morris et al., 1987). Thus one could logically assume that any temperature increase in the mixed layer would also be reflected by an increase in the second layer.

Other climate effects researchers are assuming that the sea-level average temperature increase occurs throughout the troposphere (Wuebbles, 1988). Thus, to be consistent with other research and in the absence of any better information, we are assuming that the 4°C temperature increase also occurs in the third layer.

EFFECTS OF TEMPERATURE CHANGE ON OTHER METEOROLOGICAL VARIABLES

The atmosphere is a complicated system in which many variables, such as pressure, temperature, and winds, are in dynamic balance with each other. This linkage is described mathematically by the primitive equations (Pielke, 1984). Thus any modification of the temperature may also affect other meteorological variables. These other variables may include, but are not limited to, the following:

Boundary (mixing) layer heights
Frequency and patterns of cloud cover and cloudiness
Water vapor concentrations
Wind fields, e.g., thermal winds
Stability
Emissions rates, both anthropogenic and biogenic
Frequency and intensity of climate variations

Boundary Layer Heights

One would expect that an increase in surface temperature would result in an increase in convective activity and a resultant increase in the convective mixing height. For the central California modeling domain the mixing heights were defined as the base of an inversion from temperature soundings. Since we have assumed that the 4°C temperature increase occurs uniformly throughout the vertical temperature sounding, the height of the inversion base and mixing height would remain unchanged. The mixing heights for the midwestern/southeastern modeling domain were created by the Meteorological Processor for Diffusion Analysis mixing height algorithm (Paumier et al., 1986), which estimates the convective mixing height as the base of the inversion but also contains some algorithms that may be sensitive to changes in temperature. However, changes in the mixing heights input into the RTM-III would also involve adjusting the layer-average wind, temperature, and water vapor fields. Quite a bit of uncertainty is associated with the location of the mixing height because of the spatial and temporal interpolation of the twice-daily mixing heights at radiosonde sites located 200 to 300 km. Therefore, the mixing heights for the climate change scenarios are the same ones used in the base case. As a result, the effects of temperature increases on ozone formation should be overstated by the model since the emissions are trapped in a smaller volume of air.

Cloudiness

There were clear skies throughout the period of the California episode studied here (5-10 August 1981). Thus it appears that we should assume continued clear skies for the climate change scenarios, since the appearance of clouds would be unjustified and would unreasonably confuse and complicate the analysis.

The episode selected for the midwestern/southeastern modeling domain (14 to 21 July 1980) includes periods of clouds and some precipitation. Increased cloudiness would increase precipitation, decrease ultraviolet light, and possibly increase vertical transport of pollutants, while a decrease in cloudiness would have the opposite effect. Thus increased cloudiness would most likely result in lower ozone concentrations due to reductions in UV radiation and possible increases in the occurrence of aqueous-phase chemistry. Since the specification of the increase, or decrease, of cloudiness associated with a 4°C temperature increase would be arbitrary, we have assumed that cloudiness remains unchanged. However, cloudiness should be considered as a climate change variable in future studies.

Water Vapor Concentrations

The relationship between temperature and water vapor concentrations can be determined via the Clausius-Clapeyron equation. The change in water vapor concentration in the atmosphere, as the temperature increases, depends on the supply of water at the surface. If the surface is dry, the water vapor concentration will not change. If there is a plentiful supply of water, the surface water flux would increase but the relative humidity would stay nearly constant. GCM results suggest that relative humidity would stay constant with increased temperature (Ramanathan, 1988). Thus, when atmospheric temperature T increases, the ratio of the vapor pressure to the saturation vapor pressure (i.e., relative humidity) would remain constant, i.e.:

$$r = \frac{e(T_D)}{e_s(T)} = \frac{e(T'_D)}{e_s(T + \Delta T)}$$

$$e(T'_D) = e(T_D)\frac{e_s(T + \Delta T)}{e_s(T)}$$

where T_D is the dew point and $e(T'_D)$ is the vapor pressure when the temperature has been increased by ΔT. From the above equations water vapor concentrations for increased temperature conditions can be calculated from the original water vapor concentrations by multiplying by the factor $e_s(T + \Delta T)/e_s(T)$, which can be estimated from the Clausius-Clapeyron equation as follows:

$$\lambda = \frac{\exp[21.548 - 5388/(T + \Delta t)]}{\exp[21.548 - 5388/T]}$$

Assuming a temperature increase of 4°C and ambient temperatures of 250, 275, and 300°K, we get values for λ of 1.40, 1.32, and 1.26, respectively. Thus a 4°C temperature increase will be expected to increase the water vapor concentrations by 26 to 40%.

Increases in water vapor would result in a higher rate of production of the hydroxy radical and thus higher ozone concentrations. In general, however, maximum ozone concentrations are not that sensitive to changes in water vapor concentrations at normal levels of relative humidity.

Wind Fields

It is difficult to quantify the effects of increased temperature on the wind fields. For the central California episode it appears the increased temperature could result in significant alterations of the flow fields. Because of stagnant synoptic conditions during the California episode, the flow fields in the San Joaquin Valley are dominated by thermal upslope and downslope flows. Increased surface temperature could result in stronger slope flows. In addition, the increased temperature could also alter the temperature differential between the San Joaquin Valley and air over the Pacific Ocean, resulting in modifications of the strength of the land-sea breezes.

The wind fields for the central California application were generated by the Diagnostic Wind Model, which relies on observations and parameterizations of processes to obtain its wind fields (Kessler and Douglas, 1988; Morris et al., 1987). The Diagnostic Wind Model requires hourly values of a domain-mean surface temperature and lapse rate. The surface temperature and lapse rate are used in the denominator of the expression for calculating the Froude number, which describes the blocking and deflection of the synoptic wind flows by complex terrain. The lapse rate is also used to determine the strength of the thermally generated slope flows. The assumption of a uniform increase in temperature for the future climate scenario would not affect the lapse rate but may affect the Froude number calculations. An increase of 4°C in the temperature would change the Froude number by approximately 1%. This change is very small and would not significantly alter the flow fields, especially since the wind fields in the California episode (5-10 August 1981) are dominated by stagnant conditions without large amounts of blocking and deflection effects. Thus we are assuming no changes in the wind fields for the climate change scenarios for the California modeling domain.

The wind fields for the July 1980 midwestern/southeastern episode were generated by the Limited Fine Mesh (LFM) prognostic meteorological model. In principle it could be possible to alter the radiation parameterization and initial temperature fields of a prognostic model, such as the LFM, to create new wind fields under conditions of increased temperature. However, these fields were obtained from archived LFM output and rerunning the model to obtain new wind fields is a difficult task; the effort involved would have exceeded the resources and time constraints for this study. Thus the same wind fields were used for both the base case and climate change scenarios.

It appears reasonable that a change in the thermal structure of the atmosphere due to a temperature increase would modify wind patterns. However, it is hard to quantify at this time how those patterns would change, and what effect they would have on the model calculations of changes in air quality for the climate change scenarios.

Stability

It appears reasonable that increased surface temperature would result in an increase in convective activity and a corresponding increase in the frequency of unstable atmospheric conditions. In most air quality simulation models, such as the RTM-III, changes in stability affect plume rise and dispersion processes. In the RTM-III stabilty is calculated using a method proposed by Turner (1970) that relates stability class to surface wind speed and solar insolation. Since this stabilty classification scheme does not explicitly use temperature, we have no choice but to assume that stability does not change in the climate change scenarios.

Higher plume rise for point sources may result in local increases in ozone (due to the lack of NO titration) and possibly lower ground-level ozone values downwind. The occurrence of unstable conditions earlier in the day would bring emissions of hydrocarbons and nitrogen oxides (NO_x) together earlier in the day, resulting in a longer period of photochemical activity. Thus the lack of stability changes in the climate change scenarios may understate changes in ozone concentrations.

Emissions

It is well known that increased temperature results in increased evaporation and hence increased emission of volatile organic compounds (VOC). Temperature is also a key factor in emissions from automobiles. Since automobiles are the main class of reactive hydrocarbon emitters, and a major source for NO_x emissions, these emission changes could be significant. Automobiles tend to emit more reactive hydrocarbons and less NO_x and CO at higher ambient temperatures. Higher temperatures during the summer months, as is assumed in the California and midwestern/southeastern applications of the RTM-III, would also result in increased use of air-conditioning systems and corresponding increases in emissions from power plants supplying the electricity.

Biogenic emissions are also known to increase with temperature as plant respiration increases. However, at extreme temperatures some plants will close their stomata openings to reduce moisture loss, resulting in decreased respiration and a lower rate of biogenic emissions. The net effect of increased temperature on anthropogenic and biogenic emissions is a definite increase in reactive hydrocarbons and possibly a decrease in low-level (area source) NO_x and increase in elevated (point source) NO_x, resulting in a more reactive atmosphere.

It is difficult to estimate emission rates and distribution 50 to 100 years in the future. Reactive hydrocarbon and NO_x emissions are currently controlled to meet air quality standards. In addition, automobiles that far in the future would be significantly more efficient than the current automobile fleet, and the widespread use of electric cars is a distinct possibility. On the other hand, population growth will increase emissions as more people use electricity, industrial products, and automobiles.

Given the uncertainities associated with estimating emissions so far in the future, we elected to use the base case 1980 NAPAP anthropogenic and biogenic emissions for the climate change scenarios. Future research should include efforts to estimate future emissions under increased temperature conditions.

DEFINITION OF STRATOSPHERIC OZONE REDUCTION

Several climatic and atmospheric modeling studies have indicated that the stratospheric ozone layer is decreasing due to chemical reactions with halocarbons (Cicerone et al., 1983; Prather et al., 1984), methane (Craig and Chou, 1982), and nitrous oxide (Weiss, 1981). Since stratospheric ozone is the principal attenuator of ultraviolet radiation, the reduction in the stratospheric ozone layer would result in increased penetration of UV-B to the troposphere. This phenomenon would not only likely result in an increase in skin cancer, but also in increased photochemical reaction rates for specific atmospheric pollutants. These increased photochemical rates may, in turn, result in increased production of photochemical oxidants in the troposphere.

In fact, according to a recent study, the depletion of stratospheric ozone may be a more important factor than temperature increases in the formation of ozone in the urban environment (Gery et al., 1987). That study assumed a reduction in the stratospheric ozone column of from 16.5 to 33% and calculated the effects of the stratospheric ozone reduction on air quality in several urban areas. However, since the study an international agreement to control emissions of chlorocarbons has been signed. Based on the implementation of emission reductions specified in the so-called Montreal protocol, new estimates of the stratospheric ozone reduction range from 0 to 20%, with the latest predictions being a few percent. However, it remains to be seen whether the proposed controls will be effective in the future.

Thus for the climate change scenario that includes depletion of stratospheric ozone concentrations we are assuming a 10% decrease. For the base case simulations we assume an ozone column of 0.300 cm-atm. This represents approximately the monthly average ozone column at North American latitudes during the months of July and August. Thus a 10% reduction in stratospheric ozone would result in an ozone column of 0.270 cm-atm. Photolysis rates were calculated by the method discussed by Gery et al. (1987).

DEFINITION OF MODELING SCENARIOS

Three modeling scenarios were defined to estimate the effect of future climate changes on tropospheric ozone concentrations. These scenarios consist of a base case and two future climate cases:

Base case--current meteorological and ozone column conditions

Scenario #1--4°C temperature increase and attendant increase in water vapor concentrations.

Scenario #2--4°C temperature and water vapor increases and a 10% reduction in stratospheric ozone concentrations.

The RTM-III was exercised for ozone episodes of approximately one-week duration for the central California and the midwestern/southeastern modeling domains for the base case and scenario #1. Due to limitations on time and resources for this work, scenario #2 was modeled only for four days from the midwestern/southeastern modeling episode.

UNCERTAINTIES

Before presenting the modeling results it is useful to review the uncertainties associated with assumptions in the modeling. These uncertaintes can be roughly divided into three categories: (1) uncertainty in the assumptions used to define the climate change scenarios, (2) uncertainties in the model inputs, and (3) model limitations.

Definitions of the Climate Change Scenarios

Foremost among the uncertainties in the climate change scenarios is that the 4°C temperature increase is assumed to occur uniformly throughout the modeling domain and over the diurnal cycle. If most of the increase in temperature occurs at night, rather than in the day when photochemical activity occurs, then the assumption of uniform temperature change across the diurnal cycle may overstate the ozone concentrations, since ozone formation occurs during the day. If the temperature increase above the ground is less than 4°C, the assumption of a 4°C increase aloft may also overstate the ozone concentrations.

The assumption that mixing heights will not change with the increase in temperature will overstate ozone concentrations. By not including changes in cloudiness in the climate change scenarios, the effects of increased temperature will be either over- or underestimated, depending on whether cloudiness actually increases or decreases. The fact that stability is also not adjusted for the climate change scenarios may also result in an understatement of ozone concentrations.

The uncertainties associated with the water vapor concentrations stem from the assumption that the temperature increase is uniform and that relative humidity will remain constant as the temperature increases. As for the temperature, if daytime temperature and temperatures aloft do not increase 4°C, then the assumed water vapor concentrations will be too high and the resulting effects of increased temperature on ozone concentrations will be overstated.

Finally, the effects of holding emissions constant for the climate change scenarios will, most likely, result in an understatement of ozone concentrations. A significant increase in hydrocarbon emissions can be expected with a 4°C temperature increase and the population growth expected in the next 50 to 100 years. However, no one can predict the emission reductions that will occur in the future, or the possibility of more efficient emission controls. However, higher temperatures do result in an increase in emission rates, so that neglecting this change in emissions would result in an understatement of the changes in ozone concentrations.

Model Inputs

Quite a bit of uncertainty is associated with the meteorological and emissions inputs used in the applications of the RTM-III, as is true for all air quality models. Of particular note are the wind fields over complex terrain in the central California application. The ramifications of these uncertainties should, in general, be minimal since we are examining the sensitivity of a regional oxidant model to postulated changes in future climate conditions, and any possible deviations between model input and actual conditions would be the same for both the base case and climate change cases. However, since there is quite a bit of uncertainty in the temperature and water vapor concentration fields used as input, this uncertainty does transfer over to the calculations of ozone concentrations under increased temperature conditions. Depending on the base case temperature, an increase of 4°C will produce different effects in the photochemistry rates and resultant production of ozone.

Model Limitations

In any modeling study we cannot know with full certainty whether a model is capturing all of the effects of changes in meterological and emission input data. In this study we decided to change a minimal number of variables--temperature and water vapor--for the first climate change scenario. Thus the primary uncertainty will be in the chemical mechanism used. We have attempted to limit this uncertainty by incorporating into RTM-III the latest version of the Carbon Bond IV Mechanism, the CB-IV (Gery et al., 1988).

RESULTS OF THE SIMULATIONS -- CLIMATE CHANGE SCENARIO #1

The effects of increased temperature on tropospheric ozone concentations were studied in two separate simulations using RTM-II: a six-day ozone episode (5-10 August 1981) in California and an eight-day episode (14-21 July 1980) in the midwestern/southeastern United States. The RTM-III was run using current climate conditions (the base case) and an increased temperature scenario, which was characterized by a 4°C uniform temperature increase and attendant increase in water vapor concentration assuming constant specific humidity.

An Eulerian regional oxidant model, such as the RTM-III, will report multi-level gridded fields of hourly average concentration for each species (about 30) in the chemical mechanism. Clearly, not all of this data can or needs to be presented here. Of particular importance, in terms of air quality regulations and health effects, are the effects of climate changes on the maximum daily ozone concentrations. Thus in the following paragraphs we discuss the calculated changes in maximum daily ozone concentrations due to an increase in temperature for each day of the two episode simulations.

Central California

Maximum daily ozone concentrations were calculated at each grid point in the central California modeling domain for each day of the six-day episode. The results for the base case are displayed in isopleths for each day of the episode in Figure 2-1.[2] The results for the climate change scenario are shown in Figure 2-2. The differences between the daily maximum ozone concentrations for the climate change scenario and the base case are shown in isopleths in Figure 2-3. The highest maximum daily ozone concentrations predicted by the RTM-III for each day are given in Table 2-1.

August 5, 1981

On this day the main area of elevated ozone concentration is downwind of the San Francisco Bay Area for both the base case and climate change scenario (compare Figures 2-1a and 2-2a). The increase in temperature moves the location of the highest ozone concentration closer to the urban area. In fact, the increased temperature results in ozone concentrations that exceed the primary National Ambient Air Quality Standard (NAAQS) for ozone (12 pphm) whereas no exceedance is calculated in the base case. As predicted by the RTM-III, an increase in temperature of 4°C results in an area approximately 300 km exceeding the primary ozone standard on this day.

In areas away from the San Francisco urban area the effects of the temperature increase are small (see Figure 2-3a). In many areas there is no change, but in some areas, such as downwind of Bakersfield, there is a slight increase in ozone. However, in Bakersfield itself there is a slight decrease of over 0.5 pphm. This decrease appears to be the result of increased mixed layer NO concentrations from a point source whose plume rise was reduced because of bouyancy flux due to the increase in the ambient temperature. The increase of NO emissions in the mixed layer results in the local suppression of ozone due to titration.

August 6, 1981

The highest ozone concentrations for the entire episode were calculated for both the base case and increased temperature case on this day (see Figures 2-1b, 2-2b, and 2-3b). The temperature increase results in increases in ozone throughout the modeling domain; the highest maximum daily ozone concentration increases from 15.0 pphm in the base case to 18.0 in the increased temperature scenario, a 20% increase (Table 2-1). The

---

[2] All figures for this chapter are collected at the end of the chapter.

Table 2-1. Highest Daily Ozone Concentrations Predicted by the RTM-III For Each Day of the Central California Episode For the Base Case and the Case of Increased Temperature

	Maximum Daily Ozone Concentration (pphm)		
	Base Case	Increased Temperature	Percent Increase
5 August 1981	11.8	12.1	3
6 August 1981	15.0	18.0	20
7 August 1981	11.7	13.1	12
8 August 1981	13.5	13.7	2
9 August 1981	10.5	11.2	7
10 August 1981	9.1	9.8	8

ozone peak is slightly farther downwind in the increased temperature case. The region of predicted ozone concentration in excess of the NAAQS almost doubles from 3,700 km^2 (in the base case) to 6,600 km^2. Thus under the increased temperature scenario the model predicts exceedances of the NAAQS in the city of San Francisco.

In two of the main cities in the San Joaquin Valley, Fresno and Bakersfield, the temperature increase results in an increase of approximately 0.5 pphm (8%) in the maximum daily ozone concentration. In the rest of the valley ozone increases are on the order of 0.1 pphm. At regions distant from emission sources, such as the Sierra Nevada, there is little change in the ozone concentrations.

August 7, 1981

On August 7 the highest ozone concentrations for the base case and increased temperature scenario occur at the same site, approximately 80 km downwind of San Francisco (Figures 2-1c and 2-2c). However, ozone levels increase from 11.7 in the base case to 13.1 pphm under increased temperature. Again, under increased temperature the NAAQS is exceeded, where no exceedance occurred under current climate conditions. In the heart of the Oakland urban area ozone decreases by approximately 1 pphm (Figure 2-3c). This decrease may be due to the faster photochemical reactions caused by increased temperature, such that the more reactive hydrocarbons close to the urban areas are burned out before the time of peak photochemical production in the middle of the day. This is partially confirmed by the fact that the highest ozone concentration occurs earlier in the increased temperature scenario than in the base case.

In areas outside the San Francisco Bay Area urban plume the temperature increase has very little effect on ozone concentrations; the only significant effect is a slight increase (0.5 pphm) in the vicinity of Bakersfield.

August 8, 1981

On August 8 the highest ozone level in the increased temperature scenario (13.7 pphm) is only slightly higher than the highest value in the base case (13.5 pphm) (see Figures 2-1d and 2-2d). There is almost no difference between the two cases in the areal extent of the region in excess of the NAAQS. Again, the increased temperature scenario results in a slight (0.1 pphm) decrease in ozone at the San Francisco - Oakland urban center. In the remainder of the modeling domain there are slight increases in ozone, except for a small area around western Yosemite National Park, where there is a slight decrease in ozone (Figure 2-3d).

August 9, 1981

Ozone concentrations on August 9 are lower than the previous days in both the base case and the increased temperature scenario. Because of a shift in wind to the northwest, the highest daily ozone concentration is located southeast of the San Francisco Bay Area near Stockton. Over the northwestern portion of the modeling domain the temperature increase results in an increase in ozone (from 0.1 pphm in the base case to 2.0 pphm). Again the temperature increase has little effect on ozone concentrations in the remainder of the modeling domain, away from the influences of the San Francisco Bay Area urban plume (Figure 2-3e).

August 10, 1981

On August 10 an increase in wind speeds from the northwest results in a "tongue" of ozone spreading out from the San Francisco Bay Area down the San Joaquin Valley (Figures 2-1f and 2-2f). Although the highest ozone concentration on 10 August is the lowest for the six-day episode, for both the base case (9.1 pphm) and increased temperature scenario (9.8 pphm), ozone concentrations within the San Joaquin Valley are both higher and more widespread than on previous days. Throughout the entire modeling domain the ozone concentrations in the increased temperature scenario are higher than in the base case.

Midwestern/Southeastern Region

Maximum daily ozone concentrations were calculated at each grid point in the midwestern/southeastern U.S. for an eight-day ozone episode (July 14-21, 1980). The results for the base case are shown in isopleths in Figure 2-4. The results for the first climate change scenario are shown in Figure 2-5. The differences between the climate change scenario and the base case are shown in isopleths in Figure 2-6. The highest maximum daily ozone concentrations predicted by RTM-III for each day are given in Table 2-2.

July 14, 1980

On the first day of the episode the increased temperature has almost no effect on the ozone concentrations compared to the base case (Figures 2-4a and 2-5a). In fact, the plot showing differences between the two cases (Figure 2-6a) reveals that there are about equal areas with increases and decreases in ozone and these differences rarely exceed 0.1 pphm in magnitude. The exception is in the vicinity of Pittsburg, where the increased temperature scenario results in a decrease in ozone of approximately 1 pphm. For a region of this size it would take over one day to minimize the effects of the initial conditions; thus, we cannot tell if this decrease is significant or just an artifact of the initial conditions. The highest ozone concentrations calculated for the base case and increased temperature case are the same (11.3 pphm).

July 15, 1980

On July 15 the highest ozone concentrations for the base case (11.5 pphm) and the increased temperature scenario (11.9 pphm) both occur in the urban plume downwind of Chicago. Except for an area stretching from Arkansas to Alabama, ozone concentrations are higher everywhere under the increased temperature scenario. The highest increase (approximately 1 pphm) occurs on the border between Minnesota and Iowa (Figure 2-6b).

July 16, 1980

The highest ozone concentration for the base case on July 16 (12.5 pphm) occurs in the urban plume downwind of Detroit. Under the increased temperature scenario the highest concentration (13.0 pphm) is still downwind of Detroit but the predicted area of exceedances of the ozone NAAQS increases by almost a factor of three from approximately 9,800 km^2 in the base case to 27,000 km^2. In the increased temperature scenario increases in ozone are mainly in the upper midwestern, southwestern, and southeastern portions of the modeling domain (Figure 2-6c). In three areas with elevated ozone (>10 pphm) in the base case--the Ohio River valley, New Orleans, and Iowa--the increases in ozone in the increased temperature scenario are less (<0.2 pphm) than is seen downwind of Detroit.

July 17, 1980

On July 17 ozone levels in the increased temperature scenario are higher than in the base case over almost the entire modeling domain (Figures 2-4d, 2-5d, and 2-6d). Significant increases, greater than 0.5 pphm, occur over an area connecting the cities of Chicago and Detroit. The highest calculated ozone concentration in the region is 12.0 pphm, compared to 11.7 pphm for the base case. There are slight increases in ozone (0.1 to 0.5 pphm) in other areas of base case predicted elevated ozone concentrations (>10 pphm), i.e., Nashville, New Orleans, and Iowa. However, in the increased temperature scenario ozone levels over eastern Kansas are lower than in the base case (10.7 pphm compared to 11.7 pphm).

July 18, 1980

On July 18 ozone concentrations throughout the entire modeling domain increase significantly under the increased temperature scenario. Increases in excess of 1 pphm occur over Iowa, Wisconsin, and Pennsylvania; in most of the modeling domain increases are in excess of 0.5 pphm. The highest ozone concentration under the increased temperature scenario is 12.1 pphm, an exceedance of the NAAQS.

Table 2-2. Highest Maximum Daily Ozone concentrations Predicted by the RTM-III for Each Day of the Midwestern/Southeastern Episode For the Base Case and the Case of Increased Temperature

Date	Maximum Daily Ozone Concentration (pphm)		
	Base Case	Increased Temperature	Percent Increase
14 July 1980	11.3	11.3	0.0
15 July 1980	11.5	11.9	3.5
16 July 1980	12.5	13.0	4.0
17 July 1980	11.7	12.0	2.6
18 July 1980	11.2	12.1	8.0
19 July 1980	13.8	14.8	7.2
20 July 1980	11.1	11.2	0.9
21 July 1980	12.6	12.3	-2.4

July 19, 1980

Urban plumes from St. Louis, Chicago, Detroit, and emissions from the Ohio River valley create a region of elevated ozone concentration covering Indiana, Illinois, Ohio, and Michigan. The highest calculated ozone concentrations of the episode occur on this day downwind of Detroit over Toronto (Figures 2-4f and 2-5f): 13.8 pphm in the base case and 14.8 pphm in the increased temperature case. In the latter case ozone levels are higher than in the base case over most of the region; the most significant increases (0.5 to 1 pphm) occur in Minnesota, Iowa, Wisconsin, and Michigan.

July 20, 1980

On July 20 the only significant increases in ozone under the increased temperature scenario occur in the upper northwestern portion of the region (Figures 2-4g, 2-5g, and 2-6g). The highest ozone concentration calculated for the base case on this day (11.1 pphm) occurs over Pittsburgh; for the increased temperature case it is 11.2 pphm, also over Pittsburgh. A more dramatic increase in ozone due to the increase in temperature occurs downwind of Chicago, from 10.7 pphm in the base case to 11.2 pphm.

July 21, 1980

On the last day of the episode the increased temperature results in significant ozone increases over a large portion of the region compared to the base case (Figure 2-6h). The main exception is near the center of the western boundary, where ozone under the increased temperature scenario is less than in the base case (12.3 pphm compared to 12.6 pphm). However, significant increases occur around Chicago, where the maximum daily ozone concentration in the Chicago plume increases from 11.1 in the base case to 12.3 pphm in the increased temperature scenario. Despite the fact that the highest ozone concentration on this day is lower in the increased temperature scenario than in the base case, the area of ozone concentrations in excess of the NAAQS increases from approximately 9,800 km^2 in the base case to 16,900 km^2 in the increased temperature scenario.

RESULTS OF THE SIMULATIONS -- CLIMATE CHANGE SCENARIO #2

Because of limitations on the study, simulations of climate change scenario #2 were limited to four days of the midwestern/southeastern episode and the California episode was not simulated. Here we briefly examine the results of the simulation of the four days (July 14-17, 1980) in the midwestern/southeastern U.S. episode. In this second climate change scenario the temperature is assumed to increase by 4°C, as in scenario #1, and photolytic rates are assumed to increase due to a 10% reduction in the ozone column. Predicted maximum daily ozone concentrations for the second climate change scenario are shown in isopleths in Figure 2-7, and isopleths showing the differences between this case and the base case are shown in Figure 2-8.

As noted by Gery et al. (1987), the effects of increased ultraviolet irradiance or temperature on tropospheric ozone concentrations depends on the oxidant-forming potential of the system. This in turn is generally a function of meteorological conditions and the efficiency of the atmospheric system in converting oxidant precursors to oxidants. For some atmospheric systems the increased energy results in increased reactivity in the morning hours, depleting enough oxidant precursors from the system to limit afternoon ozone production to levels lower than the base case.

For example, on July 14 of the modeled episode the patterns of increases and decreases in ozone for the two climate change scenarios are similar. This seems to indicate that the ozone formation potential for this day is precursor limited. Over most of the region the maximum daily ozone concentrations for the two scenarios differ by only 0.1 pphm; the biggest difference occurs in the northeastern portion of the modeling domain. The highest ozone concentration for all three scenarios on 14 July occurs over the Ohio River valley, where the value under increased UV and temperature conditions is 11.6 pphm compared to 11.3 pphm for both the base case and first climate change scenario. Thus for the Ohio River Valley, the ozone formation potential may not be precursor limited. Differences in the two climate change scenarios occur on the Pennsylvania-Ohio border; under increased temperature alone (scenario #1) ozone is approximately 1 pphm lower than in the base case, whereas under scenario #2 (increased temperature and UV) ozone is only 0.1 pphm lower than in the base case.

On the other three days of the episode under the second climate change scenario, ozone levels are slightly lower (0 to 0.3 pphm) than under scenario #1. Both climate change scenarios produce a similiar pattern of increases and decreases in concentrations when compared to the base case for this episode. This is illustrated by the highest daily maximum ozone concentrations for July 15-17: the values under the second climate change scenario lie between the base case and first climate change case (see Table 2-2).

These results are consistent with those found by Gery et al., who showed that under conditions of increased temperature and UV radiation the highest ozone concentrations were frequently lower in cities with less oxidant precursors. This is because the increased energy, due to an increase in temperature and/or UV radiation, burns out the oxidant precursors earlier in the day, resulting in less oxidant precursors in the afternoon, the period of maximum ozone formation potential. The rather coarse grid spacing used in the midwestern/southeastern modeling domain (approximately 50 km on a side) reduces the peak precursor concentrations from the urban areas because of dilution in the large grid cells.

IMPLICATIONS OF THE ANALYSIS FOR AIR QUALITY CONTROLS

Although this preliminary model sensitivity analysis may be useful in anticipating the kinds of air quality controls that may be needed in responding to potential global climate changes, the uncertainties associated with predicting just how the climate may be modified preclude any definitive discussion here of regulatory controls. These preliminary modeling results can only indicate possible general trends in exceedances of the ozone standard and increases in the number of people exposed to unhealthy levels of ozone as a result of global climate change.

Our study indicates that under most conditions (i.e., immediately downwind of urban areas) increased temperature tends to (1) increase ozone concentrations, (2) move the location of the peak ozone concentration closer to urban areas, and (3) expand the area in which ozone concentrations exceed the primary ozone standard of 12 pphm. Thus the modeling study indicates that global warming will not only lead to more exceedances of the primary ozone standard over a larger area, but also to an increase in the number of people exposed to these elevated ozone concentrations. Maps of the ozone concentrations in the vicinity of the San Francisco Bay Area for the base case and first climate change scenario clearly show the increase in areas of exceedances of the NAAQS due to increases in temperature (Figure 2-9). Similar maps for the midwestern/southeastern modeling domain are given in Figure 2-10. A crucial question is whether future increases in global temperature will jeopardize the goal of attainment of the ozone standard in regions in the United States and increase the number of people exposed to unhealthy levels of ozone concentrations.

Census data from 1980 were mapped onto the two modeling regions (central California and midwestern/southeastern U.S.) to determine the number of people that may be exposed to higher levels of ozone concentrations as a result of increased ambient temperature. Table 2-3 presents estimates of the number of people-hours exposed to ozone concentrations in excess of 8, 12, and 16 pphm for the base case and the increased temperature case for the two modeling regions. These estimates were obtained by multiplying the population in a grid cell by the total number of hours that the predicted hourly ozone concentration in that grid cell exceeded 8, 12, or 16 pphm. Thus the figures in Table 2-3 are overstatements of the actual population exposure since people tend to spend 80 to 90% of their time indoors, and indoor ozone concentration levels are typically 10 to 70% of the outdoor level.

Table 2-3 indicates that approximately three times as many people in the central California modeling domain and 60% more people in the midwestern/southeastern modeling domain will be exposed to hourly ozone concentrations in excess of the NAAQS as a result of a 4°C temperature increase. In addition, the modeling

Table 2-3. **Number of People-Hours of Exposure to Ozone Concentrations in Excess of 8, 12, and 16 pphm For the Base Case and the Increased Temperature Case (Climate Change Scenario #1)**

	Exposure to $O_3 \geq 8$ pphm	Exposure to $O_3 \geq 12$ pphm	Exposure to $O_3 \geq 16$ pphm
Central California			
Base Case	70,509,216	660,876	0
Increased Temperature	102,012,064	2,052,143	92,220
Midwestern/Southeastern U.S.			
Base Case	1,722,590,208	29,805,348	0
Increased Temperature	1,956,205,568	47,528,944	0

results suggest that, with the increase in temperature, people in central California will be exposed to ozone concentrations in excess of 16 pphm whereas under current temperature conditions the modeled ozone concentrations do not exceed 16 pphm.

In air quality regulation, geographic areas are divided into air basins for purposes of classifying air quality, although air basins are sometimes further divided into local regions. A region is considered "nonattainment" of an air quality standard (NAAQS) if its estimated exceedance rate of the NAAQS is more than once per year over three years. Exceedances are counted in terms of days. The number of monitors recording an exceedance or the number of hours is not a factor in establishing an exceedance. Thus whether two monitors in a region measure an exceedance of the NAAQS or one monitor measures several hours of exceedance on the same day, that day counts as one exceedance of the NAAQS for that region.

In the RTM-III simulation of the six-day central California episode the number of exceedances of the NAAQS for the entire modeling domain doubles from two to four days due to increases in temperature (Table 2-1). For the eight-day episode in the midwestern/southeastern U.S the number of days in which predicted ozone concentrations exceed the NAAQS increased from three for the base case to five for the increased temperature case. These exceedances occur in several different areas: Chicago, New Orleans, Iowa, Illinois, and downwind of Detroit.

To estimate the increases in exceedances and attainment status due to future increases in temperature we estimated the number of exceedances in each grid cell of the central California and midwestern/southeastern modeling domains. As discussed above, attainment or nonattainment is usually defined for entire air basins, although the definition of air basins is somewhat arbitrary and in some cases, at the discretion of the EPA, subregions within air basins are classified separately.

Table 2-4 gives the population exposed to exceedances of the NAAQS for ozone of 12 pphm. According the the RTM-III calculations for the California episode, a 4°C temperature increase will increase the number of exceedances of the NAAQS from 2 to 3 and increase the number of people exposed to an exceedance.

Out of a total of 5.5 million people living in the central California modeling domain in 1980, the percentage of people exposed to one exceedance of the NAAQS increases from 3% (175,080 people) for the base case to 8% (456,782 people) for the temperature increase case. Approximately 70,000 and 26,000 additional people would be exposed to, respectively, 2 and 3 exceedances of the ozone standard.

Increased temperature also expands the area of exceedances. Regions experiencing one, two, and three exceedances of the ozone NAAQS increase, respectively, from 5,200 to 7,100 km^2, 3,000 to 4,400 km^2, and 0 to 1,600 km^2.

Similiar results are seen for the midwestern/southeastern modeling domain. With an increase in temperature of 4°C, approximately 360,000 people would be exposed to two exceedances of the ozone standard. Out of approximately 35 million people in the midwestern/southeastern modeling domain, the percentage of people exposed to one exceedance of the NAAQS would increase from 25% (in the base case) to almost 30%.

These results must be viewed with caution. As discussed earlier, numerous simplifying assumptions were made in modeling the impacts of climate change on ozone, and these assumptions add significantly to the quantitative uncertainty normally inherent in air quality modeling. Some of these assumptions, e.g., that the increase in temperature occurs everywhere, will tend to overstate the effects of increased temperature, while others, e.g., that hydrocarbon emissions do not increase under increased temperature conditions, tend to understate the impacts. The climate change scenarios presented here are simplistic and most likely do not completely describe the changes in climate associated with global warming.

The model's calculations of ozone under the simplified climate change scenarios discussed here should thus be viewed as possible trends rather than as conclusive impacts. The basic results of this modeling exercise are that increases in temperature will likely result in increases in maximum daily ozone concentrations, increases in the areas impacted by high ozone concentrations, and increases in the number of people exposed to unhealthy levels of ozone. Under these circumstances, emission control requirements currently planned to achieve attainment of the ozone standard may not be sufficient.

Table 2-4. Population Exposed to Exceedances of the National Ambient Air Quality Standard for Ozone (12 pphm) for the Base Case and Increased Temperature Case (Climate Change Scenario #1). Population Figures Represent the Total Population in all Model Grid Cells With a Specified Number of Exceedances

	Pop. in Grid Cells with 1 Exceed.	Pop. in Grid Cells with 2 Exceed.	Pop. in Grid Cells with 3 Exceed.
Central California			
Base Case	175,080	122,625	0
Increased Temperature	456,782	192,625	26,548
Midwestern/Southeastern U.S.			
Base Case	8,741,510	0	0
Increased Temperature	10,199,734	359,753	0

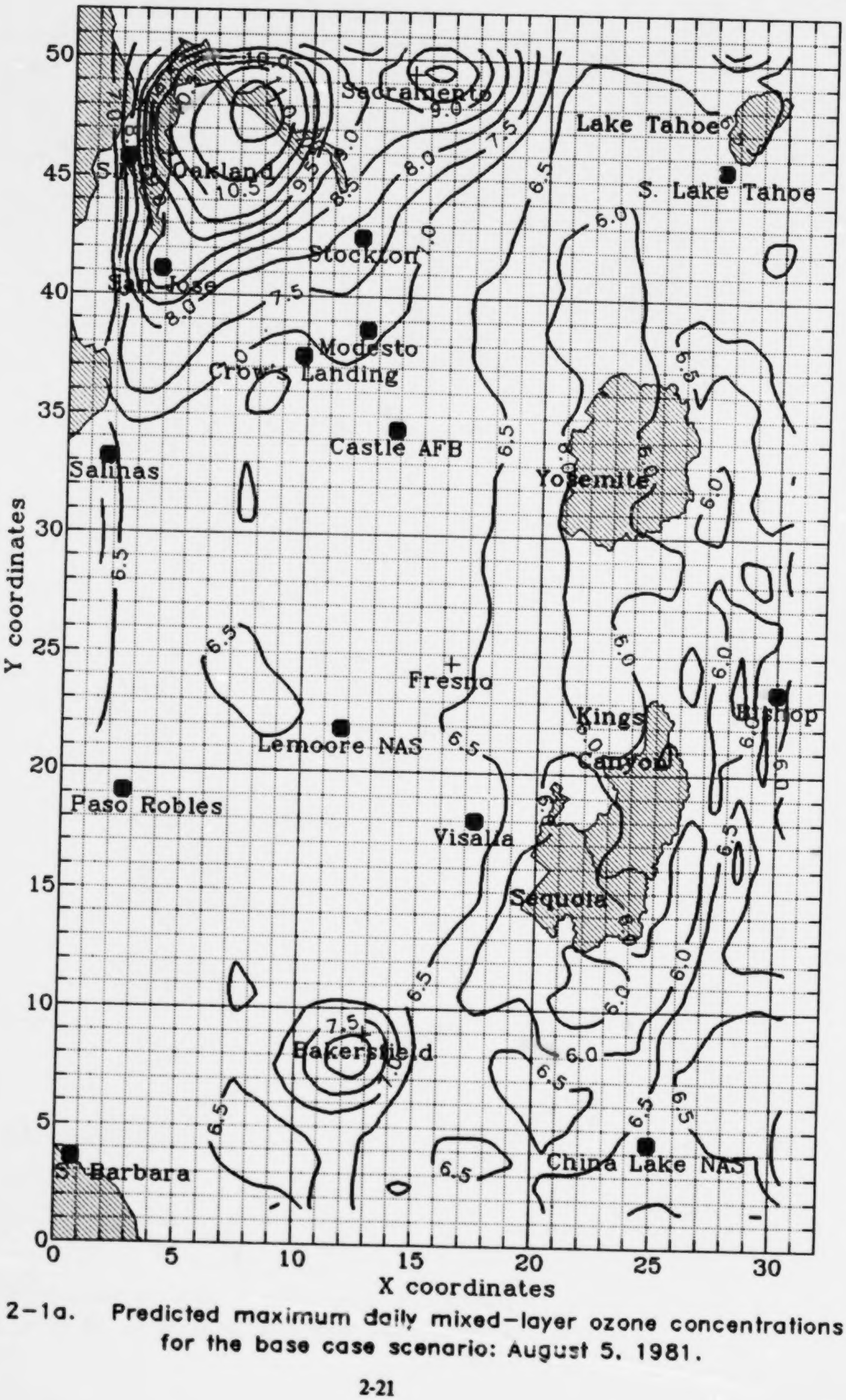
Y coordinates
X coordinates
0
5
10
15
20
25
30
35
40
45
50
Sacramento
Lake Tahoe
S. Lake Tahoe
S.F.
Oakland
Stockton
San Jose
Modesto
Crow's Landing
Castle AFB
Salinas
Yosemite
Fresno
Lemoore NAS
Kings Canyon
Bishop
Paso Robles
Visalia
Sequoia
Bakersfield
S. Barbara
China Lake NAS
10.5
10.0
9.5
9.0
8.5
8.0
7.5
7.0
6.5
6.0

Figure 2–1a. Predicted maximum daily mixed–layer ozone concentrations (pphm) for the base case scenario: August 5, 1981.

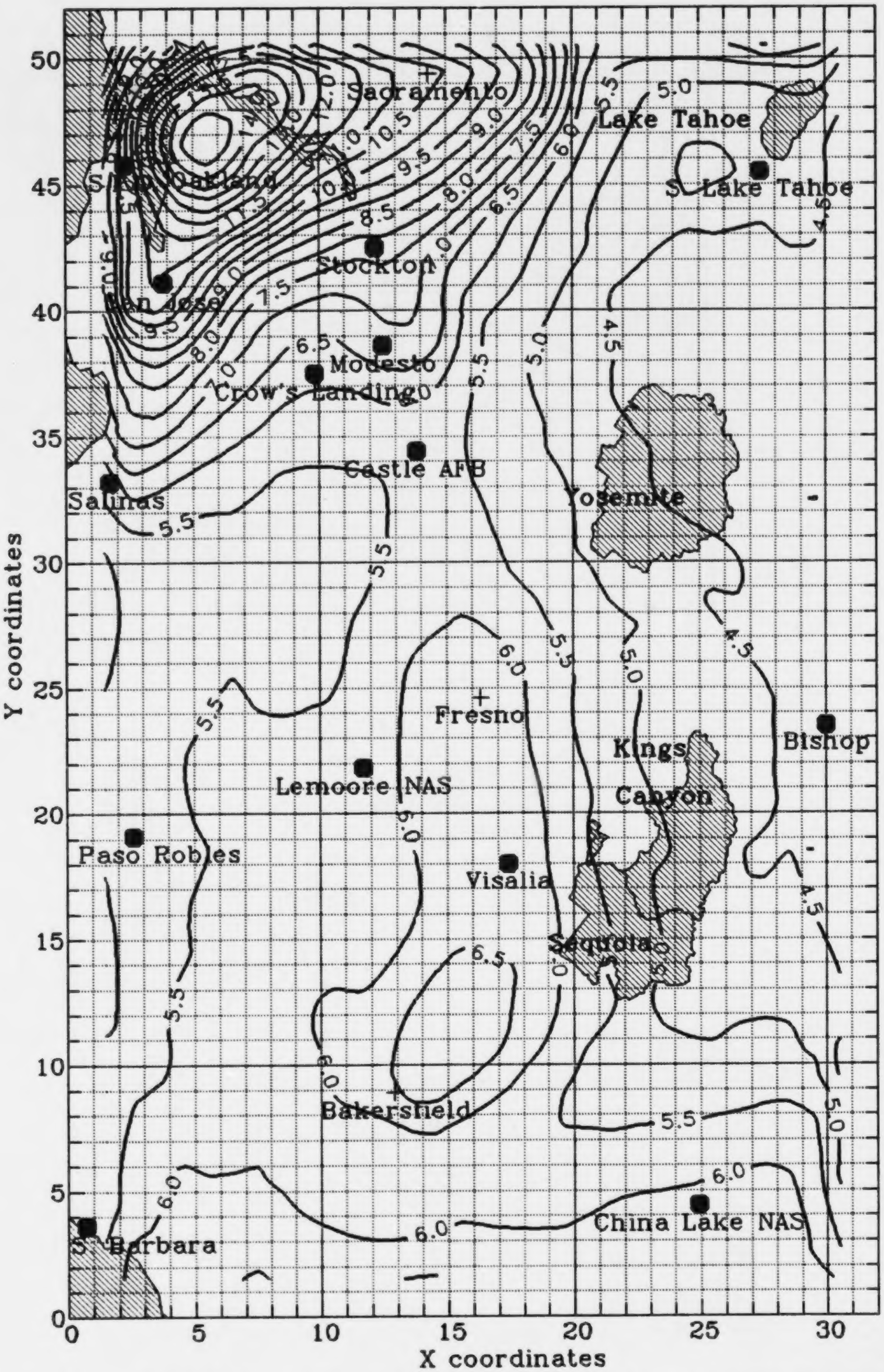
Sacramento
Lake Tahoe
S. Lake Tahoe
S.F.
Oakland
Stockton
San Jose
Modesto
Crow's Landing
Castle AFB
Salinas
Yosemite
Fresno
Kings
Canyon
Bishop
Lemoore NAS
Paso Robles
Visalia
Sequoia
Bakersfield
China Lake NAS
S. Barbara
14.0
12.0
10.5
10.0
9.5
9.0
8.5
8.0
7.5
7.0
6.5
6.0
5.5
5.0
4.5
Y coordinates
X coordinates
0
5
10
15
20
25
30
35
40
45
50

Figure 2–1b. Predicted maximum daily mixed–layer ozone concentrations (pphm) for the base case scenario: August 6, 1981.

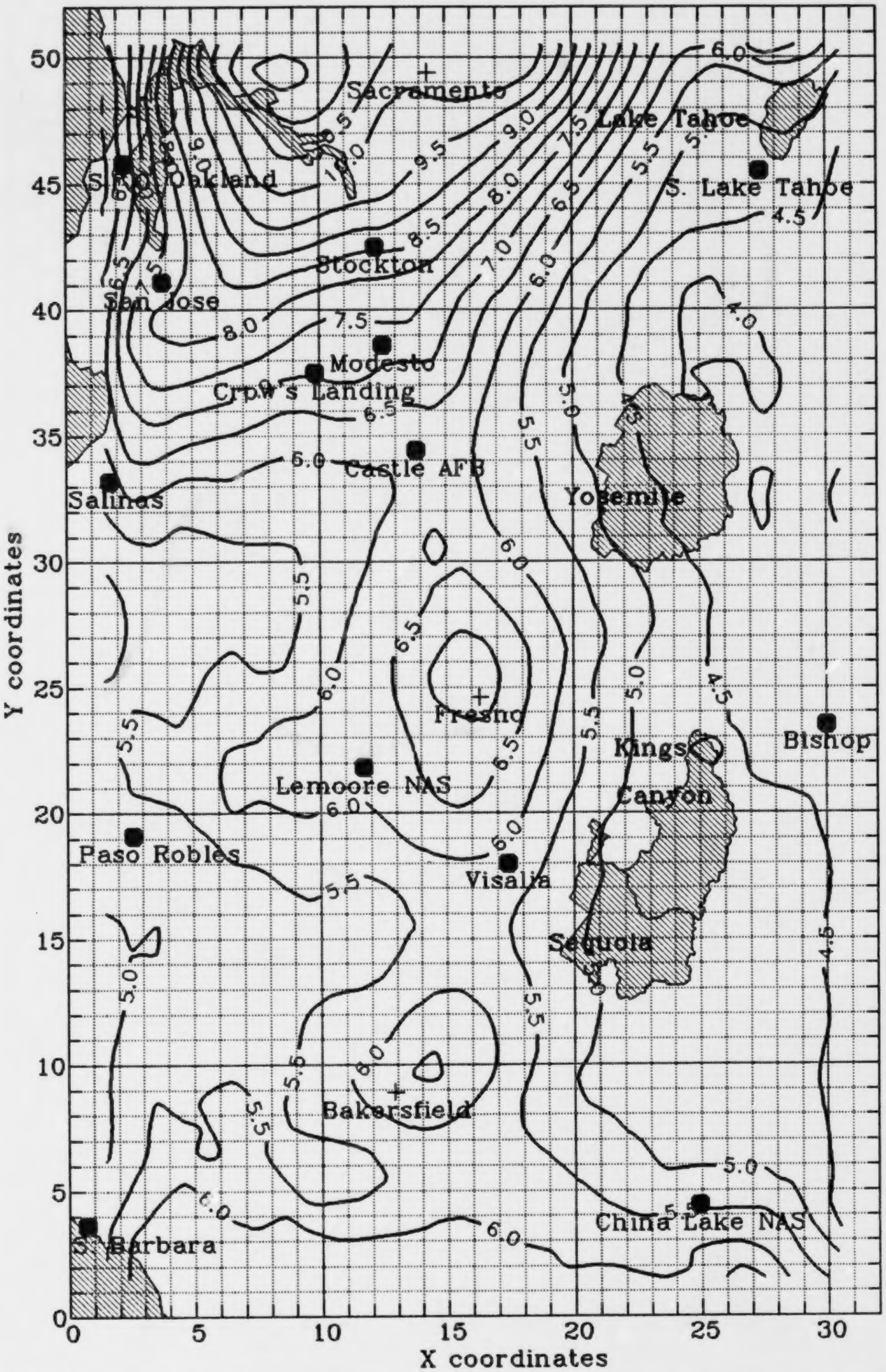
Y coordinates
X coordinates
0
5
10
15
20
25
30
35
40
45
50
Sacramento
Lake Tahoe
S. Lake Tahoe
S.F./Oakland
Stockton
San Jose
Modesto
Crow's Landing
Castle AFB
Salinas
Yosemite
Fresno
Kings
Canyon
Bishop
Lemoore NAS
Paso Robles
Visalia
Sequoia
Bakersfield
China Lake NAS
S. Barbara
6.0
9.0
9.5
10.0
8.5
8.0
7.5
7.0
6.5
5.5
5.0
4.5
4.0

Figure 2-1c. Predicted maximum daily mixed-layer ozone concentrations (pphm) for the base case scenario: August 7, 1981.

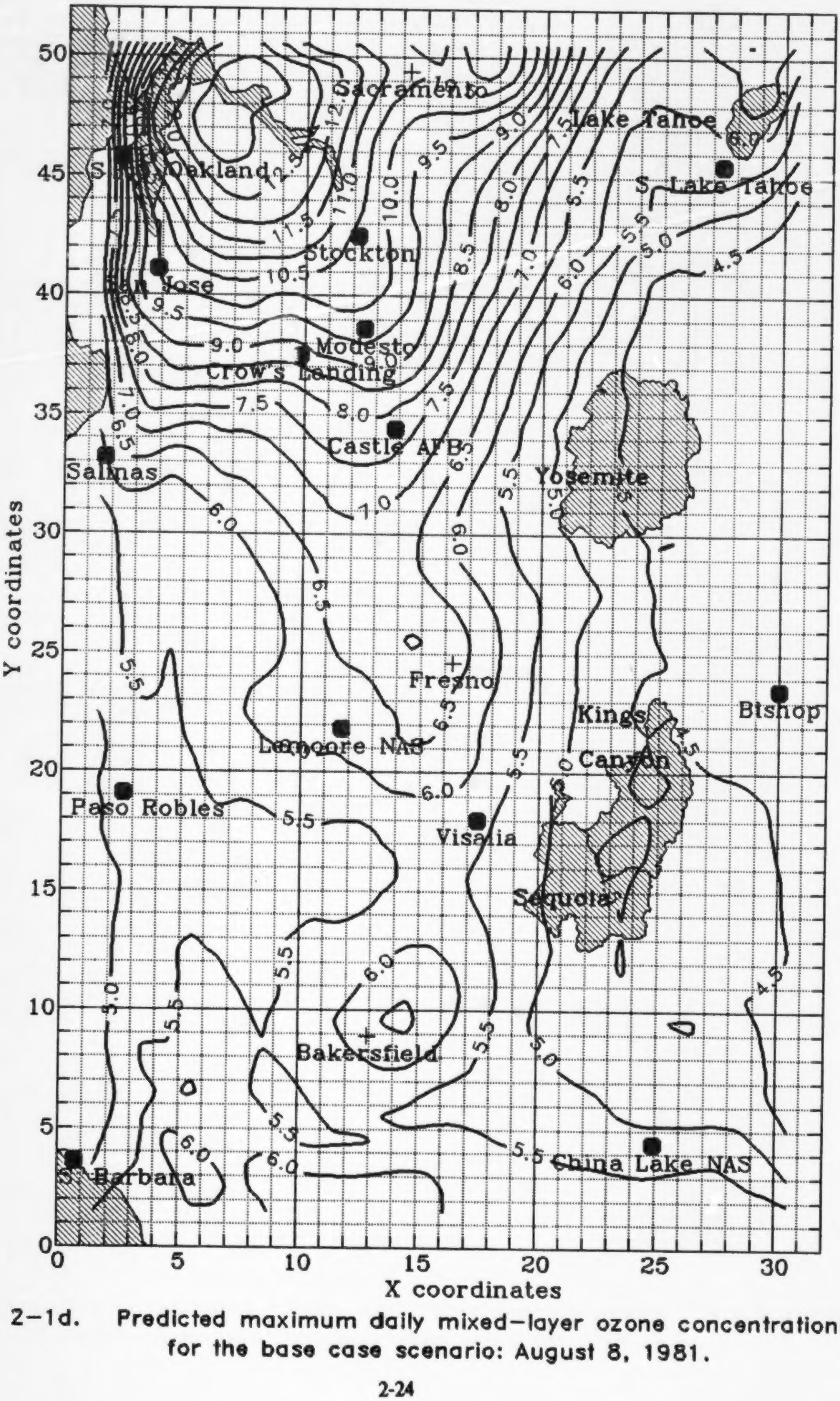
Y coordinates
X coordinates
0
5
10
15
20
25
30
35
40
45
50
Sacramento
Lake Tahoe
S. Lake Tahoe
Oakland
Stockton
San Jose
Modesto
Crow's Landing
Castle AFB
Salinas
Yosemite
Fresno
Kings
Canyon
Bishop
Lemoore NAS
Paso Robles
Visalia
Sequoia
Bakersfield
China Lake NAS
S. Barbara
12.0
11.5
11.0
10.5
10.0
9.5
9.0
8.5
8.0
7.5
7.0
6.5
6.0
5.5
5.0
4.5

Figure 2-1d. Predicted maximum daily mixed-layer ozone concentrations (pphm) for the base case scenario: August 8, 1981.

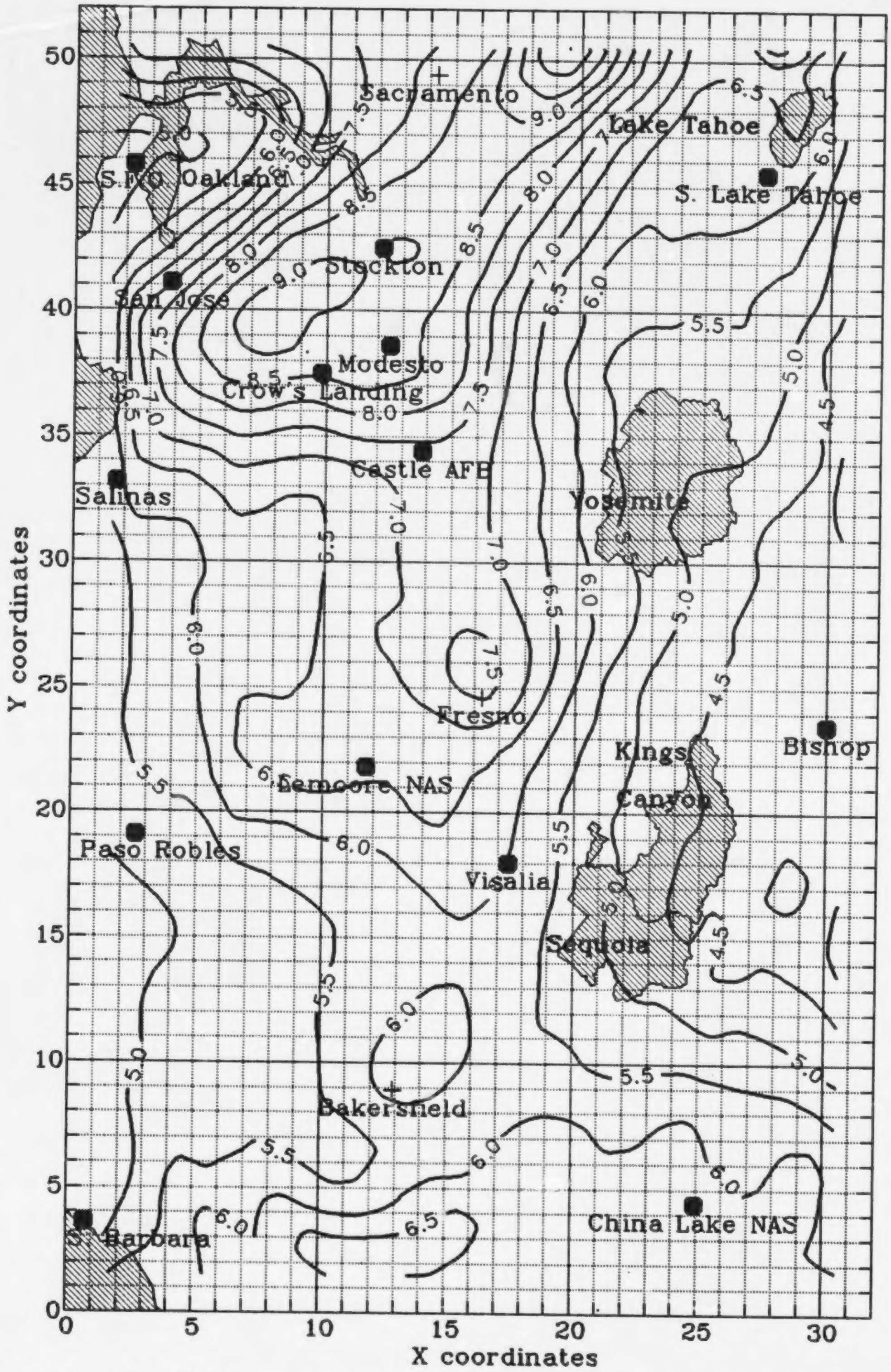
Sacramento
Lake Tahoe
S.F. Oakland
S. Lake Tahoe
Stockton
San Jose
Modesto
Crow's Landing
Castle AFB
Salinas
Yosemite
Fresno
Kings Canyon
Bishop
Lemoore NAS
Paso Robles
Visalia
Sequoia
Bakersfield
China Lake NAS
S. Barbara
Y coordinates
X coordinates
0
5
10
15
20
25
30
35
40
45
50
4.5
5.0
5.5
6.0
6.5
7.0
7.5
8.0
8.5
9.0

Figure 2–1e. Predicted maximum daily mixed–layer ozone concentrations (pphm) for the base case scenario: August 9, 1981.

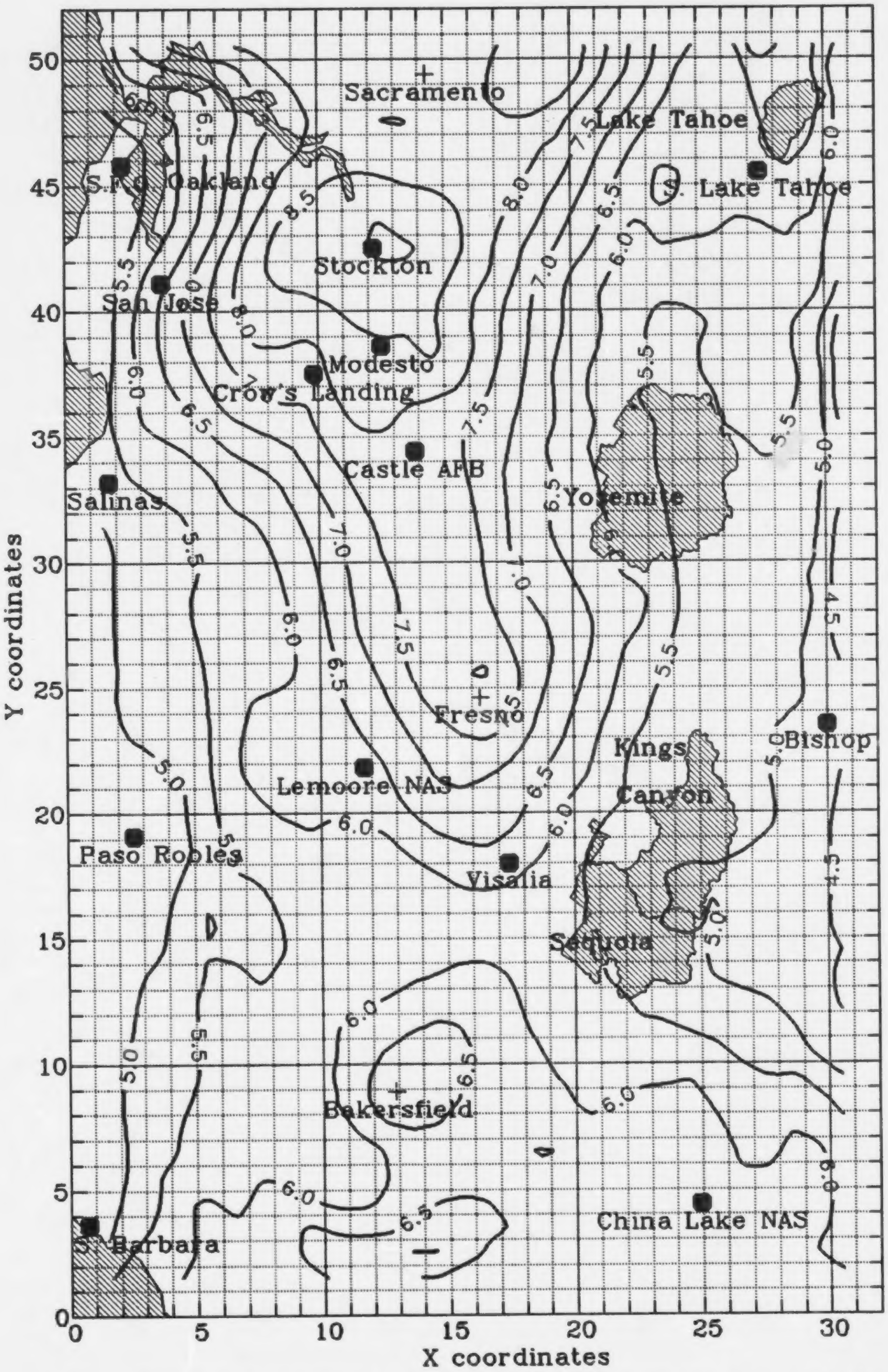
Sacramento
Lake Tahoe
S.F. Oakland
S. Lake Tahoe
Stockton
San Jose
Modesto
Crow's Landing
Castle AFB
Salinas
Yosemite
Fresno
Kings
Canyon
Bishop
Lemoore NAS
Paso Robles
Visalia
Sequoia
Bakersfield
China Lake NAS
S. Barbara
Y coordinates
X coordinates
0
5
10
15
20
25
30
35
40
45
50
4.5
5.0
5.5
6.0
6.5
7.0
7.5
8.0
8.5

Figure 2-1f. Predicted maximum daily mixed-layer ozone concentrations (pphm) for the base case scenario: August 10, 1981.

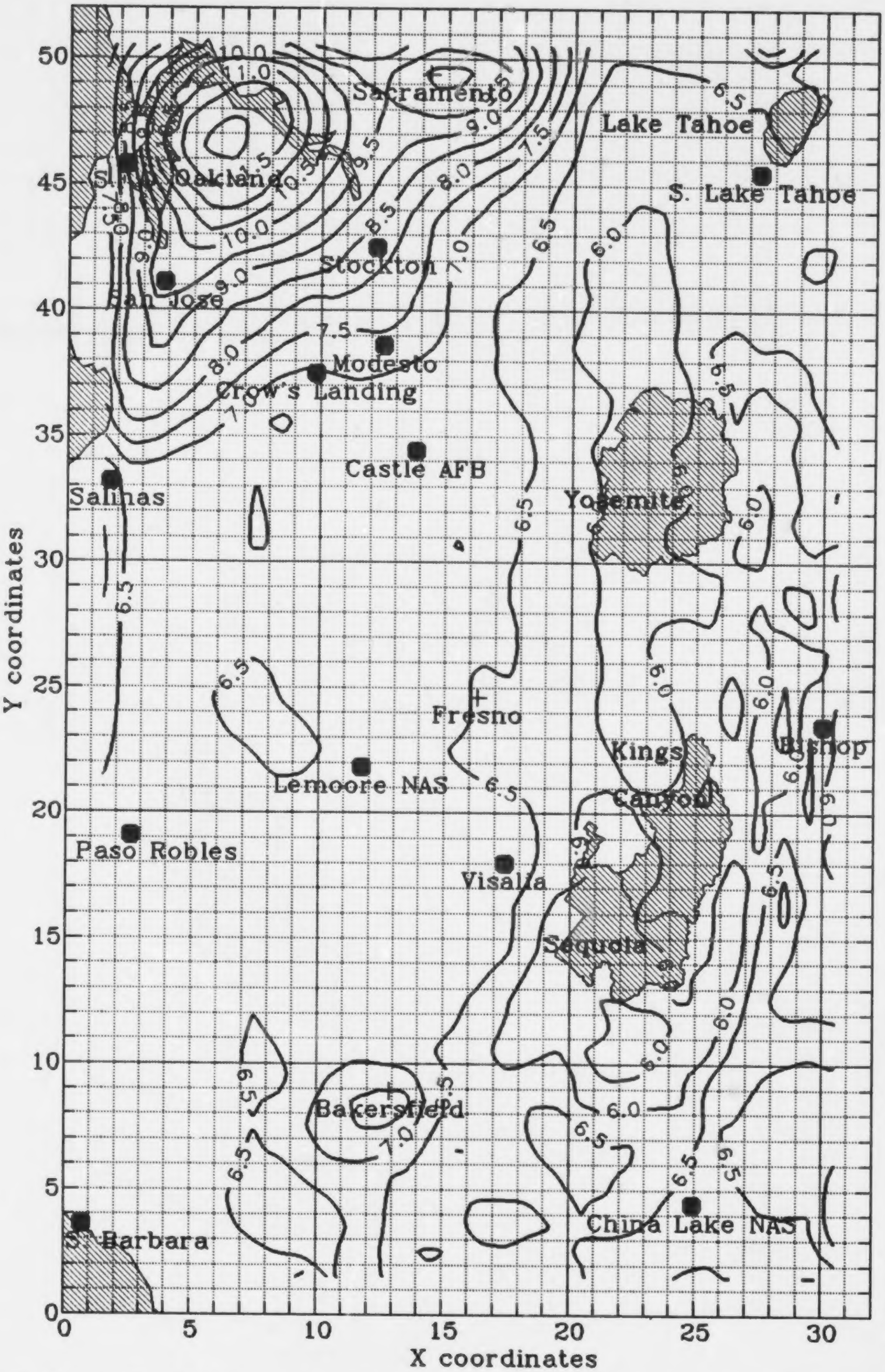
Sacramento
Lake Tahoe
S. Lake Tahoe
S.F.
Oakland
San Jose
Stockton
Modesto
Crow's Landing
Castle AFB
Salinas
Yosemite
Fresno
Kings Canyon
Bishop
Lemoore NAS
Paso Robles
Visalia
Sequoia
Bakersfield
China Lake NAS
S. Barbara
10.0
11.0
10.5
9.5
9.0
8.5
8.0
7.5
7.0
6.5
6.0
Y coordinates
X coordinates
0
5
10
15
20
25
30
35
40
45
50

Figure 2–2a. Predicted maximum daily mixed-layer ozone concentrations (pphm) for climate sensitivity scenario #1 (temp. and water increase): August 5, 1981.

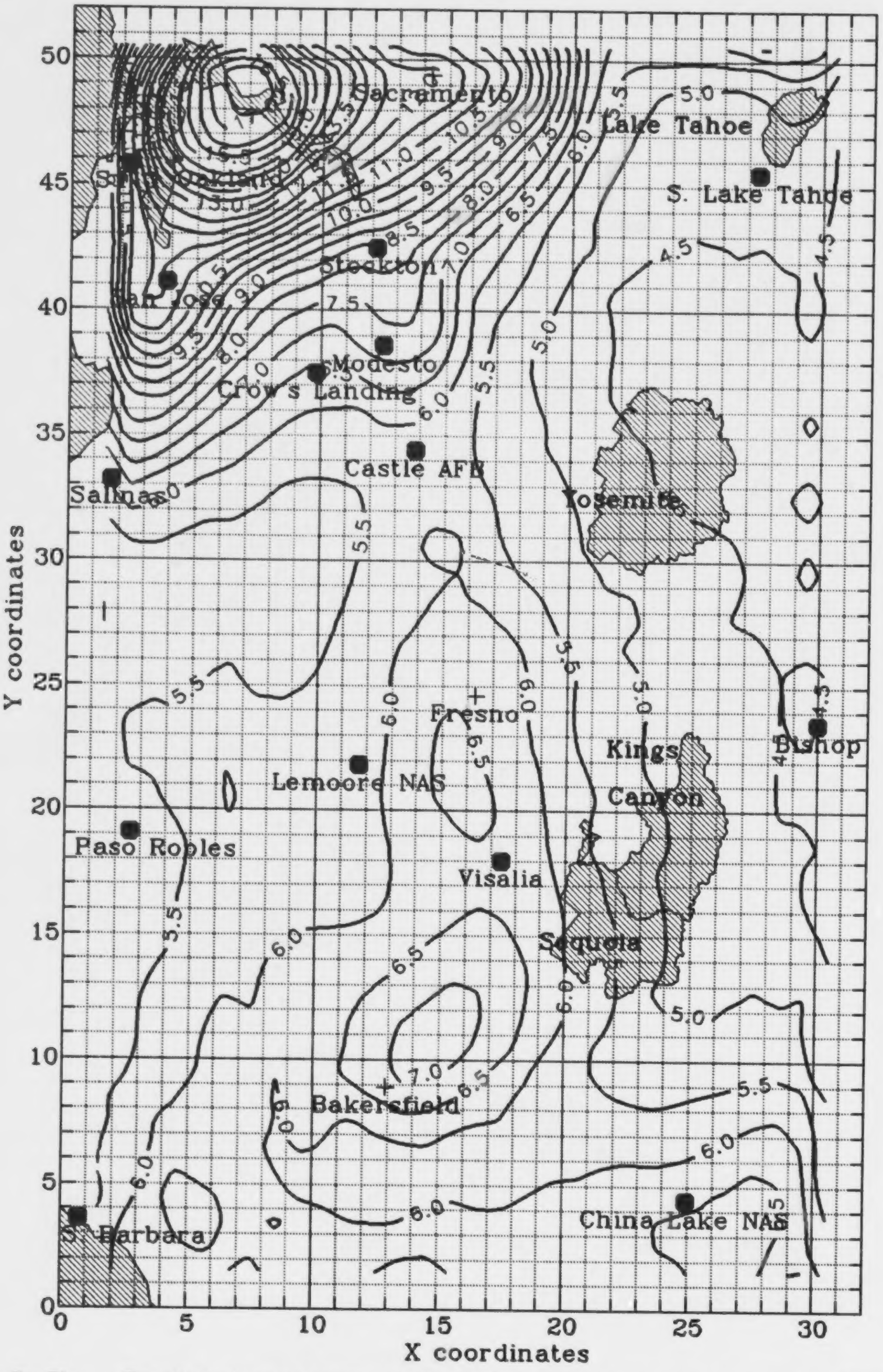
Sacramento
Lake Tahoe
S. Lake Tahoe
SF
Oakland
Stockton
San Jose
Modesto
Crow's Landing
Castle AFB
Salinas
Yosemite
Fresno
Kings
Canyon
Bishop
Lemoore NAS
Paso Robles
Visalia
Sequoia
Bakersfield
China Lake NAS
S. Barbara
13.0
11.0
10.5
10.0
9.5
9.0
8.5
8.0
7.5
7.0
6.5
6.0
5.5
5.0
4.5
Y coordinates
X coordinates
0
5
10
15
20
25
30
35
40
45
50

Figure 2-2b. Predicted maximum daily mixed-layer ozone concentrations (pphm) for climate sensitivity scenario #1 (temp. and water increase): August 6, 1981.

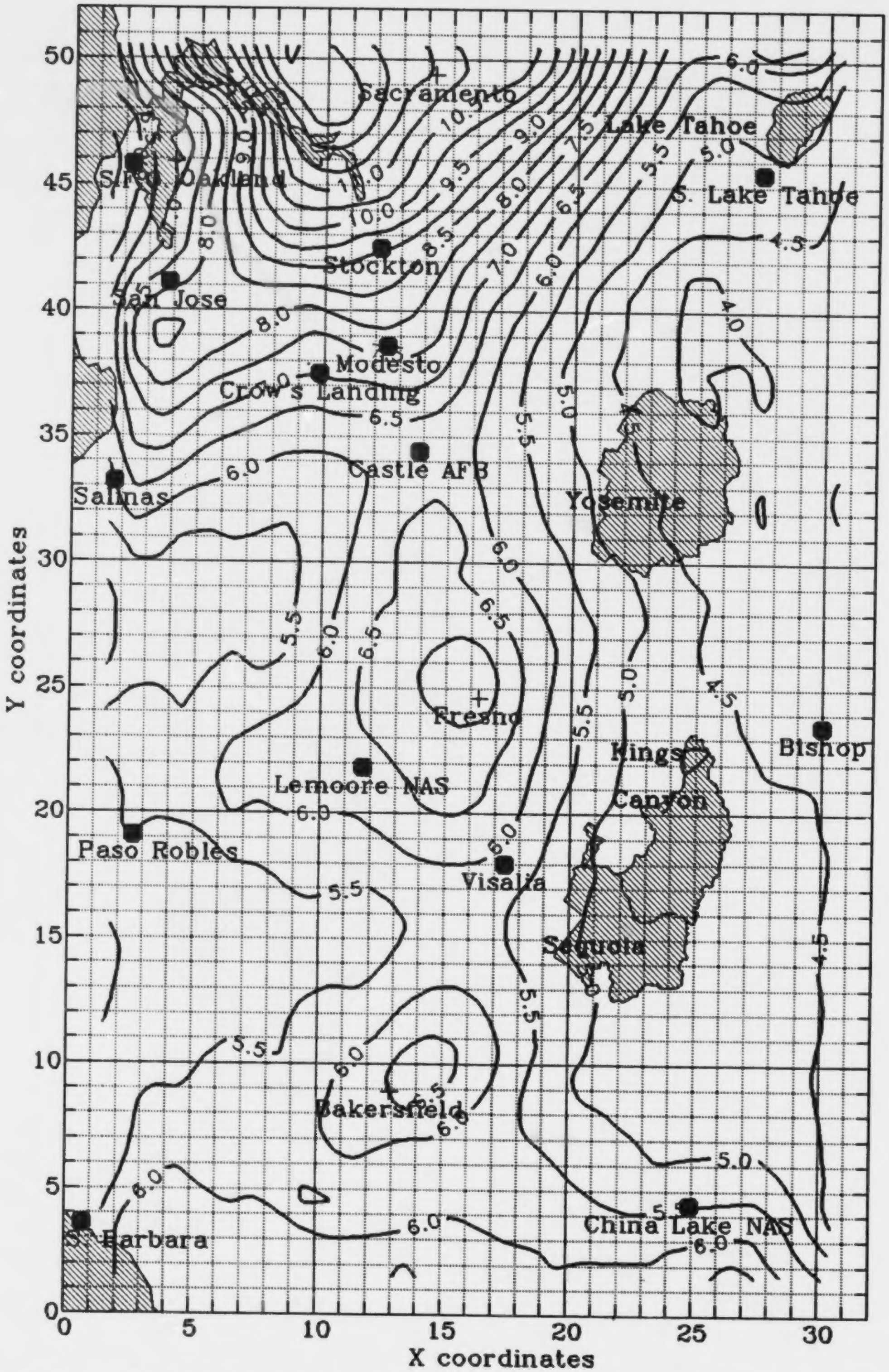
Sacramento
Lake Tahoe
S.F. Oakland
S. Lake Tahoe
Stockton
San Jose
Modesto
Crow's Landing
Castle AFB
Salinas
Yosemite
Fresno
Kings Canyon
Bishop
Lemoore NAS
Paso Robles
Visalia
Sequoia
Bakersfield
China Lake NAS
S. Barbara
10.0
9.5
9.0
8.5
8.0
7.5
7.0
6.5
6.0
5.5
5.0
4.5
4.0
Y coordinates
X coordinates
0
5
10
15
20
25
30
35
40
45
50

Figure 2-2c. Predicted maximum daily mixed-layer ozone concentrations (pphm) for climate sensitivity scenario #1 (temp. and water increase): August 7, 1981.

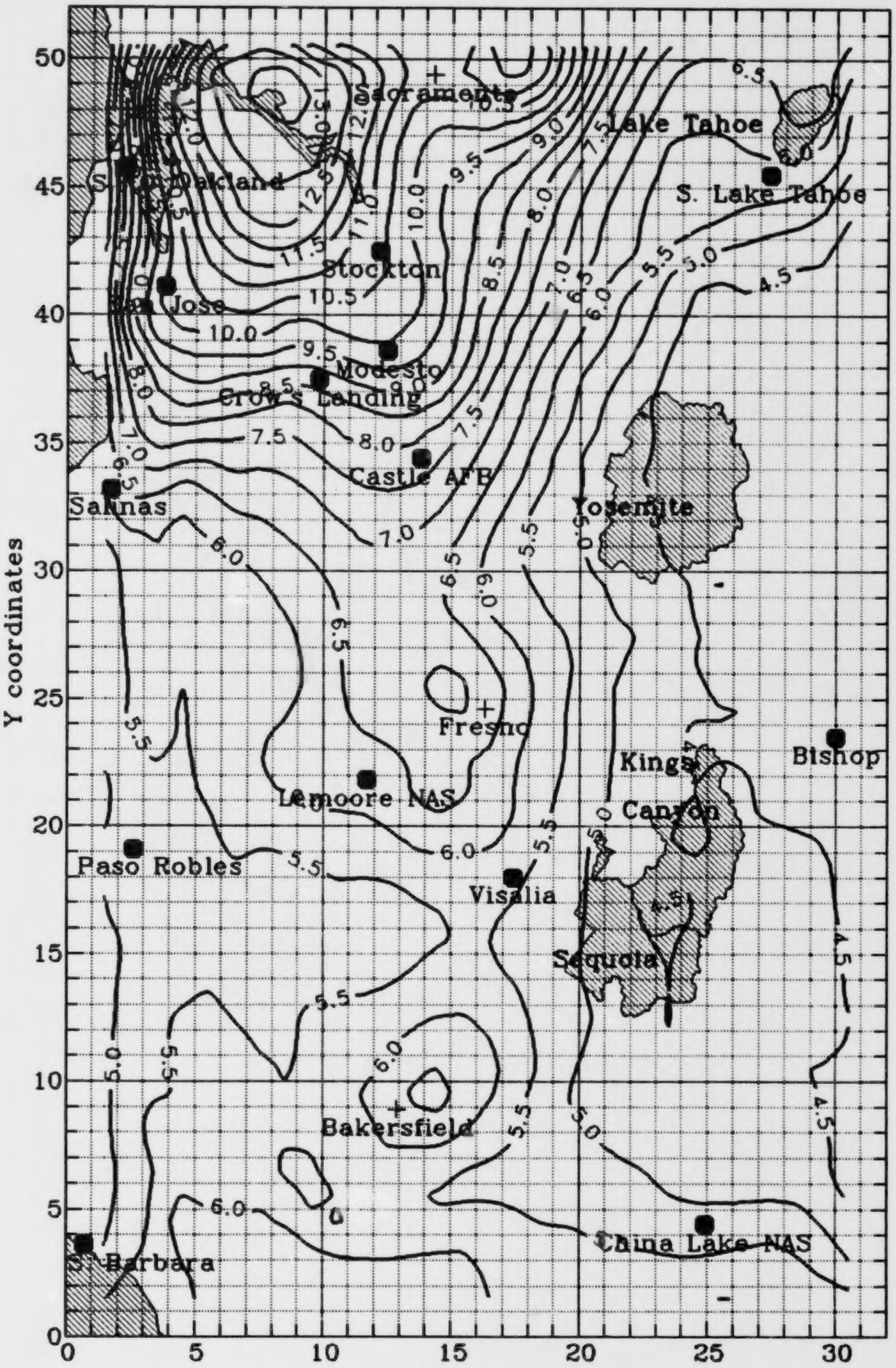
Y coordinates
X coordinates
0
5
10
15
20
25
30
35
40
45
50
Sacramento
Lake Tahoe
S. Lake Tahoe
S.F. Oakland
Stockton
San Jose
Modesto
Crow's Landing
Castle AFB
Salinas
Yosemite
Fresno
Kings Canyon
Bishop
Lemoore NAS
Paso Robles
Visalia
Sequoia
Bakersfield
China Lake NAS
S. Barbara
12.5
12.0
11.5
11.0
10.5
10.0
9.5
9.0
8.5
8.0
7.5
7.0
6.5
6.0
5.5
5.0
4.5

Figure 2-2d. Predicted maximum daily mixed-layer ozone concentrations (pphm) for climate sensitivity scenario #1 (temp. and water increase): August 8, 1981.

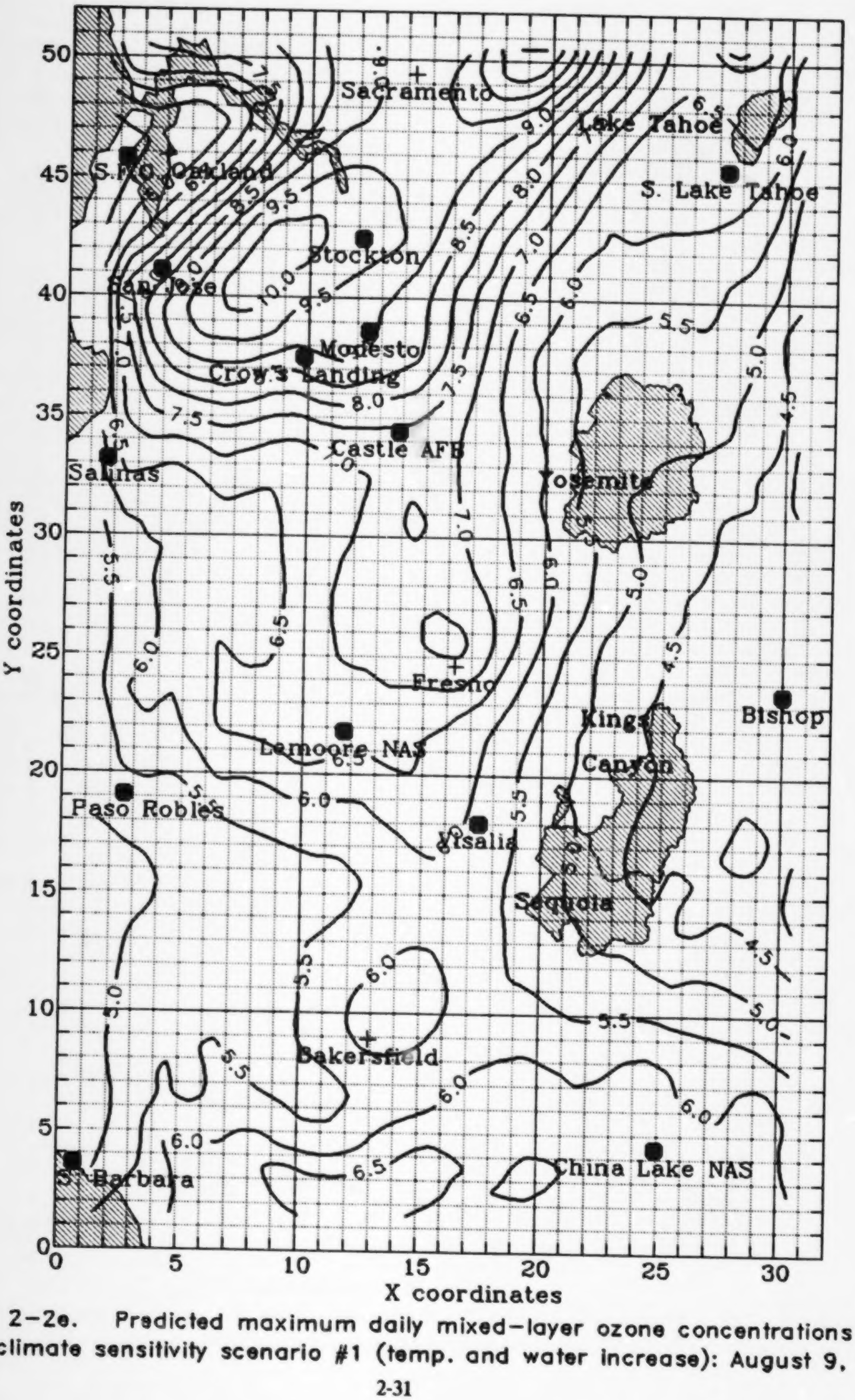
Sacramento
Lake Tahoe
S. Lake Tahoe
S.F.
Oakland
Stockton
San Jose
Modesto
Crow's Landing
Castle AFB
Salinas
Yosemite
Fresno
Kings
Canyon
Bishop
Lemoore NAS
Paso Robles
Visalia
Sequoia
Bakersfield
China Lake NAS
S. Barbara
10.0
9.5
9.0
8.5
8.0
7.5
7.0
6.5
6.0
5.5
5.0
4.5
Y coordinates
X coordinates
0
5
10
15
20
25
30
35
40
45
50

Figure 2-2e. Predicted maximum daily mixed-layer ozone concentrations (pphm) for climate sensitivity scenario #1 (temp. and water increase): August 9, 1981.

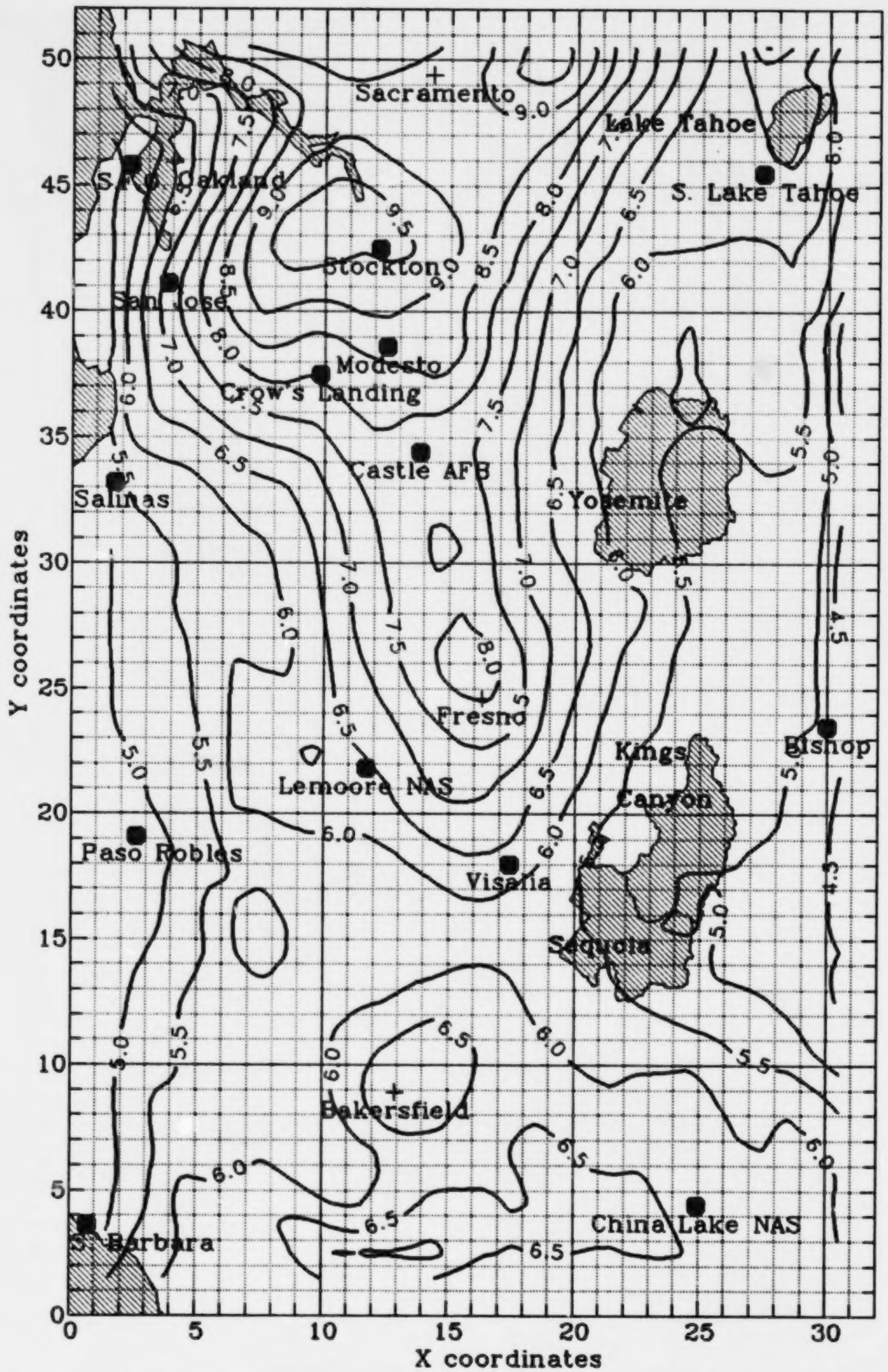
Sacramento
Lake Tahoe
S. Lake Tahoe
S.F.
Oakland
Stockton
San Jose
Modesto
Crow's Landing
Castle AFB
Salinas
Yosemite
Fresno
Kings
Canyon
Bishop
Lemoore NAS
Paso Robles
Visalia
Sequoia
Bakersfield
China Lake NAS
S. Barbara
9.0
9.5
8.5
8.0
7.5
7.0
6.5
6.0
5.5
5.0
4.5
Y coordinates
X coordinates
0
5
10
15
20
25
30
35
40
45
50

Figure 2–2f. Predicted maximum daily mixed–layer ozone concentrations (pphm) for climate sensitivity scenario #1 (temp. and water increase): August 10, 1981.

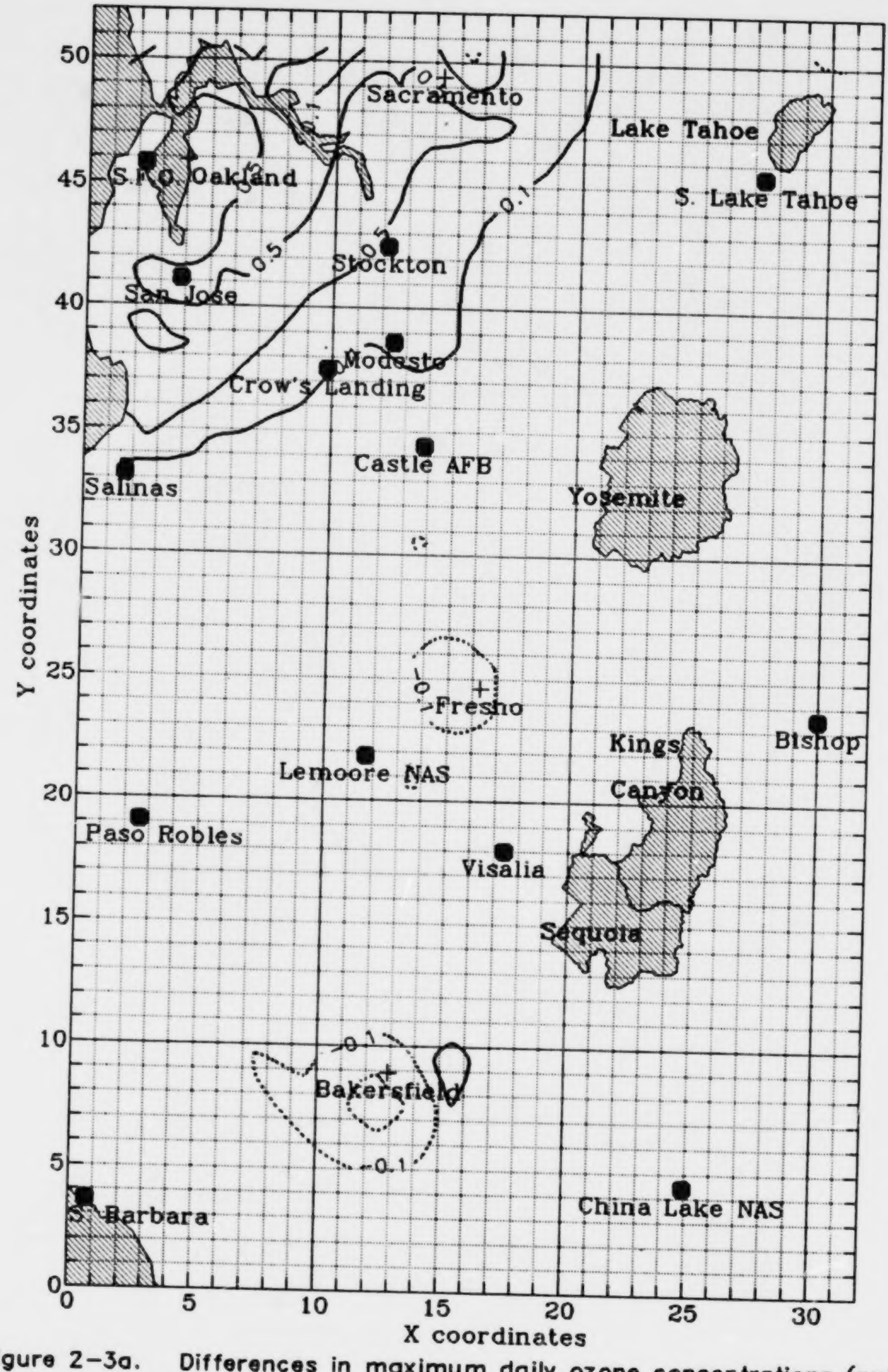
Sacramento
Lake Tahoe
S.F.O. Oakland
S. Lake Tahoe
Stockton
San Jose
Modesto
Crow's Landing
Castle AFB
Salinas
Yosemite
Fresno
Kings
Canyon
Bishop
Lemoore NAS
Paso Robles
Visalia
Sequoia
Bakersfield
S. Barbara
China Lake NAS
0.5
0.1
-0.1
Y coordinates
X coordinates
0
5
10
15
20
25
30
35
40
45
50

Figure 2–3a. Differences in maximum daily ozone concentrations (pphm) (climate sensitivity senario#1 – base case): August 5,1981.

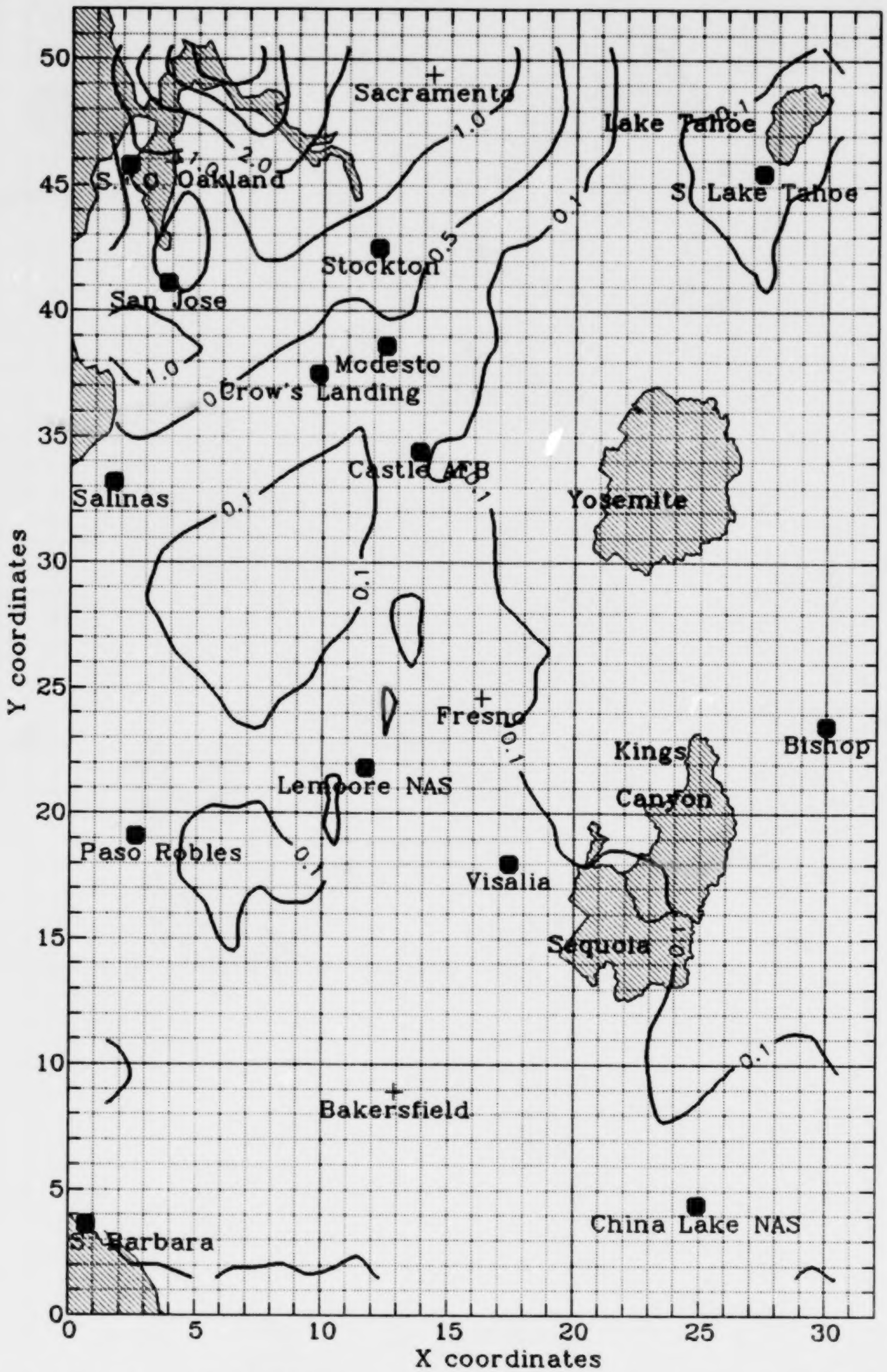
Sacramento
Lake Tahoe
S. Lake Tahoe
S.F.
Oakland
Stockton
San Jose
Modesto
Crow's Landing
Castle AFB
Salinas
Yosemite
Fresno
Kings
Canyon
Bishop
Lemoore NAS
Paso Robles
Visalia
Sequoia
Bakersfield
China Lake NAS
S. Barbara
1.0
2.0
0.5
0.1
Y coordinates
X coordinates
0
5
10
15
20
25
30
35
40
45
50

Figure 2-3b. Differences in maximum daily ozone concentrations (pphm) (climate sensitivity senario#1 – base case): August 6,1981.

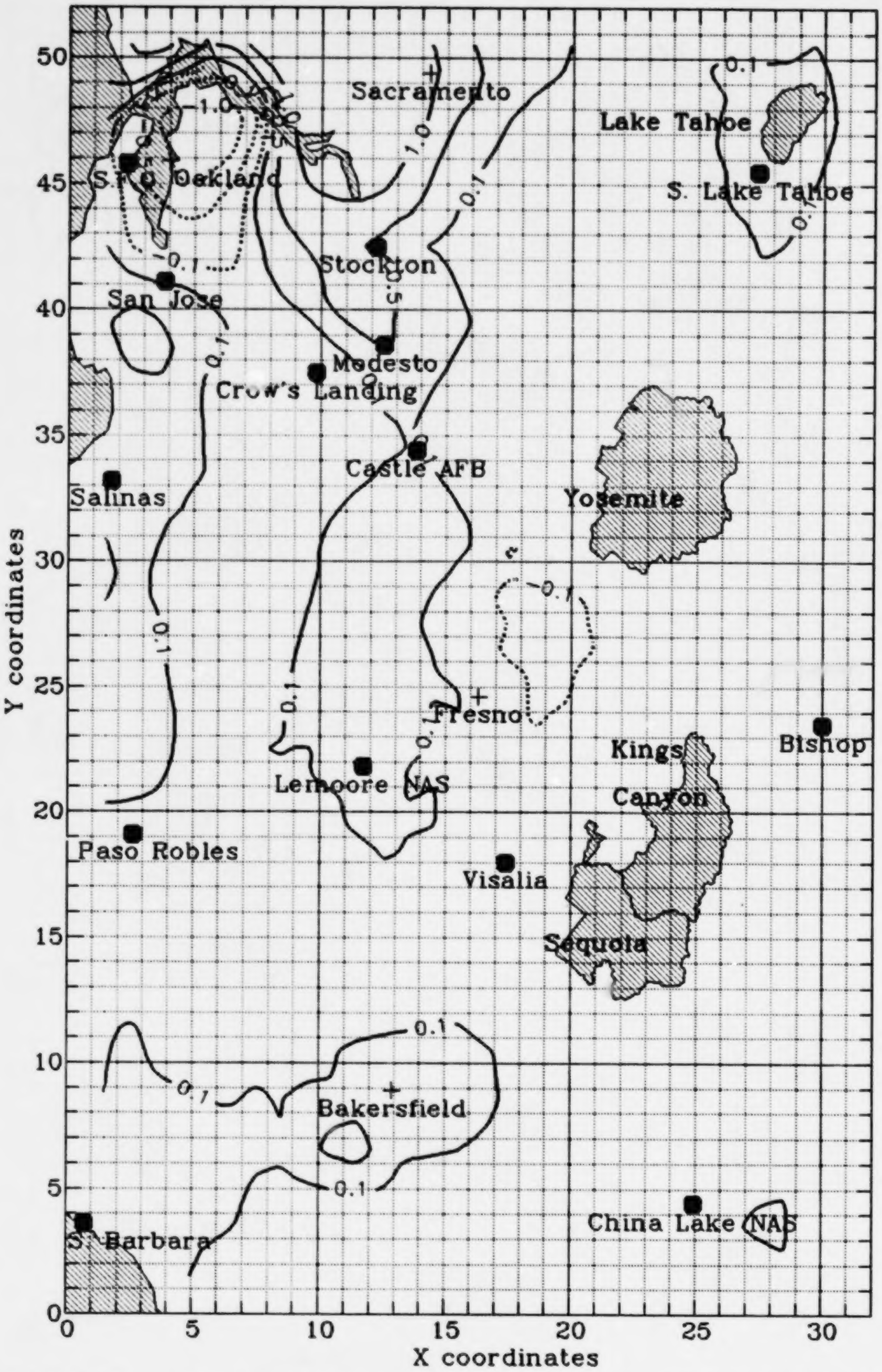
Y coordinates
X coordinates
0
5
10
15
20
25
30
35
40
45
50
Sacramento
Lake Tahoe
S. Lake Tahoe
S.F.
Oakland
Stockton
San Jose
Modesto
Crow's Landing
Castle AFB
Salinas
Yosemite
Fresno
Kings
Canyon
Bishop
Lemoore NAS
Paso Robles
Visalia
Sequoia
Bakersfield
S. Barbara
China Lake NAS
0.1
-0.1
1.0
-1.0
0.5

Figure 2–3c. Differences in maximum daily ozone concentrations (pphm) (climate sensitivity senario#1 – base case): August 7,1981.

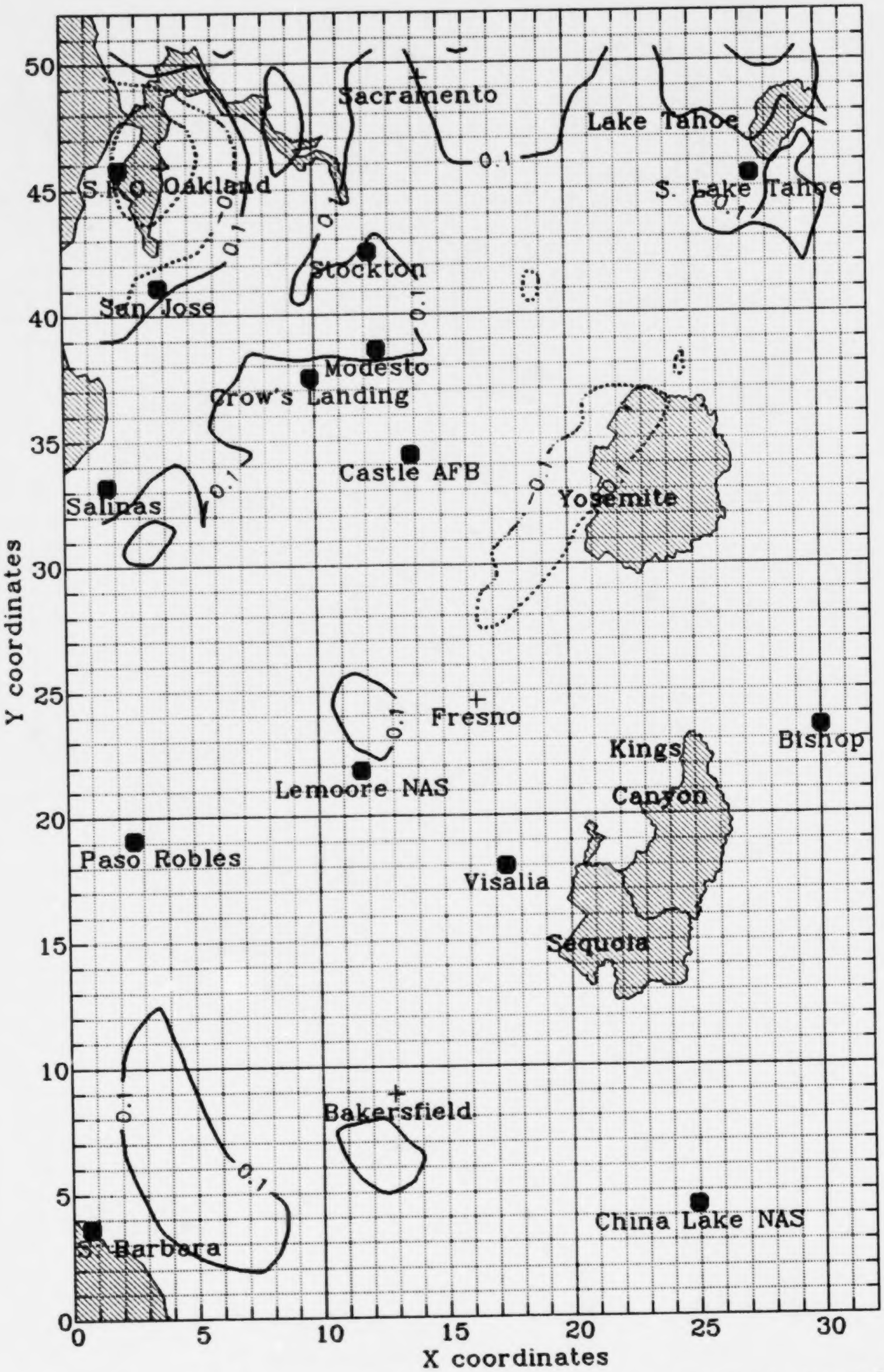
Sacramento
Lake Tahoe
S.F.O.
Oakland
S. Lake Tahoe
Stockton
San Jose
Modesto
Crow's Landing
Castle AFB
Yosemite
Salinas
Fresno
Kings
Canyon
Bishop
Lemoore NAS
Paso Robles
Visalia
Sequoia
Bakersfield
China Lake NAS
S. Barbara
0.1
-0.1
Y coordinates
X coordinates
0
5
10
15
20
25
30
35
40
45
50

Figure 2–3d. Differences in maximum daily ozone concentrations (pphm) (climate sensitivity senario#1 – base case): August 8,1981.

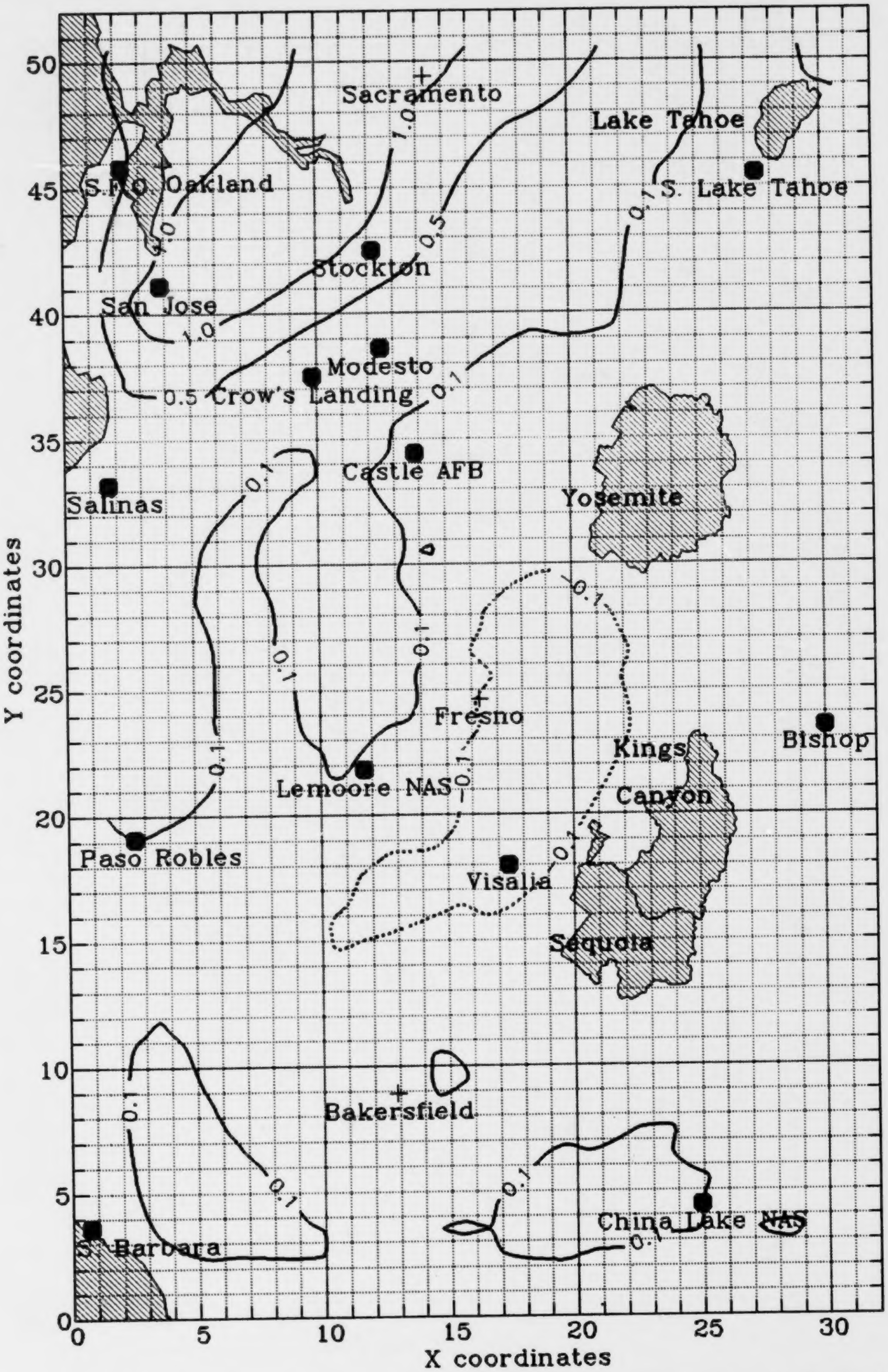
Sacramento
Lake Tahoe
S.F.O.
Oakland
S. Lake Tahoe
Stockton
San Jose
Modesto
Crow's Landing
Castle AFB
Salinas
Yosemite
Fresno
Bishop
Kings
Canyon
Lemoore NAS
Paso Robles
Visalia
Sequoia
Bakersfield
China Lake NAS
S. Barbara
1.0
0.5
0.1
-0.1
Y coordinates
X coordinates
0
5
10
15
20
25
30
35
40
45
50

Figure 2–3e. Differences in maximum daily ozone concentrations (pphm) (climate sensitivity senario#1 – base case): August 9,1981.

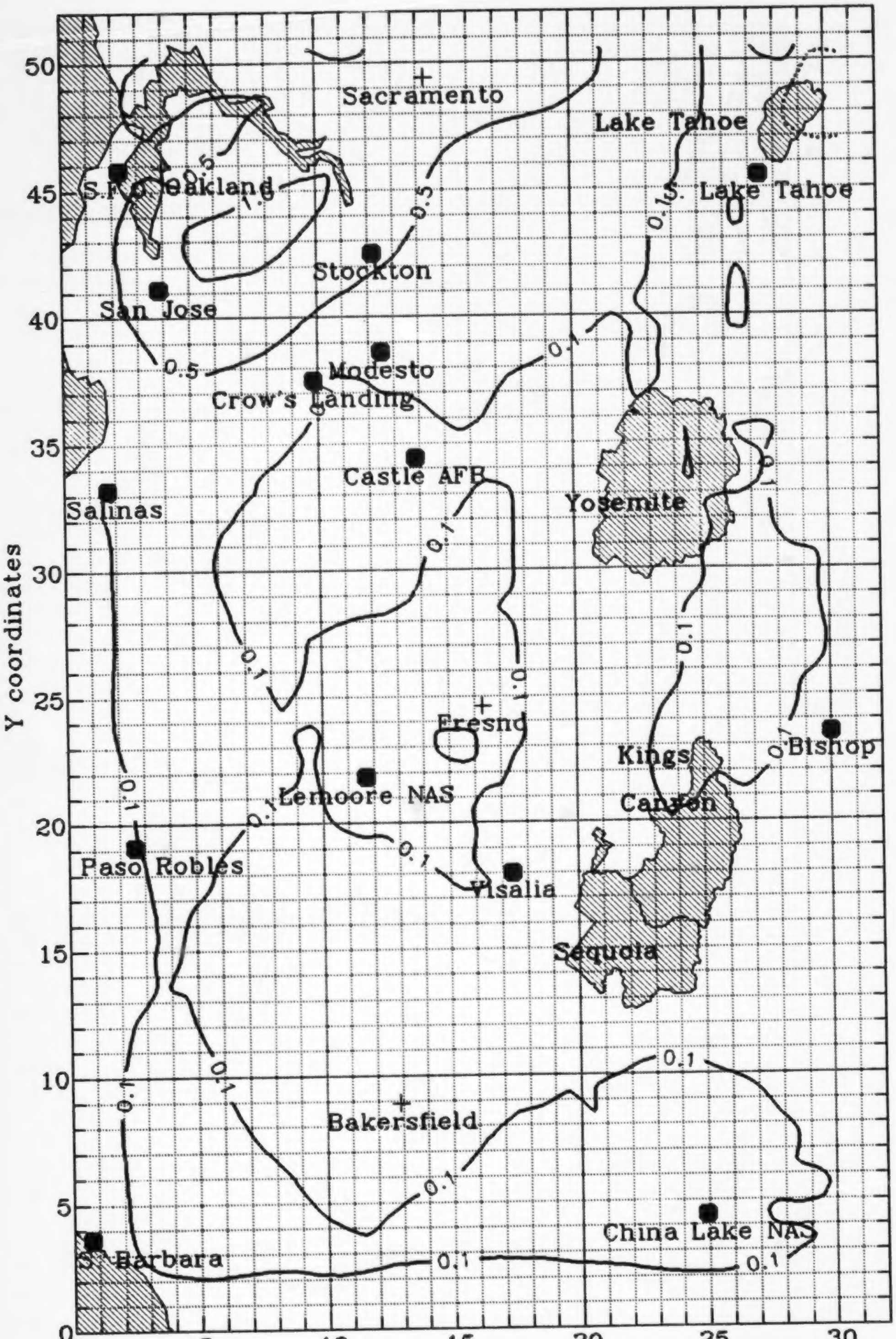
Sacramento
Lake Tahoe
S. Lake Tahoe
S.F.
Oakland
Stockton
San Jose
Modesto
Crow's Landing
Castle AFB
Salinas
Yosemite
Fresno
Kings
Canyon
Bishop
Lemoore NAS
Paso Robles
Visalia
Sequoia
Bakersfield
China Lake NAS
S. Barbara
0.5
1.5
0.1
Y coordinates
X coordinates
0
5
10
15
20
25
30
35
40
45
50

Figure 2–3f. Differences in maximum daily ozone concentrations (pphm) (climate sensitivity senario#1 – base case): August 10,1981.

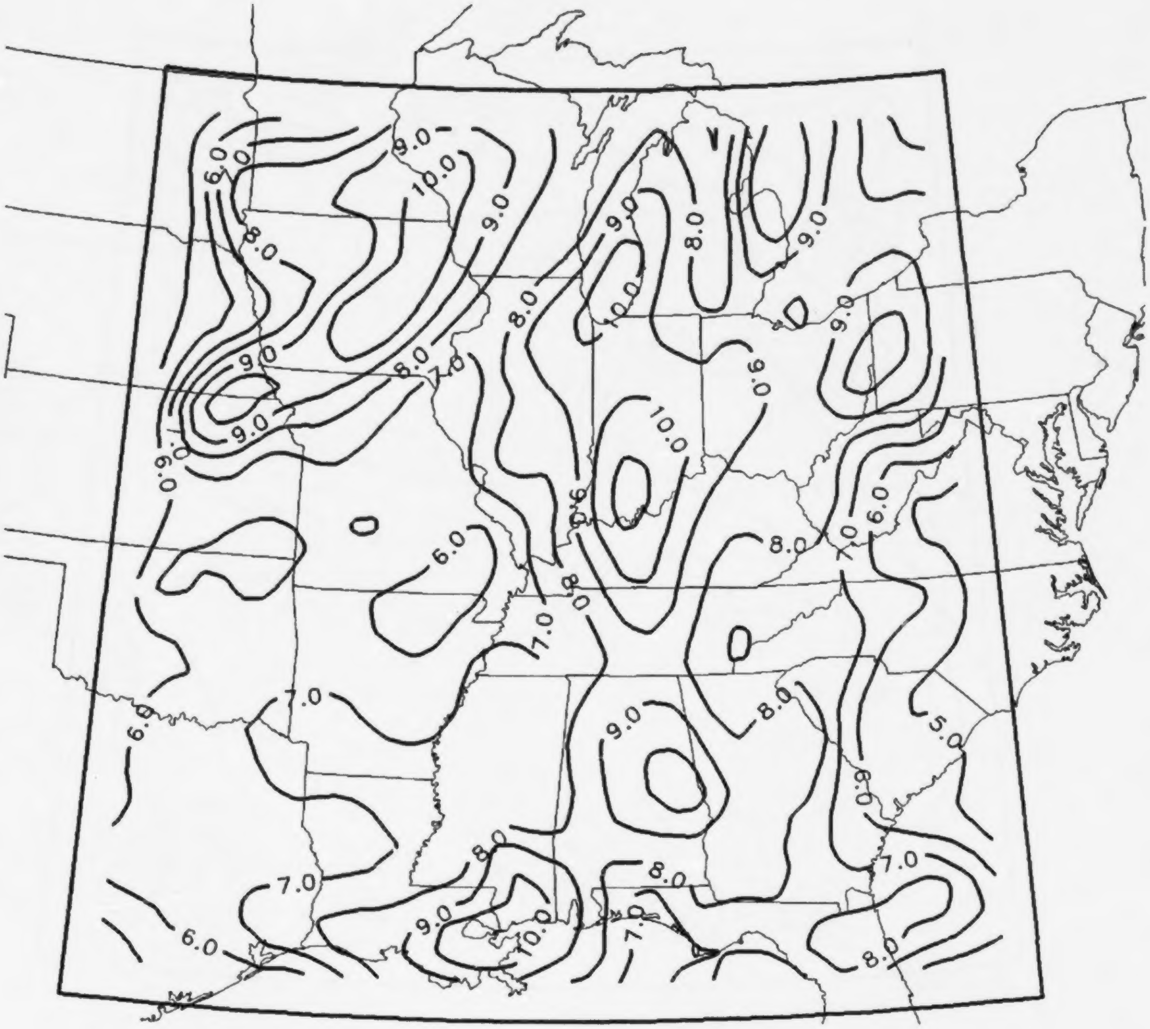
6.0
9.0
10.0
9.0
8.0
9.0
8.0
10.0
9.0
8.0
9.0
9.0
8.0
7.0
9.0
9.0
10.0
6.0
9.0
6.0
8.0
7.0
6.0
8.0
7.0
6.0
9.0
8.0
5.0
6.0
8.0
7.0
8.0
7.0
6.0
9.0
10.0
7.0
8.0

Figure 2–4a. Predicted maximum daily mixed–layer ozone concentrations (pphm) for the base case scenario: July 14, 1980.

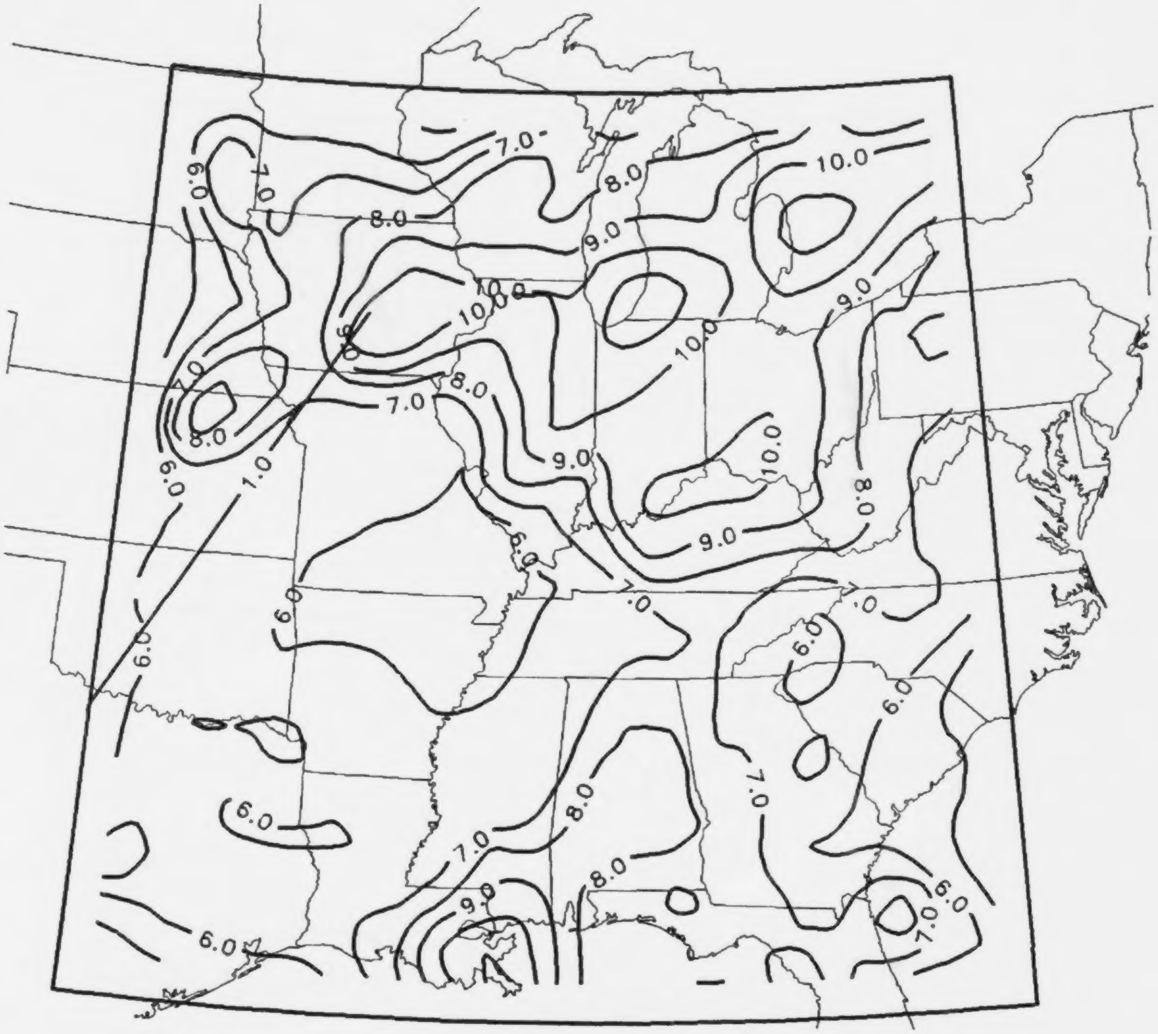
7.0
10.0
6.0
7.0
8.0
8.0
8.0
9.0
9.0
10.0
10.0
9.0
10.0
9.0
7.0
8.0
8.0
8.0
6.0
1.0
9.0
10.0
8.0
9.0
6.0
7.0
7.0
6.0
6.0
6.0
6.0
7.0
8.0
6.0
7.0
9.0
8.0
6.0
7.0
6.0

Figure 2–4b. Predicted maximum daily mixed–layer ozone concentrations (pphm) for the base case scenario: July 15, 1980.

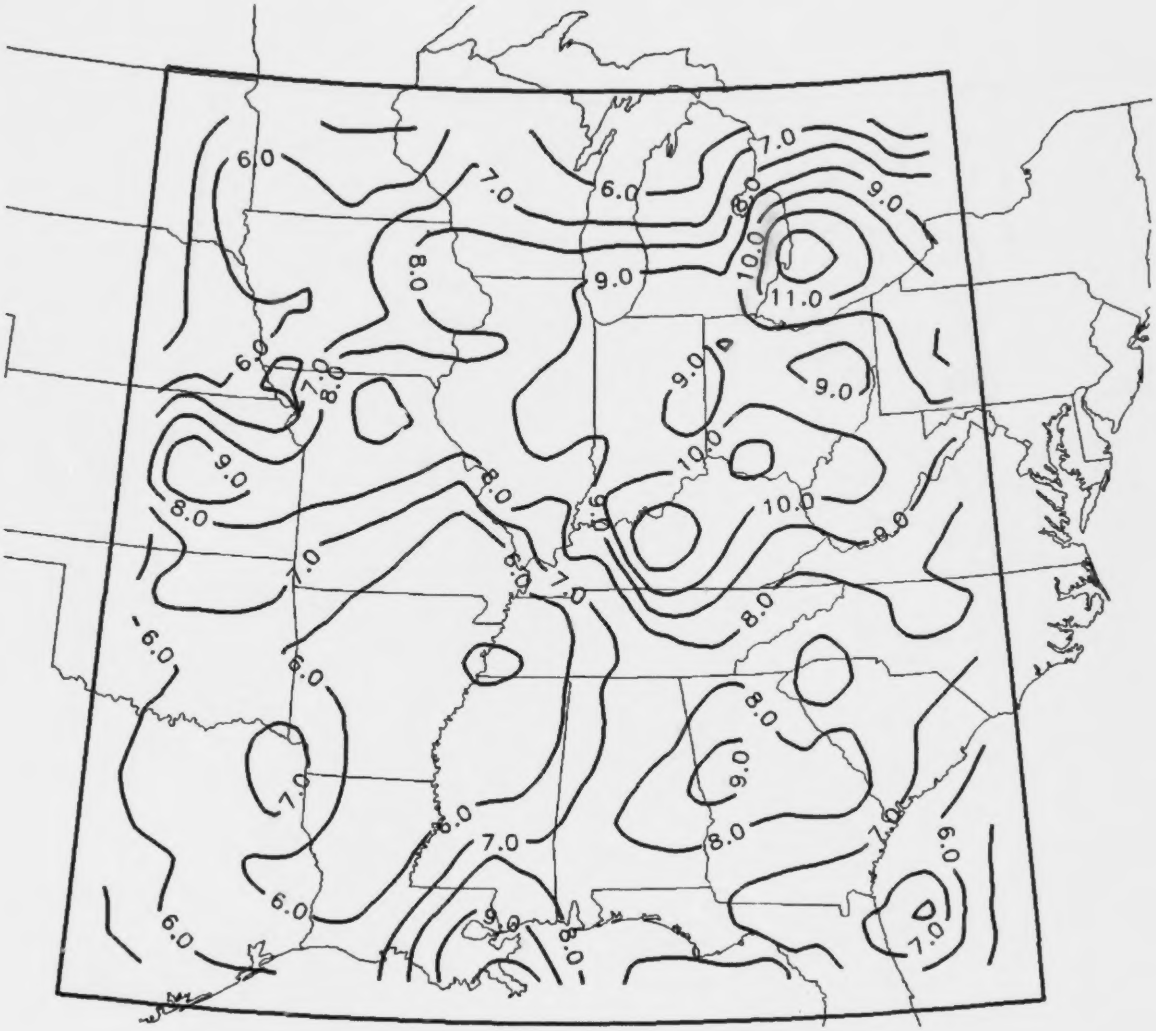
6.0
7.0
6.0
7.0
9.0
8.0
10.0
11.0
9.0
8.0
9.0
6.0
7.0
8.0
9.0
9.0
8.0
8.0
10.0
10.0
9.0
9.0
8.0
7.0
7.0
8.0
6.0
6.0
8.0
9.0
7.0
8.0
7.0
8.0
7.0
6.0
6.0
6.0
9.0
8.0
7.0

Figure 2-4c. Predicted maximum daily mixed-layer ozone concentrations (pphm) for the base case scenario: July 16, 1980.

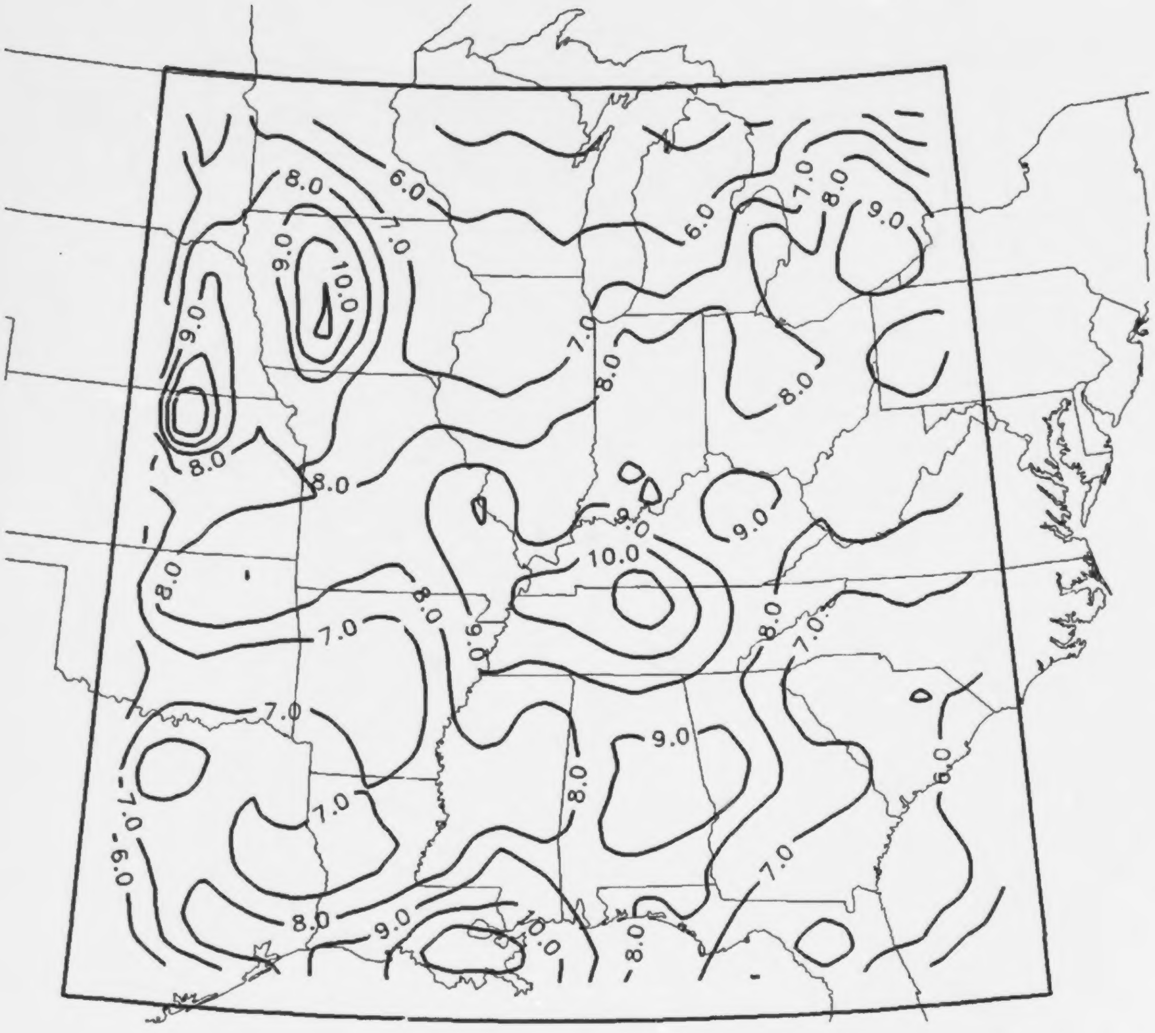
8.0
6.0
7.0
9.0
10.0
9.0
6.0
7.0
8.0
9.0
7.0
8.0
8.0
8.0
8.0
9.0
9.0
10.0
8.0
8.0
7.0
9.0
8.0
7.0
7.0
9.0
7.0
8.0
6.0
7.0
6.0
7.0
8.0
9.0
10.0
8.0

Figure 2–4d. Predicted maximum daily mixed–layer ozone concentrations (pphm) for the base case scenario: July 17, 1980.

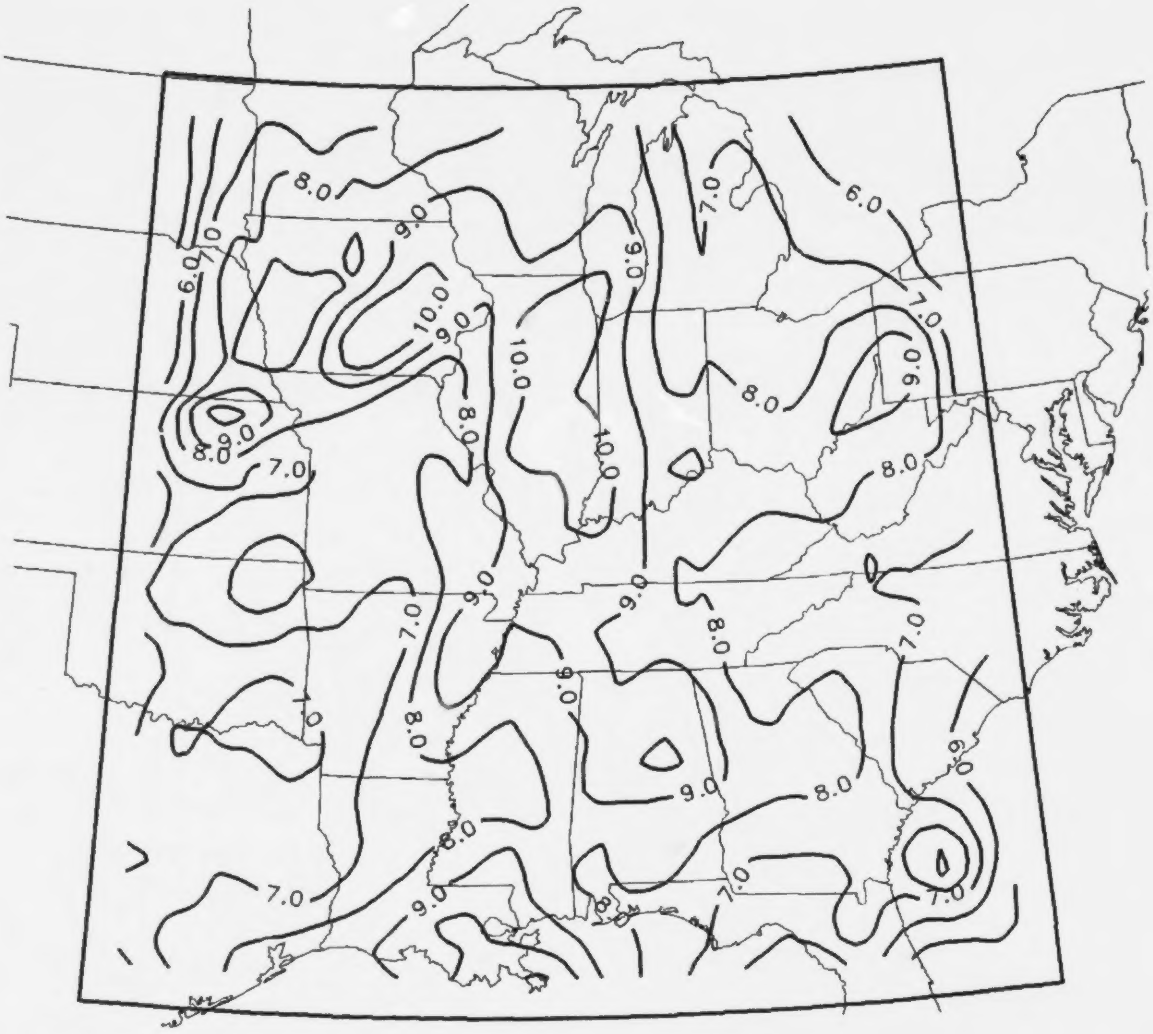

8.0
9.0
7.0
6.0
10.0
9.0
9.0
10.0
7.0
6.0
7.0
9.0
8.0
9.0
8.0
10.0
8.0
9.0
8.0
7.0
9.0
9.0
7.0
8.0
7.0
9.0
8.0
0
9.0
8.0
9.0
8.0
9.0
7.0
9.0
7.0
8.0
7.0
7.0

Figure 2–4e. Predicted maximum daily mixed–layer ozone concentrations (pphm) for the base case scenario: July 18, 1980.

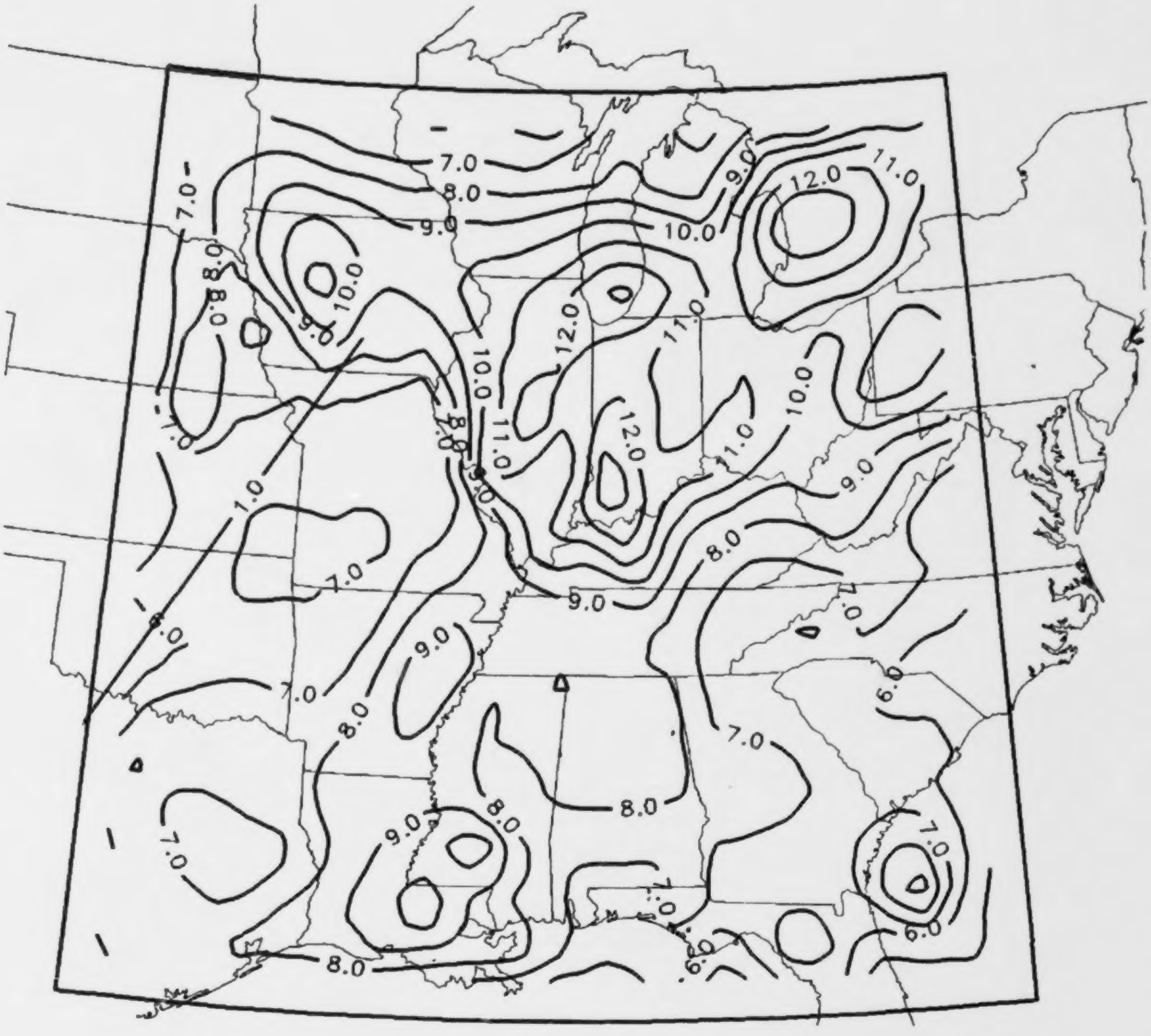
7.0
8.0
9.0
10.0
9.0
11.0
12.0
11.0
7.0
8.0
8.0
10.0
9.0
10.0
12.0
11.0
10.0
11.0
12.0
11.0
9.0
1.0
8.0
7.0
9.0
8.0
7.0
9.0
7.0
6.0
6.0
7.0
8.0
7.0
8.0
9.0
8.0
8.0
7.0
7.0
6.0
6.0
6.0
8.0

Figure 2–4f. Predicted maximum daily mixed–layer ozone concentrations (pphm) for the base case scenario: July 19, 1980.

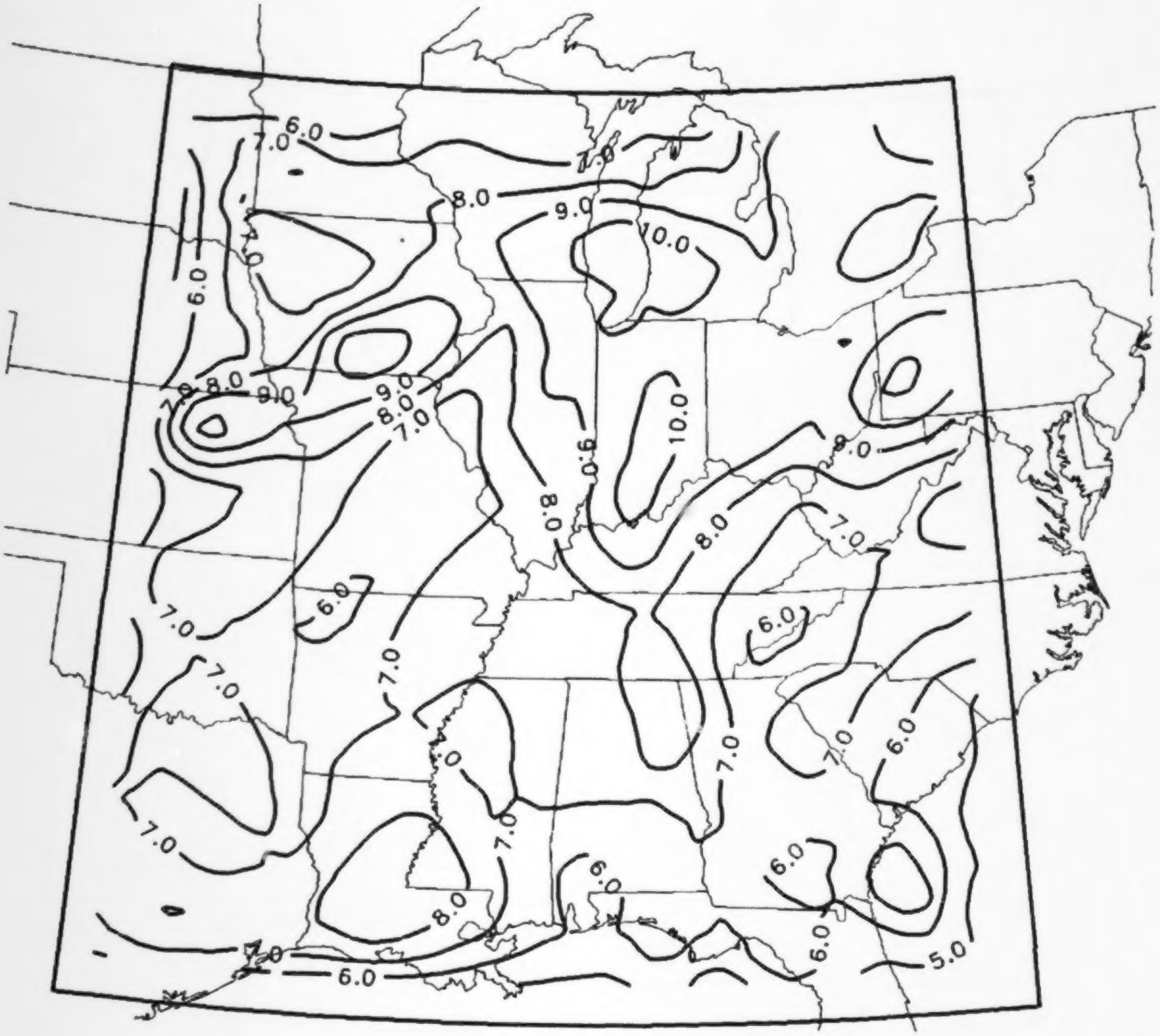
6.0
7.0
7.0
8.0
9.0
10.0
6.0
7.0
8.0
9.0
9.0
8.0
7.0
10.0
9.0
8.0
9.0
8.0
7.0
6.0
7.0
6.0
7.0
7.0
7.0
7.0
7.0
7.0
6.0
7.0
6.0
8.0
6.0
6.0
6.0
7.0
6.0
5.0

Figure 2–4g. Predicted maximum daily mixed–layer ozone concentrations (pphm) for the base case scenario: July 20, 1980.

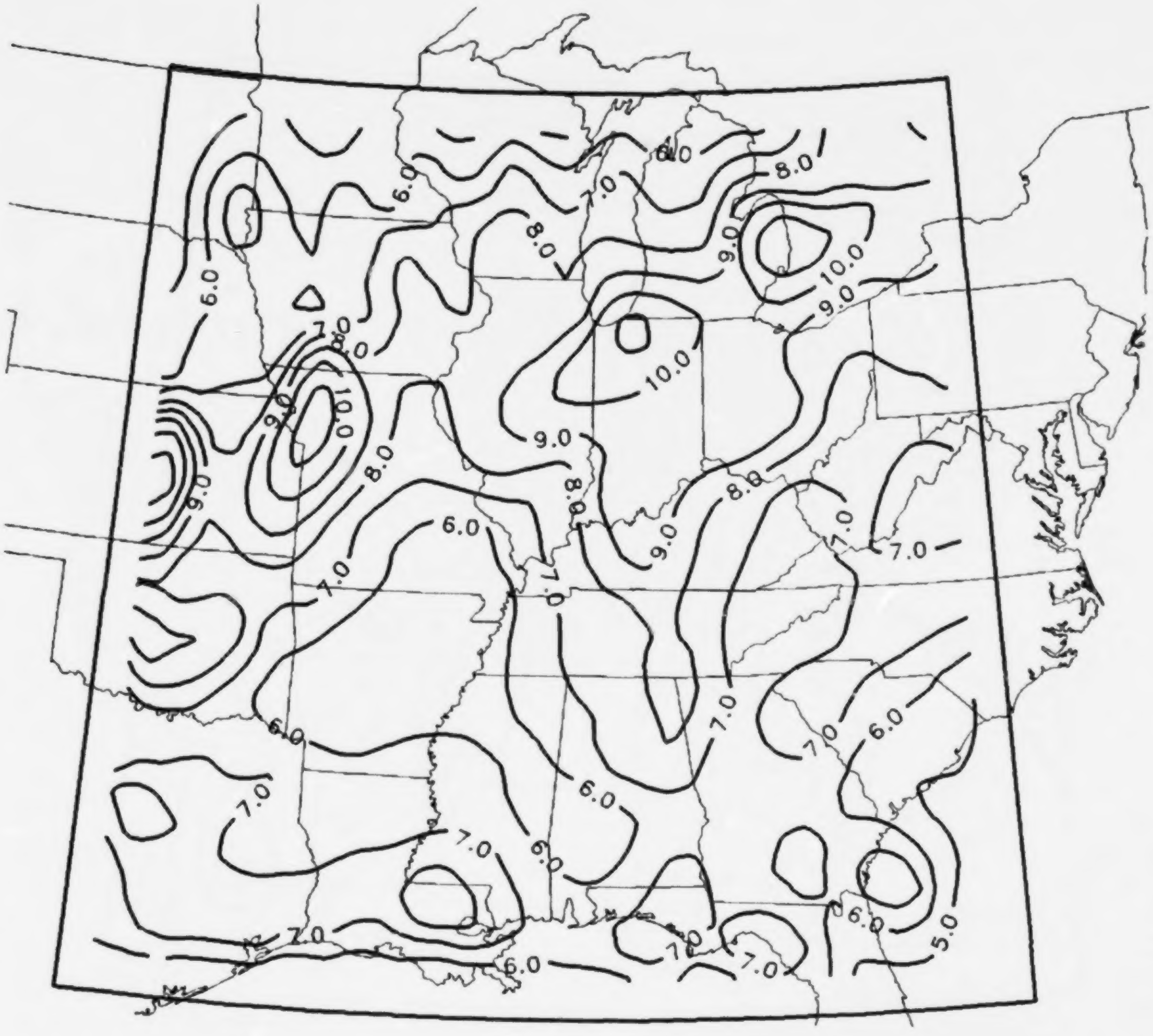
6.0
6.0
8.0
7.0
8.0
9.0
10.0
9.0
6.0
7.0
8.0
10.0
9.0
10.0
8.0
9.0
9.0
8.0
8.0
9.0
7.0
7.0
6.0
7.0
7.0
7.0
6.0
6.0
7.0
7.0
6.0
7.0
6.0
7.0
6.0
5.0
6.0
7.0
7.0
6.0

Figure 2–4h. Predicted maximum daily mixed–layer ozone concentrations (pphm) for the base case scenario: July 21, 1980.

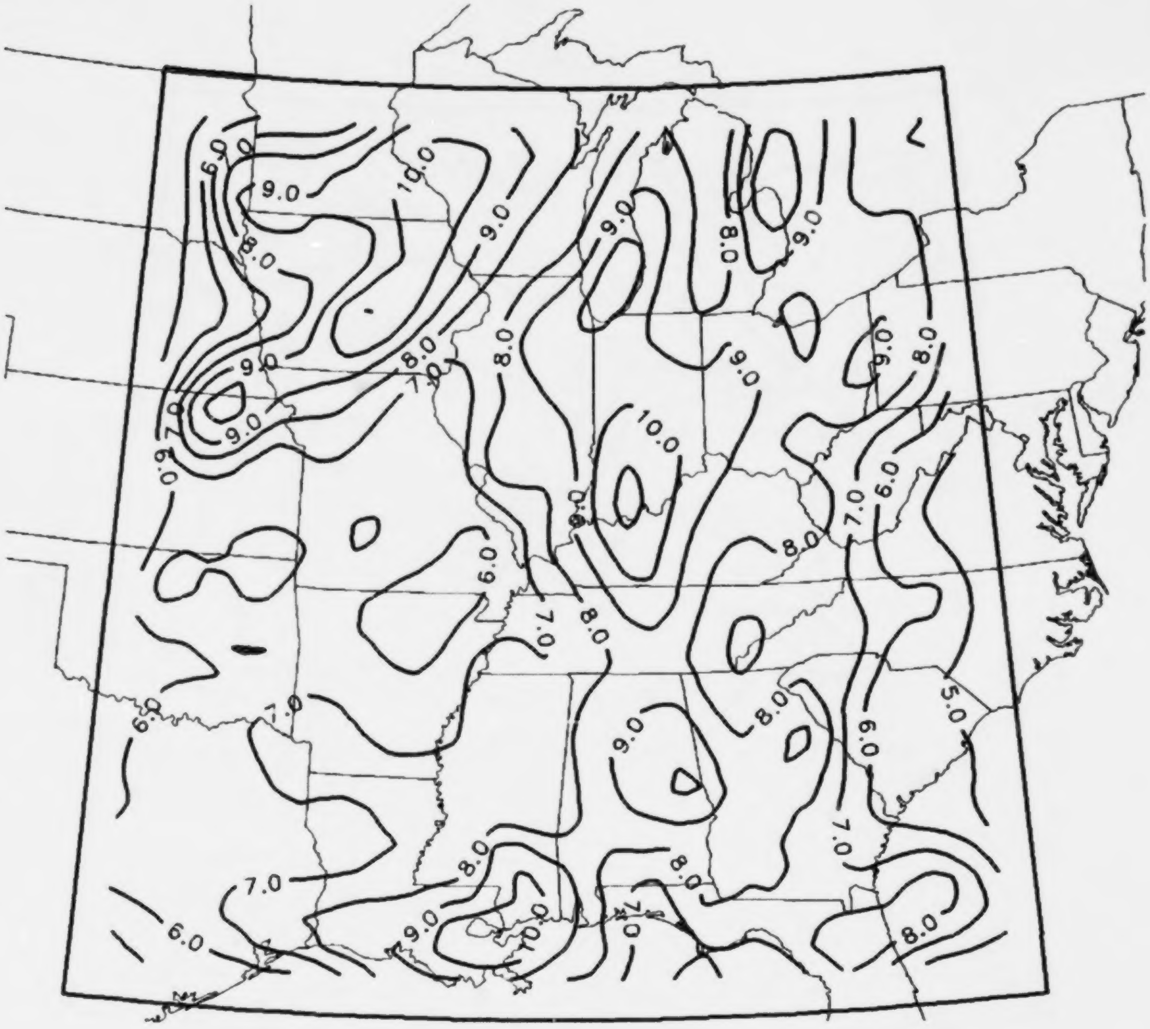
6.0
9.0
10.0
9.0
9.0
8.0
9.0
8.0
9.0
8.0
7.0
9.0
8.0
9.0
9.0
7.0
6.0
10.0
9.0
8.0
8.0
7.0
6.0
6.0
7.0
8.0
7.0
6.0
5.0
6.0
9.0
8.0
7.0
8.0
8.0
7.0
9.0
10.0
7.0
6.0
8.0

Figure 2–5a. Predicted maximum daily mixed–layer ozone concentrations (pphm) for climate sensitivity scenario#1: July 14, 1980.

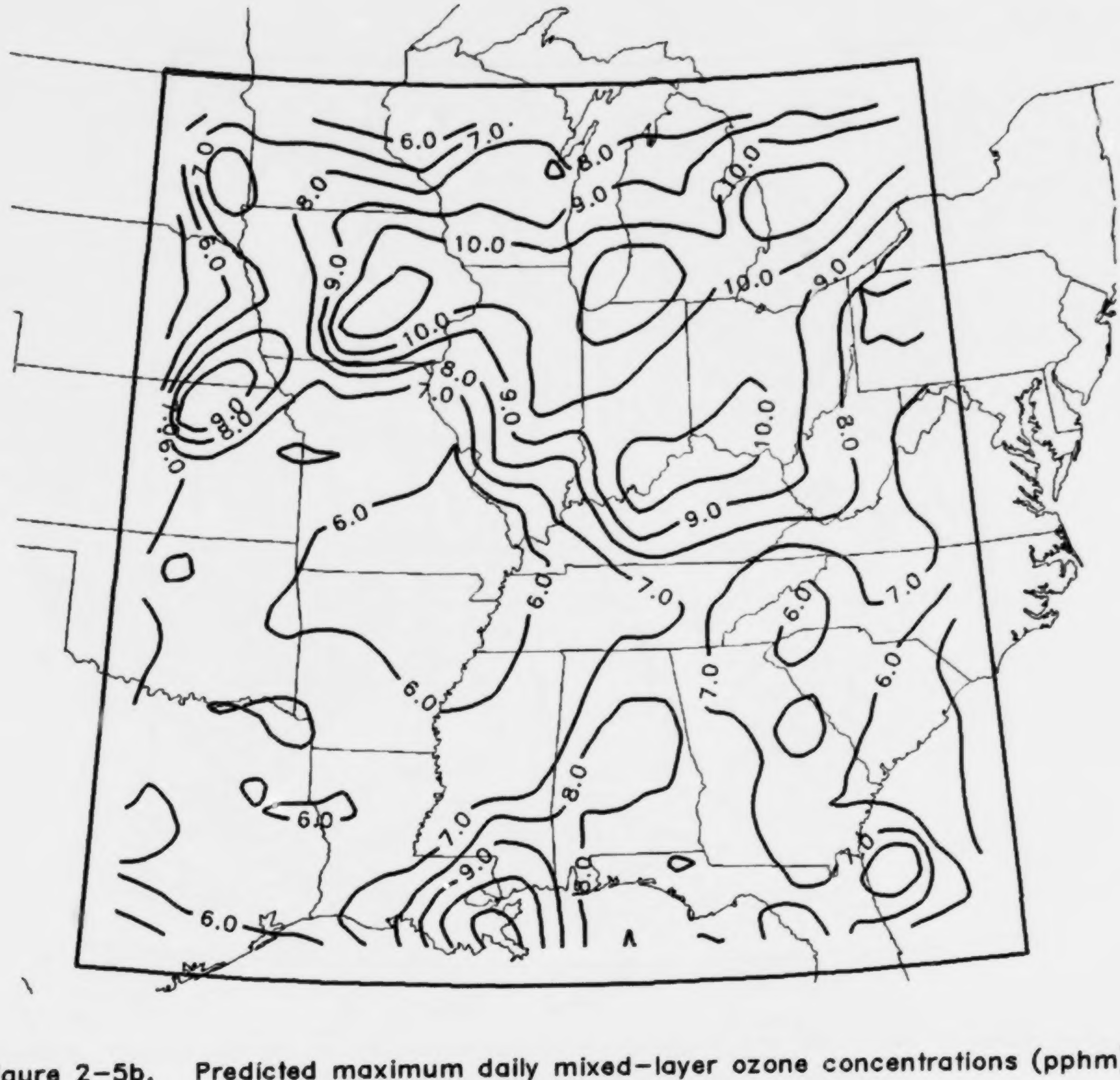
6.0
7.0
8.0
9.0
10.0
9.0
10.0
8.0
7.0
6.0
9.0
10.0
9.0
8.0
9.0
8.0
7.0
6.0
9.0
10.0
8.0
9.0
6.0
7.0
6.0
6.0
7.0
6.0
7.0
6.0
6.0
8.0
7.0
9.0
7.0
6.0

Figure 2-5b. Predicted maximum daily mixed-layer ozone concentrations (pphm) for climate sensitivity scenario#1: July 15, 1980.

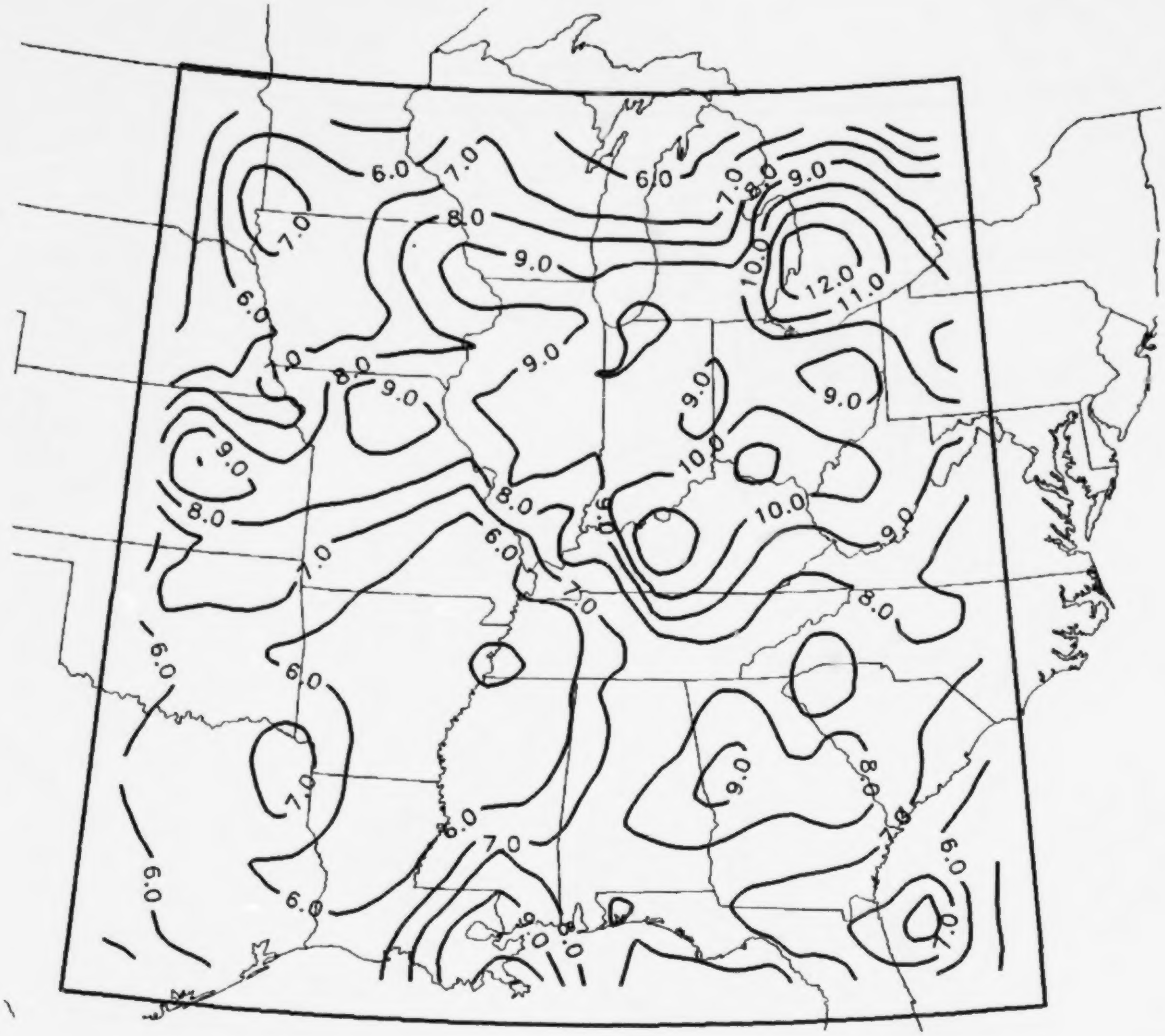
6.0
7.0
8.0
9.0
6.0
7.0
8.0
9.0
7.0
10.0
12.0
11.0
6.0
7.0
8.0
9.0
9.0
9.0
9.0
10.0
9.0
8.0
8.0
6.0
9.0
10.0
7.0
7.0
9.0
8.0
6.0
6.0
7.0
9.0
8.0
7.0
6.0
7.0
6.0
6.0
6.0
6.0
7.0

Figure 2-5c. Predicted maximum daily mixed-layer ozone concentrations (pphm) for climate sensitivity scenario#1: July 16, 1980.

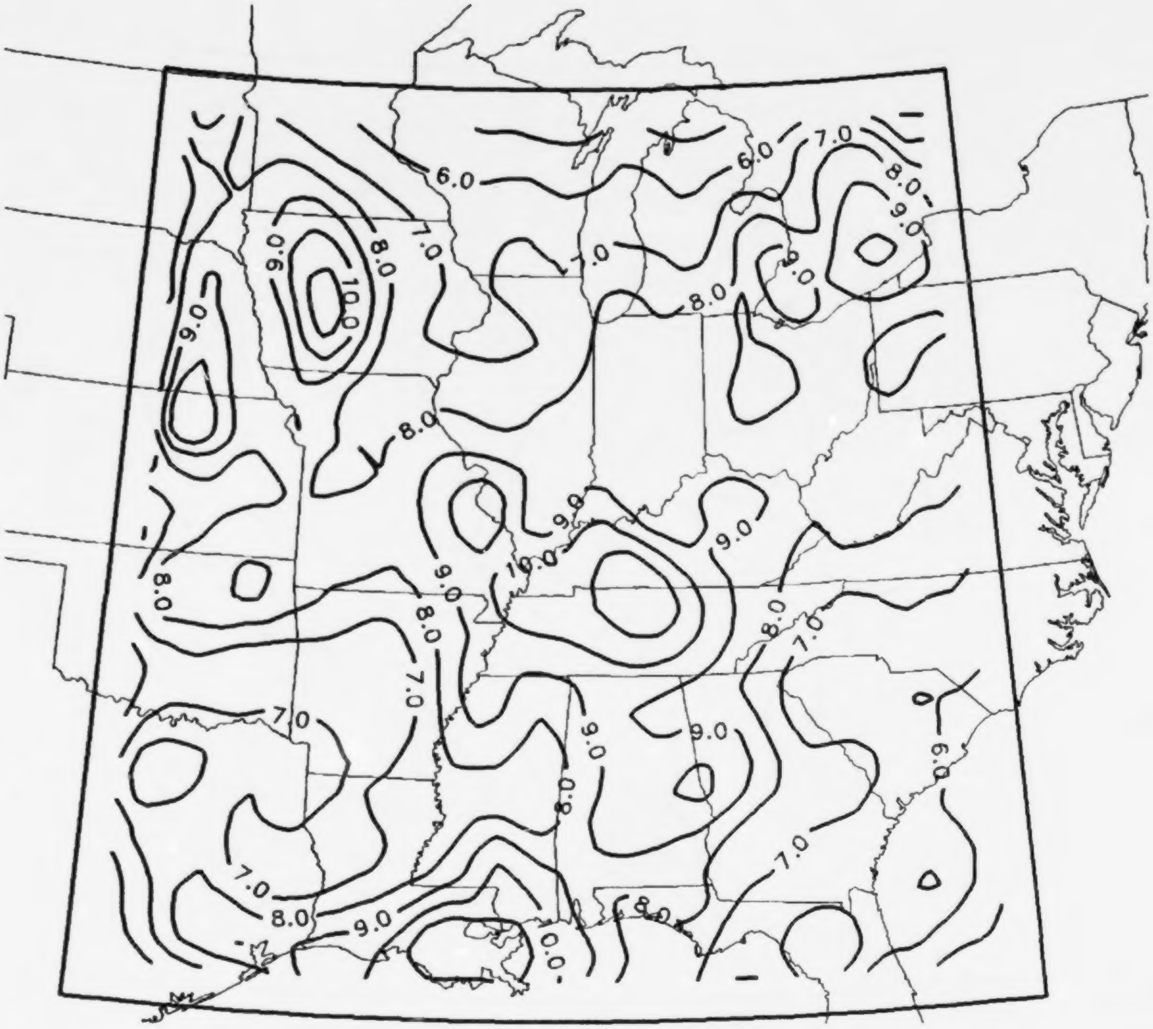
6.0
6.0
7.0
8.0
9.0
9.0
8.0
10.0
7.0
7.0
8.0
9.0
9.0
8.0
9.0
9.0
10.0
8.0
9.0
8.0
7.0
8.0
7.0
7.0
9.0
9.0
8.0
6.0
7.0
7.0
8.0
9.0
10.0
8.0

Figure 2–5d. Predicted maximum daily mixed–layer ozone concentrations (pphm) for climate sensitivity scenario#1: July 17, 1980.

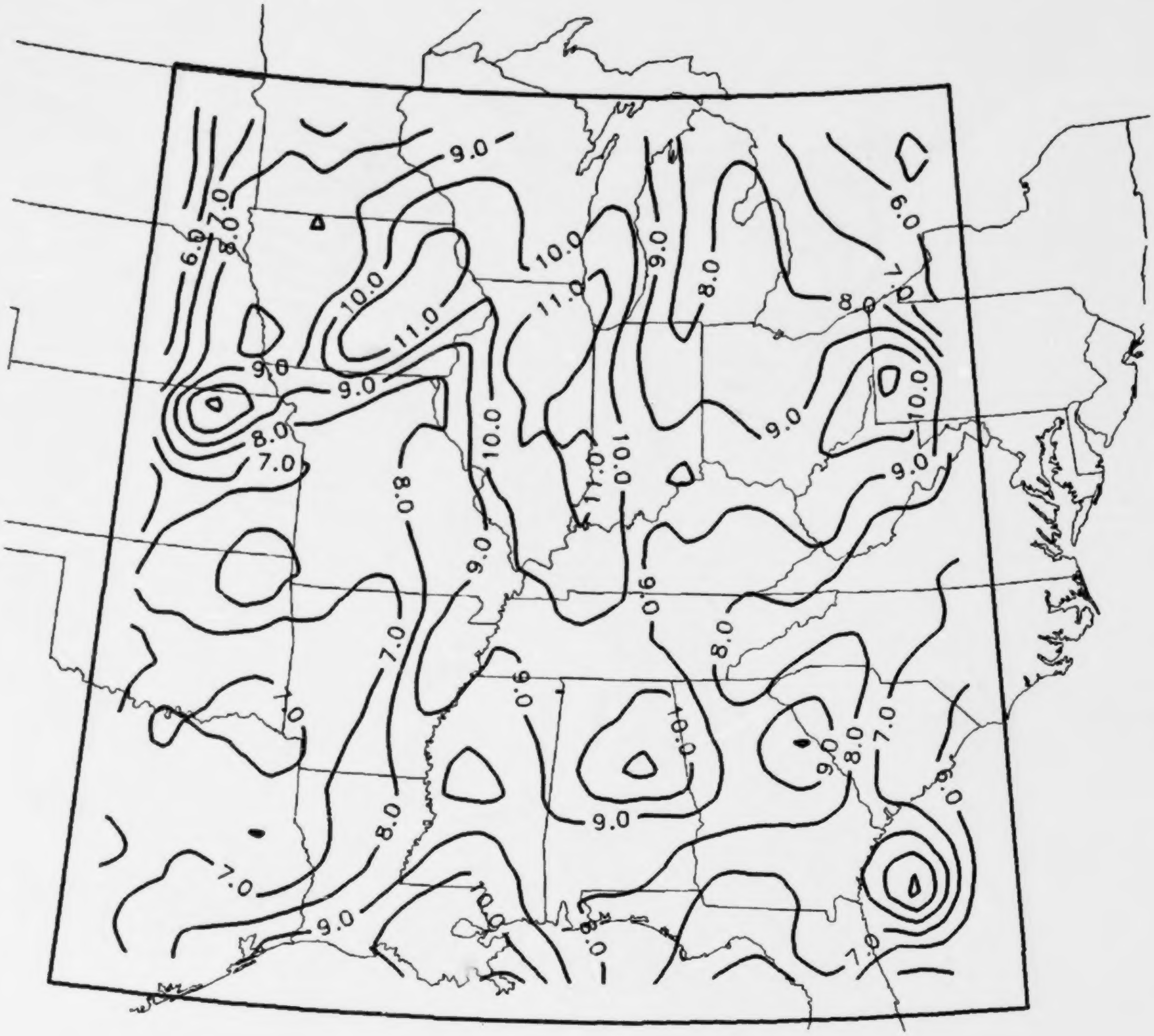
9.0
6.0
7.0
8.0
10.0
11.0
10.0
11.0
9.0
8.0
6.0
7.0
8.0
9.0
9.0
9.0
8.0
7.0
10.0
10.0
11.0
9.0
10.0
8.0
9.0
9.0
7.0
8.0
9.0
10.0
9.0
8.0
7.0
0
9.0
8.0
6.0
7.0
9.0
10.0
9.0
7.0

Figure 2–5e. Predicted maximum daily mixed–layer ozone concentrations (pphm) for climate sensitivity scenario#1: July 18, 1980.

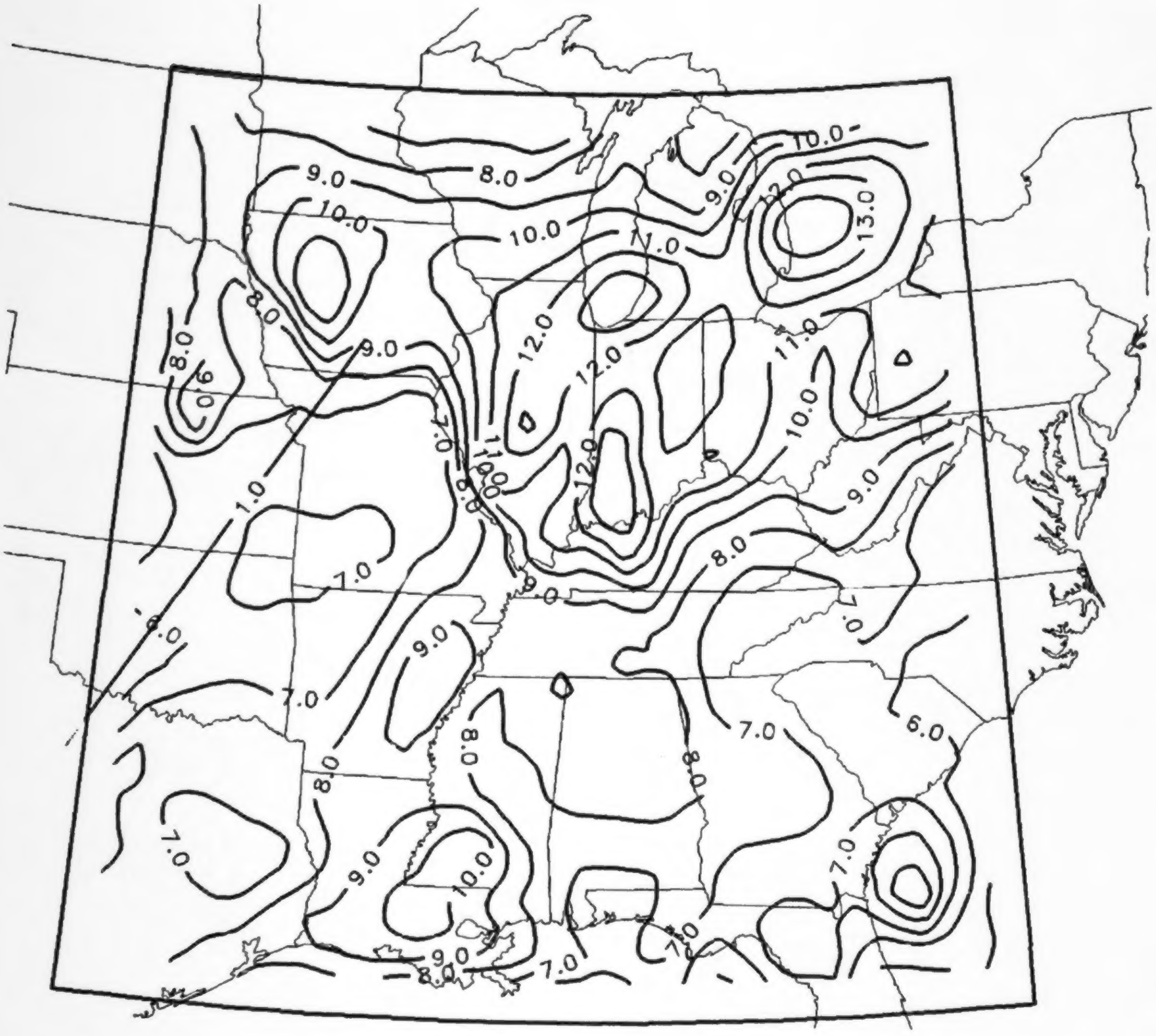
10.0
9.0
8.0
10.0
10.0
11.0
9.0
12.0
13.0
8.0
8.0
9.0
9.0
12.0
12.0
11.0
10.0
7.0
11.0
10.0
8.0
12.0
1.0
9.0
8.0
7.0
9.0
8.0
6.0
9.0
7.0
7.0
6.0
8.0
8.0
8.0
7.0
7.0
9.0
10.0
9.0
8.0
7.0
7.0

Figure 2–5f. Predicted maximum daily mixed–layer ozone concentrations (pphm) for climate sensitivity scenario#1: July 19, 1980.

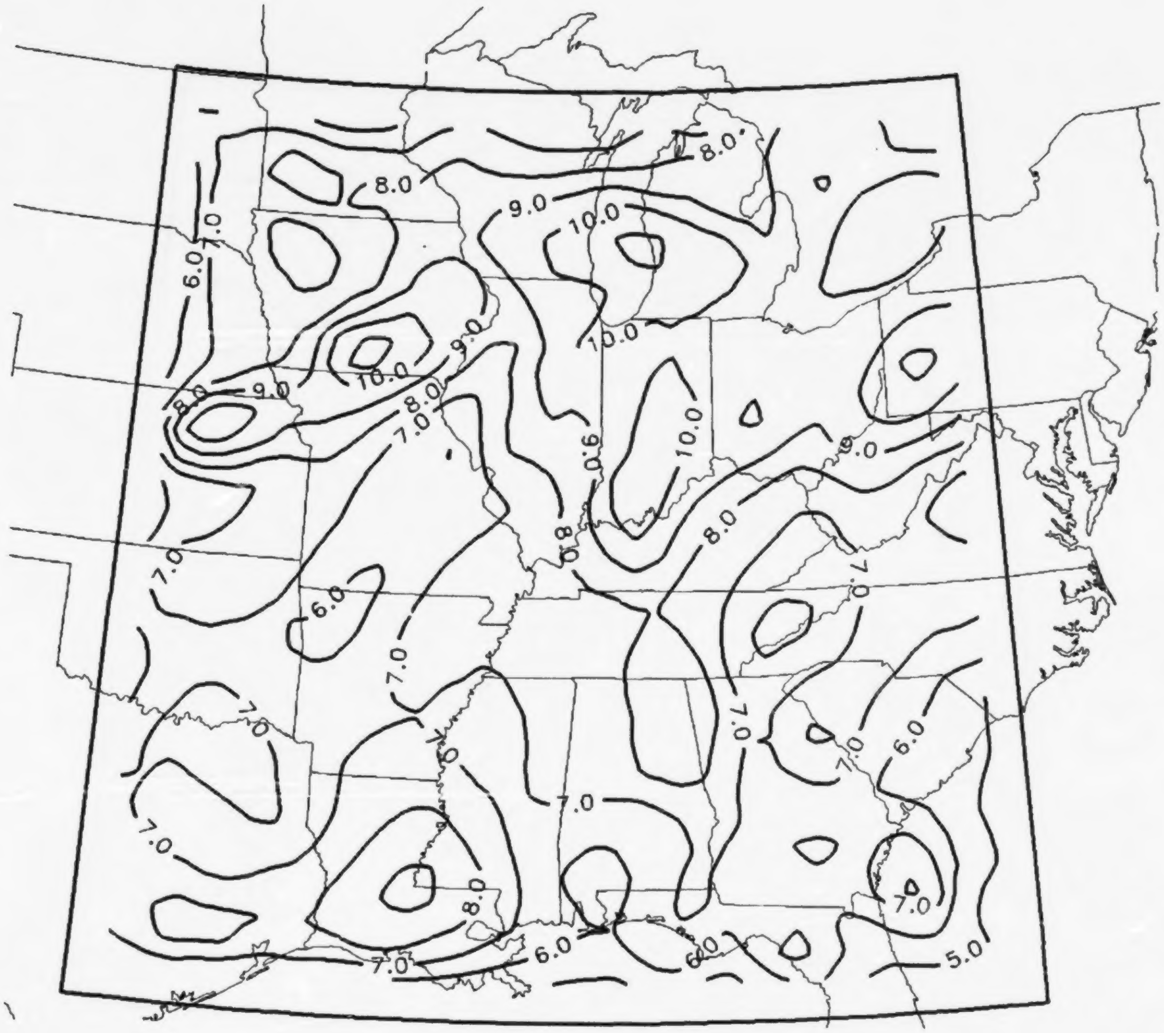
8.0
8.0
9.0
10.0
7.0
6.0
9.0
10.0
9.0
8.0
9.0
8.0
7.0
9.0
10.0
10.0
9.0
8.0
8.0
7.0
7.0
6.0
7.0
7.0
7.0
7.0
7.0
7.0
6.0
7.0
7.0
8.0
7.0
6.0
6.0
7.0
5.0

Figure 2–5g. Predicted maximum daily mixed–layer ozone concentrations (pphm) for climate sensitivity scenario#1: July 20, 1980.

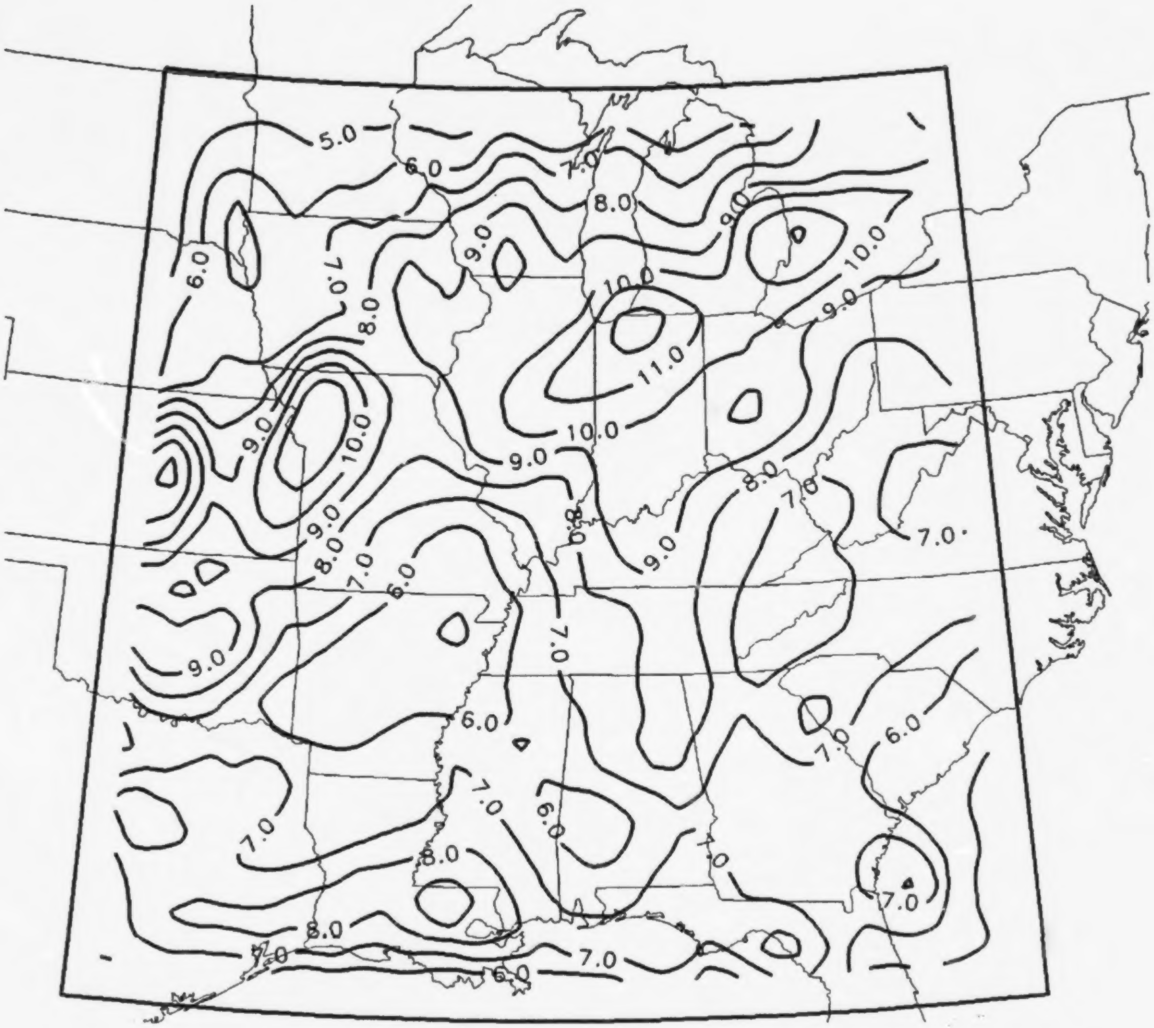
5.0
6.0
7.0
8.0
9.0
10.0
11.0
10.0
9.0
6.0
7.0
8.0
9.0
10.0
9.0
8.0
7.0
6.0
9.0
8.0
7.0
9.0
7.0
6.0
7.0
6.0
7.0
8.0
7.0
7.0
6.0
7.0
8.0
7.0
6.0
7.0
7.0

Figure 2–5h. Predicted maximum daily mixed–layer ozone concentrations (pphm) for climate sensitivity scenario#1: July 21, 1980.

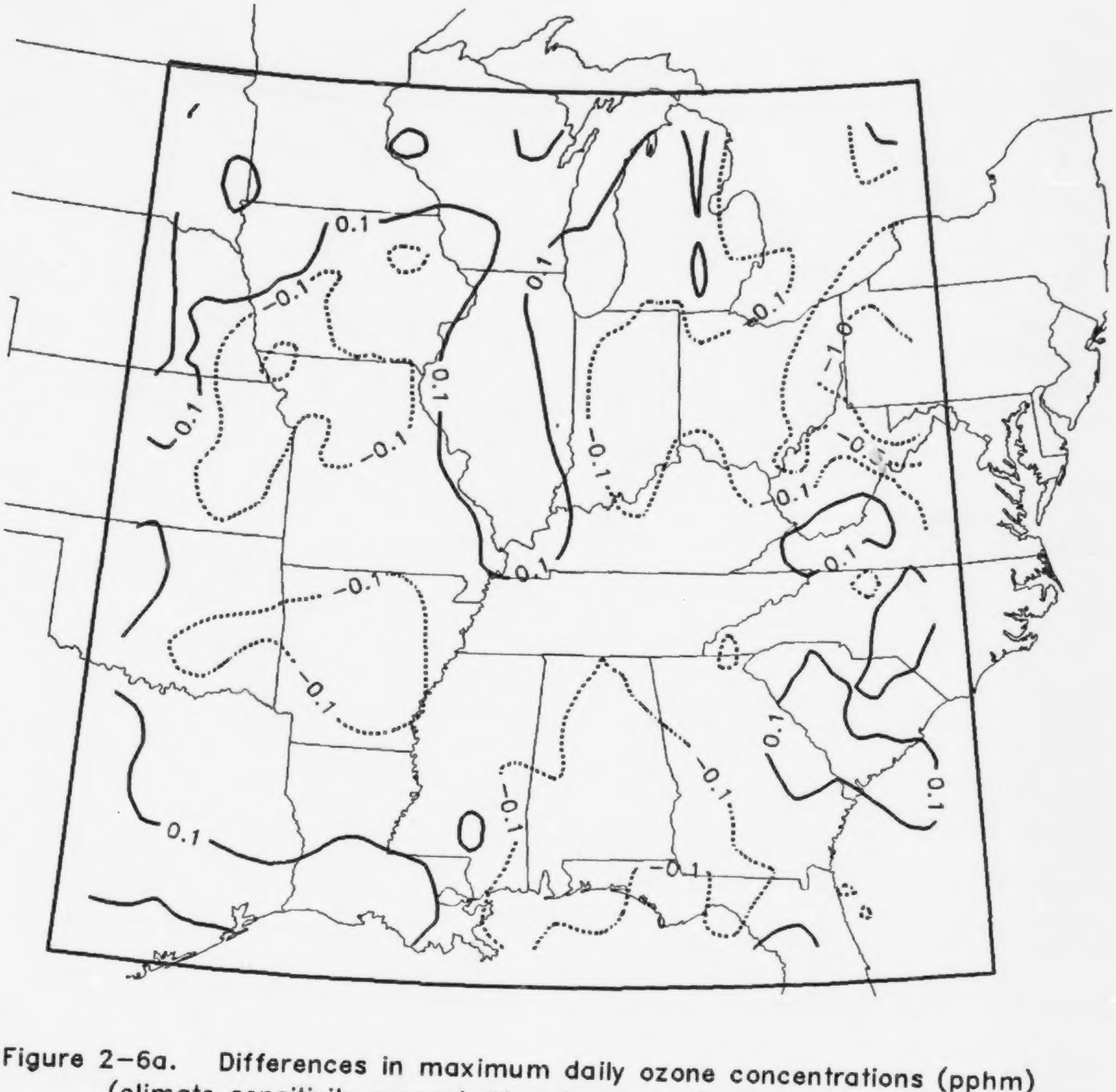
0.1
-0.1
0.1
-0.1
0.1
-0.1
0.1
-0.1
-1.0
-0.1
0.1
0.1
-0.1
-0.1
0.1
-0.1
-0.1
0.1
0.1
-0.1

Figure 2–6a. Differences in maximum daily ozone concentrations (pphm) (climate sensitivity scenario#1 – base case): July 14, 1980.

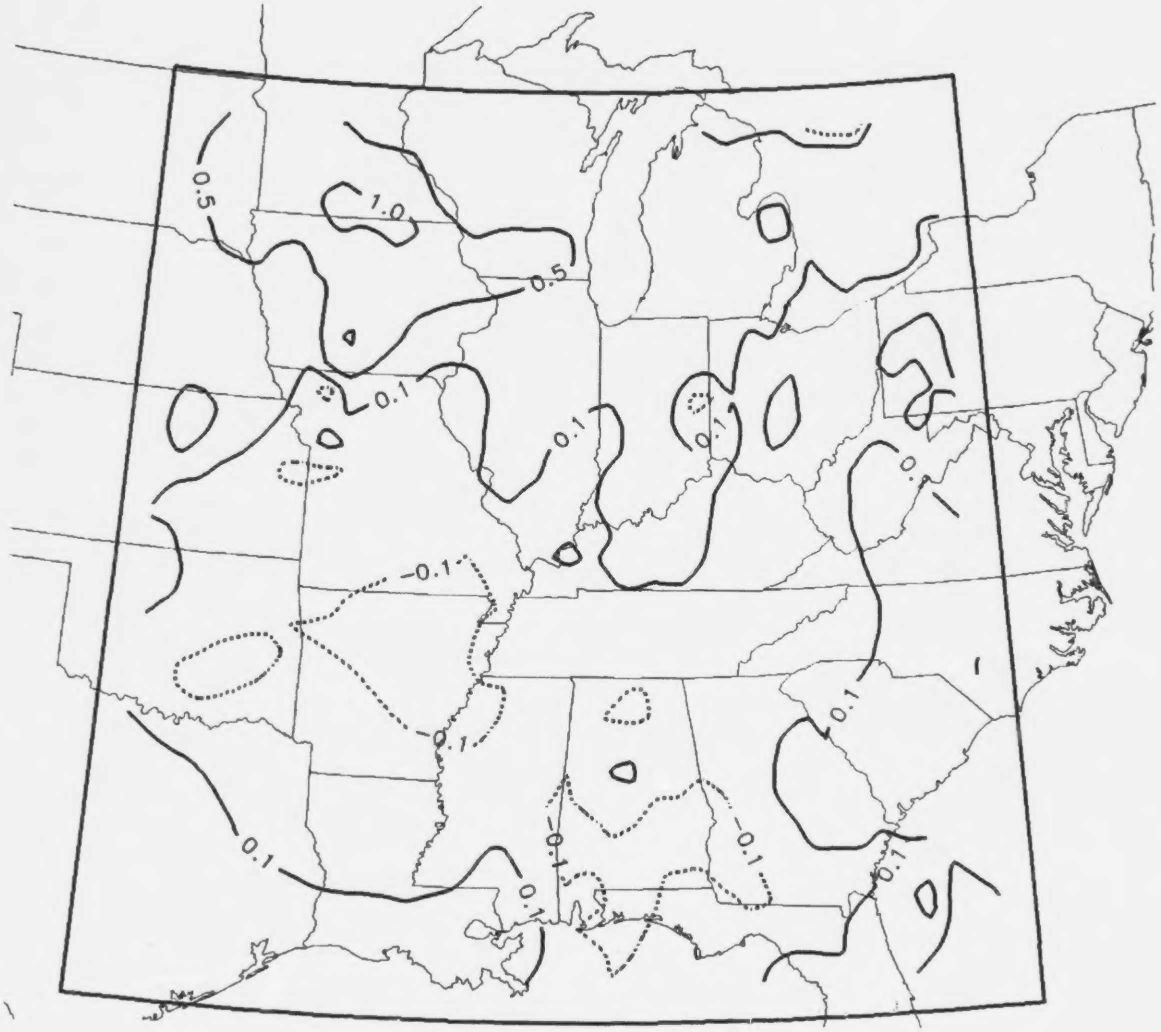
0.5
1.0
0.5
-0.1
0.1
0.1
-0.1
-0.1
0.1
0.1
0.1
-0.1
-0.1
0.1
0.1
0.1

Figure 2–6b. Differences in maximum daily ozone concentrations (pphm) (climate sensitivity scenario#1 – base case): July 15, 1980.

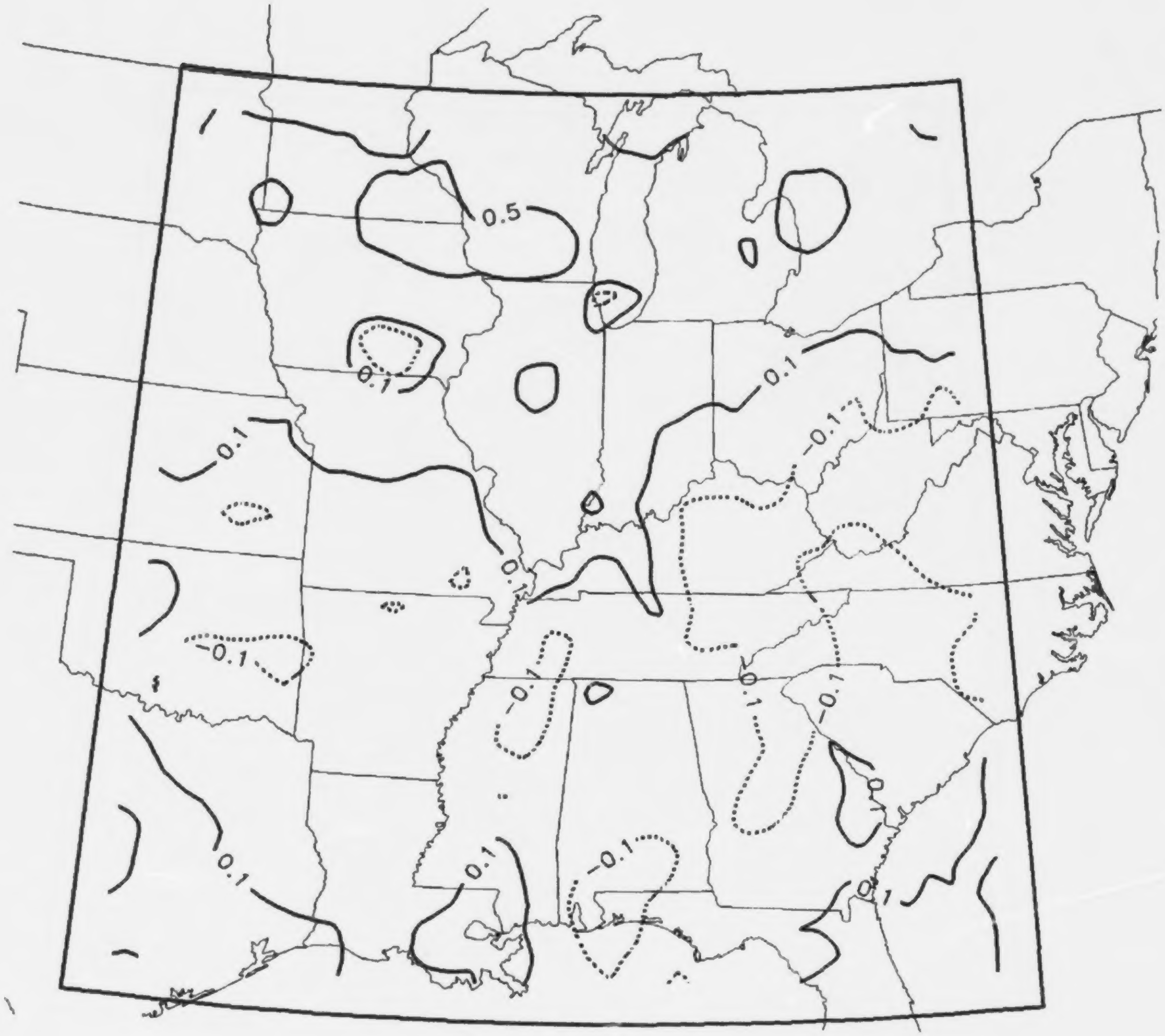
0.5
0.1
0.1
0.1
0.1
-0.1
-0.1
-0.1
-0.1
-0.1
-0.1
0.1
0.1
-0.1
0.1
0.1

Figure 2–6c. Differences in maximum daily ozone concentrations (pphm) (climate sensitivity scenario#1 – base case): July 16, 1980.

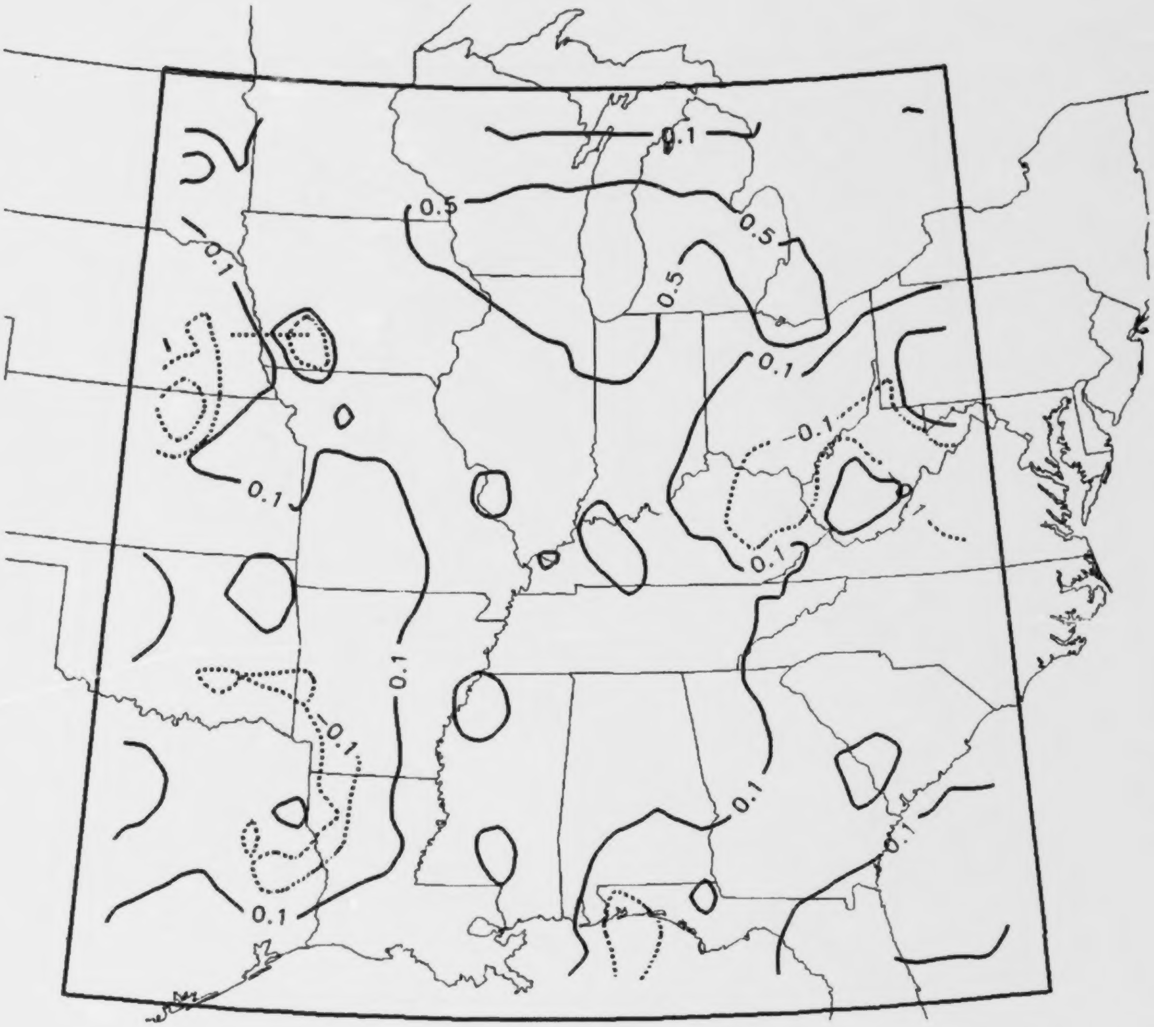
0.1
0.5
0.5
0.5
0.1
0.1
0.1
-0.1
0.1
0.1
0.1
0.1
0.1
0.1
0.1

Figure 2-6d. Differences in maximum daily ozone concentrations (pphm) (climate sensitivity scenario#1 - base case): July 17, 1980.

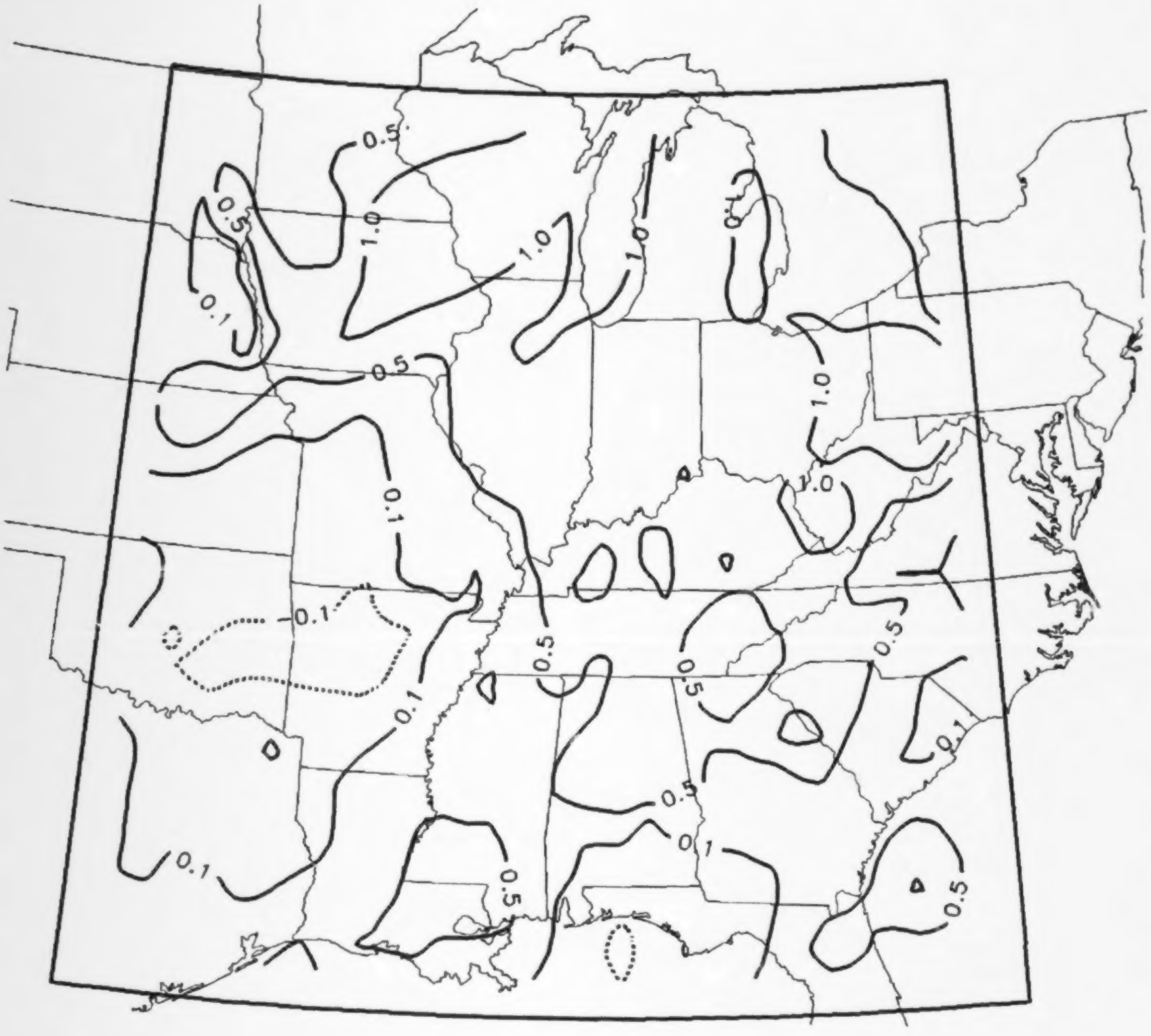
0.5
0.5
1.0
1.0
1.0
1.0
0.1
0.5
1.0
1.0
0.1
0.1
0.5
0.5
0.5
0.1
0.1
0.5
0.1
0.5
0.1
0.5

Figure 2−6e. Differences in maximum daily ozone concentrations (pphm) (climate sensitivity scenario#1 − base case): July 18, 1980.

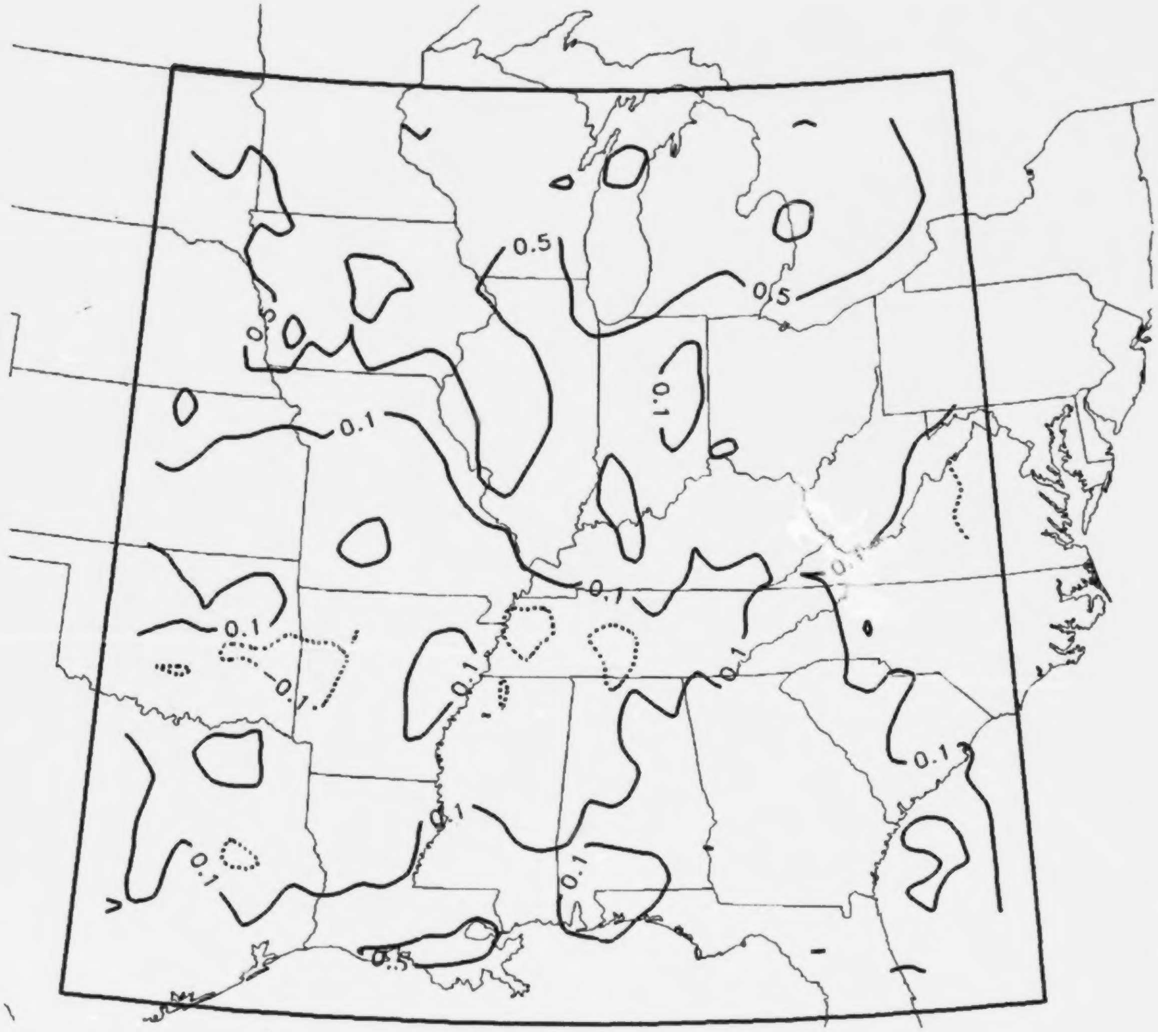
0.5
0.5
0.5
0.1
0.1
0.1
0.1
0.1
-0.1
0.1
0.1
0.1
0.1
0.1
0.1
0.1
0.5

Figure 2-6f. Differences in maximum daily ozone concentrations (pphm) (climate sensitivity scenario#1 - base case): July 19, 1980.

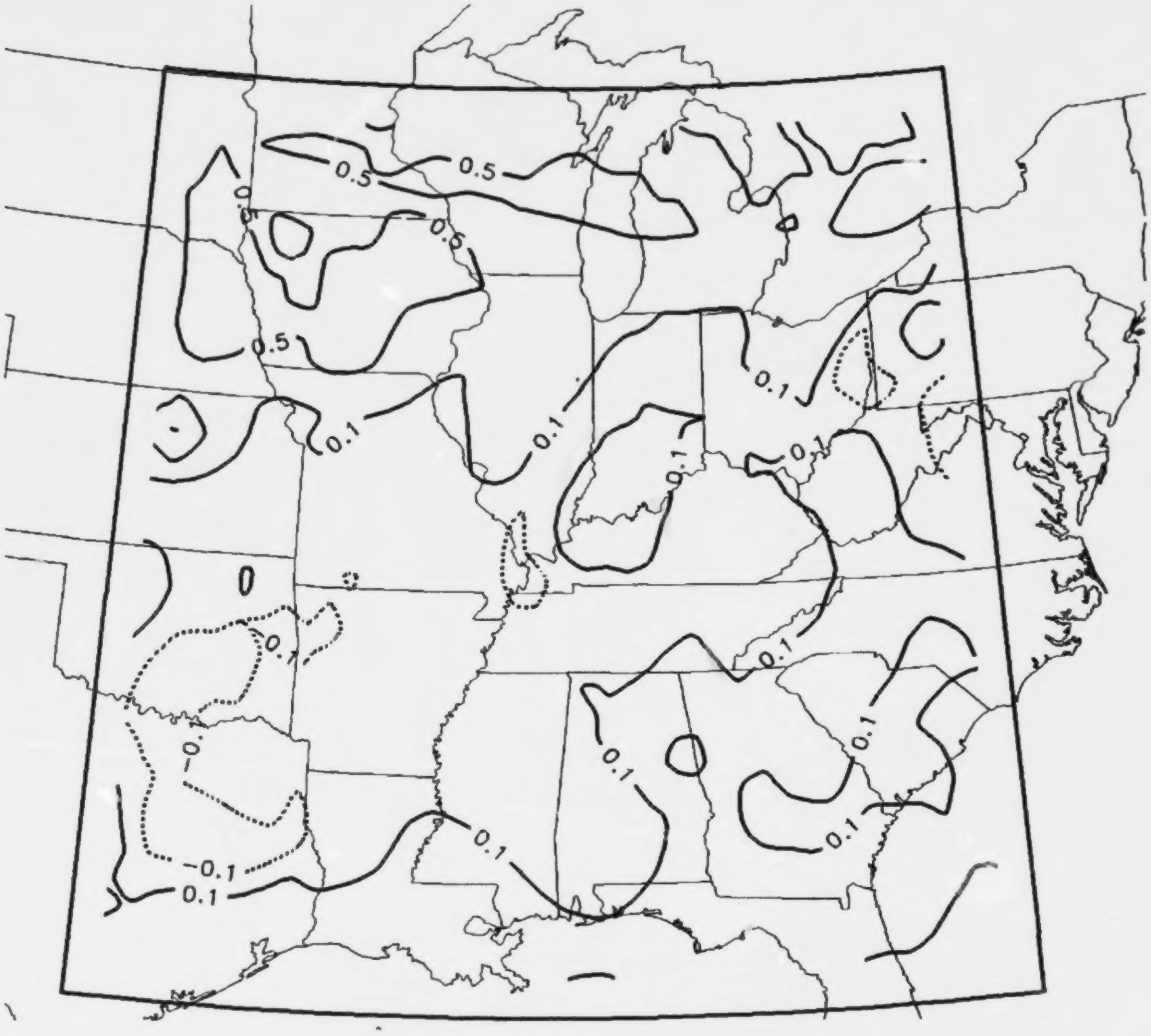
0.5
0.5
0.5
0.5
0.5
0.5
0.1
0.1
0.1
0.1
0.1
0
0.1
0.1
0.1
0.1
0.1
0.1
-0.1
0.1

Figure 2-6g. Differences in maximum daily ozone concentrations (pphm) (climate sensitivity scenario#1 - base case): July 20, 1980.

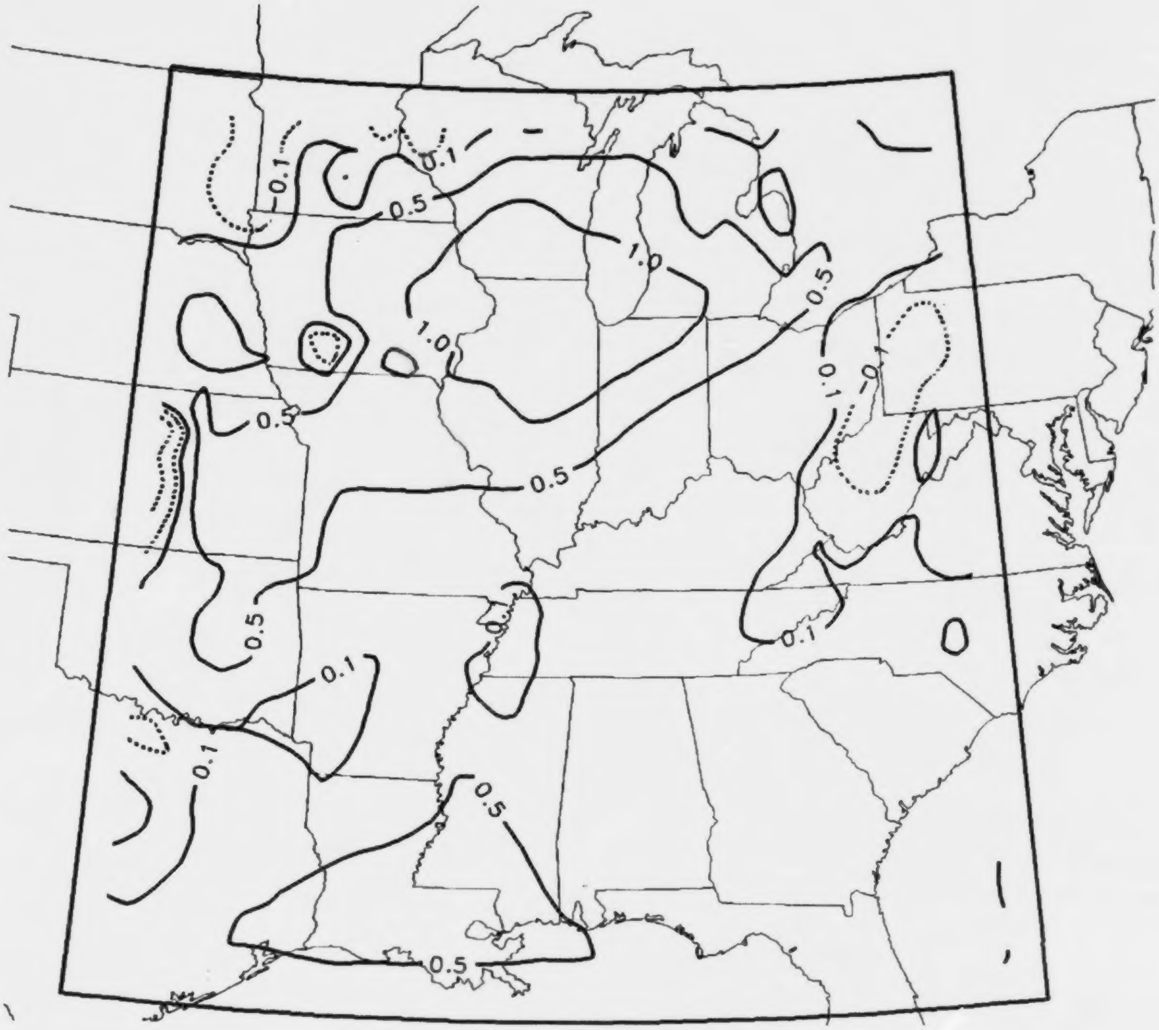
0.1
0.1
0.5
1.0
1.0
0.5
0.5
0.5
0.1
0.1
0.5
0.5
0.1
0.1
0.1
0.5
0.5
0.1

Figure 2–6h. Differences in maximum daily ozone concentrations (pphm) (climate sensitivity scenario#1 – base case): July 21, 1980.

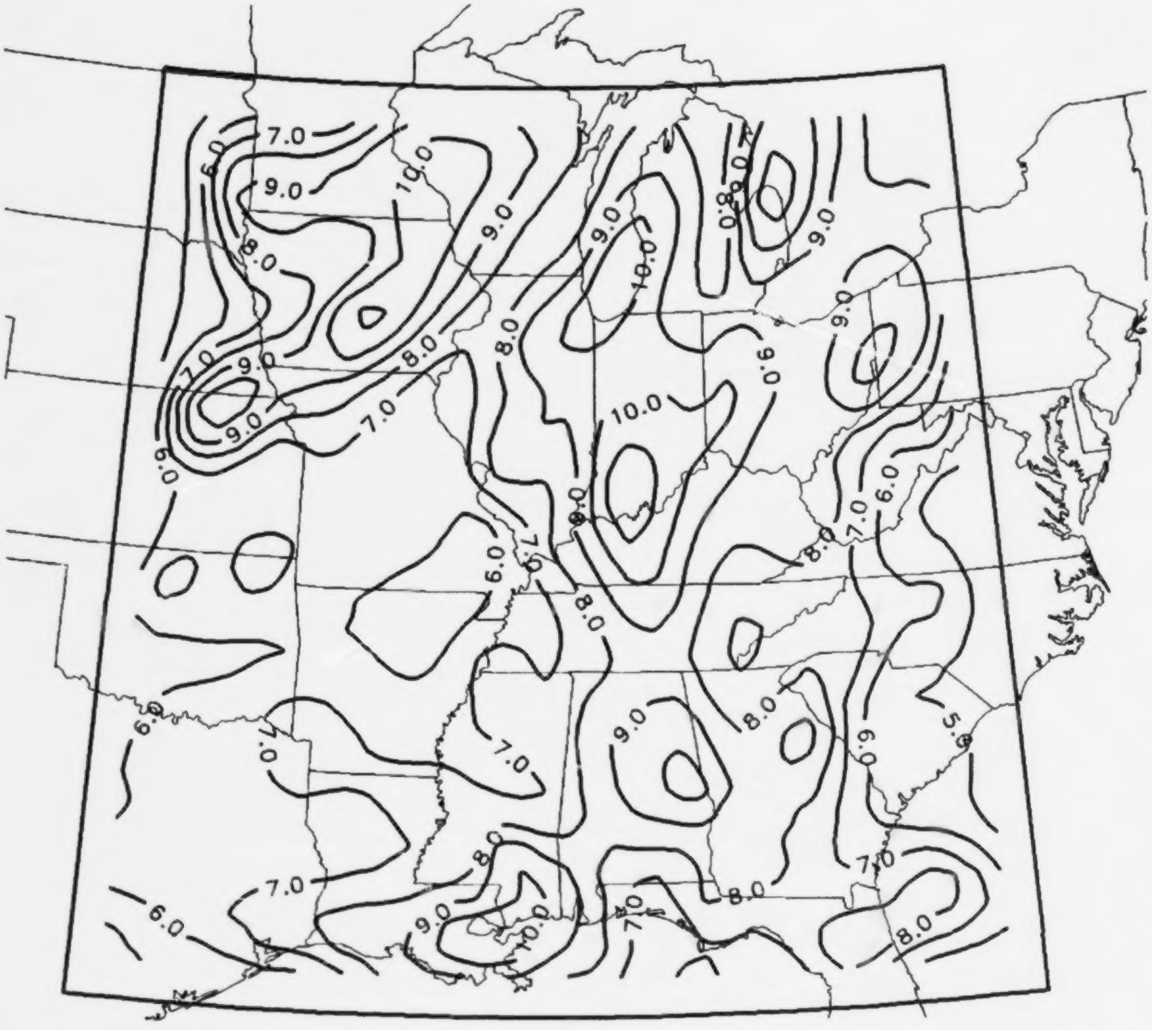
7.0
6.0
9.0
10.0
9.0
8.0
9.0
10.0
8.0
9.0
8.0
7.0
9.0
9.0
8.0
7.0
9.0
9.0
10.0
6.0
7.0
6.0
8.0
9.0
8.0
6.0
7.0
9.0
8.0
7.0
9.0
5.0
8.0
7.0
7.0
6.0
9.0
10.0
7.0
8.0
8.0

Figure 2–7a. Predicted maximum daily mixed–layer ozone concentrations (pphm) for climate sensitivity scenario#2: July 14, 1980.

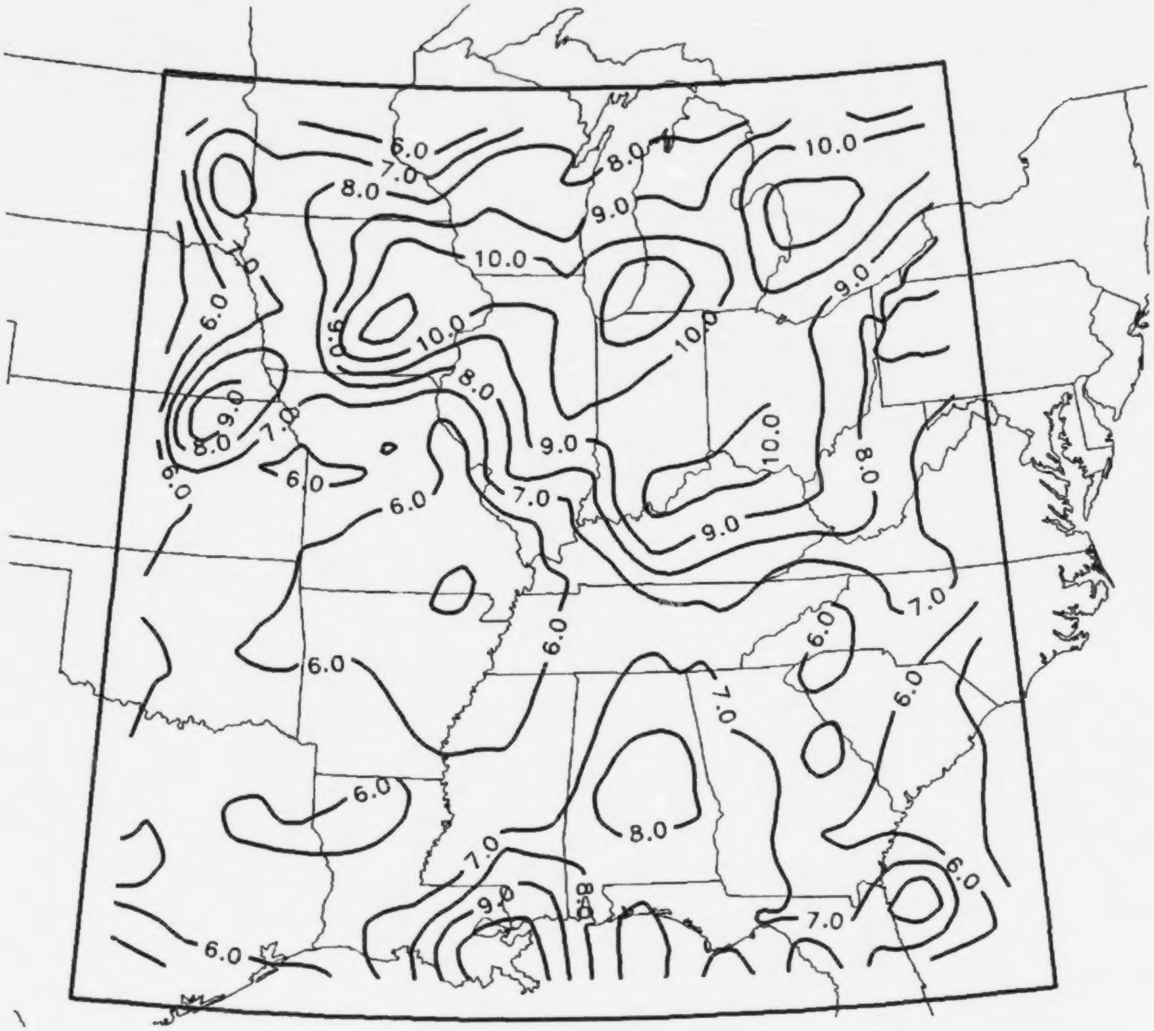
6.0
7.0
8.0
8.0
10.0
9.0
10.0
6.0
9.0
10.0
10.0
9.0
6.0
9.0
8.0
7.0
8.0
6.0
9.0
6.0
6.0
7.0
10.0
8.0
9.0
7.0
6.0
6.0
6.0
7.0
6.0
7.0
6.0
8.0
7.0
9.0
8.0
6.0
7.0
6.0

Figure 2-7b. Predicted maximum daily mixed-layer ozone concentrations (pphm) for climate sensitivity scenario#2: July 15, 1980.

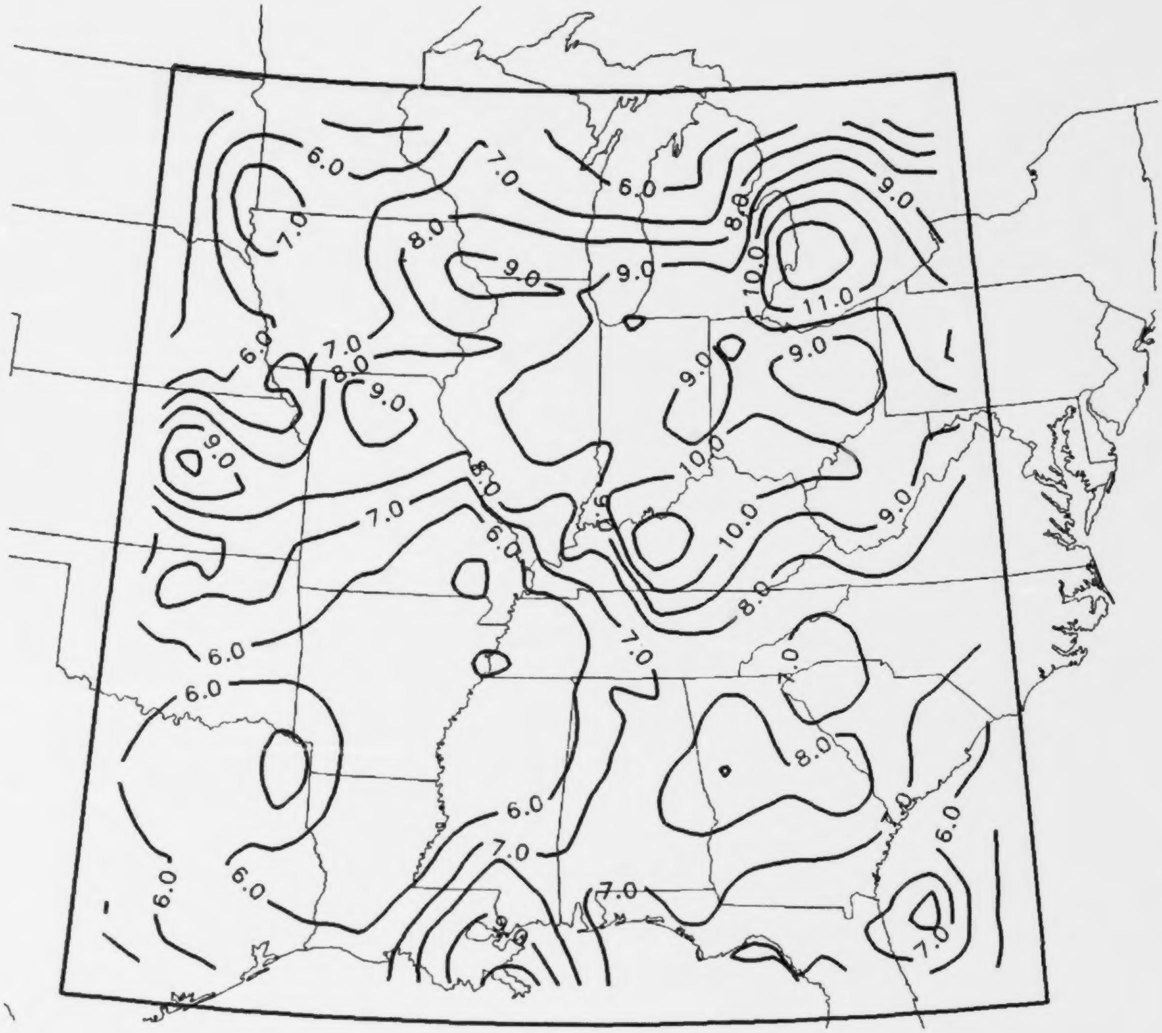
6.0
7.0
6.0
9.0
7.0
8.0
9.0
9.0
8.0
10.0
11.0
6.0
7.0
8.0
9.0
9.0
9.0
9.0
8.0
10.0
7.0
6.0
9.0
10.0
9.0
8.0
6.0
7.0
6.0
7.0
8.0
7.0
6.0
6.0
7.0
7.0
6.0
9.0
6.0
7.0

Figure 2–7c. Predicted maximum daily mixed–layer ozone concentrations (pphm) for climate sensitivity scenario#2: July 16, 1980.

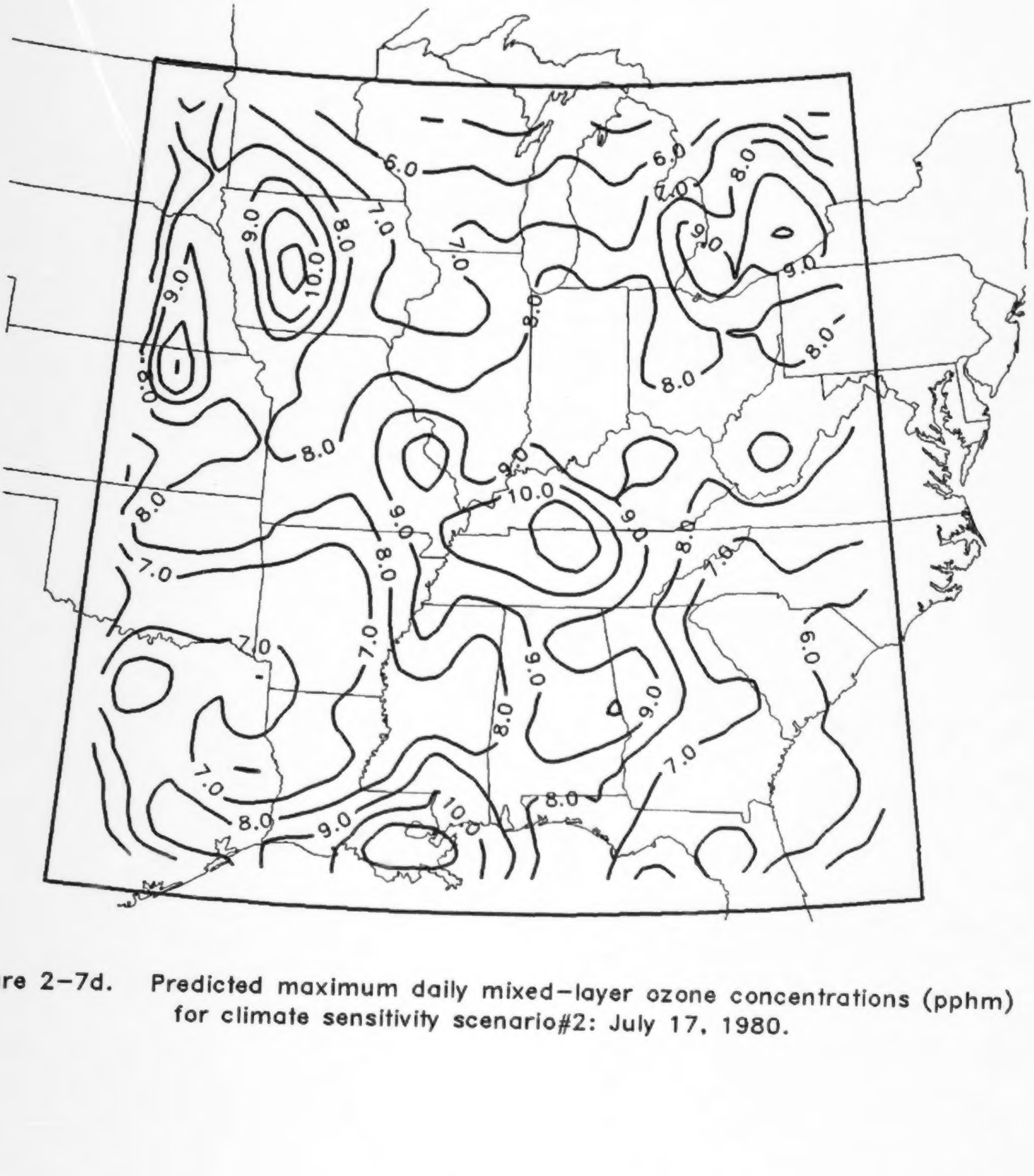
6.0
6.0
8.0
7.0
9.0
8.0
7.0
9.0
10.0
7.0
8.0
9.0
9.0
9.0
8.0
8.0
8.0
8.0
9.0
10.0
9.0
8.0
9.0
7.0
8.0
7.0
7.0
7.0
6.0
9.0
8.0
9.0
7.0
7.0
8.0
8.0
9.0
10.0

Figure 2-7d. Predicted maximum daily mixed-layer ozone concentrations (pphm) for climate sensitivity scenario#2: July 17, 1980.

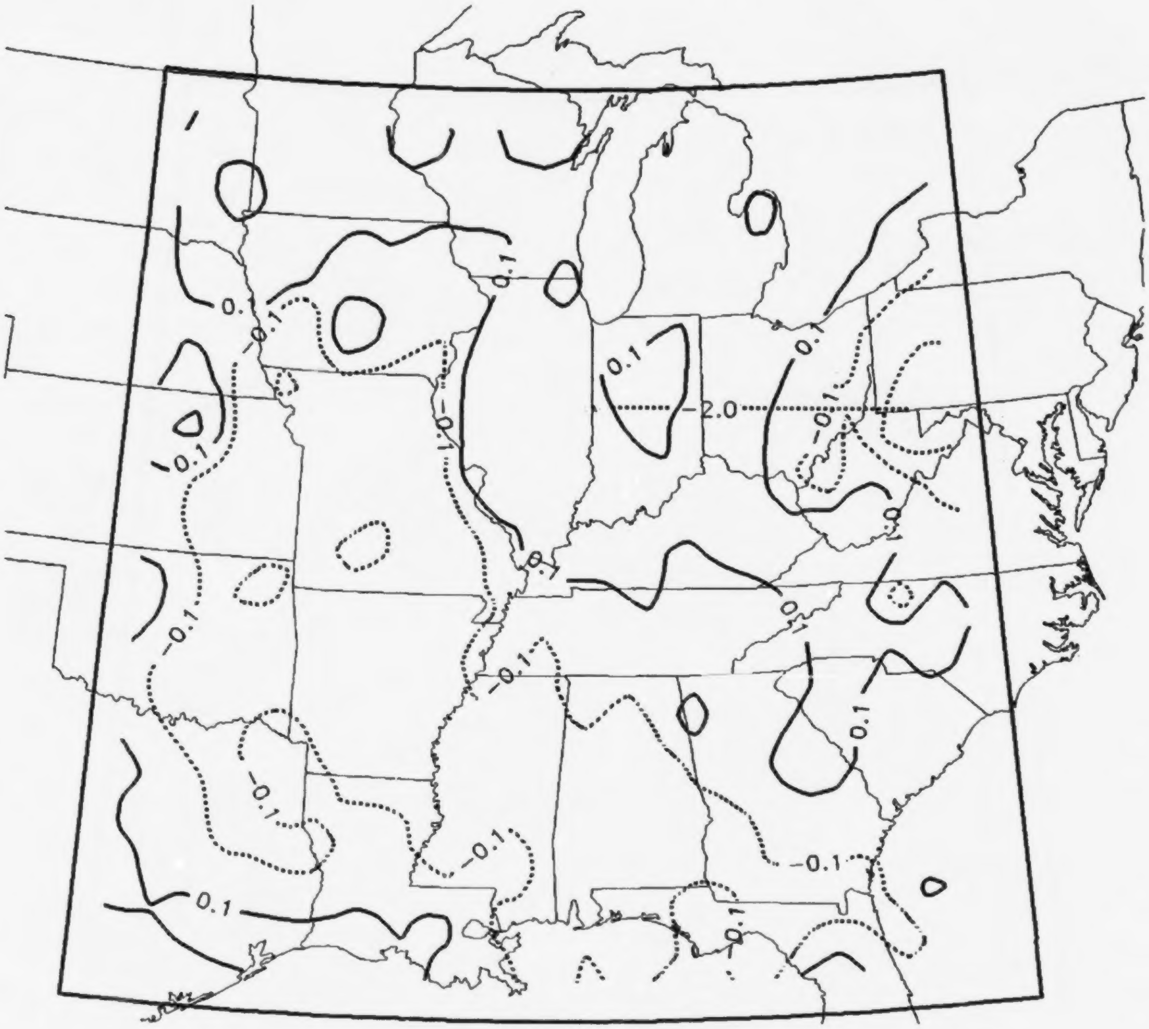
0.1
-0.1
0.1
0.1
0.1
2.0
-0.1
-0.1
0.1
-0.1
-0.1
0.1
0.1
-0.1
-0.1
0.1
-0.1
-0.1
0.1
0.1
-0.1

Figure 2—8a. Differences in maximum daily ozone concentrations (pphm) (climate sensitivity scenario#2 – base case): July 14, 1980.

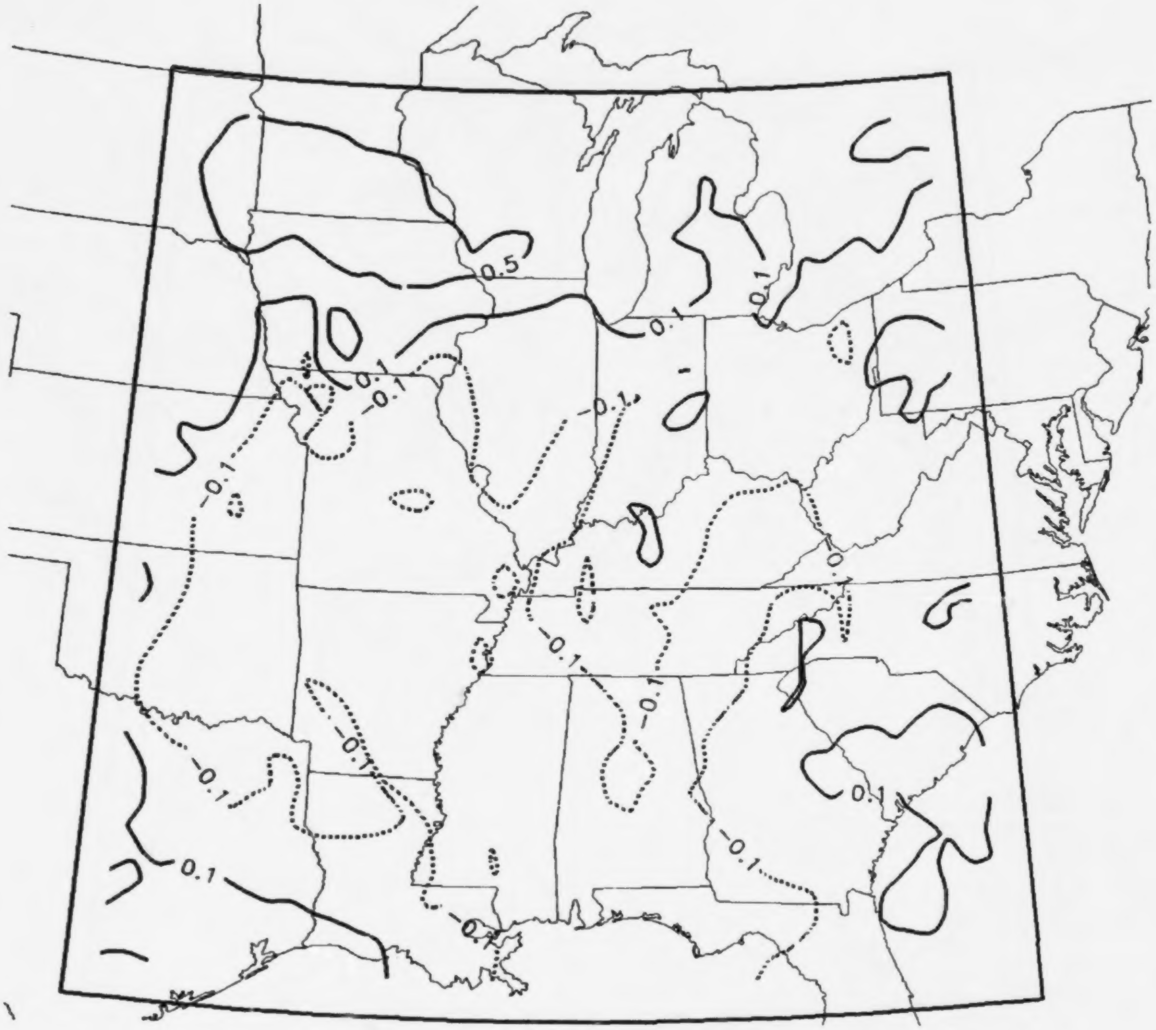
0.5
0.1
0.1
-0.1
-0.1
-0.1
-0.1
-0.1
-0.1
-0.1
-0.1
-0.1
-0.1
0.1
0.1
0.1
-0.1

Figure 2–8b. Differences in maximum daily ozone concentrations (pphm) (climate sensitivity scenario#2 – base case): July 15, 1980.

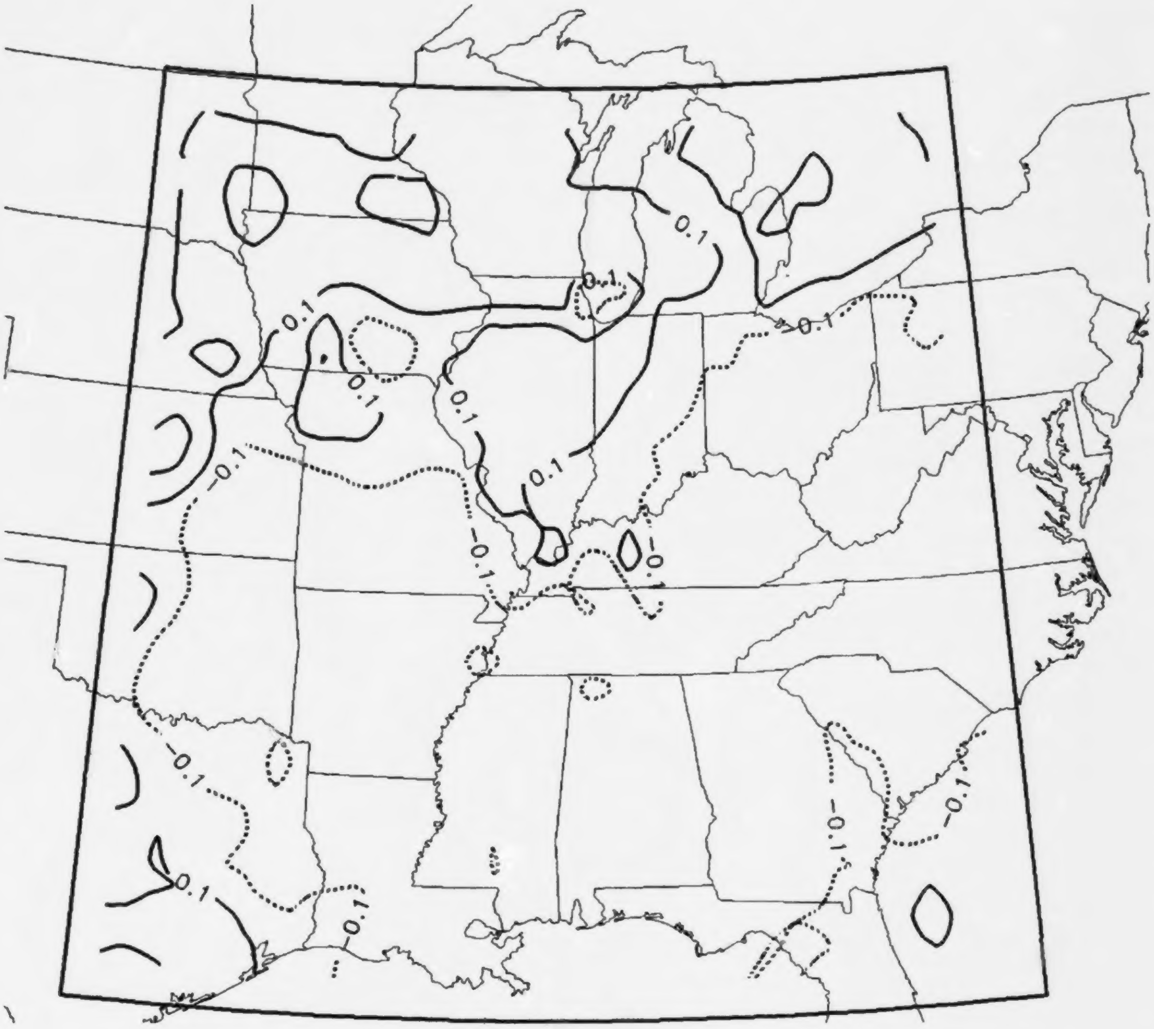
0.1
0.1
-0.1
0.1
0.1
-0.1
0.1
0.1
-0.1
0
-0.1
0.1
-0.1
-0.1
-0.1

Figure 2–8c. Differences in maximum daily ozone concentrations (pphm) (climate sensitivity scenario#2 – base case): July 16, 1980.

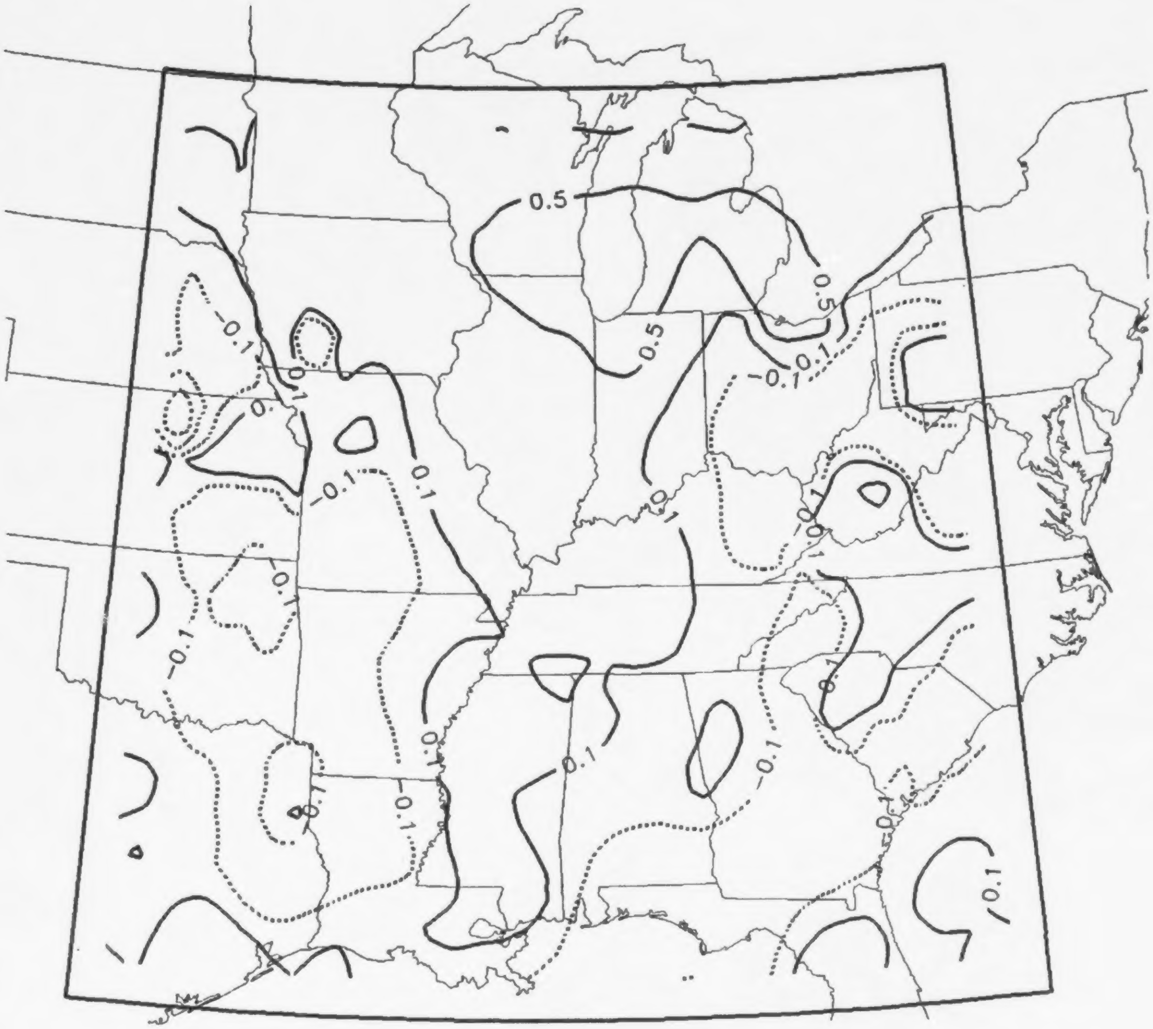
0.5
0.5
0.5
-0.1
-0.1
0.1
0.1
-0.1
0.1
0.1
-0.1
-0.1
0.1
0.1
-0.1
0.1
0.1
-0.1
0.1
-0.1
0.1
-0.1
0.1
0.1
-0.1

Figure 2-8d. Differences in maximum daily ozone concentrations (pphm) (climate sensitivity scenario#2 - base case): July 17, 1980.

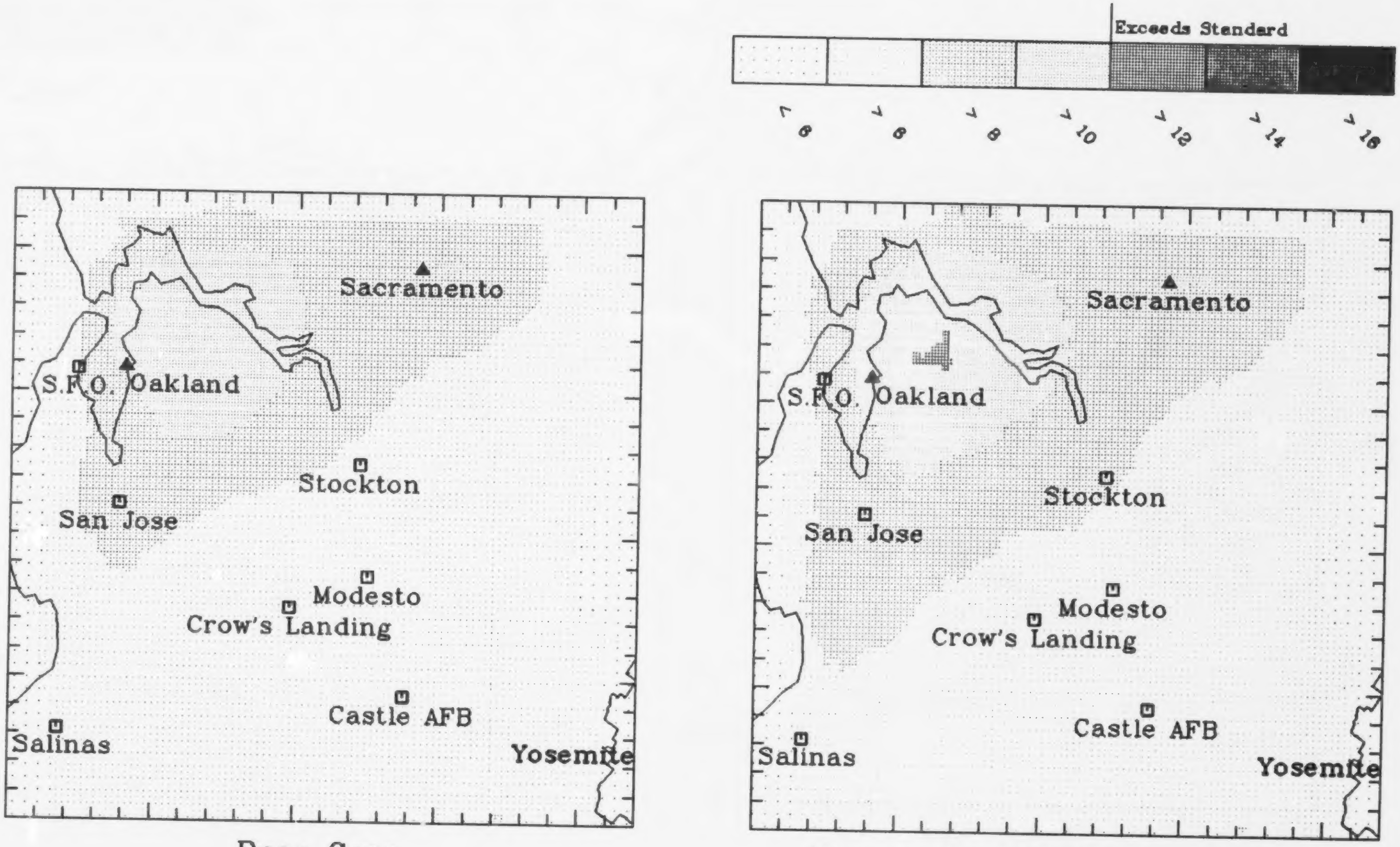
Exceeds Standard
< 6
> 6
> 8
> 10
> 12
> 14
> 16
S.F.O.
Oakland
Sacramento
Stockton
San Jose
Modesto
Crow's Landing
Castle AFB
Salinas
Yosemite

Base Case

Climate Sensitivity Scenario #1

FIGURE 2-9a. **Comparison of predicted maximum daily ozone concentrations (pphm) for the base case and climate sensitivity scenario #1 (temperature and water increase) for August 5, 1981**

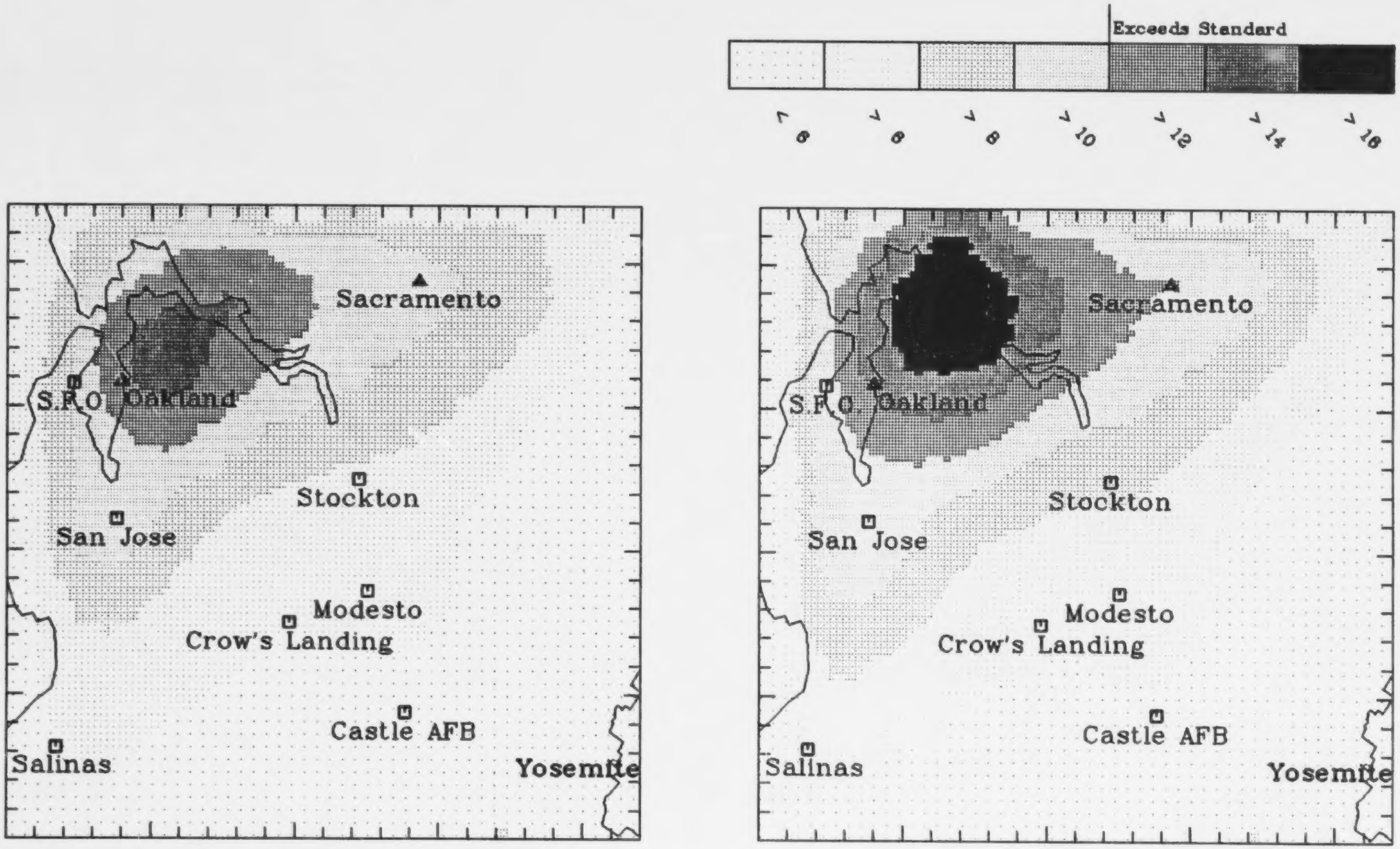

Exceeds Standard
< 6
> 6
> 8
> 10
> 12
> 14
> 16
Sacramento
S.F.O.
Oakland
Stockton
San Jose
Modesto
Crow's Landing
Castle AFB
Salinas
Yosemite

Base Case

Climate Sensitivity Scenario #1

FIGURE 2-9b. **Comparison of predicted maximum daily ozone concentrations (pphm) for the base case and climate sensitivity scenario #1 (temperature and water increase) for August 6, 1981**

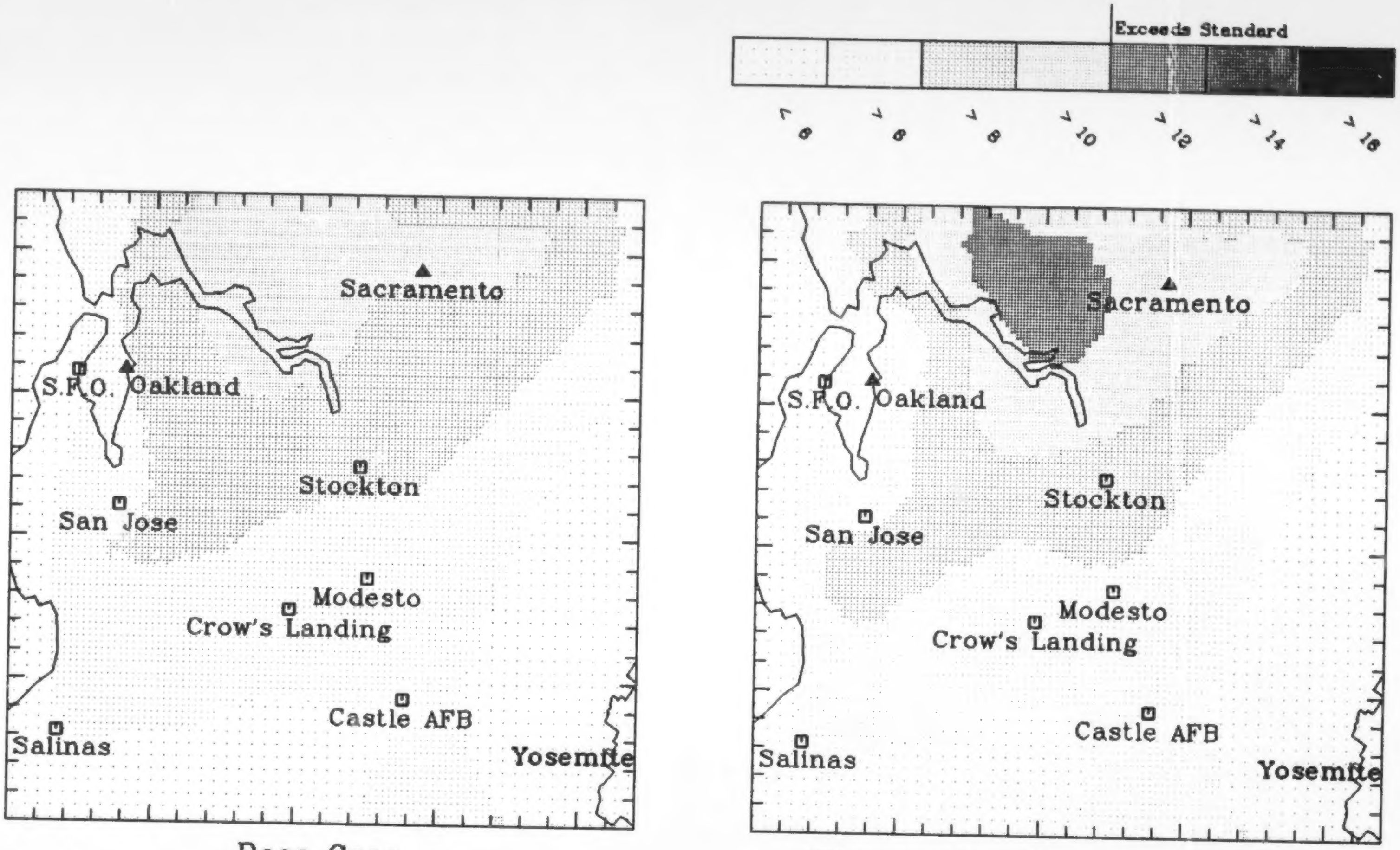
Exceeds Standard
< 6
> 6
> 8
> 10
> 12
> 14
> 16
Sacramento
S.F.O.
Oakland
Stockton
San Jose
Modesto
Crow's Landing
Castle AFB
Salinas
Yosemite

Base Case

Climate Sensitivity Scenario #1

FIGURE 2-9c. **Comparison of predicted maximum daily ozone concentrations (pphm) for the base case and climate sensitivity scenario #1 (temperature and water increase) for August 7, 1981**

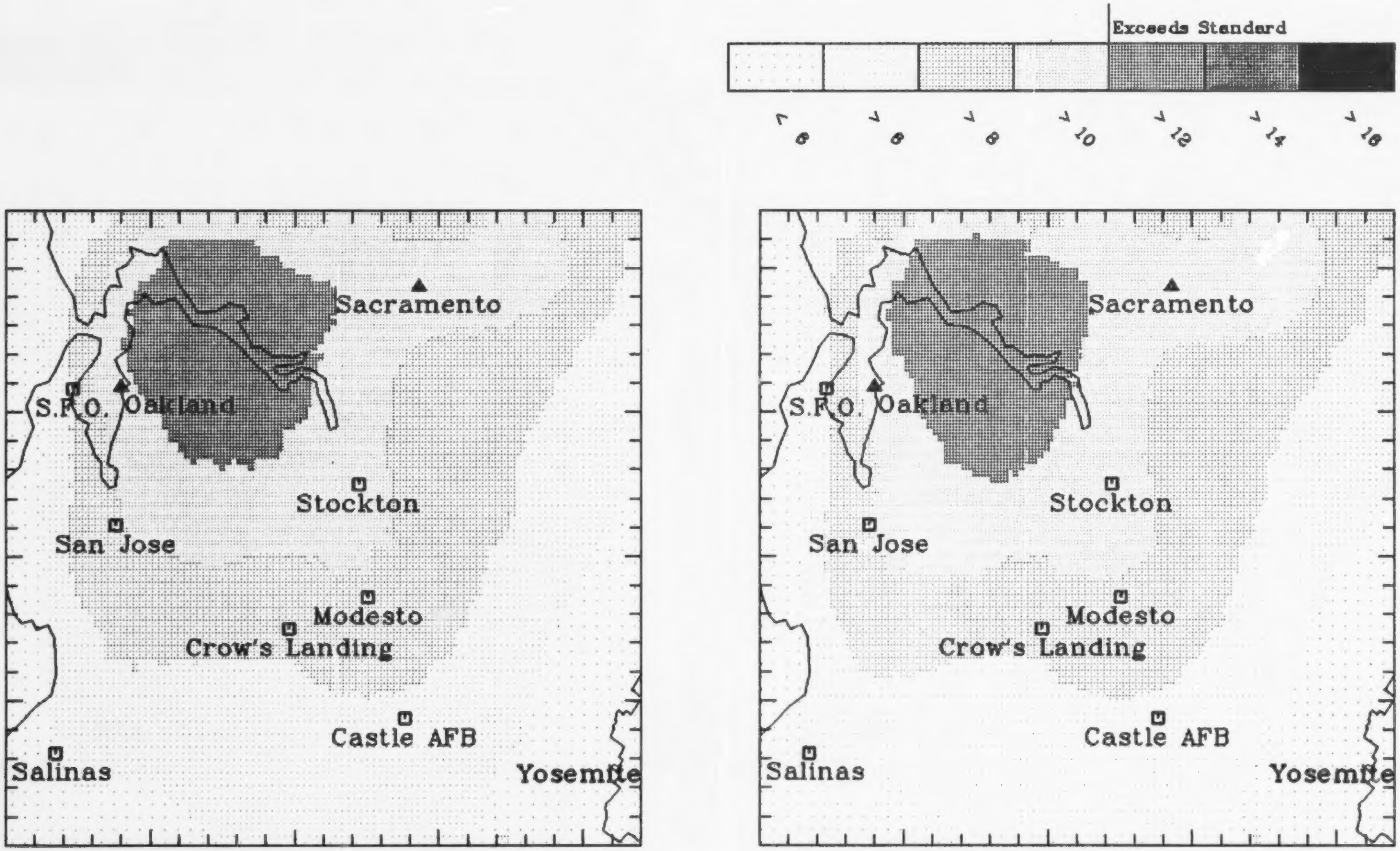
Exceeds Standard
< 6
> 6
> 8
> 10
> 12
> 14
> 16
Sacramento
S.F.O.
Oakland
Stockton
San Jose
Modesto
Crow's Landing
Castle AFB
Salinas
Yosemite

Base Case

Climate Sensitivity Scenario #1

Morris

FIGURE 2-9d. **Comparison of predicted maximum daily ozone concentrations (pphm) for the base case and climate sensitivity scenario #1 (temperature and water increase) for August 8, 1981**

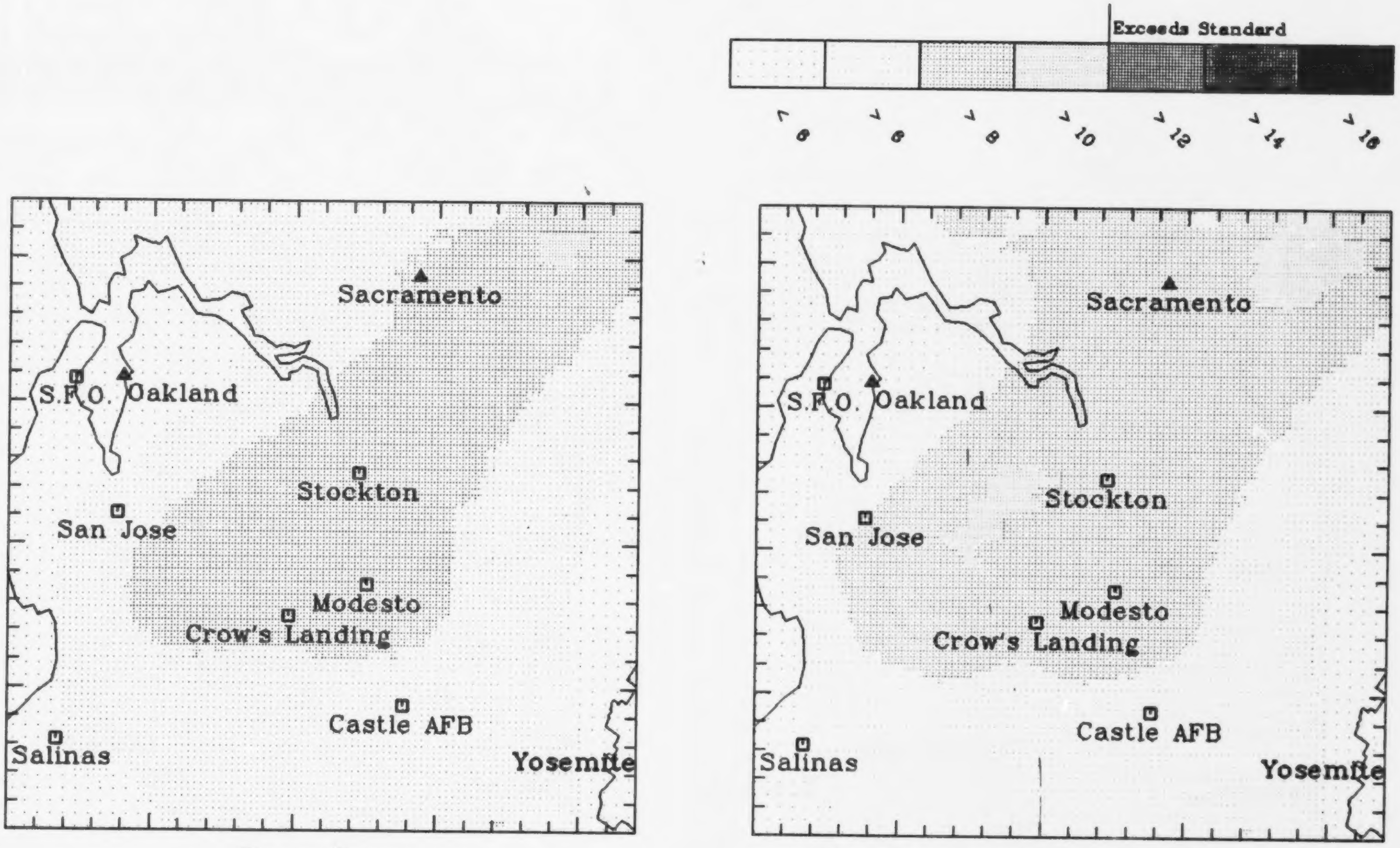
Exceeds Standard
< 6
> 6
> 8
> 10
> 12
> 14
> 16
Sacramento
S.F.O.
Oakland
Stockton
San Jose
Modesto
Crow's Landing
Castle AFB
Salinas
Yosemite

Base Case

Climate Sensitivity Scenario #1

FIGURE 2-9e. **Comparison of predicted maximum daily ozone concentrations (pphm) for the base case and climate sensitivity scenario #1 (temperature and water increase) for August 9, 1981**

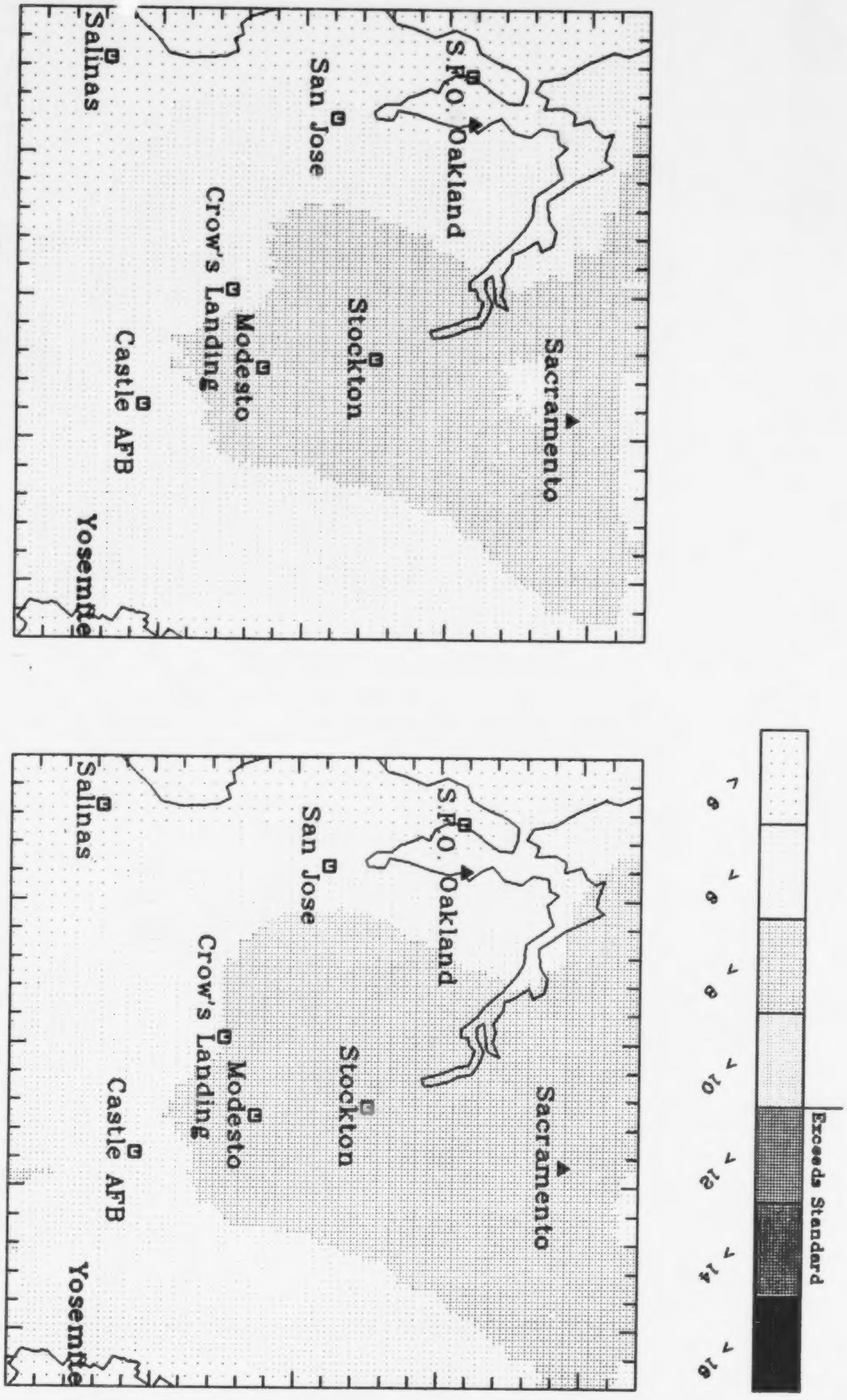
Sacramento
Stockton
Oakland
S.F.O.
San Jose
Crow's Landing
Modesto
Castle AFB
Salinas
Yosemite
Base Case
Climate Sensitivity Scenario #1
< 6
> 6
> 8
> 10
> 12
> 14
> 16
Exceeds Standard

FIGURE 2-9f. Comparison of predicted maximum daily ozone concentrations (pphm) for the base case and climate sensitivity scenario #1 (temperature and water increase) for August 10, 1981

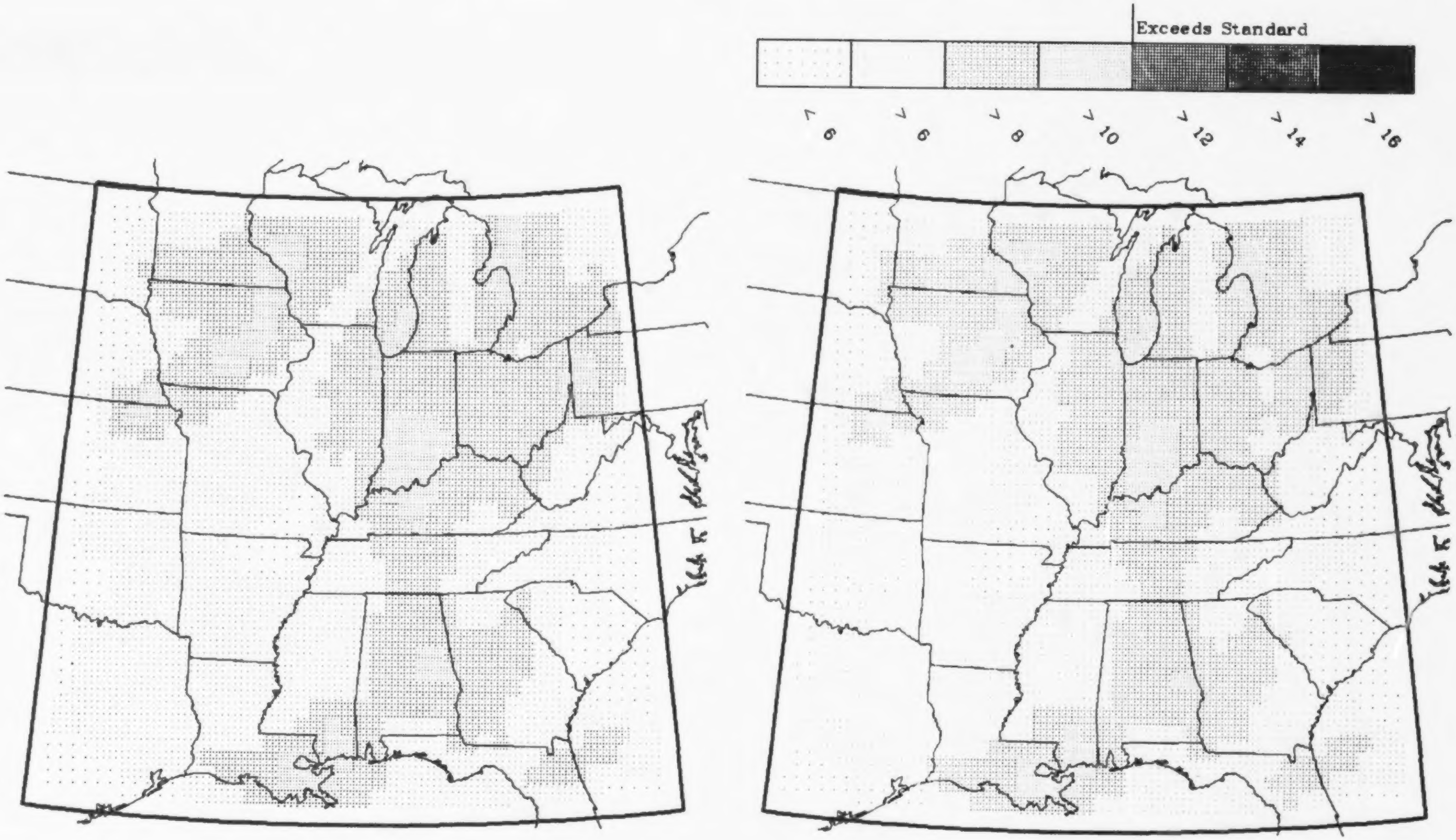
Exceeds Standard
< 6
> 6
> 8
> 10
> 12
> 14
> 16

Base Case

Climate Sensitivity Scenario #1

FIGURE 2-10a. **Comparison of predicted maximum daily ozone concentrations (pphm) for the base case and climate sensitivity scenario #1 (temperature and water increase) for July 14, 1980**

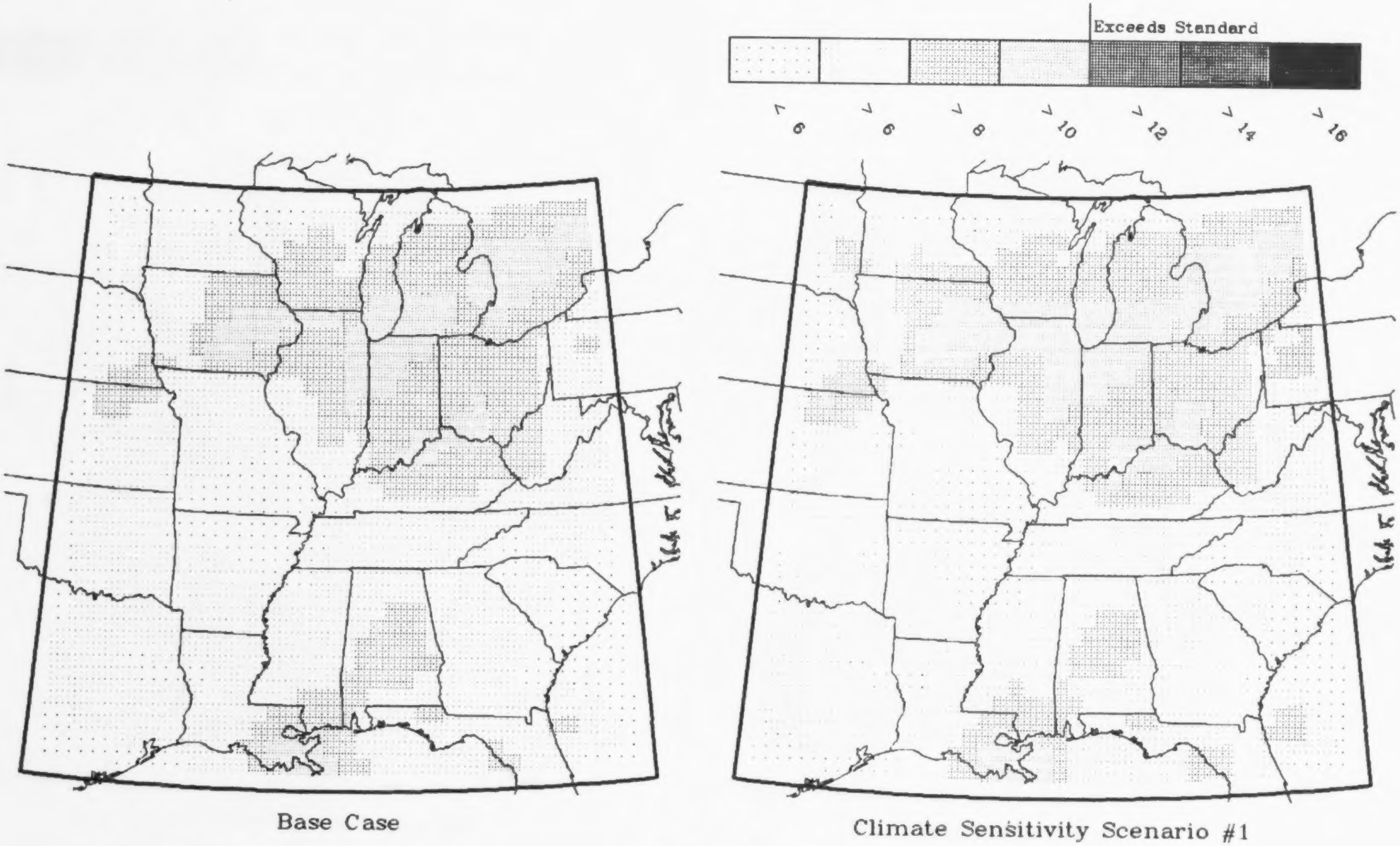

Exceeds Standard
< 6
> 6
> 8
> 10
> 12
> 14
> 16

Base Case

Climate Sensitivity Scenario #1

FIGURE 2-10b. Comparison of predicted maximum daily ozone concentrations (pphm) for the base case and climate sensitivity scenario #1 (temperature and water increase) for July 15, 1980

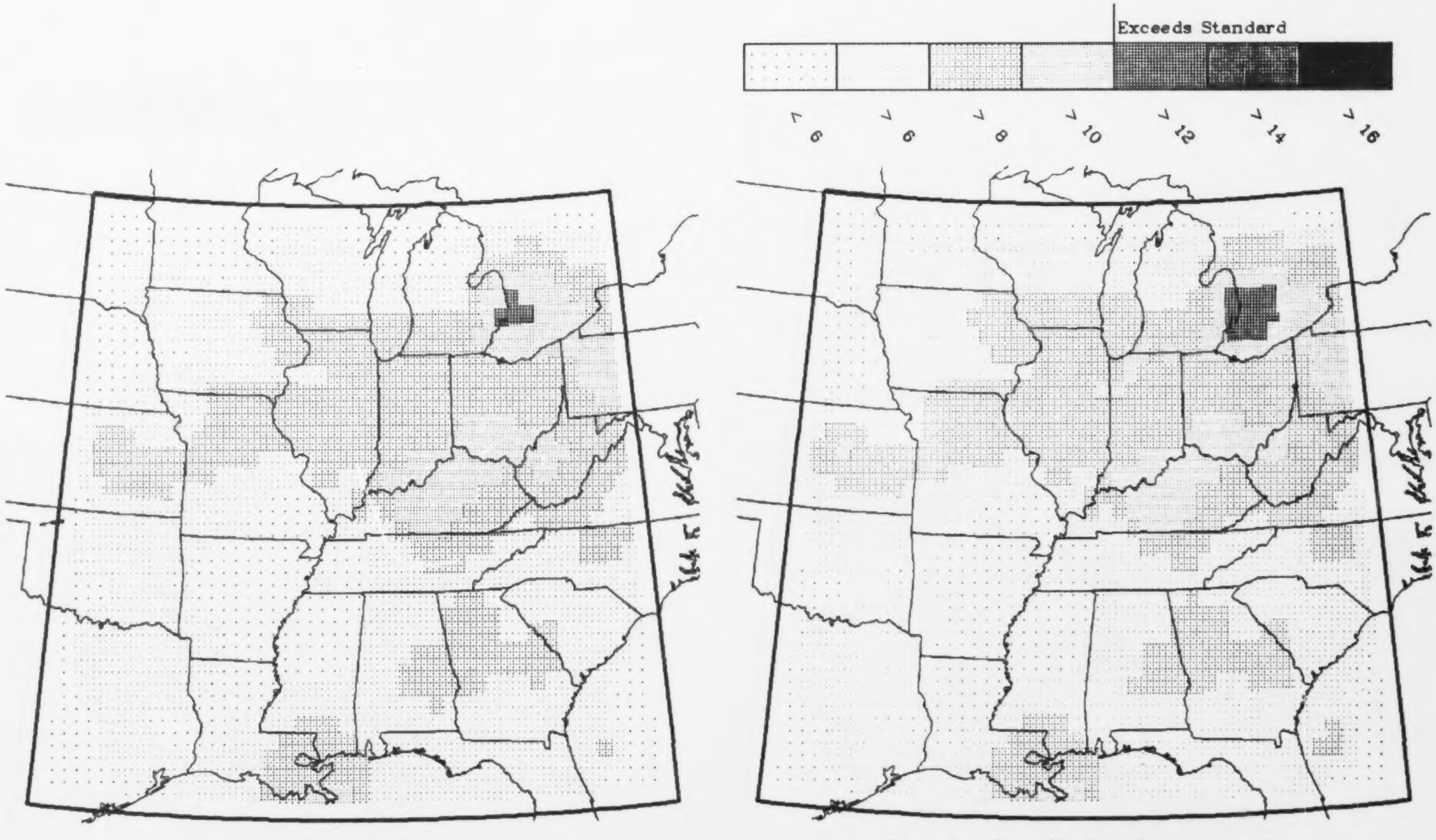
Exceeds Standard
< 6
> 6
> 8
> 10
> 12
> 14
> 16

Base Case

Climate Sensitivity Scenario #1

FIGURE 2-10c. **Comparison of predicted maximum daily ozone concentrations (pphm) for the base case and climate sensitivity scenario #1 (temperature and water increase) for July 16, 1980**

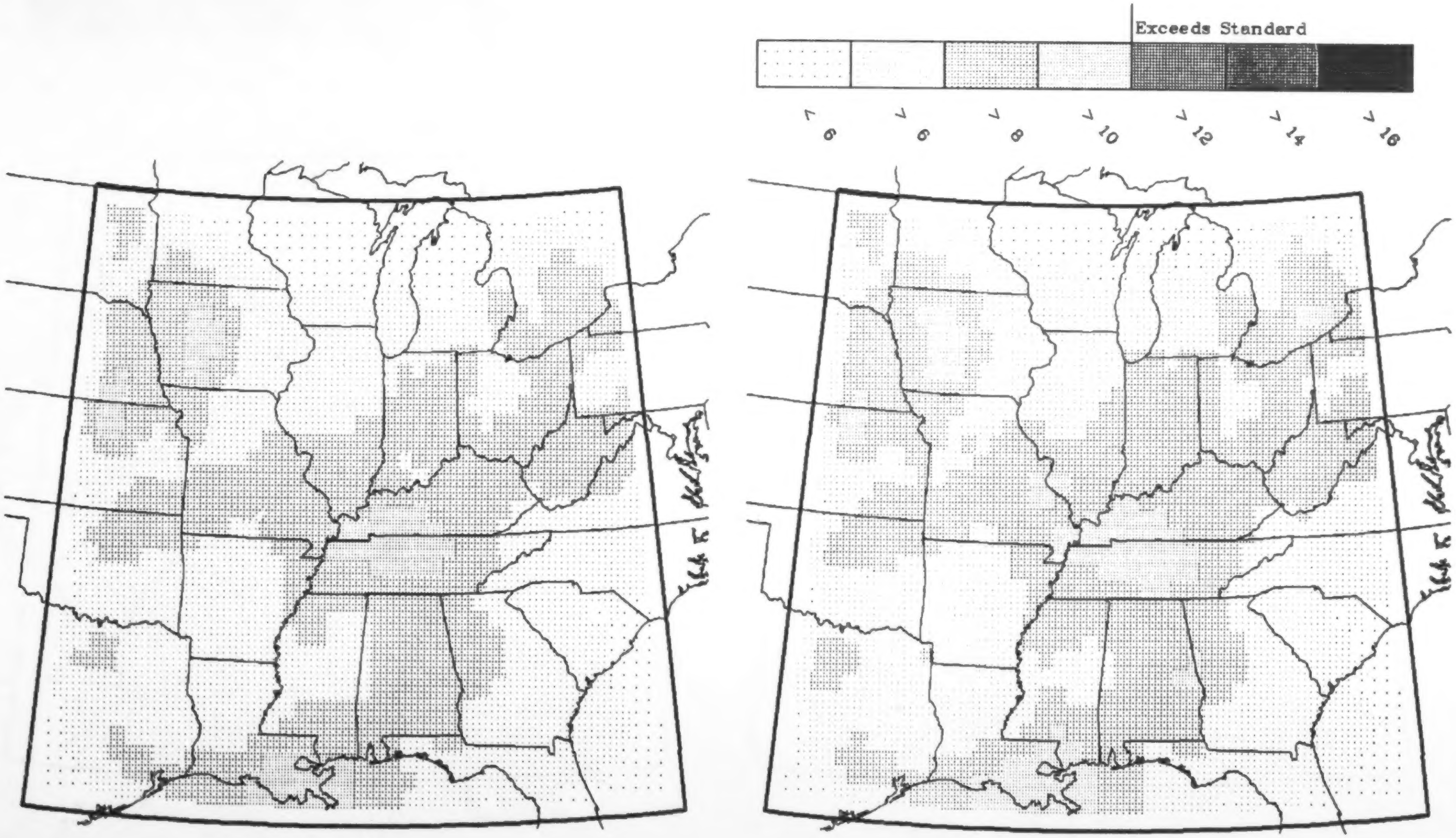
Exceeds Standard
< 6
> 6
> 8
> 10
> 12
> 14
> 16

Base Case

Climate Sensitivity Scenario #1

FIGURE 2-10d. **Comparison of predicted maximum daily ozone concentrations (pphm) for the base case and climate sensitivity scenario #1 (temperature and water increase) for July 17, 1980**

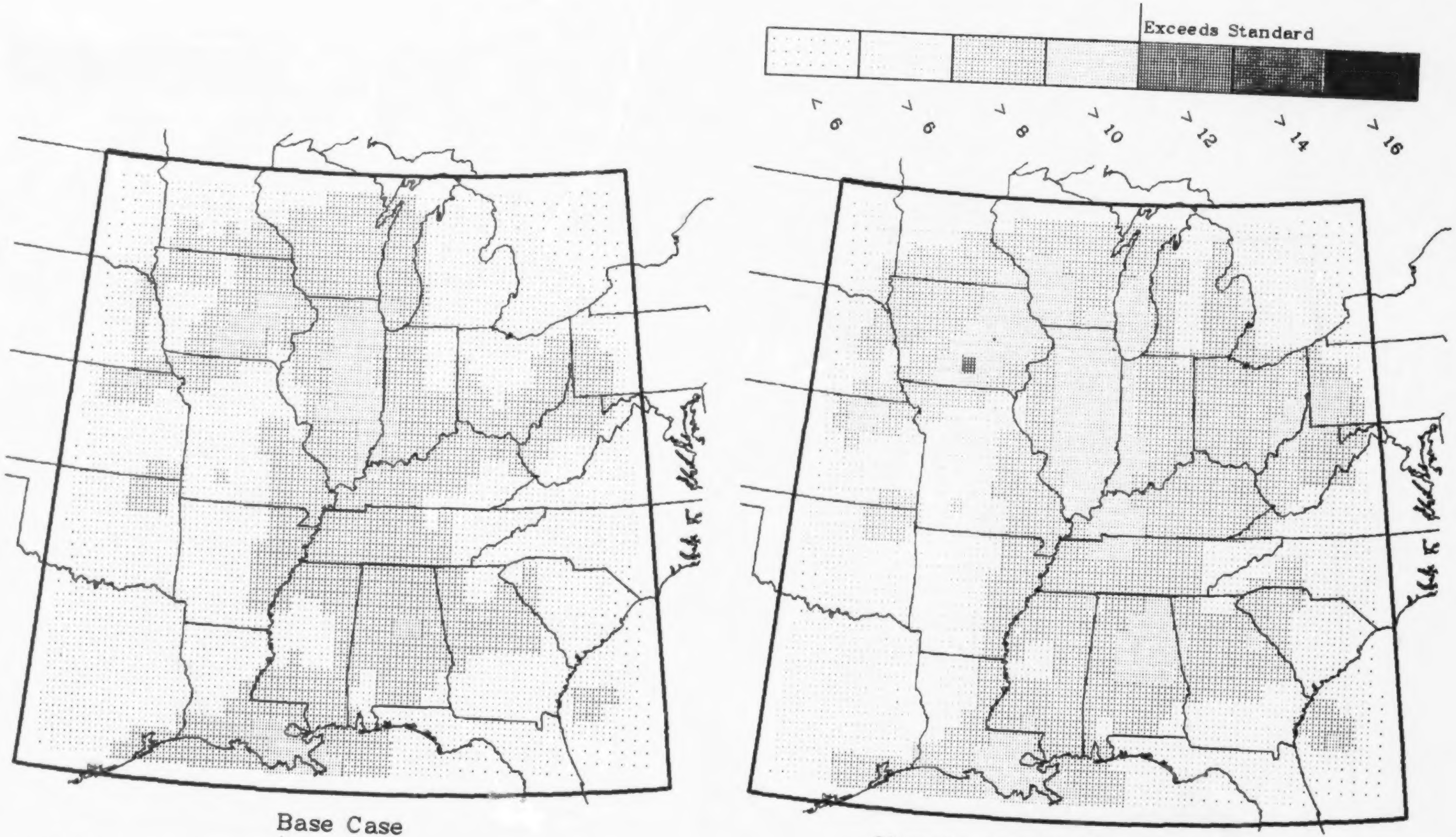
Exceeds Standard
< 6
> 6
> 8
> 10
> 12
> 14
> 16

Base Case

Climate Sensitivity Scenario #1

FIGURE 2-10e. **Comparison of predicted maximum daily ozone concentrations (pphm) for the base case and climate sensitivity scenario #1 (temperature and water increase) for July 18, 1980**

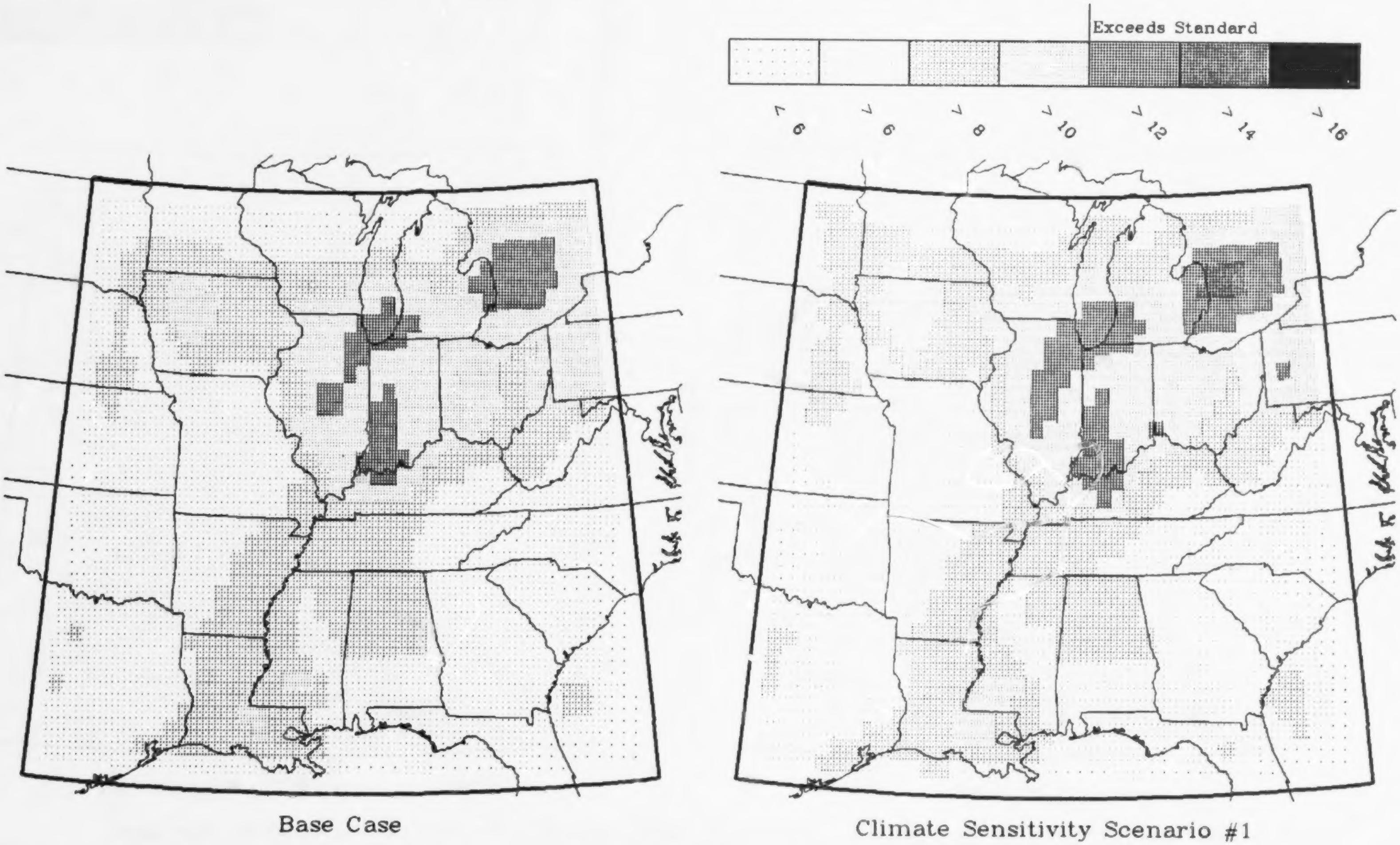
Exceeds Standard
< 6
> 6
> 8
> 10
> 12
> 14
> 16

Base Case

Climate Sensitivity Scenario #1

FIGURE 2-10f. **Comparison of predicted maximum daily ozone concentrations (pphm) for the base case and climate sensitivity scenario #1 (temperature and water increase) for July 19, 1980**

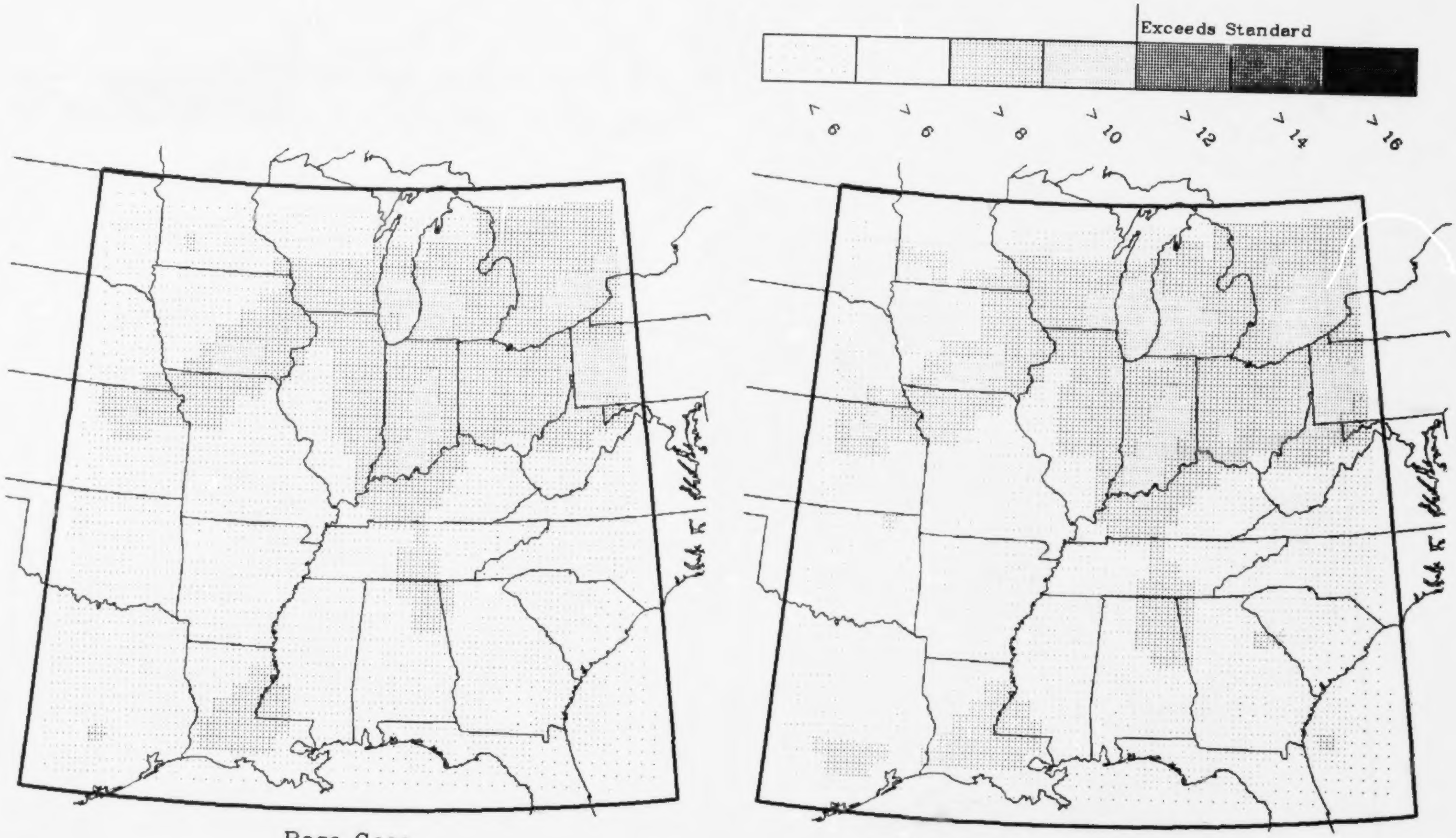
Exceeds Standard
< 6
> 6
> 8
> 10
> 12
> 14
> 16

Base Case

Climate Sensitivity Scenario #1

FIGURE 2-10g. **Comparison of predicted maximum daily ozone concentrations (pphm) for the base case and climate sensitivity scenario #1 (temperature and water increase) for July 20, 1980**

Morris

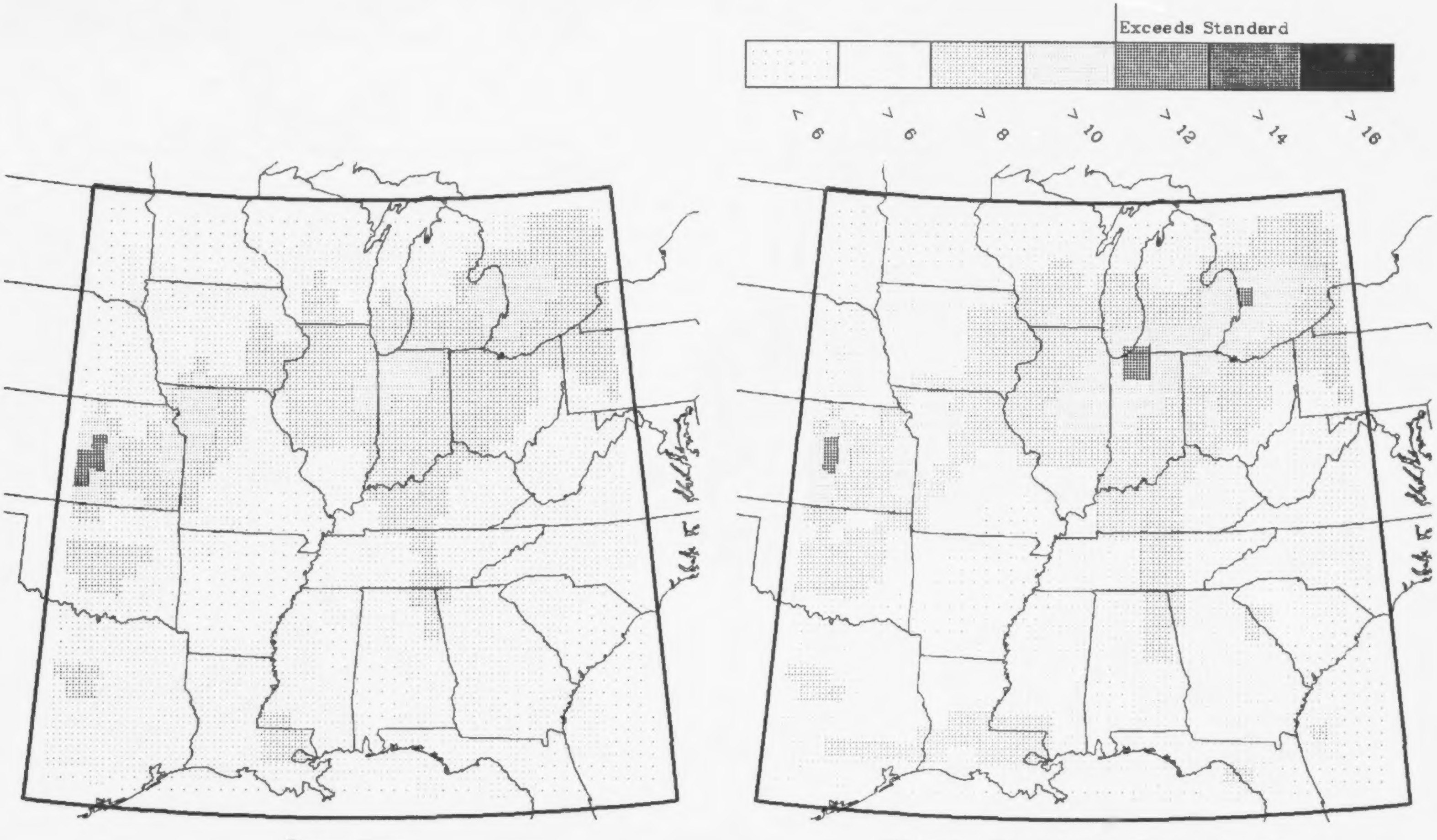
Exceeds Standard
< 6
> 6
> 8
> 10
> 12
> 14
> 16

Base Case

Climate Sensitivity Scenario #1

FIGURE 2-10h. **Comparison of predicted maximum daily ozone concentrations (pphm) for the base case and climate sensitivity scenario #1 (temperature and water increase) for July 21, 1980**

CHAPTER 3

THE SENSITIVITY OF OZONE CONCENTRATIONS TO CLIMATE VARIABILITY

Changes in climate that are forecast to occur in the next several decades will probably manifest themselves as changes in the frequency distribution of climatic variables. For example, a global warming might (1) shift the frequency distribution of temperatures toward warmer values, decreasing the chances of cold temperatures occurring, or (2) change the shape of thedistribution to include a higher frequency of high temperatures, so that the chances of cold temperatures occurring remain the same. In other words, future frequency distributions of climatic variables will largely be made up of events that have occurred historically, but their chances of occurring will change. Therefore, we are justified in using historical data to examine the impact of future meteorological conditions on ozone concentration. In so doing, we can gain insight into the sensitivity of ozone to potential changes in specific meteorological variables. We can also gain insight into which meteorological variables are associated with particular weather regimes, which is useful for introducing realistic climatic perturbations into an air quality model.

We performed an analysis to:

(1) Assess the sensitivity of ozone concentrations to meteorological variables.

(2) Evaluate methods of grouping the meteorological variables into weather types that are associated with ozone concentrations.

If such groups prove to be useful in characterizing various levels of ozone, additional analyses can be performed in the future to (1) produce realistic estimates of the type and degree of climatic perturbation that might occur according to predictions of global climate models, and (2) determine the sensitivities of ozone concentrations to climatic perturbations.

Because data inputs to air quality models are a convenient source of relatively complete information on meteorological variables that influence ozone concentrations, we examined the data inputs and ozone predictions for three applications of the PHOXA version of the RTM-III. The main difference between this version and the RTM-III used in the study discussed in Section 2 is that the PHOXA version includes an early version of the CBM-IV chemical mechanism (Whitten and Gery, 1985).

METHODOLOGY

The analysis consisted of several steps:

(1) Meterological variables that potentially influence ozone concentrations were selected.

(2) Measures of these variables were developed, through spatial and temporal averaging, that would best relate them to ozone concentrations.

(3) The measures were grouped into climatic types that are associated with ozone concentrations.

(4) The feasibility of using such grouping schemes to predict ozone concentrations was assessed.

Selection of Meteorological Variables

The RTM-III model inputs include all climatic information needed to model ozone formation and transport. These variables, which together constitute the "world" according to the RTM-III model, are the following:

(1) At each of the RTM-III layers, gridded and time-dependent arrays of:
  temperature
  wind speed and direction
  water vapor mixing ratio

(2) Gridded and time-dependent arrays of:
  mixing height
  emission rates of ozone precursors
  exposure class
  precipitation rates
  cloud cover

(3) Time-dependent boundary conditions of chemical species at the sides and top of each model layer.

In addition, the RTM-III derives the radiative flux for photochemical reactions (based on the date and time of day, latitude, and cloud cover).

To make the selection of meteorological variables as straightforward aspossible, it is necessary to develop simple techniques for reducing the thousands of data points available for each day to a dozen or so which have the greatest predictive power for maximum daily ozone concentrations. The following reduction techniques were used:

(1) Variables were combined into composite indexes based on a knowledge of chemistry, dispersion, and emissions. For example, wind speed and the mixing height can be multiplied into a product which is sometimes known as the 'ventilation'.

(2) Redundant data were eliminated by combining or removing intercorrelated variables and deemphasizing areas where there is no need for representation by a classification variable. For example, water vapor mixing ratios and temperatures are of interest only in the mixed layer, where the bulk of ozone formation takes place.

(3) Data were systematically averaged in time and space.

(4) Variables were extracted from the model. For example, the algorithm for producing estimates of radiative flux for photochemistry was taken out of RTM and used in conjunction with other input variables to make estimates of radiative flux.

One complicating factor is that the maximum daily ozone is usually affected by the meteorology of the preceding hours. In addition, there is occasionally a substantial buildup and carryover of ozone concentrationsfrom one day to the next. Since we have classified each day separately, we have not treated multi-day serial correlation of ozone levels.

Once a dozen or so candidate variables have been selected, an objective method can be applied to simplify the selection. The creation of a correlation matrix for all of the discriminatory variables will reveal redundancy in the form of correlation between variables. Those variables can then be combined into more powerful variables, or simply eliminated if their ability to predict ozone is poor.

Classification of Meteorological Variables

The goal of the analysis is to provide a scheme for classifying each day of RTM-III input data and evaluate the ability of such a scheme to predict ozone concentrations. There are two separate ways to proceed. The first is to divide the days on the basis of ozone levels. For example, one can define three ranges of ozone concentration and then lump the days, first by ozone, and then by meteorology. This method insures a significant discrimination of ozone levels.

The second approach is to classify days only on the basis of meteorological variables, and to treat ozone as a dependent variable. While this approach results in unique meteorological classes, each class can include such a wide range of ozone concentrations that the meteorological variables would not be useful in predicting levels of ozone.

For our purposes it was more efficient to use the former method, i.e., define ranges of ozone, then classify the days falling under each ozone class by meteorology. In this way the usefulness of the meteorological variables in characterizing ozone levels (which is the information we seek) can be evaluated in a straightforward manner. For example, if one meteorological class is associated with more than one ozone class, the meteorological variables included in that class are probably not good indexes of ozone concentration.

THE DATA BASE

RTM-III Simulations

The data base for this analysis was developed from three RTM-III simulations (Table 3-1).

Eastern U.S. Simulation: This simulation was performed over a domain that encompasses nearly all of the eastern United States and a large portion of the Midwest (Figure 3-1). The modeling period, 15 August to 15 September 1978, included several ozone episodes in various parts of the domain. The highest maximum daily ozone predictions generally occurred in areas in or downwind of major emission areas, such as the mid-Atlantic seaboard and the Ohio River valley. The cell size in this simulation, 80 x 80 km, was the largest of the three simulations.

Midwestern/Southeastern US Simulation: The midwestern domain extends from the Great Plains to just west of the mid-Atlantic seaboard, and from the northern Great Lakes area to central Florida (Figure 3-2). This domain overlaps about two-thirds of the modeling domain for the eastern United States simulation. The simulation includes three separate ozone episodes. The first episode (April 1980) features elevated ozone concentrations in eastern Texas and Louisiana. The second episode (July 1980) features elevated ozone concentrations primarily in the Ohio-Indiana region. In the third episode (August 1980), both of the aforementioned regions experience high ozone concentrations.

Central California Simulation: The central California domain is the smallest of the three, covering an area roughly bounded by the Pacific coast and Sierra Nevada, and the San Francisco Bay Area and Tehachapi Mountains (Figure 3-3). The episode is brief and features elevated ozone concentrations throughout the San Joaquin Valley and San Francisco Bay Area. Features unique to this simulation are the small grid cell size (10 x 10 km), an air flow regime dominated by thermodynamic processes acting on complex terrain, and a lack of cloud cover during the episode. Unlike the other lengthier simulations, this brief episode does not include periods of relatively low ozone concentrations.

RTM-III Input Variables

Meteorological variables influencing the formation and dispersion of ozoneare contained in RTM-III gridded input fields. Of these, five are thought to have a significant influence on ozone concentrations and are

TABLE 3-1. RTM-III simulations used in the historical data analysis.

Region	Domain	Cell Size	Number of Subregions	Subregion Days	Episode
Northeastern USA	2080 x 1840 km	80 x 80 km	3	93	15 August - 15 September 1978
Midwestern USA	1855 x 1942 km	45 x 55 km	4	32 15 12	17-25 April 1980 7-21 July 1980 18-29 August 1980
Central California	320 x 520 km	10 x 10 km	2	12	5-10 August 1981
				164	

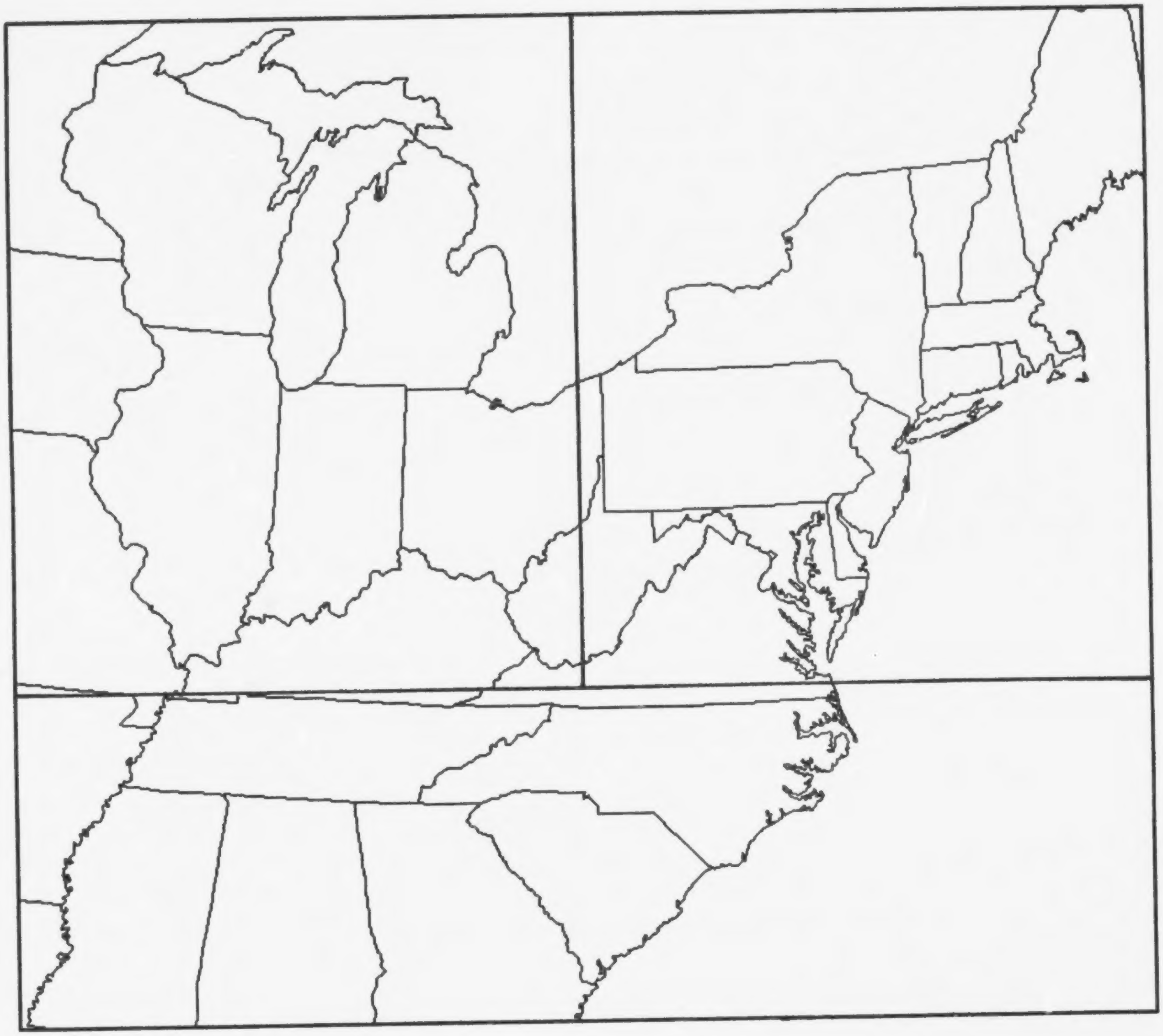

FIGURE 3-1. Northeastern United States modeling region with subregions.

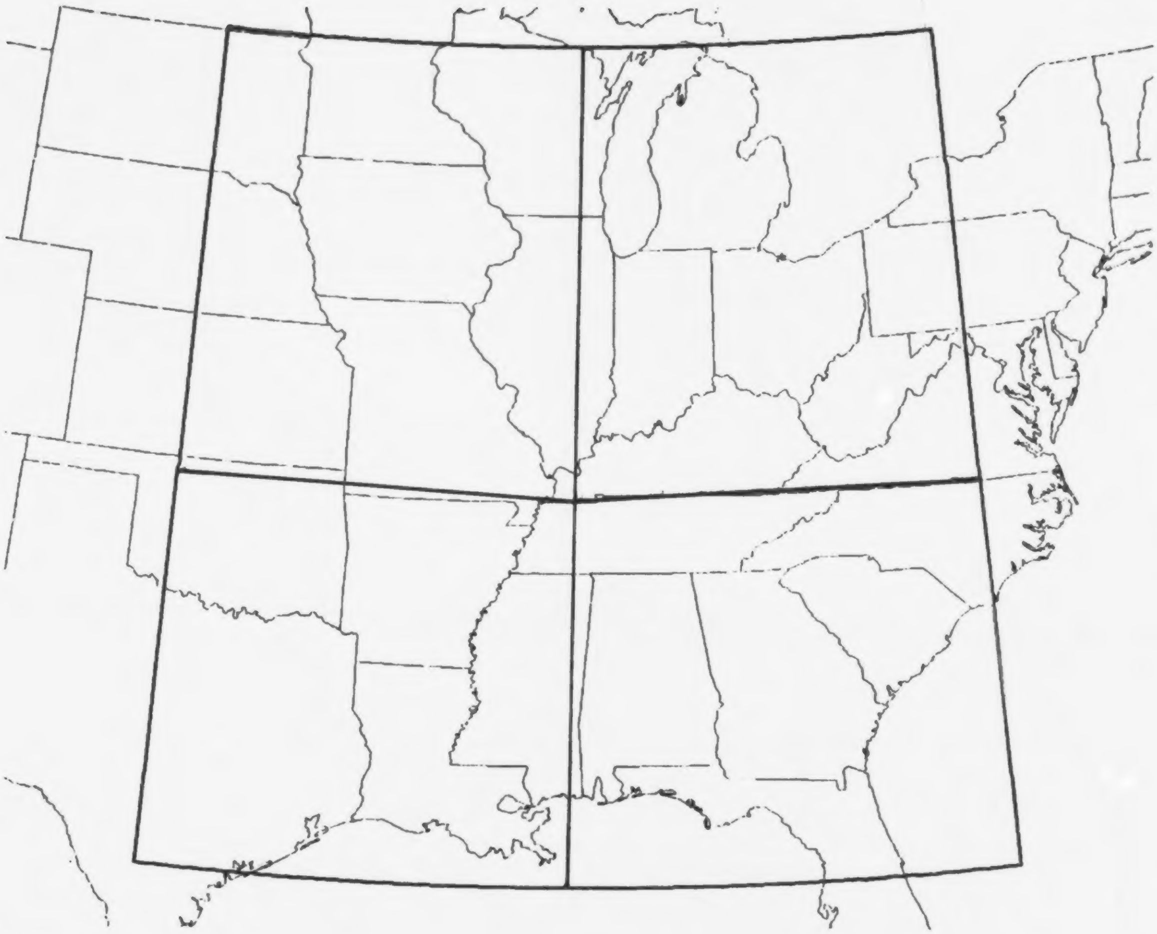

Figure 3-2. The midwestern United States modeling region, with subregions.

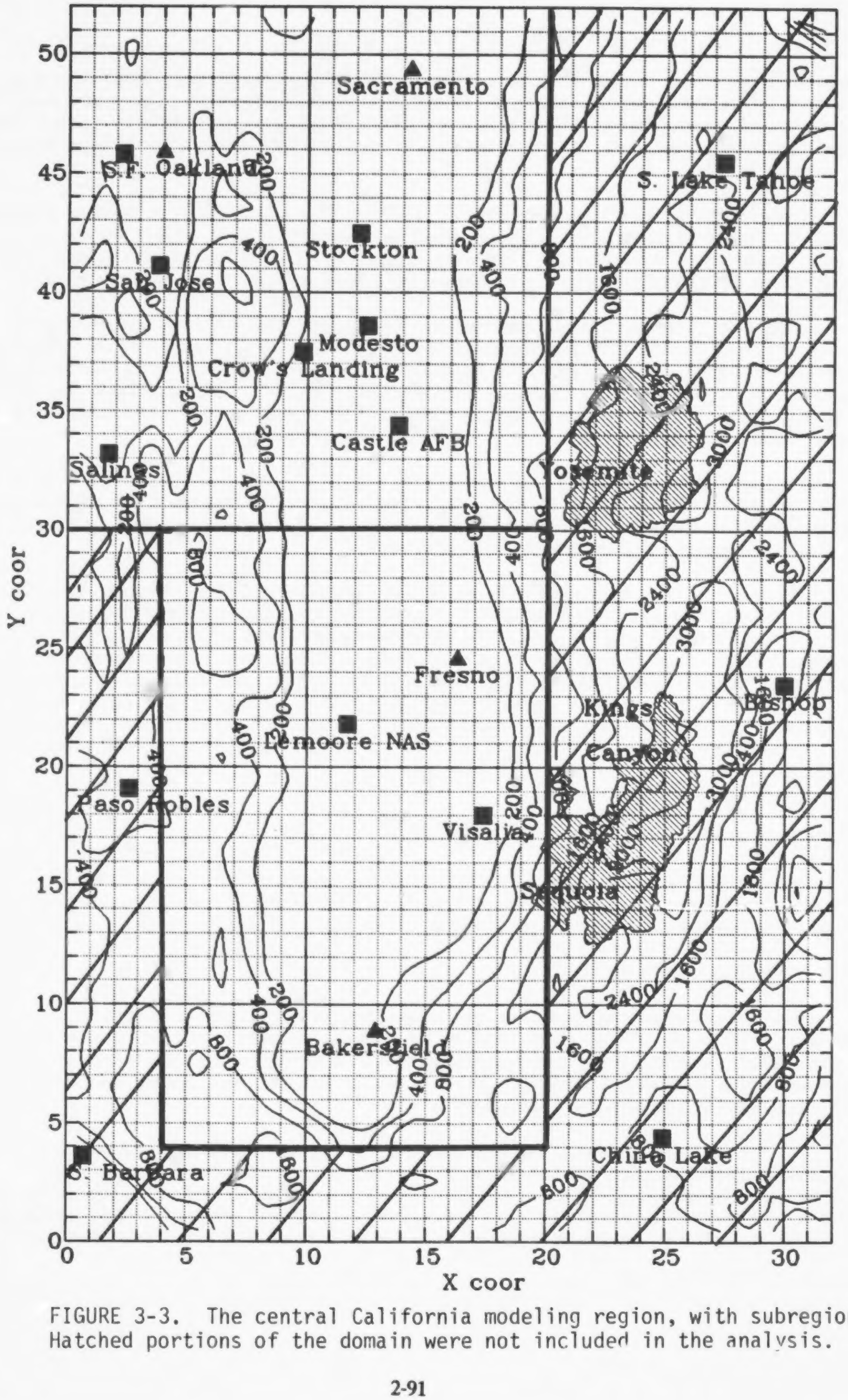
Y coor
X coor
0
5
10
15
20
25
30
35
40
45
50
Sacramento
S.F. Oakland
S. Lake Tahoe
Stockton
San Jose
Modesto
Crow's Landing
Castle AFB
Salinas
Yosemite
Fresno
Kings
Canyon
Bishop
Lemoore NAS
Paso Robles
Visalia
Sequoia
Bakersfield
China Lake
S. Barbara
200
400
800
1600
2400
3000

FIGURE 3-3. The central California modeling region, with subregions. Hatched portions of the domain were not included in the analysis.

relevant to climate change studies. They are: wind speed, mixing height, temperature, water vapor mixing ratio, and solar radiation. Wind speed and mixing height might also be effectively combined into one variable, termed ventilation (wind speed x mixing height), that is a measure of the general capability of the atmosphere to transport and disperse pollutants. Solar radiation is calculated by RTM-III from cloud cover, latitude, time of year, and time of day.

A model is, by definition, reality simplified. The way in which the input variables influence the calculations of ozone will not be the exact way in which they influence ozone in reality. For our purposes, it is important to understand the basic differences between the "RTM-III world" and reality, as they apply to our analysis. These differences deal primarily with approximations of vertical structure and processes:

Vertical Stratification: RTM-III employs a four-layer vertical structure: three prognostic layers (mixed, inversion, and above inversion) and one diagnostic surface layer within the mixed layer. Because the mixed layer is not stratified into more finely divided layers, phenomena that vary with height in the mixed layer in reality are represented by a layer average in RTM-III. Such phenomena include temperature lapse rate, wind speed increase with height, and directional wind shears. When RTM-III is used to study the effects of climatic change, the earth's skin temperature is approximated by the mixed-layer temperature.

Vertical Motion: RTM-III does not address the concept of inversion strength. Gases do not diffuse through the inversion base (defined by the mixing height), but material may pass through this barrier by horizontal transport from areas of higher mixing height to areas of lower mixing height, or through positive vertical velocities produced by convergence in the wind field.

In reality, the inversion strength varies as a function of the amount of subsidence and the temperature lapse rate. Material may pass through the inversion base if it possesses sufficient energy to do so. For example, plumes of warm air or vertical flow produced by cloud pumping can produce updraft venting of material through the inversion base. As previously mentioned, RTM-III has no provision for inhomogeneities in the temperature/energy structure of the mixed layer that might lead to such events. For our purposes, this means that the RTM-III formulation tends to isolate the surface layer from other vertical layers, minimizing the influence of meteorological variables above the mixing height and maximizing the influence of those in the mixed layer. This property of RTM led us to concentrate only on the mixed-layer values of the meteorological variables in this analysis.

SELECTION OF VARIABLES FOR THE ANALYSIS

In an RTM-III simulation, meteorological variables are defined at each grid point every hour or three hours; ozone concentrations are predicted each hour at each grid point. To develop indexes that relate the meteorological variables to ozone concentrations, spatial and temporal averaging scales must be determined.

Spatial Grouping of Variables

Since the goal of this study is to investigate relationships between meteorological variables and regional ozone concentrations, the obvious choice is to average variables over each modeling domain. In practice, however, averaging over such large areas smooths over much of the interesting ozone events occurring within the domain; that is, variability in ozone concentrations and the meterological variables, which is necessary for the development of robust statistical relationships, is reduced.

The reason for this problem is that large regional modeling domains encompass several major emission source areas and are often larger than the typical synoptic scale of a particular weather regime (e.g., storm, high-pressure ridge). For example, in the northeastern U.S. simulation, southern New England experienced an ozone episode on 16 August in which predicted ozone concentrations exceeded 10 pphm; meanwhile, the Chicago area experienced much different conditions, with predicted ozone concentrations near background levels (<6 pphm).

To avoid averaging over highly variable ozone patterns and to maximize the strength and coherence in the relationships among variables, each modeling domain was divided into subregions. Each subregion encompasses an area in which the patterns of ozone concentrations vary in a coherent fashion. The divided modeling domains are shown in Figures 3-1 to 3-3. The northeastern U.S. was divided into three subregions: northwestern, covering the Ohio Valley and much of the Great Lakes; northeastern, covering the northeast corridor; and southern, covering the southern one-third of the domain.

The domain for the midwestern U.S. was divided into four equal subregions: northwestern, which includes the Chicago, St. Louis, and Kansas City urban areas; northeastern, which includes the Ohio River valley and Great Lakes region; southeastern, covering the southeastern states; and southwestern, which includes the Dallas, Houston, and New Orleans urban areas.

The central California domain, although relatively small, contains large gradients in many of the meteorological variables because of the presence of large elevational gradients. We found that those areas of large gradients (i.e., the western slope of the Sierra Nevada and the coastal mountains) would have required excessive subdividing to produce subregions that exhibited an appreciable amount of homogeneity. Therefore, the Sierra Nevada and part of the Coast Range were omitted from the analysis. That part of the domain showing relatively little elevational gradient was divided into two subregions, northern and southern. The northern subregion includes the San Francisco Bay Area, Stockton, and Sacramento; the southern subregion covers the southern San Joaquin Valley, including Fresno and Bakersfield.

Temporal Grouping of Variables

The effects of climate change on exceedances of the primary 1-hour ozone standard is the chief interest in this study; therefore, we have chosen the maximum daily one-hour average concentration as the measure of ozone. The maximum daily ozone concentration is influenced by meteorological processes occurring throughout the day, so it is necessary to choose one or more measurement periods for each variable that potentially best relate it to the maximum hourly ozone concentration. The meteorological variables of concern are wind speed, mixing height, temperature, watervapor mixing ratio, solar radiation, and rainfall (Table 3-2).

Wind speed is a measure of the rate of advection and transport, and is often a good indicator of the weather regime affecting an area. Low windspeeds are typically associated with slow-moving high-pressure systems and stagnant air masses, which are often characterized by above average ozone concentrations. High wind speeds are often associated with weather disturbances or the advection of new air masses into an area; both are characterized by relatively low ozone concentrations. Wind speed may affect both the nocturnal buildup and afternoon dispersion of ozone. Therefore, the selected data periods for wind speed are (1) average windspeed over all hours of the day preceding the ozone maximum, and (2) average wind speed during the afternoon, before the ozone peak occurs. The timing of the maximum daily ozone varies depending on location, weather regime, and time of year; however, for the sake of consistency, 1800 hours was chosen as the time of ozone maximum. Maximum ozone values typically occur before this time, so the selected data periods for windspeed will typically include more hours than actually occur before the ozone maximum.

Mixing height is a measure of the depth of the atmosphere over which most emission, transport, transformation, and dispersion processes occur. Generally, small mixing depths are conducive to the buildup of pollutants, resulting in higher ozone concentrations. Elevated mixing heights allow a relatively large amount of vertical dispersion, resulting in lower ozone concentrations. As in the case of wind speed, the mixing height may affect both the nocturnal buildup and afternoon dispersion of ozone. Therefore, the selected data periods for mixing height are the same as for wind speed.

Temperature influences photolysis reaction rates, and so is of greatest importance during daylight hours. Maximum temperatures and peak ozone concentrations often occur at the same time, and temperature can directly influence ozone production and destruction during the buildup of ozone. Therefore, the selected data periods for temperature are (1) average mixed-layer temperature over all daylight hours up to the ozone maximum (1800 hours), and (2) the maximum daily mixed-layer temperature.

TABLE 3-2. RTM-III input variables expected to be important in the formation and buildup of ozone concentrations.

Variable	Temporal Resolution	Vertical Specification	Data Selected for Analysis
Wind speed	3 hours*	Mixed layer	0-1800 average; afternoon (1200-1800) average
Mixing height	3 hours*	Mixed layer	0-1800 average; afternoon (1200-1800) average
Temperature	3 hours*	Mixed layer	Daylight (0700-1800) average; maximum 3-hour value
Humidity	3 hours*	Mixed layer	Daylight (0700-1800) average; maximum 3-hour value
Solar radiation	3 hours**	Surface	Daily (0-2400) total; morning (0-1200) total
Ventilation	3 hours*	Mixed layer	0-1800 average; afternoon (1200-1800) average
Rainfall	1 hour**	Surface	Daily total (0-2400)

* One hour in the central California simulation.
** Not available in the central California simulation.

Humidity influences the rates and dispositions of many chemical reactionsin the atmosphere. It can affect the rate of ozone destruction during the night, but its primary effect is on ozone production during the day. Maximum water vapor mixing ratios often occur near the time of the peak daily ozone concentration, and can affect the rates of ozone formation and destruction at this time. Therefore, the selected data periods for humidity are (1) the average water vapor mixing ratio in the mixed layer during the daylight hours leading up to the ozone maximum (1800 hours), and (2) the daily maximum mixed layer water vapor mixing ratio.

Solar radiation directly dictates photolysis rates and thus is importantduring all daylight hours, especially the morning hours. A value for solar radiation is calculated by RTM-III by considering cloud cover and sun angle. The selected data periods are: (1) total solar radiation received at the surface during the day, and (2) total solar radiation received at the surface during the morning hours.

Rainfall scavenges ozone and its precursors from the atmosphere and therefore has a negative relationship with maximum daily ozone concentration. Also, rainfall is usually accompanied by increased windspeeds, mixing heights, and cloudy skies, which also tend to depress ozone concentrations. The accumulated rainfall in an area serves as a measure of the ozone-producing potential of the atmosphere, so the selected data period is total daily rainfall.

Ventilation, defined as the product of the mixed layer wind speed and depth of the mixed layer, is a measure of the overall ability of the atmosphere to transport and disperse pollutants, both vertically and horizontally. It is not a primary meteorological variable, but has a strong influence on the buildup of pollutants during the night; during the day, atmospheric ventilation directly influences the maximum concentrations of ozone in the mixed layer. The selected data periods for ventilation are the same as for wind speed and mixing height.

Ranges of the Meteorological Variables within Episodes

If robust relationships are to be developed between the meteorological variables and ozone concentrations, there must be sufficient variability in both the independent and dependent variables. Table 3-3 shows the mean and range of values for predicted ozone and the meteorological variables for each modeling domain and episode. In the northeastern simulation (Table 3-3a) all meteorological variables exhibit a relatively large range of values. Average rainfall is very low, primarily due to the averaging of spotty rainfall events over relatively large subregions. The temperature range is substantial (about 12 K) and the water vapor mixing ratio varies over a factor of two. Maximum ventilation is over 10 times the minimum, and maximum solar radiation is about three times the minimum. Ranges of mixing height and wind speed reveal that most of the range in ventilation (mixing height x wind speed) is accounted for by variation in the wind speed, which ranges over a factor of 10; mixing height ranges over a factor of two to three. Maximum ozone varies least, ranging over a factor of less than two. However, the minimum of 0.047 ppm is essentially a background ozone concentration, while the maximum of 0.082 ppm indicates that high values are widespread over a subregion. (Predicted maximum ozone concentrations rarely exceed 0.12 ppm for any grid cell in any simulation analyzed.)

Episode 1 in the midwestern region, in April, is characterized by relatively low temperatures and water vapor mixing ratios; both have somewhat larger ranges than in the northeastern episode (Table 3-3b). Temperature ranges over about 15 K, and water vapor mixing ratios vary over a factor of three. Mixing heights are relatively high, averaging 30-40% higher than in the northeastern episode; in contrast, rainfall is low. The ranges and values of the other variables are roughly similar.

Episode 2 in the midwestern region occurred in July; this is reflected inthe highest temperatures and water vapor mixing ratios of any of the simulations (Table 3-3c). In general, the ranges of the descriptive measures are somewhat less than those in the northeastern episode; the range of ozone concentrations is almost identical to the two previously discussed episodes, but the average is higher.

Episode 3 in the midwestern region, in August, exhibits means, maxima, and minima similar to episode 2, except that solar radiation and mixing heights (and hence, ventilation) are slightly lower (Table 3-3d).

Table 3-3a. Ranges of Calculated Measures and Daily Ozone Concentrations for the Northeastern United States Modeling Region (All Subregions Included), 15 August - 14 September 1978

Variable	N	Minimum	Maximum	Mean
Rainfall (inches)	93	0.00002	0.183	0.033
Daylight temperature (°K)	93	285.6	297.4	293.0
Maximum temperature (°K)	93	286.5	298.1	294.0
Average water vapor (ppm)	93	9108	21,826	15,588
Maximum water vapor (ppm)	93	9652	22,690	16,156
Average ventilation (km^2/m)	93	2.65	36.00	13.37
Afternoon ventilation (km^2/m)	93	4.90	57.80	21.33
Daily radiation (w/m^2)	93	858	2548	1928
Morning radiation (w/m^2)	93	337	1079	803
Average mixing height (m)	93	439	924	659
Afternoon mixing height (m)	93	779	1904	1125
Average wind speed (m/s)	93	1.67	11.67	5.27
Afternoon wind speed (m/s)	93	1.67	10.83	5.17
Maximum ozone (ppm)	93	0.047	0.082	0.065

Table 3-3b. **Ranges of the Calculated Measures and Daily Ozone Concentrations for the Midwestern United States Modeling Region, Episode 1 (All Subregions Included), 17 - 25 April 1980**

Variable	N	Minimum	Maximum	Mean
Rainfall (inches)	36	0.00008	0.07677	0.00900
Daylight temperature (°K)	36	276.5	293.4	286.6
Maximum temperature (°K)	36	279.6	295.6	288.0
Average water vapor (ppm)	36	5406	15,207	9036
Maximum water vapor (ppm)	36	5689	15,877	9818
Average ventilation (km^2/m)	36	7.13	29.03	15.02
Afternoon ventilation (km^2/m)	36	9.30	54.28	25.51
Daily radiation (w/m^2)	36	1388	2467	1962
Morning radiation (w/m^2)	36	361	942	654
Average mixing height (m)	36	669	1187	881
Afternoon mixing height (m)	36	1088	2594	1625
Average wind speed (m/s)	36	2.67	8.33	4.86
Afternoon wind speed (m/s)	36	2.33	7.83	4.39
Maximum ozone (ppm)	36	0.053	0.086	0.070

Table 3-3c. Ranges of the Calculated Measures and Daily Ozone Concentrations for the Midwestern United States Modeling Region, Episode 2 (All Subregions Included), 7 - 21 July 1980

Variable	N	Minimum	Maximum	Mean
Rainfall (inches)	56	0.00097	0.08065	0.02081
Daylight temperature (°K)	60	292.6	302.20	298.7
Maximum temperature (°K)	60	294.8	305.0	300.7
Average water vapor (ppm)	60	16,522	27,461	22,249
Maximum water vapor (ppm)	60	17,467	28,674	23,284
Average ventilation (km^2/m)	60	5.45	25.49	12.14
Afternoon ventilation (km^2/m)	60	8.50	36.89	17.84
Daily radiation (w/m^2)	60	1630	2688	2255
Morning radiation (w/m^2)	60	468	913	740
Average mixing height (m)	60	505	963	709
Afternoon mixing height (m)	60	761	1727	1117
Average wind speed (m/s)	60	2.17	8.33	4.74
Afternoon wind speed (m/s)	60	2.17	7.67	4.36
Maximum ozone (ppm)	60	0.057	0.091	0.072

Table 3-3b. Ranges of the Calculated Measures and Daily Ozone Concentrations for the Midwestern United States Modeling Region, Episode 1 (All Subregions Included), 17 - 25 April 1980

Variable	N	Minimum	Maximum	Mean
Rainfall (inches)	36	0.00008	0.07677	0.00900
Daylight temperature (°K)	36	276.5	293.4	286.6
Maximum temperature (°K)	36	279.6	295.6	288.0
Average water vapor (ppm)	36	5406	15,207	9036
Maximum water vapor (ppm)	36	5689	15,877	9818
Average ventilation (km^2/m)	36	7.13	29.03	15.02
Afternoon ventilation (km^2/m)	36	9.30	54.28	25.51
Daily radiation (w/m^2)	36	1388	2467	1962
Morning radiation (w/m^2)	36	361	942	654
Average mixing height (m)	36	669	1187	881
Afternoon mixing height (m)	36	1088	2594	1625
Average wind speed (m/s)	36	2.67	8.33	4.86
Afternoon wind speed (m/s)	36	2.33	7.83	4.39
Maximum ozone (ppm)	36	0.053	0.086	0.070

Table 3-3d. Ranges of the Calculated Measures and Daily Ozone Concentrations for the Midwestern United States Modeling Region, Episode 3 (All Subregions Included), 18 - 29 August 1980

Variable	N	Minimum	Maximum	Mean
Rainfall (inches)	48	0.00174	0.10169	0.02507
Daylight temperature (°K)	44	291.6	301.1	296.2
Maximum temperature (°K)	44	292.2	304.0	297.2
Average water vapor (ppm)	44	16,283	26,964	21,102
Maximum water vapor (ppm)	44	16,485	28,365	22,166
Average ventilation (km^2/m)	48	3.09	21.09	8.54
Afternoon ventilation (km^2/m)	48	6.27	30.91	14.55
Daily radiation (w/m^2)	48	1361	2283	1846
Morning radiation (w/m^2)	48	358	812	599
Average mixing height (m)	48	377	777	543
Afternoon mixing height (m)	48	747	1436	1015
Average wind speed (m/s)	48	2.17	8.33	4.41
Afternoon wind speed (m/s)	48	2.17	8.00	4.05
Maximum ozone (ppm)	48	0.056	0.089	0.073

Table 3-3e. Ranges of the Calculated Measures and Daily Ozone Concentrations for the Central California Modeling Region, 5 - 10 August 1981

Variable	N	Minimum	Maximum	Mean
Rainfall[a] (inches)	--	--	--	--
Daylight temperature (°K)	12	298.6	303.5	301.3
Maximum temperature (°K)	12	300.9	307.3	304.5
Average water vapor (ppm)	12	4814	8350	6433
Maximum water vapor (ppm)	12	6887	8959	7690
Average ventilation (km^2/m)	12	1.68	5.24	3.25
Afternoon ventilation (km^2/m)	12	3.51	13.64	7.59
Daily radiation (w/m^2)[b]	--	--	--	--
Morning radiation (w/m^2)[b]	--	--	--	--
Average mixing height (m)[c]	--	--	--	--
Afternoon mixing height (m)[c]	--	--	--	--
Average wind speed (m/s)[c]	--	--	--	--
Afternoon wind speed (m/s)[c]	--	--	--	--
Maximum ozone (ppm)	12	0.074	0.091	0.081

[a] No rainfall in region during episode.
[b] Skies were cloud-free during episode.
[c] Not used in analysis; see text.